An urban heat island study for building and urban design

A thesis submitted to The University of Manchester for the degree of Doctor of Philosophy in the Faculty of Engineering and Physical Sciences

2011

Henry Kei Wang Cheung

School of Mechanical, Aerospace and Civil Engineering

Table of content

List of figures

List of tables

Notation for canyon model

A = the surface area of the slab [m^2]

C = the cloud cover ($0 \leq C \leq 1$)

C_d = the discharge coefficient, which for a sharp-edged opening, is 0.6 [dimensionless]

C_p = the specific heat capacity [J m^{-3} K^{-1}]

H = average height of buildings in canyon [m]

k = conductivity of the slab [W m^{-1} K^{-1}]

L = length of street canyon[m]

Q_{ac} = convective heat exchange between the air within the canyon and the inside canyon surface [W]

Q_{as} = the convective, turbulent flux heat transfer and advective heat loss to the air from the slab [W]

Q_{canyon} = the heat conduction at the canyon's inside surface [W]

Q_{cie} = the heat flow from the canyon slabs, to (or from) the interiors of the buildings and to the earth under the bottom, base slab [W],

Q_e = heat lost to earth [W]

Q_l = the net long wave irradiance emitted from the slab surface [W]

Q_{lc} = long wave radiation from the canyon [W]

q_s = the horizontal global solar irradiance flux [Wm^{-2}]

Q_s = the horizontal global solar irradiance, [W]

Q_{sabc} = solar irradiance absorbed by the inside of the canyon [W]

Q_{slab} = the heat into the slab [W]

SVF = the sky view factor [dimensionless]

T = the time [s]

t_{ao} = the external air temperature [°C]

t_c = the temperature of the middle of the canyon slabs[°C]

t_{ca} = the air temperature in the canyon [°C]

t_{ci} = the building interior temperature [°C]

t_{cie} = the average canyon building interior and earth temperature [°C]

t_{co} = the outside surface temperature of buildings inside the canyon [°C]

t_e= the earth temperature [°C]

t_s = temperature of the middle of the slab [°C]

t_{so} = the outside (upper) surface temp slab [°C]

V = the volume of the canyon [m^3]

W = width of street canyon [m]

x = thickness of the slab [m]

α = absorption of solar irradiance into the slab.

ρ = the density of the slab [kg m^{-3}]

τ = the time constant [s].

Abstract

A lot of research has been conducted in the past decades on urban heat island (UHI) all over the world. Nevertheless, the UHI effect has not been included in weather data used by building services engineers to design buildings and size their heating and cooling plants. This research was carried out to investigate the UHI effect in Greater Manchester by setting up fixed point monitoring stations over the city. Woodford Met Office ground observation station was selected to be the rural reference point. A multiple regression model was developed to incorporate the heat island effect into the Manchester weather data for engineering usage.

It was found that the urban heat island intensity (the difference between the rural and urban area temperatures) can be as high as 8^{o}C in summer and 10^{o}C in winter in Manchester. Clear and calm nocturnal temperature data was used (when maximum heat island occurs[1]) to find the relationship between the UHI intensity and sky view factor (SVF), distance away from the city centre, evapotranspiration fraction (EF), wind speed, cloud cover and rural reference temperature. Results indicate that all factors have a negative linear relationship with UHI intensity.

All measured data were fed into a statistical software package to create general linear regression models. Validation showed that these models were capable of predicting average UHI effect to a good accuracy. The maximum heat island effect peaks are not so accurate. However, an analytical model was developed based on energy balance equations to predict the maximum heat island effect. Validation shows a good prediction for summer but not so good for winter. This is probably due to the lower average UHI intensity in winter than in summer.

Declaration

No portion of the work referred to in the thesis has been submitted in support of an application for another degree or qualification of this or any other university or other institute of learning.

Copyright Statement

Acknowledgement

I would like to thank my supervisors, Prof. Geoff Levermore, Dr. John Parkinson and Prof. Yong Wang for all their invaluable supervision and suggestions. Your valuable comments, help and advice on the development of this work enable the formation of the platform of this thesis. I am grateful for their patience that drove me to complete this research project.

Also thank you to Prof. Patrick Laycock for his advice and comments on the statistical part of the thesis and Dr Richard Watkins for his comments on this thesis.

This work was funded as part of the COPSE project under an EPSRC grant EP/F038178/1. I'm very grateful for the co-operation of the local authorities within the Greater Manchester area who were very supportive in giving permission for establishing the array of monitoring stations.

I would like to dedicate this thesis to my parents to fully support me to bring this thesis to a completion.

Thanks you to Mr. Paul Townsend, Mr. David Jones, Mrs. Carolyn Levermore and Miss Theresa Yong for their grateful assistance during my preparation of this thesis.

Finally, I would like to thank all my friends for their encouragement and support.

CHAPTER 1

Introduction

CHAPTER 1 Introduction

Over the last few decades, urbanisation has been spreading rapidly over the world. Population Reference Bureau (2007)[2] suggested that half of the world's population would be living in city areas by 2008. In Europe, an increase in the urban population from 73% by 2000 to 80% in 2030[3] is predicted. Global warming and pollution are some of the consequences of urbanisation. These consequences will not only affect human beings but can also modify earth's climate. Urban heat island (UHI) is an example of this. Urban heat island is a phenomenon when air / surface temperature in an urban area is higher in comparison to rural areas. Figure 1.1 shows the typical temperature variation over a city with urban heat island effect [Stone & Rodger[4] (2001)].

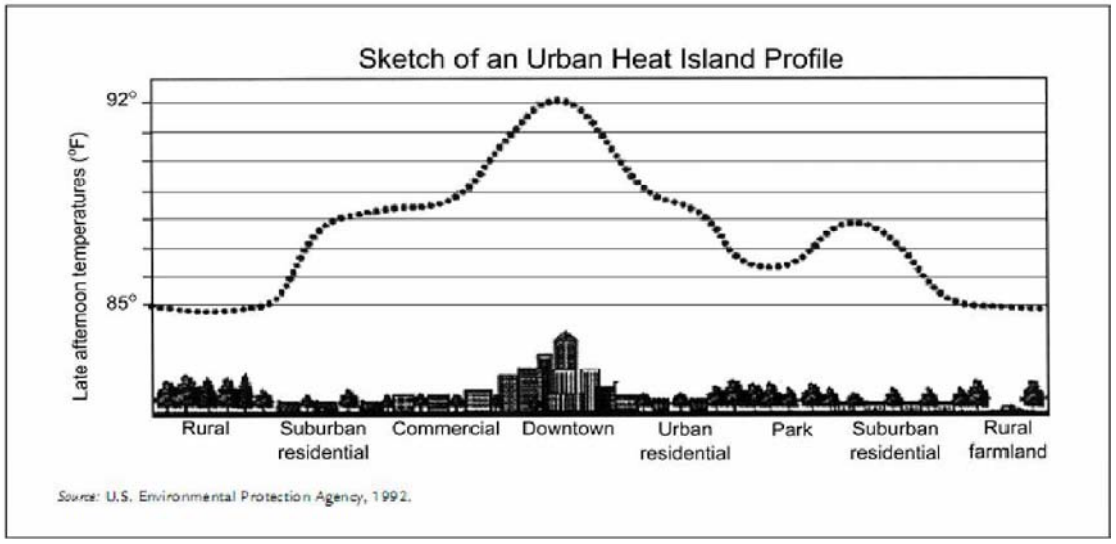

Figure 1.1 Temperature profile of a typical UHI [Stone & Roger[4], (2001)]

The air temperature difference between urban and rural areas is called the urban heat island intensity [Lowry[5] (1977), Magee *et al.,*[6] (1999), Kim and Baik[7] (2005)]. A positive intensity value shows an urban heat island; whilst a negative value represents an urban cool island (i.e. air temperature for the urban area is lower than the rural

surroundings). According to Arnfield[8] (2003) and Kanda[9] (2007), there have been a lot of scientific papers published on the topic of urban heat island over the last decade. A lot of models have been developed to predict the urban heat island effect. Furthermore, research has also been conducted to investigate the urban heat island in different countries such as Sweden, Hong Kong, London and Korea etc [Eliasson[10] (1996), Giridharan *et al.,*[11] (2007), Watkins *et al.,*[12] (2002), Wilby[13] (2003), Baik *et al.,*[14] (2006)].

The urban heat island can have a large impact on building and urban design. Urban heat island in winter can reduce the energy consumption in heating system (this might be revised if the surplus heat causing the heat island is due to the anthropogenic heating released caused by poor building insulation) while the heat island effect in summer would cause increasing energy consumption in air-conditioning. Therefore it is important to investigate and quantify the urban heat island effect.

UK climate impacts program (UKCIP02) scientific report[15] indicated the impact to the climate under four CO_2 emission scenarios. The Adaptation Strategies for Climate Change in the Urban Environment [ASCCUE[16] (2006)] project investigated the impact of climate change on building integrity in Manchester. The outcomes of the ASCCUE project included basic surface temperature models which were produced for the different CO_2 emission scenario mentioned in UKCIP02 and the urban morphology type mapping (details will be covered in chapter 7.4) for Greater Manchester. Although the surface temperature model can reflect heat island effect caused by different land use, the effect caused by urban geometry was not included. Sustainable Cities: Options for Responding the Climate change impacts and outcomes [SCORCHIO[17] (2009)] project performed ground and air transects to investigate the

urban heat island in Greater Manchester. A GIS-based supporting tool was created for urban design. Urban heat island effect in Greater Manchester was investigated in SCORCHIO project by transects. These transects were only conducted over a few clear sunny days in a year. However, air transects can only measure the surface temperature. Similar to the limitation of ASCCUE project, the canyon effect was not investigated. Therefore, with limited data and no canyon analysis, a more comprehensive investigation for urban heat island effect is required in Greater Manchester.

Although urban heat island effect in Greater Manchester had been investigated previously, the temperature monitoring scale was small. The effect of canyons has not been investigated. Deliverables from previous projects were not sufficient to provide a simple solution to engineer for building design. Therefore, the urban heat island effect in Greater Manchester is investigated in this project with large scale temperature monitoring and simple models developed so that engineers can quantify the heat island effect in their designs.

CHAPTER 2

Objectives and Aim

CHAPTER 2 Objectives, Aims and hypothesis

2.1 Project Background

One of the main predicted effects of climate change was the increase of air temperature. IPCC (2007)[18] suggested an increase of 1.1°C to 6.4°C by the end of this century depending on the different emission scenarios. The IPCC report (2007)[18] also indicated that 33% of total greenhouse gas emissions were produced by human activity contributing toward global warming. About 50% of the CO_2 emissions in UK were contributed by buildings. Building overheating in summer is likely to be increased and more energy would be used for air conditioning in buildings to provide extra cooling as a consequence of global warming [Chow *et al.,*[19] (2002), Konopacki and Akbari[20] (2002), Parkinson *et al.,*[21] (2004)].

Heating, ventilation and air conditioning plants are usually designed based on the steady state calculation method with weather data from CIBSE Guide [CIBSE[22] (2006)]. However, all these weather data were historical data with no future expectations. They were obtained mainly from local airports with Met Office weather stations. Some of these data were over 20 years [Leveremore *et al.,*[23] (2006)]. Designers use extreme weather data, sometimes without considering the probability of the occurrence, resulting in an over-estimated plant designed. Cost and energy is then wasted as a consequence.

UKCIP updated the UKCP02 data in 2009 (UKCP09)[24] including a weather generator which can produce probabilistic weather data with grid size of five kilometres for three different greenhouse gas emission scenarios. This weather generator is a stochastic first-order Markov chain processor and the days are

independent (not smoothly joined at midnight) and adjacent grids are not coincident temporally (one grid box could be sunny and the adjacent grid box pouring with rain). In order to use these future probabilistic weather data, building designers should consider the different combinations of weather conditions with different probability. COPSE (Coincident Probabilistic climate change weather data for a Sustainable built Environment) [COPSE[25] (2008)], of which this work is a part, aims to provide an explanation of the probabilistic design and developing different scenarios to assist building designers in selecting UKCP data. Although urbanity (a simple ratio between 0 and 1 to indicate the make up of the grid) was included partly in the UKCP data, this work examines the urban heat island for Manchester in the COPSE project to include the urban heat island with the UKCP weather data[26].

2.2 Project aim and objectives

This thesis is part of an EPSRC funded research project COPSE. The main objective of COPSE is to develop a scheme to produce (or revise) a new set of weather data (mainly to revise the air temperature) for building services engineers. The overall aims for COPSE were listed below[25]:

1. Develop new design criteria based on CKCP09 outputs for domestic and non domestic buildings based on probabilistic future weather data from UKCP09 scenarios.
2. Establish methodologies to transform UKP09 probabilistic data into design data for buildings and developing new Design Reference year (DRY)
3. Develop methods to modify the weather data to reflect urban heat island effect so that the localised weather data could be generated from UKCP based output.

4. Assess the potential of adaptation for carbon emission reduction from new and refurbished buildings under new methodology and data.

This thesis is the outcome of one of the work packages of COPSE which aims to investigate the urban heat island effect. The objectives of this thesis were that large scale temperature monitoring will be performed in Greater Manchester and temperature data could be used to calculate urban heat island intensity. The specific objectives of this project are:

To develop a new model/procedure to adjust the weather data so that the revised weather data set can reflect the urban heat island effect in local canyons. By using this localised weather data, additional building services plant load could be calculated more accurately. This new weather data set could be based on historical weather data or UKCP data with five kilometres grid.

2.3 Hypotheses

From the aims above, the objectives for this project are developed into the following hypotheses. There are four hypotheses in this project:

1. There is an urban heat island effect in Greater Manchester.
2. Urban geometry contributes to urban heat island effect.
3. This urban heat island effect can be modelled statistically or empirically and reasonably simply.
4. Weather data can be used with the model to reflect urban heat island effect in Greater Manchester.

CHAPTER 3

Literature review

CHAPTER 3 Literature Review

3.1 Introduction

Urban heat was first mentioned by Luke Howards (1810s)[27] in the 1810s. He found "an artificial excess of heat" in London compared with its rural area. Mitchell (1953)[28] commenced his research in America during the 1950s. A lot of research regarding the urban heat island effect was undertaken around the world in the past decades [Gartland[29] (2008)].

Morris *et al.,*[30](2000) found the maximum heat island intensity could reach 2.4^{o}C in winter in Melbourne. The maximum heat island intensity was found to be 6.5^{o}C in Mexico City by Jauregui[31] (1997) using hourly daytime temperature. Moll *et al.,* (1996)[32] found a maximum heat island intensity of 7^{o}C in Atlanta. In Brussels, Van Weverberg *et al.,*[33] (2008) found that there was a stronger heat island effect in summer under clear skies with calm conditions. Yamashita[34] (1996) found a stronger heat island intensity of 4-5^{o}C in winter and 1.0-1.5^{o}C in summer in Tokyo. A maximum UHI intensity of 7-8^{o}C was found in Barcelona [Moreno[35] (1994)] by comparing the daily maximum temperature with the temperature obtained from the airport. Gedzlman *et al.,*[36] (2002) found that the maximum heat island effect occurred in the mid-night under clear condition in New York. Montavez *et al.,*[37] (2000) also found a heat island intensity of 3-3.5^{o}C in Granada, Spain. Santamouris[38] (1998) found that the daytime temperature difference varied from 4-15^{o}C warmer than the outside town area in Athens. It can be seen that the heat island effect was clearly evident but the intensity varied from place to place.

Urban cool island was also found in extreme hot or cold environments. Using transect

data in summer during periods with the maximum temperature, Ludwing[39] (1968) found an approximate of 1°C urban cool island in Dallas. A negative heat island intensity of -4°C was found by Steinecke[40] (1999) in Reykjavik, Iceland during all day daytime in summer. This was because the low summer sun casts shadows on buildings in northern cities. Due to the high latitude of the Iceland, the solar angle in winter is very low. High rise buildings in the city centre can block the low angle solar irradiance from entering the street canyon. Thus, the air temperature in the canyon is much lower than rural area where got plenty of sunshine in early morning in Iceland. Brazel *et al.,*[41] (2000) also found a negative heat island during the day in the desert city of Phoenix. However, a positive heat island intensity of 3-8°C was still found during the night. Apart from the locations, there was also research studies investigating the UHI intensities in different seasons [Kolokotroni and Giridharan[42] (2008), Giridharan and Kolokotroni[43] (2009)]. It was found that the average urban heat island intensities at night were similar in magnitude for both seasons.

A large scale temperature monitoring project was performed by Watkins[44] (2002) in London. He used 80 sensor-loggers to measure the air temperature over Greater London. It was found that the averaged urban heat island was about 3-4°C at night in London. The maximum urban heat island intensity was recorded at 8°C in some occasions. Watkins also showed good relationships between UHI intensity and causal factors such as wind speed, distance from city centre, rural temperature and wind direction. He did not study canyons in detail and he analysed the data he measured statistically, using individual parameter correlations, and did not develop a UHI or canyon model. Watkins' work is the basis of the UHI section in CIBSE Guide A[22].

Although different magnitudes of urban heat island were recorded for different parts

of the world, Peterson *et al.,*[45] (1999) indicated the influence of urbanisation on the global mean temperature was very little. McCarthy *et al.,*[46] (2009) found that the urban heat island effect would increase with climate change by using regional climate model simulation.

3.2 Effect of urban heat island

Apart from the temperature influences, the welfare and health of inhabitants could also be affected by local heat waves. More than 800 people died during the heat wave in Chicago in 1995 [Changnon *et al.,*[47] (1996)]. The hot summer in 2003 in Europe also caused 15,000 deaths due to heat related illness in Paris [Wright *et al.,*[48] (2005)]. Urban heat island will also cause increase in air pollutants. Sarrat *et al.,*[49] (2006) indicated the impact of urban heat island in Paris on the concentration of ozone and nitrogen oxide (NO_x) in their research. Urban heat island also increases the energy demand used for cooling. This in turn causes extra heat to be dumped into the urban area further exacerbating the urban heat island effect [Voogt[50] (2004)].

3.3 Factors affecting urban heat island

Oke (1978)[1] defined urban boundary layer in his book as "a local to meso-scale phenomenon whose characteristics are governed by the nature of the general urban surface" and urban canopy layer as "Beneath roof-level and produced by micro-scale process operating in the street between buildings". Voogt[50] (2004) further defined three types of urban heat island: canopy layer heat island, boundary layer heat island and surface heat island. The definition of canopy layer, boundary layer will be explained later in chapter 4.

Many factors affect the urban heat island. Memon *et al.,*[51] (2008a) stated that the main urban heat island generation was caused by anthropogenic heat from vehicles, air conditioners and power plant, as well as heat re-radiated and stored in the urban structure. Memon *et al.,*[51] (2008a) also suggested that there were two classes of influencing factors for urban heat island: controllable and uncontrollable. Figure 3.1 below shows all the generation factors. Uncontrolled factors are weather parameters such as cloud cover, windspeed, diurnal conditions, seasons and anticyclone conditions. Controllable factors can be further divied into population related factors (such as anthropogenic heat and air pollutants) and urban designed related factor (such as sky view factor, green areas, building materials). Solar irradiance has influence on both controllable and uncontrollable factors and will affect the urban heat island directly.

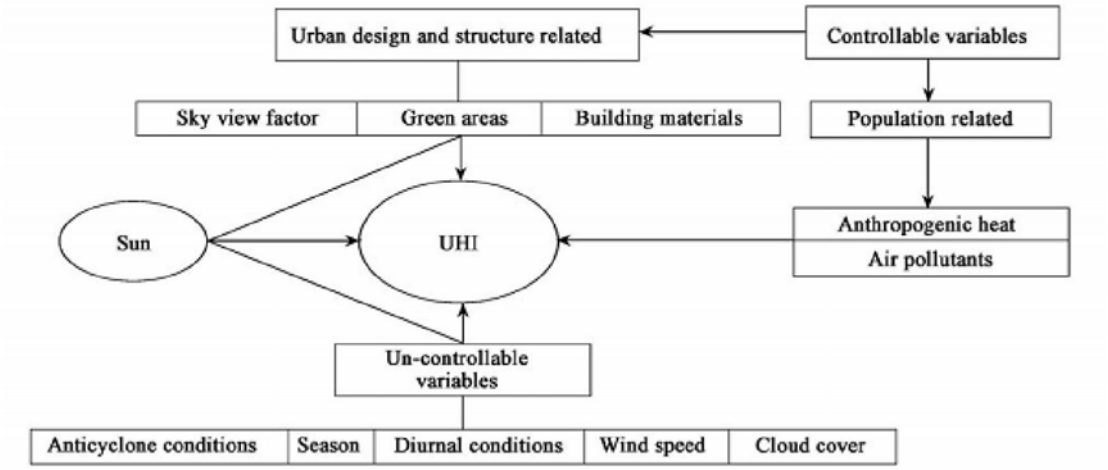

Figure 3.1 Factors affecting the generation of urban heat island [Memon *et al,.*[50] (2008a)]

It is believed that urban heat island is formed by the mutual inter-action between different environmental factor and human factors [Memon *et al.,*[52] (2008b), Unger *et al.,*[53] (2001)]. However, it has still not been thoroughly understood [Hafner and Kidder[54] (1999), Poreh[55] (1996)].

Canyon geometry is one of the most important factors that affect the urban heat island Oke[1] (1978). The shape of a canyon limits the amount of solar irradiance entering as well as the escape of long wave radiation. Canyon geometry could be expressed in terms of either height to width ratio or sky view factor (SVF). SVF details are covered in section 7.2. Oke[56] (1981) indicated the importance of urban geometry towards the formation of urban heat island in his model (refer to section 5.1.1 for details). The long wave irradiation to the sky would decrease if there was a low sky view factor because part of the sky was blocked by tall buildings. Oke[56] presented the relation between UHI intensity and urban geometry as equation 3.1 and equation 3.2 where $\Delta T_{\mathrm{u-r}}$ is the air temperature difference between urabn and rural area, *H* and *W* refer to the height and width of the street canyon and ψ_{sky} is the sky view factor.

$$\Delta T_{\mathrm{u-r}} = 7.54 + 3.97\ln({}^{H}/_{W}) \qquad \text{eq 3.1}$$

$$\Delta T_{\mathrm{u-r}} = 15.27 - 13.88\psi_{\mathrm{sky}} \qquad \text{eq 3.2}$$

Yamashita *et al.,*[57] (1986) performed research in five cities near Tokyo regarding the relation between SVF and air temperature. A 'fairly strong relationship' between SVF and air temperature was found. Eliasson[58] (1992) investigated the relation between surface temperature and SVF. Equation 3.3 states her findings where T_{s} is the surface temperature and ψ_{sky} is the sky view factor.

$$T_{\mathrm{s}} = 7.1 - 4.7 \times \psi_{\mathrm{sky}} \qquad \text{eq 3.3}$$

In her later research [Eliasson[10] (1996)], she concluded that surface temperature was affected by the sky view factor but not air temperature. Goh and Chang[59] (1999) investigated the relationship of maximum and minimum air temperature difference ($\Delta T_{\mathrm{a,max}}$) in estates with respect to median weighted canyon Height to Width ratios ($^{H}/_{W_{\mathrm{median}}}$)in Singapore. The relationship is shown in equation 3.4

$$\Delta T_{\mathrm{a,max}} = 0.952\ {}^{H}/_{W_{\mathrm{median}}} - 0.021 \qquad \text{eq 3.4}$$

They compared the result with Oke's[56] by applying a logarithmic fit, and their model was significant at 5% confidence level. Santos *et al.,*[60] (2003) showed the relationship of air temperature (T_a) as SVF (ψ_{sky}) in equation 3.5.

$$T_a = 27.75 - 2.56 \times \psi_{sky} \quad \text{eq 3.5}$$

Unger[61] (2004) used a new approach by dividing a city into small areas. The relationship of air temperature difference with SVF was investigated separately in each small area before joining together. Equation 3.6 summarises the finding where $\Delta T_{a,yea}$ is the air temperature difference and ψ_{sky} is the sky view factor.

$$\Delta T_{a,yea} = 5.90 - 4.620 \times \psi_{sky} \quad \text{eq 3.6}$$

It can be seen from previous research that urban geometry seems to be one of the factors that determines the urban heat island intensity. Most of the literature shows a negative linear relationship between urban geometry (either represented by SVF or H/W ratio) and heat island intensity but the relationships are different in the linear parameters. This variation is caused by the size of the city, i.e. the extent of building mass. As the equations cited in the literature are for different cities and the conditions of the measurements not always clear, no single equation is likely be applicable in a general way. It is for this reason that the relationship between SVF and urban heat island intensity in Manchester has to be investigated.

Apart from urban geometry, the type of land use also plays an important role in the formation of urban heat island. Land with green cover tends to lose heat quicker via evapotranspiration. Eumorfopoulou and Kontoleon (2009)[62] performed experiments on two buildings to compare the thermal behaviour of a bare wall and a plant-covered wall. Their results indicated a lower temperature on a plant-covered wall compared with a bare wall. Jusuf *et al.,*[63] (2007) investigated the different land use types which contributed to the most significant increase in ambient temperature in Singapore.

Their result indicated that different land usage would influence the urban ambient temperature. However, the sequence of land use type affecting ambient temperature was different in day time when compared with night time. S Gill *et al.,*[64] (2007) used an energy balance model and a surface runoff model to predict the influence of green roofs on surface temperature. Her results suggested that surface temperature could be kept the same as the baseline for 1961-1990 if 10% green areas were added to high residential area. However, a reduction of 10% in green roofs in the same area might result an increase of 7^{o}C to 8.2^{o}C surface temperature in 2080s under high emission case. Eliasson *et al.,* (2003)[65] found that the type of surface cover also had an impact on the local air temperature variation. Golany[66] (1996) also pointed out that there is a correlation between the urban morphology and the climate. Upmanis *et al.,*[67] (1998) and Upmanis and Chen[68] (1999) performed research in urban parks in Sweden. Their result indicated the existence of urban parks also had an effect on the air temperature of the surrounding built up areas. Bottyan *et al.,*[69] (2005) analyzed the digital satellite image with the measured weather data and concluded that there was a linear relationship between the urban heat island intensity with built-up ratio (how much city is built up) and its sub-urban extensions.

Taha[70] (1997) analysed field monitoring data and meteorological simulation and concluded that near surface climate could be changed by modifying the surface albedo and surface vegetation. Giridharan *et al.,*[71] (2004) also performed measurements to investigate the influence of surface albedo, sky view factor and height to floor area ratio to urban heat island. All factors were found to contribute to the urban heat island.

Anthropogenic heat is another source of urban heat island formation. Heat released from vehicles and building plants would promote the heat island effect if it cannot be

dissipated quickly due to the urban geometry as mentioned earlier. Hamilton *et al.,*[72] (2009) investigated the effect of anthropogenic heat emission in London on the local climate. They used four urban environmental models to represent different urban densities in London, to compare the net shortwave radiation and anthropogenic heat emission. Their results indicated that the total heat emission from buildings was about 3 to 25 times greater than incident solar radiation in winter and 0.04 to 0.4 times greater in summer depending on the urban density form. Smith *et al.,* (2009)[73] developed a model to estimate anthropogenic heat fluxes in the Manchester area. The model indicated a 23Wm^{-2} of anthropogenic heat flux in Manchester city centre compared to the average value of 6.12Wm^{-2} over the whole of Greater Manchester.

Wind and cloud can also affect the formation of urban heat island. Heat energy could be dissipated at a quicker rate from urban canyon if strong wind is present. On the other hand, cloud cover in rural area could reduce the removal of heat by reducing the long wave irradiation from earth to sky. Morris *et al.*[30]*,* (2001) found in their research that the urban heat island intensity was inversely proportional to about the fourth root of both wind speed and cloud cover amount. Eliasson[10] (1996) used meteorological data obtained from the monitoring stations in Sweden to analyze the influence of wind effect and cloud cover to the intra-urban air temperature. Her result showed that urban heat island intensity decreased with increasing wind speed and cloud cover.

Research was also carried out to investigate the relation between UHI intensity and altitude of city. Tereshchenko and Filonov[74] (2001) compared heat island studies from two different cities at different altitudes and concluded that the occurrence of urban heat island was not related to the latitude or altitude of a city.

The literature mentioned above shows how the different factors affect the formation of urban heat island or heat island intensity. However, it was not easy to determine which factor contributes the most toward the heat island. There was no large scale temperature monitoring work performed before in the Manchester area. This piece of research could fill the gap.

3.4 Literature review on energy exchange models

Solar energy reaches the earth as short wave radiation during the day. Part of this solar energy is absorbed by the earth's surface and building envelopes. The rest of the solar energy is reflected to the atmosphere. Some of this reflected energy would be reflected downward as long wave radiation by the cloud. At night-time, there is no incoming short wave radiation, however, heat energy absorbed by the earth and building during day is released as long wave radiation to the "cold" sky. The difference in thermal properties and canyon geometry of urban and rural areas may result in a difference in the heat releasing process contributing to the urban heat island effect[75]. Apart from the thermal properties and canyon geometry there were other factors such as anthropogenic heat and evapotranspiration which affects the formation of the urban heat island as mentioned by Oke[56] (1981). Equation 3.7 shows the basic energy balance concept used by most models. Solar energy from the sun (Q_s) is absorbed by the slab surface, αQ_s. Some of this is absorbed into the mass of the slab (Q_{slab}), with long wave radiation emitted from the slab (Q_l), added to which there is heat loss from the slab due to advection and convection (Q_{ac}), and if the surface is wet or has vegetation, evapotranspiration (Q_{ev}). There is also anthropogenic heat gain (Q_a) from human activities, especially road traffic and buildings. These are contained in the below equation. There are also many complex equations to establish these

individual terms in this equation.

$$\alpha Q_s + Q_a = Q_{slab} + Q_l + Q_{as} + Q_{ev} \quad \text{eq. 3.7}$$

Where

Q_s = Horizontal global solar irradiance [W]

Q_{slab} = Heat into the slab [W]

Q_l = Long wave irradiance emitted from slab surface [W]

Q_{ac} = Convective heat loss to the air above slab [W]

Q_{ev} = Heat release from evapotranspiration [W]

Q_a = Anthropogenic Heat [W]

α = Absorption of solar irradiance into the slab

Kolokotroni *et al.*[76], (2010) mentioned four types of models in her researches: Climatology models, Empirical models, Computational fluid dynamic (CFD) models and statistical models. Climatology model is usually of meso-scale, they will not be considered in this thesis because they cannot be used to reflect local micro climate. CFD models will also not be considered in this thesis because detailed air velocities and directions are required over small gridded volumes. These measurements and details are not available for Greater Manchester. Empirical energy balance models, artificial neural network (ANN) models and statistical models are most suitable for the work described in this thesis and these will be discussed.

3.4.1 Artificial neural network (ANN) model

Artificial neural network analysis consists of different elements (neurons) which are

interlinked with each other. This method was considered appropriate for UHI research to analyse the relationship between each causal factors of UHI effect that maybe complicated and non linear[76]. Santamouris *et al.,*[77] (1999) developed a multiple neural network model based on back propagation procedure to estimate the air temperature data obtained from four urban measurement stations on an hourly basis. The result of Santamouris's research indicated the neural network model they developed can predict air temperature reasonably accurately. Kolokotroni *et al.,* [78] (2009) and Kolokotroni *et al.,*[76] (2010) also used a back propagation artificial neural network model to predict hourly air temperature in London. The simulation result from the model matched with the measured air temperature. Artificial neural network technique was also used by Gobakis *et al.*[79], (2011) to predict the air temperature in Athens Greece. However ANNs are effectively "black boxes" that fit parameters to the data by training the neural pathways but not providing any explicit correlations or equations. Also the ANNs models for one city such as Athens, having been trained on Athens data would not provide output for Manchester without a lot more training and setting up. It was felt that the explicit equations and correlations related to the underlying physics or the statistical and empirical models would be more suited to this work.

3.4.2 Statistical models

Statistical models using statistical packages such as Statistical Package for Social Science (SPSS) have also been developed to investigate the UHI effect. Giridharan and Kolokotroni[43] (2009) and Kolokotroni and Giridharan[76] (2010) used statistical approaches to investigate the relationships between urban heat island intensity and different factors in London for both summer and winter. In their research, each

weather parameter was divided into three categories. For example, wind speed was divided into below $10ms^{-1}$, below $5ms^{-1}$ and below $2.5ms^{-1}$. Cloud cover levels were divided into clear sky, partially cloudy and cloudy. Other weather parameter could be controlled using this division method. However, the total number of data set for each analysis is reduced. This may end up with a poor significance level on the results. The result of Kolokotroni and Giridharan[42] (2008) gave poor significances (significant level larger than 0.05) which suggest that the grouping of data could have been better. Watkins[44] (2002) also used basic statistical methods for his London analysis but primarily relied on individual correlations between parameters. Statistical model should be more accurate when there is a large amount of data available because it allows for better control of key variables.

3.4.3 Empirical energy balance model

Kanda[9] (2007) had reviewed the urban heat island publications in the past decade. He classified urban canyon model into two categories. The first one was to make use of resistance network analogy [Masson[80] (2000) Masson *et al.* [81], (2002); Arnfield[82] (2000); Kusaka *et al.,*[83] (2001); Kanda *et al.,*[84] (2005)]. Resistance is the inverse of the conductance used for U-values and makes heat transfer analogous to an electrical circuit. The other one was the addition of sink/source term to the original energy equation [Uno *et al.,*[85] (1989); Ashie *et al.,*[86] (1999); Vu *et al.,*[87,88] (1999) (2002); Martilli[89] (2003); Tanimoto *et al.,*[90] (2004); Kondo *et al.,*[91] (2005)]. In order to find a suitable model which can be used to modify weather data for engineering used, the model itself must be simple enough. Therefore, only simple resistance energy models will be reviewed. Grimmond *et al.*[92,93] (2010) (2011) investigated 33 energy balance models and concluded that no model performs perfectly in all heat fluxes. A canyon

scale dynamic thermal modelling software[94] was also developed in another EPSRC funded project[95] named "The development of a Local Urban Climate and its application to the Intelligent Development of cities (LUCID)" to investigate the surface / air temperature and heat fluxes of building in a canyon. In order to find a heat island model for engineering usage (the main objective of this project), the model itself has to be simple enough. Therefore, only simple resistance network analogy model will be looked at in details in this section. Table 3-1 shows some of these models

Table 3-1 shows some of these models.

Models	Published year	Canyon included
Oke's Hardware model[56]	1981	Yes
Tso's Model[96,97]	1990-1991	No
Johnson's SHIM model[98,75]	1991	Yes
Mills Model[99]	1993	Yes
Masson's TBE model[80,81]	2000	Yes
Kusaka's Single-layer Urban Canopy model[83]	2001	Yes
Erell's CAT Model[100]	2006	Yes

Table 3-1 A list of energy balance models

3.4.1 Oke's canyon model

One of the earliest energy balance models developed to simulate the urban canyon effect was the "urban" model developed by Oke[56] (1981). This urban model (shown in below figure 3.2) was a hardware model built with polystyrene, plywood and

polyethylene film.

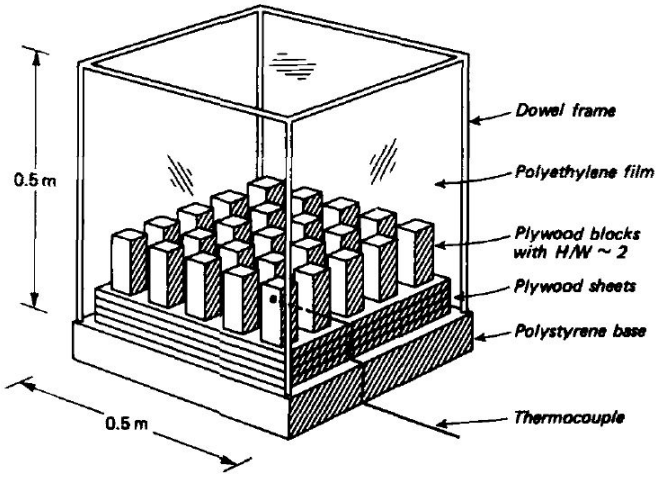

Figure 3.2 Oke's urban model[56]

A rural model was also created in a similar way with a greater number of plywood sheets but fewer plywood blocks to ensure both rural and urban models had the same volume of the same construction material. Different height to width ratio had been used in the model to simulate different street canyon. Oke[56] (1981) intended to use these models to look at passive radiative cooling rates after sunset between urban and rural landscapes in a cloudless and calm night. The models were left in a room at a warmer temperature (20^{o}C) until equilibrium was reached and then moved into the cold chamber to observe the rate of cooling. The results of the simulation were also compared with actual data obtained from field observation as validation.

The hardware model developed by Oke clearly demonstrated the difference in passive radiative cooling effect after sunset between urban and rural condition in a clear and calm night. Nevertheless there were limitations in this model. Firstly, the models were left in a cold room with a constant cooler temperature but the actual air temperature varies after sun-set. The cooling rates of the landscapes are expected to vary. Secondly, this model only estimated the cooling effect in a calm and clear night. Although the

result indicated a nice relation between the heat island intensity and the urban geometry, there would not be many clear and calm nights in the real world. Finally this model was not practical. It was a hardware model. A new model would need to be built every time when a specific street canyon is simulated.

3.4.2 Tso's Model

Gill[101] (2009) and Whitford[102] (2001) examined a number of models for use in the ASCCUE[16] project and found that the Tso model[96,97] was the most appropriate. This was also used in the SCORCHIO[17] project although a limited empirical statistical model [Smith[73] (2009)] primarily related to distance from the city centre and morphology was also used. However, the Tso model was developed for Kuala Lumpur in Malaysia and adjustments had to be made for Manchester. It used a clear sky solar model and not variable solar data that is available in the current work. Tso[96,97] (1990, 1991) used the basic energy balance equation (equation 3.7) The model has six assumptions as follow:

1. No horizontal transfer or movement of meteorological parameters within the model
2. Turbulent diffusivities for water vapour and heat were assumed to be given by the near-neutral value for momentum.
3. The turbulent fluxes of water vapour and heat in the surface boundary layer were assumed to be stable.
4. All wind speed, specific humidity and temperature were assumed to be constant at the level of surface boundary layer.
5. A unique roughness length was assumed over the urban canopy.

6. Anthropogenic heat sources were assumed to be zero in the model.

All these energy balance equations were linearised to produce simultaneous differential equations which can be solved eventually. The concept of the model was to use the surface temperature of an area to calculate the surface balance (Gill[101] 2009). Whitford *et al.,*[103] (2001) further developed and customized the model by inputting all the simultaneous energy balance equations into Mathematica.

This model divided a day into three periods: Daytime, night time and pre-dawn. By starting with an estimated air and soil temperature, both soil and surface temperature at the end of each period were found and used as the starting values of the next period. A convergence test will start to perform at the end of the pre-dawn period by comparing the temperatures in this period with the same value of the previous day. The output of the model includes the soil and surface temperature in terms of a graph against time for a day. It also states the maximum and minimum temperature for the corresponding time.

Sensitivity tests were performed on two parameters of this model, the evaporating fraction and the building mass per land. These two parameters were selected because Gill S[101] (2009) indicated that they are the most dominant factors. The result of the sensitivity tests indicated the surface temperature varies when either parameter changes. However, it was also found that there is no input parameter to indicate the canyon geometry. In another words, the model would be capable of simulating the effect due to land use and mass of concrete, but not the canyon effect. Therefore, it is not an ideal model for this project.

3.4.3 SHIM model

The Surface Heat Island Model (SHIM) was first mentioned by Johnson G.[98] (1991). He suggested two approaches: the partial differential equation approach and the force-restore method. Fully implementation can be performed by solving partial differential equation. However Johnson simplified the model by replacing the partial differential equation on different surfaces with ordinary differential equations. The model took account of the heat conduction through different vertical and horizontal surfaces as well as radiative transfer between sky and all these surfaces. Johnson validated his model with field data and concluded that the model was suitable for the analysis of urban heat island under 'ideal' night condition.

Oke[75] (1991) used this model to find out the relative importance of different causes of urban heat island including urban geometry, thermal property, combined effect of urban geometry and thermal property, anthropogenic heat and surface emissivity. His findings included:

1. Street canyon geometry had a crucial effect on long-wave heat lost in a canyon which leads towards the formation of urban heat island.
2. The thermal admittance differences between urban and rural alone can form a heat island
3. Anthropogenic heat released from building with poor wall insulation under cold weather can match the influence of urban geometry and thermal admittance on heat island.

Although SHIM model could predict the importance for the different causes of urban heat island, the output of the model was surface temperature instead of air temperature.

Furthermore, the model had no wind data input. The model could only be used in 'ideal' night conditions which might not be realistic. This model therefore would not be practical for engineer to use to estimate heat island effect based on existing weather data.

3.4.4 Mills' Model

Mills[99] (1993) created his model based on two sub-models: the urban canyon windfield and the urban canyon energy budget. He based the model on a concept that a traversal air flowing towards a canyon would induce a vortex in the canyon (see figure 3.4). When combined with the energy budget model, the effect of advection could be brought into the model. Mills also performed sensitivity tests for his model. The most important finding of his model was the stability of the energy balance between urban canopy layer and urban boundary layer. The urban canopy layer (also called urban canyon layer) refers to the area underneath the average height of the buildings in the canyon while the urban boundary layer (above the canopy layer) refers to the boundary in the troposphere where the wind is unaffected by the urban, built environment. The cross layer energy balance did not have significant changes even when a lot of changes had been made to the input parameters at urban canopy layer.

Compared with SHIM model, Mills's model could be widely used because it was not limited to clear and calm night condition. However, this model was not suitable for this project because it focuses on the energy change between the canopy layer and the boundary layer and needs more information and data than that from basic

meteorological data that was going to be available in this project. Wind speed and direction were only available at three sites around Greater Manchester and none in the city centre. Also detailed geometries of the canyons would not be available for detailed turbulence analysis.

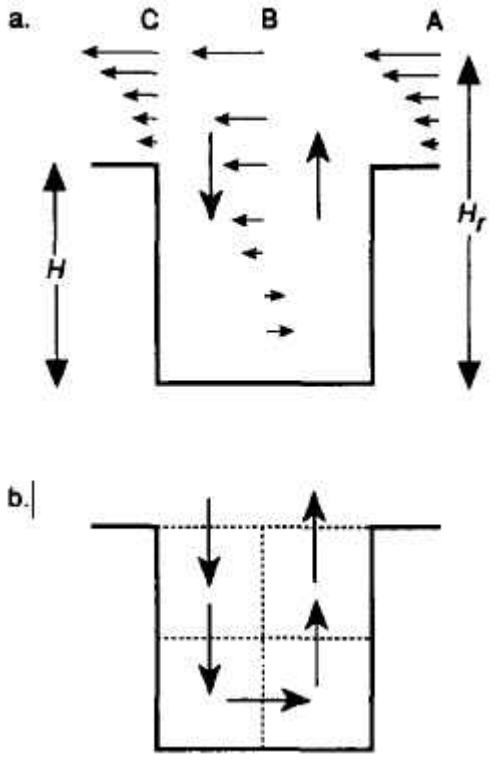

Figure 3.3 Air flow towards canyon induce a vortex in the canyon[99]

3.4.5 Masson's TEB model

Masson[80] (2000) used a Town Energy Budget (TEB) scheme model to simulate the turbulent heat and ground fluxes with relation to general urban canyon. City geometry was required in the model so that the energy exchanges between cities and the atmosphere can be represented. Masson concluded that the TEB model behaved correctly with what was known from the urban climatology. Masson *et al.,*[81] (2002)

used the TEB scheme on two cities: Mexico City and Vancouver. The result indicated that surface temperature, partitioning between turbulent and storage heat fluxes and net radiation were all correctly simulated in both sites.

TEB model is a meso-scale model, instead of looking at the energy balance of a canyon, it focused on grid size of a few hundred meters therefore it cannot be used to represent canyon climate and so was not suitable for this project.

3.4.6 Kusaka's Single-layer Urban Canopy model

Kusaka *et al,*[83]. (2000) developed a single-layer urban canopy model which included the shadowing from building and radiation reflection. The model can be used to find out surface temperature and heat fluxes from roof, wall and road. The results from their model were compared with the observations and they agreed closely. However, this mode is a column model, which means it can only focus on a single block, although surface temperature and heat fluxes from all surface can be calculated from the model, there is no interaction between different blocks. In other words, this model can only used to simulate one building, but not building inside a canyon.

3.4.7 Erell's model

Erell and Williamson[100] (2006) developed a canyon temperature model based on energy balance equations. Weather data obtained from nearby metrological station can be used in the model to predict the canyon effect in a canyon with similar meso-scale climate conditions. The model simulates the urban canyon effect on radiant exchange, energy stored in ground and building surfaces, moisture level through latent heat flux,

sensible heat flux from each surface and the air flow in street based on the wind above roof. Model calibration was performed and after the validation, the CAT model indicated that the model can make air temperature prediction accurately in the canyon in Adelaide Australia.

Considering the nature of the model, it should be capable of being combined with UKCP weather data to reflect the canyon effect. However, there are two disadvantages. Firstly the weather data used in the model should have a similar meso-scale climate condition as the canyon. The weather data available for Greater Manchester is about 15 miles from Manchester city centre. The local city centre climate could be a lot different from the reference point. Secondly, there is no morphological input to the model as it was assumed to be the same as the source weather station. Vegetation is one of the most important factors affecting the urban heat island and therefore, this model cannot be used for the purpose of this project. Kolokotroni *et al.,*[78] (2009) used CAT model to simulate the heat island effect in London. However, it was found that the model behaves differently from its original usage in Australia. It was believed that this is due to the longer period of overcastting sky in London. Manchester has even more overcast sky than London. Therefore, this model is considered as not suitable for use in this project.

One of the hypotheses in this project was to demonstrate the urban heat island effect with a simple model for building services engineering usage. Kershaw *et al.*[104]*,* (2010) developed a mechanism to add in the urban heat island effect on to UKCP data. They used the urban factor (urbanity from UKCP data) of a particular grid and its nearby grids to determine an urban area. Air temperatures were then calculated for concentric circles centred at the urban area with different radius. This is a very brief method of

adding in the urban heat island effect onto UKCP data. The temperature adjustment was based on linear relation. Canyon effect due to the canyon geometry as well as the effect of vegetation cannot be reflected. Therefore, this is not a good method to be adopted by engineers.

After reviewing some of the existing models, none of them could fulfill the main requirements of being relatively easy to apply and for the input parameters to be readily available. It is for this reason that a new canyon model would be developed in this project.

CHAPTER 4

Methodology

CHAPTER 4 Methodology

4.1 Introduction

In order to investigate the urban heat island effect in Greater Manchester, it is essential to monitor and record the temperature around the city. Near ground (up to a few meters above ground) surface temperature was logged in this project instead of ground surface temperature. Air temperatures were recorded over Greater Manchester using different weather monitoring stations. Other weather parameters such as cloud level, wind speed, wind direction, rainfall and air temperatures could be obtained from Met Office ground observation station around Manchester (Woodford, Ringway and Hulme Library). These data could be incorporated into a heat canyon model to calculate the air/surface temperature in an urban canyon. These results could be validated by comparing with the actual air temperature measured from seven canyons in the Manchester city centre. After validation, this canyon model could be used by engineers during design to estimate the heat island effect around Manchester. In order to monitor and record air temperature, a suitable monitoring method should be selected. In this chapter, the selection of monitoring method and the location of monitoring stations will be discussed. The selection of sensor-loggers and the associate calibrations as well as data processing technique will be discussed in the next chapter.

4.2 Selection of monitoring methods

In order to analyse the urban heat island effect, the air temperature distribution over the whole city will need to observed and recorded. Nevertheless there are different

methods of doing this.

4.2.1 Satellite image

Satellite image is one of the easiest ways to observe the surface temperature distribution over a city. The temperature distribution can be seen directly from the thermal image. However, the cost of obtaining satellite image from different sources may be very expensive. Also this gives the surface radiant temperature, primarily of roofs and roads, not the dry bulb air temperature which is usually significantly different.

4.2.2 Ground / Air Transect

Temperature measuring and logging device can be mounted on cars or flights to perform measurements around the city. The cost for ground transect (by car) can be quite cheap, however, a certain number of personnel is required at the same time to perform a transect measurement. This had been used in the SCORCHIO[17] project but the results were limited.

4.2.3 Fixed point monitoring

Fixed monitoring stations can be set at different locations across the city to log temperature or other weather parameters. This is the most comprehensive way of monitoring urban heat island effect because the cost of the whole monitoring activity can be controlled by controlling the number of monitoring stations.

A permanent fixed point measurement method was therefore adopted for this project to measure comprehensively the urban heat island in Greater Manchester.

4.3 Selection of monitoring locations

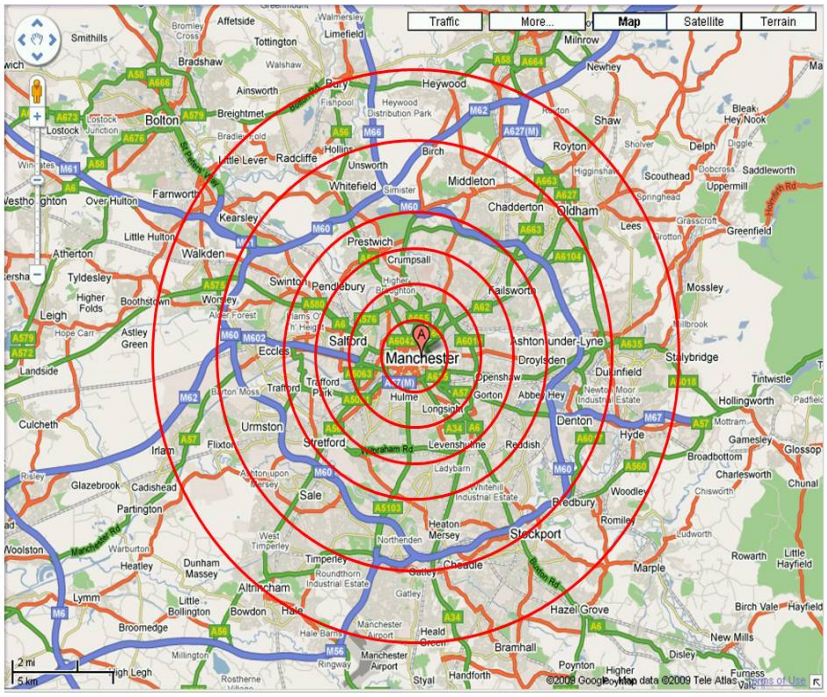

Figure 4.1 Radial distance away from Manchester city centre

Eight radial transects centred on Piccadilly Gardens, considered to be the centre of Manchester, were selected with monitoring stations positioned at one mile spacing for the first four miles and two miles apart thereafter. Figure 4.1 shows the radial directions away from the city centre. All stations were placed at four metres above ground level on street lampposts facing to the pedestrian pavement. Figure 4.2 shows all the sensor-loggers installed in Greater Manchester. There are 11 monitoring stations located inside different street canyons of central Manchester area. These stations are very important because the result from these stations can be used to investigate the canyon effect which cannot be found outside the city centre.

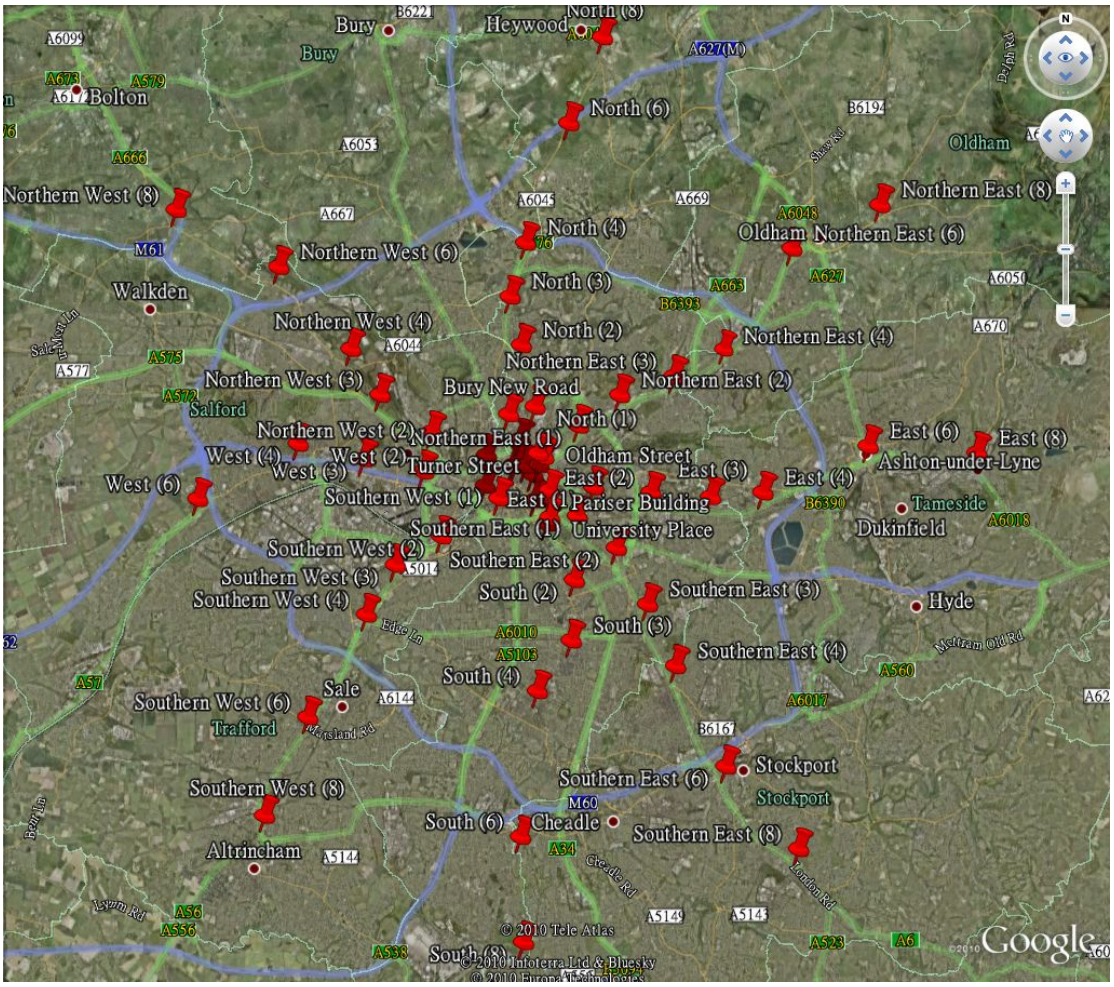

Figure 4.2 All sensor-logger locations in Greater Manchester

Eight different local councils were involved in this project: Manchester, Rochdale, Oldham, Tameside, Stockport, Trafford, Salford and Bolton. Each of these councils was contacted separately for erecting the monitoring stations. Some of the councils had their own management team for the street lighting while others would have a contractor to look after the lamp posts in their area. The first step of setting up the monitoring station is to identify the suitable lamp posts. Some of the lampposts (with concrete column) were usually not allowed to have anything attached to them. Once all the lamp posts were identified in an area by the author, the lamp post numbers or locations were submitted to the council for approval. Meanwhile, one single contractor was selected for the installation process for the whole project so that they

can have all documents (such as method statement, H&S requirement etc.) ready submitted to the council. Once approval was granted in written form, the contractor could start to attach all the monitoring stations. This was in some cases a long procedure and hence the sensor-loggers were put in at different times. The central Manchester city centre ones being the first. All the work above took about a year to complete and was all done by the author.

4.4 Conclusion

Different temperature monitoring methods as well as monitoring locations were discussed and sites around Greater Manchester decided, including the use of canyon data (which had not been done specifically in London by Watkins[44] (2002) or LUCID[95] project) in the chapter. The selection and calibration of temperature sensor-logger is discussed in the next chapter. The procedures of data collection and data processing are also discussed in the next chapter.

CHAPTER 5

Temperature sensor-logger and Data collection

CHAPTER 5 Temperature sensor-logger and data collection

5.1 Introduction

Temperature monitoring methods and the location of monitoring stations was discussed in the last chapter. In this chapter, the selection of temperature sensor-loggers will be discussed. In order to measure air temperature accurately, a radiation shield was designed and fabricated by the author to accommodate the temperature sensor-logger. A radiation test was performed on this radiation shield to investigate its performance. Calibrations were also performed on all temperature sensor-loggers before installation in field. All this work was published in a paper[105] however more detailed content will be discussed in this chapter. Finally, the data collection and processing procedure will also be discussed in this chapter.

5.2 Selection of temperature sensor-logger

In order to perform the measurement of the urban heat island in Greater Manchester, a suitable temperature sensor had to be selected. Three temperature sensors were compared: Rotronic, Tinytag and I-button (as shown in figure 5.1). The Rotronic[106] has dimensions of 128mm (H) x 109mm (W) x 42mm (D), It is capable of recording temperatures from -30^{o}C to 70^{o}C with a minimum logging interval of five seconds. Tinytag[107] has a dimension of 34mm (H) x 51mm (W) x 80mm (D). It is capable of recording temperatures from -40^{o}C to 80^{o}C at minimum logging interval of one second. I-button[108] has a radius of 9 mm and height of 6mm. It can measure temperatures from -20^{o}C to 85^{o}C with minimum logging interval of one second.

Figure 5.1 Rotronic, Tinytag and I-button temperature sensor-loggers

The response time for a step change was found by experiment. Response time was important because the temperature data collected would be used to compare with Met office data for the UHI intensity calculation. Readings from a sensor-logger with slow response time might not be accurate. Three sensor-loggers were placed inside the laboratory HVAC unit as well as an alcohol thermometer. The laboratory HVAC unit consisted of an air duct at 600mm (W) x 600mm (H) x 2000mm (L), a variable speed centrifugal fan, 3 heating coils and one DX cooling coil. Due to the lack of a certified device, the alcohol thermometer was used as the reference because it had been calibrated before by a technician using boiling water and melting ice. All sensors were started logging temperatures at their minimum logging interval for an accurate result. The fan inside the laboratory HVAC unit was switched on for 20 minutes to allow stabilisation of temperatures inside the unit. Two 1 kW heating coils were then switched on afterwards whilst the fan was still on. Temperature readings from the

thermometer were recorded every minute. The two heating coils were then switched off after two hours and the sensors were left to cool down. Figure 5.2 shows the temperature variation. It can be seen that Rotronic had the best response time for the step change in temperature. However, it would be impossible to use in large scale measurement for urban heat island due to its cost and size. It was also suggested that Tinytag and I-button should be further investigated. Finally, high resolution I-button was selected for the temperature measurement of this project due to its cost, size and flexibility. An experimental report can be found in Appendix A.

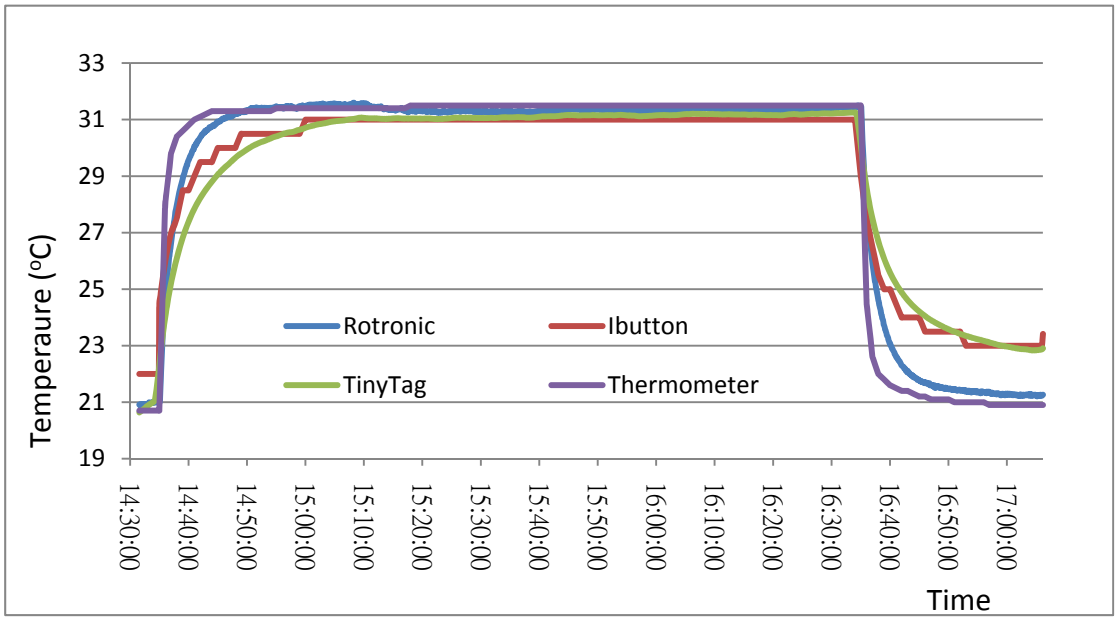

Figure 5.2 Temperature of three sensors against time response to a step change

5.3 Fabrication of radiation shield

5.3.1 Original design of radiation shield

The monitoring station consisted of a radiation shield bracket and a temperature sensor-logger. In order to obtain more accurate results, a radiation shield is required. The radiation shield was used to shelter the sensor from the rain and solar radiation. A sufficient ventilation rate should also be ensured to avoid accumulation of hot air

inside the shield. There was no readymade shield available in the market for this particular sensor-logger. Watkins *et al.,*[12] (2002) was approached first because similar temperature monitoring was performed in London before. However, the stainless steel shields were very expensive. Other radiation shields available in the market were also been investigated, nevertheless, they are either too expensive or not suitable to be attached on the street lamppost. Thus, a new radiation shield was designed and made.

A radiation shield consisted of ten 15cm diameter plastic plant saucers, three 200mm length of M6 studding (screw studding with 6mm diameter) and two pieces of aluminium with an additional aluminium arm. All materials in this radiation shield were corrosion proof. Figure 5.3 shows the prototype radiation shield. See appendix B for the design drawing of the radiation shield with dimensions.

Figure 5.3 Radiation shield prototype

In order to make a shield, all plastic plant saucers were drilled with difference size

holes as shown in appendix C to accommodate different sizes of studding. All studdings were cut to the appropriate sizes. A dome nut was then placed at one end of the studding with all three studdings placed through the rectangular aluminium plate. 10 saucers were stacked onto the studdings with two M10 nuts as spacers between each pair of saucers. The first two saucers from the top did not have the central hole to ensure that no rain could fall into the cavity below. The third saucer was fitted with a bent piece of M3 studding for the sensor-logger. The other saucers were drilled with a central hole to accommodate the sensor-logger with the hook. A triangular aluminium plate was fitted to the end of the shield to provide sufficient strength together with the top rectangular aluminium plate on the other end. All three studdings were secured at the bottom by double M6 nuts and "Loktite". A final curved piece of aluminium was fitted onto the rectangular aluminium on top to form a bracket to attach to a lighting column.

Figure 5.4 shows the telescopic rod with magnet on top used to place the sensor-logger hook into the shield at four metre. I-button sensor-loggers were attached to the hook using blue tack. Figure 5.5 shows a typical sensor-logger with hook which could be hung inside the radiation shield. The function of the "Z" shaped stainless steel was to increase the length of the whole structure. This could reduce the swing angle when there is a strong wind blowing to avoid dropping. A zinc coated washer was stuck to the bottom of the aluminium so that a magnet with a rod could be used to put it into the radiation shield.

Figure 5.4 Telescopic rod used to hang sensor-logger

Figure 5.5 Typical hook design with sensor-logger

12 radiation shields and sensor-loggers were placed around Manchester central areas. However, it was found that three sensors were missing after one month. It was believed that the weight of the hook was not heavy enough. When a strong wind was blowing through the radiation shield, the wind would be directed upwards due to the layout shape of the saucers. This generated a lift that is sufficient enough to unhook the sensor from the lamppost. In order to solve this problem, a new hook was designed with a longer hook length and heavier compared with the one used previously. Figure 5.6 shows the new hook design. Apart from the slight modification of the hook, a stainless steel gate was also added to the end of a studding (Figure 5.7). The gate can be opened or closed using the telescopic rod. With this modified design, the sensor-logger will be protected from impact even if it drops. It would remain inside the shield until the next data collection.

Figure 5.6 New designed hook

Figure 5.7 Gate added to the bottom of shield

5.3.2 Improved design of radiation shield

The radiation shield designed originally was introduced to other research projects for fixed point temperature monitoring. These applications included the case study temperature measurement of the SCORCHIO project done by the University of Manchester and the measurement of the urban heat island in Bristol and Bath areas to be performed by the University of Bath. However, due to the shortage of technician time and workshop equipment, the design of the shield had to be modified slightly to reduce the number of components for the shield. The manufacturing process for most of the components could also be done by other external engineering firms. A local engineering firm was approached however, later on it was found out that this engineering firm was already dissolved. The total time spent on manufacturing these extra radiation shields were therefore much longer than expected. A detailed specification has been written so that a third party could have a better idea of constructing the shield. A copy of this specification can be found in appendix D.

5.4 Radiation Test

In order to test the efficiency of the radiation shield, a calibration experiment was performed using two 60W desk lamps as heat sources. Although the wave spectrum from the bulb will be different from the sun, this is the only available source which can be used to simulate solar irradiance without additional cost. Figures 5.8-5.10 show the set-up of the experiment. Three sensor-loggers have been used in the experiment: one inside the shield, one outside the shield under the lamp and a one at the corner of the room measuring the room air temperature.

It was assumed that 95% of the energy used by the lamp is given out as heat. That is about 57W as heat energy for each lamp. 10% of the thermal energy was assumed to be absorbed by the lamp cover. Another 10% was assumed to be radiated to the desk surface and surroundings. The diameter of the saucers used was 15 cm which gives an area of 0.0177m^2. Therefore, only 80% of thermal energy went onto the shield.

The simulated solar power is about 2580W/m^2. Although this value is much stronger than the actual solar power, it was only used to maximize the effect in the result so that the difference of using the shield can be seen clearly. There were two conditions simulated: direct sunshine with wind and direct sunshine without wind. A laboratory HVAC unit was used to provide continuous room temperature wind at a reasonable wind speed (2.5ms^{-1}).

Figure 5.8 Experimental set-up close up

Figure 5.9 Experimental Set-up

Figure 5.10 Sensors at same level

Figure 5.11 shows the temperature variation of three sensors. The first hour of the experiment simulated the no wind condition. The fan of the HVAC unit was switched on at about 11:30am. The results indicated that the radiation shield can provide a stable condition for the sensor inside to measure the actual air temperature. The maximum difference occurred where there was no "wind", with a maximum temperature difference reaching up to 7^{o}C for the sensor inside and outside the shield. A full experimental report can be found in appendix E.

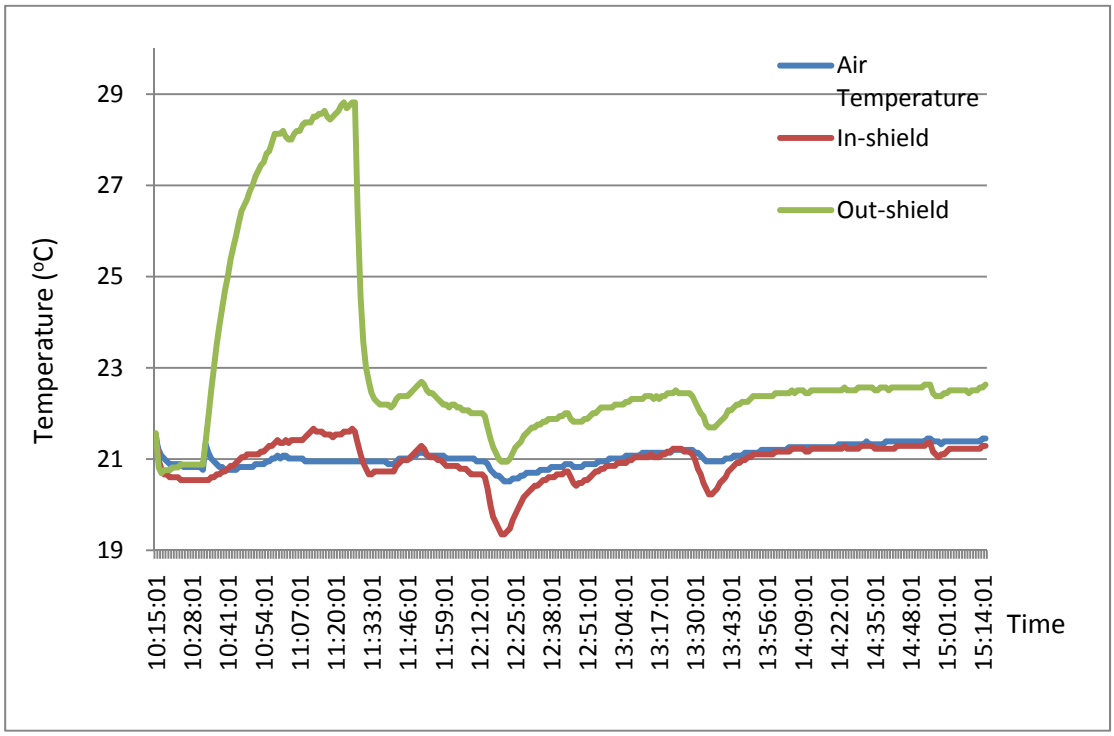

Figure 5.11 Temperature variations of three sensor-loggers inside and outside the radiation shield

5.5 Comparison between radiation shield and Stevenson screen

Further to the radiation test of the shield, another experiment was performed to compare the radiation shield with a small single louvred Stevenson Screen. The Stevenson screen used in this experiment has a length of 600mm, width of 300mm and height of 450mm. The Stevenson Screen was located on a balcony on the second floor. There was a West facing wall located about 1.2 metre east of the Stevenson screen. The Stevenson screen was placed on top of a shelf. The height of the Screen was about 1.2m above floor level. Figure 5.12 shows the location of the radiation shield as well as the orientation of the Stevenson screen. There were four sensor-loggers used in this experiment; two placed inside the Stevenson screen as shown in figure 5.13 whilst the other two were placed on the hook inside the radiation shield.

Figure 5.13 Orientation of Stevenson Screen and radiation shield (white arrow points South)

Figure 5.12 Sensor-logger locations inside Stevenson Screen

All sensor-loggers were logged at 5 minutes interval over a period of four days. The average values of two sensor-loggers inside the shield and Stevenson screen were calculated and compared.

Figure 5.14 shows the mean temperature variation of the sensor-loggers inside the shield compared with sensor-loggers inside the Stevenson screen. Table 5-1 tabulates the mean and standard deviation of the data from both sensor-loggers.

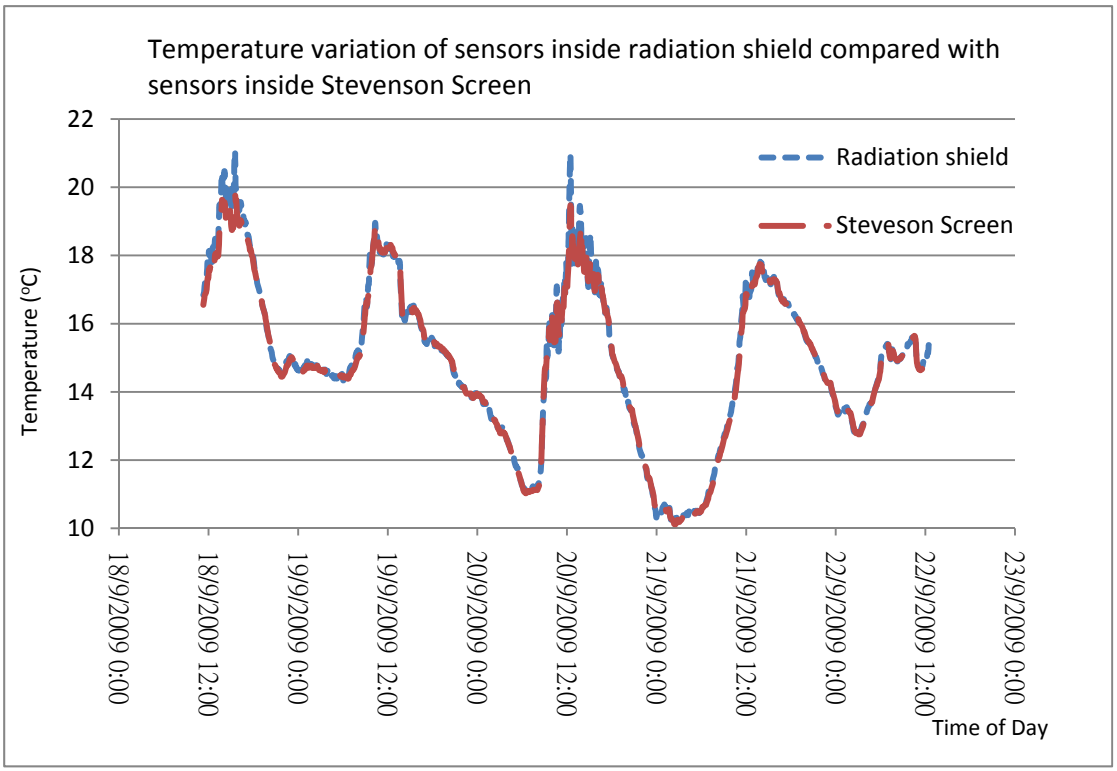

Figure 5.14 Temperature variations of sensor-loggers inside radiation shield compared with sensor-loggers inside Stevenson Screen

Sensor-logger	Mean (°C)	Standard Deviation (°C)
Stevenson Screen	14.86	2.30
Radiation Shield	14.92	2.37

Table 5-1 Means and standard deviations for temperature measured in Stevenson Screen and Radiation shield

The "Radiation shield" and "Stevenson screen" temperature were very similar. The mean temperature difference is about 0.06°C and the standard deviation difference is about 0.07°C. However, two maxima showed a difference of 1.5°C over a period of half an hour, recorded on two sunny afternoons. The temperature differences fluctuated considerably in the afternoon of 20/09/2009, from -0.5°C to +1.5°C, when there were significant solar irradiance. Furthermore, the weather in the afternoon of 22/9/2009 was cloudy with sunny spells. The result indicates a very close

performance of the radiation shield and Stevenson Screen, therefore, it can be concluded that the radiation shield is capable of sheltering the sensor from the rain and solar radiation similar to a Stevenson Screen.

5.6 Calibration of sensor-loggers

5.6.1 Calibration for 53 Sensor-loggers

In order to measure urban heat island intensity, the sensor-loggers needed to be accurately calibrated before installing in field. All sensors used in this project have been calibrated through two experiments. Both experimental reports can be found in appendix F & G respectively.

All 53 I-button temperature sensor-loggers were bought at the same time in Jan 2009. In order to simplify the calculation, each sensor was assumed to have the same error throughout the air temperature range. However there was no certified temperature logging device at that time. All sensor-loggers were placed in an oven at 30^{o}C for a night and their average temperature was found. The same experiment was performed three times with different sensor arrangements on a cardboard in the environmental chamber. The sensor-logger with the average temperature was then selected to be the reference sensor-logger. Figure 5.15 below shows the average temperatures of all 53 sensor-loggers, whilst No. 54 is the Rotronic sensor (the last bar in figure 5.15). Although Rotronic sensor has the fast response time, it can be seen that it is not as accurate as I-buttons.

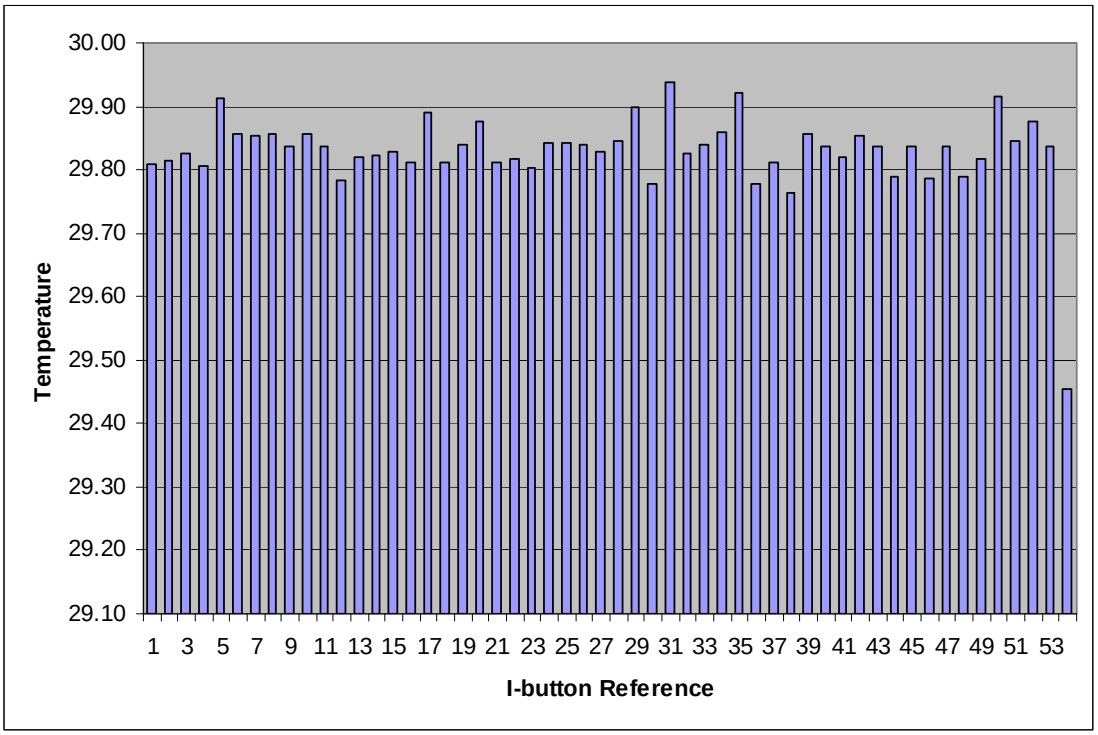

Figure 5.15 Average temperature of all 53 sensor-loggers

5.6.2 Calibration with certified sensor-logger

A calibrated sensor-logger, certified to standard EN 13005 and ISO 17025 was obtained later. The calibration experiment mentioned above was performed on the reference sensor-logger and the certified sensor-logger in the 30^{o}C oven. The calibration certification of the certified sensor-logger indicated a different error value at different test point. As a result, it was decided that the same calibration experiment in a colder (6^{o}C) environment is required to be repeated. The actual error of the reference sensor was then found using interpolation.

Table 5-2 shows the results. An average value of -0.154^{o}C was used as the adjustment for reference sensor-logger, and adjustment values for the other sensor-loggers based on this value.

	Difference	Mean
Difference at 30°C	0.026 °C	-0.154°C
Difference at 6°C	-0.333 °C	

Table 5-2 Difference of reference sensor-logger against certified sensor-logger

5.6.3 Calibration of additional sensor-loggers

Additional temperature sensor-loggers were purchased later to replace those sensor-loggers lost previously. These sensor-loggers were checked with the same warm and cold calibration tests.

10 sensor-loggers were bought and numbered from 54 to 63. The certified sensor-logger was labelled "A". All 10 sensor-loggers were placed in the environmental chamber with the certified sensor-logger at 30°C for several hours. After this warm test, all sensor-loggers were put inside a fridge with the same arrangement for cold test. However, there was a temperature difference of 1°C between individual sensor-loggers. This was believed to be as consequence of the insufficient air movement inside the refrigerator. The accuracy of the test was then improved by wrapping all sensor-loggers with four layers of aluminium foil. All sensor-loggers were now closely packed together whilst the aluminium foil provided quicker heat conduction between them to reduce the temperature gradient between the sensor-loggers. In order to further improve accuracy, the cold test experiment was performed three times to obtain an average value.

It can be seen from figures 5.16 and 5.17 that the maximum temperature difference between individual sensor-loggers dropped to about 0.13°C using the aluminium foil

wrapping. The mean temperature of each sensor-logger in both the warm and cold tests and the difference from the certified sensor-logger A could also be seen. The mean and standard deviations for both warm and cold tests are tabulated in table 5-3.

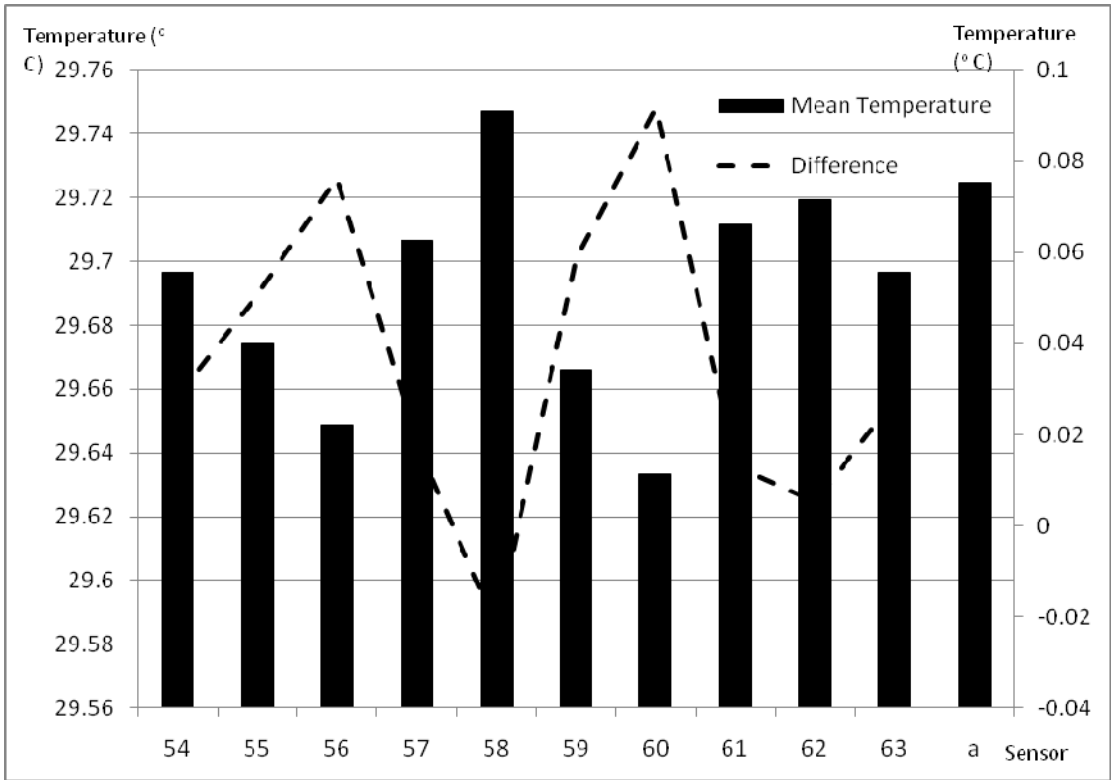

Figure 5.16 Average temperature against each sensor-logger at 30°C (Warm test)

Warm Test	Mean	29.693 °C
	Standard Deviation	0.034 °C
Cold Test	Mean	6.614°C
	Standard Deviation	0.021 °C

Table 5-3 Means and standard deviations for both the warm and cold tests

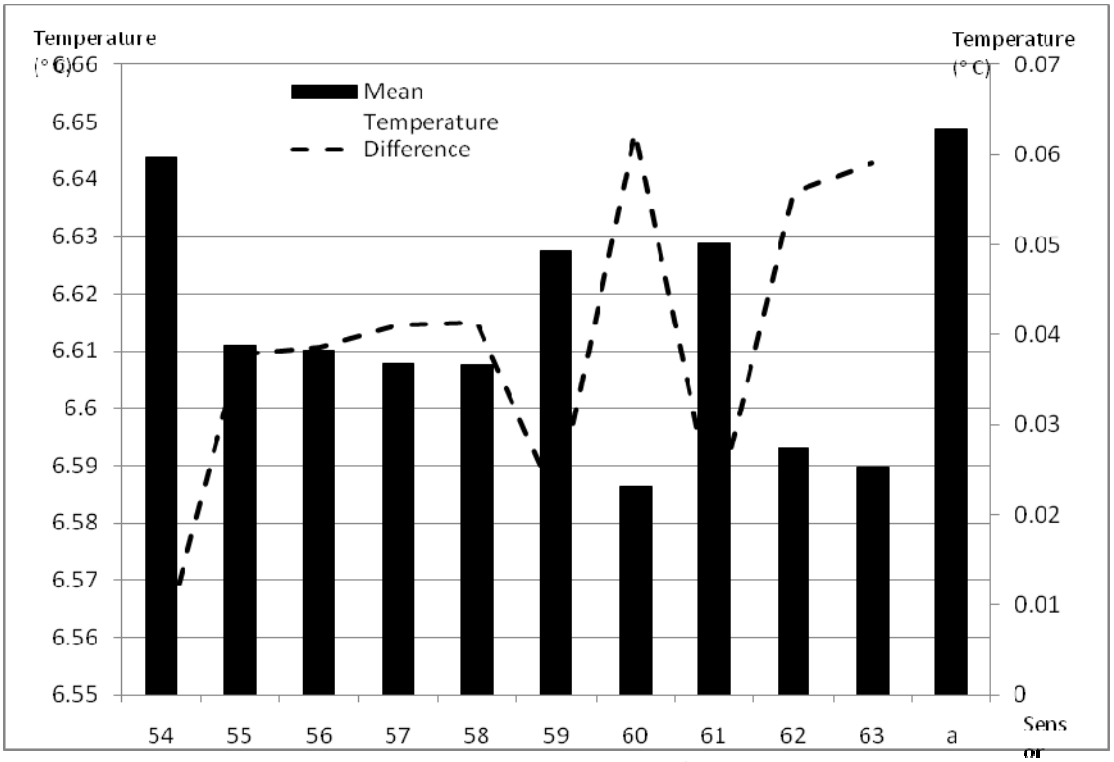

Figure 5.17 Average temperature against each sensor-logger at 6°C (Cold test)

5.7 Collection and organisation of Data

Data collection and processing was an essential part of this project. There was a lot of data collected in this project (1 Gb). An effective way of organizing the data could reduce the time for performing data analysis. These procedures are discussed in this chapter.

5.7.1 Data collection

The sensor-loggers used in this project had an internal memory of 8kB. According to the data provided by the manufacturer[108] the battery life is expected to last for three years when measuring at 30 minutes intervals. 30 minutes logging interval was used because it can give a better resolution for any time lag between different sensor-loggers. On another hand, the battery inside the sensor-logger will be

consumed a lot quicker with shorter logging intervals. A shorter logging interval also means more frequent data collection process which will be expensive and time consuming. Four types of data would be recorded: Date, time, temperature unit and temperature reading. Each sensor-logger is capable of storing three months data without being overwritten. Data would be collected from all sensor-loggers in two directions (out of eight directions where the sensor-loggers were located) for one data collection section takes about three hours to do. Five sections of data collection are therefore required every two months. Data collection was recommended to be performed on an overcast day. This is because precipitation or direct solar irradiance might reach the sensor-logger during data collection process and affect accuracy of the next temperature logging.

The data was collected during the weekend in the early mornings for all the city centre sensor-loggers and any off-peak time during the weekdays for other sensor-loggers to avoid traffic congestion. One and a half hour was usually required for collecting data from the 6 sensor-loggers in one radial direction. A laptop installed with software named “OnewireViewer” (downloaded from supplier’s website) was used to download the data. A user guideline for this software was produced by the author for this project so that others could understand the data collection procedure easily. A copy of this guideline is found in appendix H.

5.7.2 Data organisation

Raw data downloaded from the sensor-loggers was shown in a text file with four columns indicating date, time, temperature unit and temperature reading. These text

files were opened with Microsoft Excel. The “unit” column was removed because all readings from all sensor-loggers were preset to degrees centigrade. A master data sheet in Excel was created with individual worksheets to indicate the readings from every single sensor-logger. An example of the work sheet is shown in figure 5.18. An individual adjustment value was found from the calibration experiment for every single sensor-logger and this value was added onto the original measured temperature reading.

All sensor-loggers were set to synchronise with the clock (was set to GMT) on PC before their usage for the first time. No synchronisation would be done afterwards so that the time slot can always be the same on one sensor-logger. However, the sensor-loggers did not commence data collection simultaneously. In order to compare the temperature readings accurately, all readings were interpolated to start at the same 30 minutes interval.

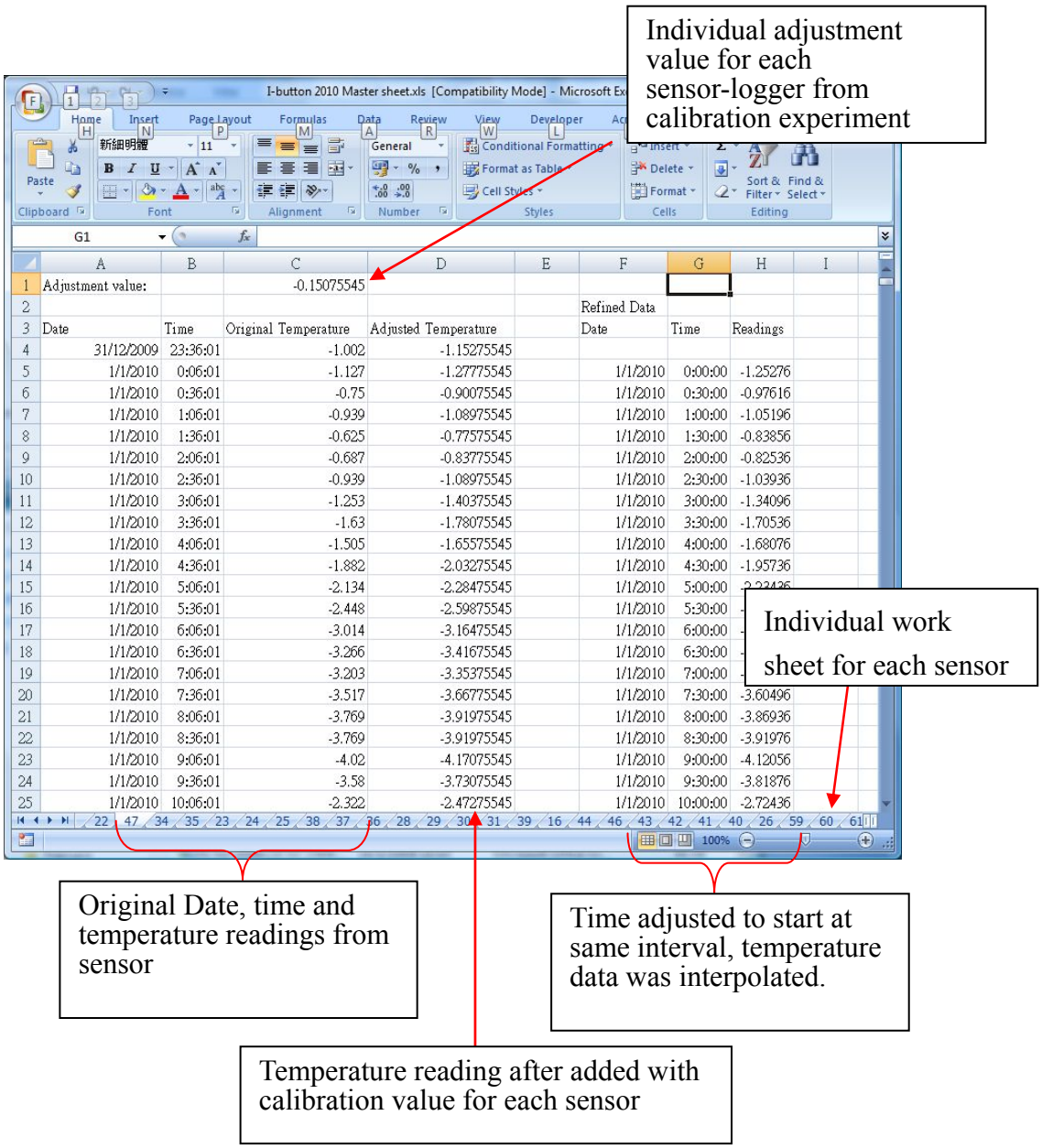

Figure 5.18 Data work sheet example

All interpolated temperature readings from the sensor-loggers were transferred to a separate work sheet as shown in figure 5.19. The location of each sensor-logger could also be found within this work sheet. Furthermore, weather data (see section 5.8 for more details) from other weather stations was added. Finally, urban heat island intensity of each point could be found by subtracting the simultaneous temperature reading from the rural reference point.

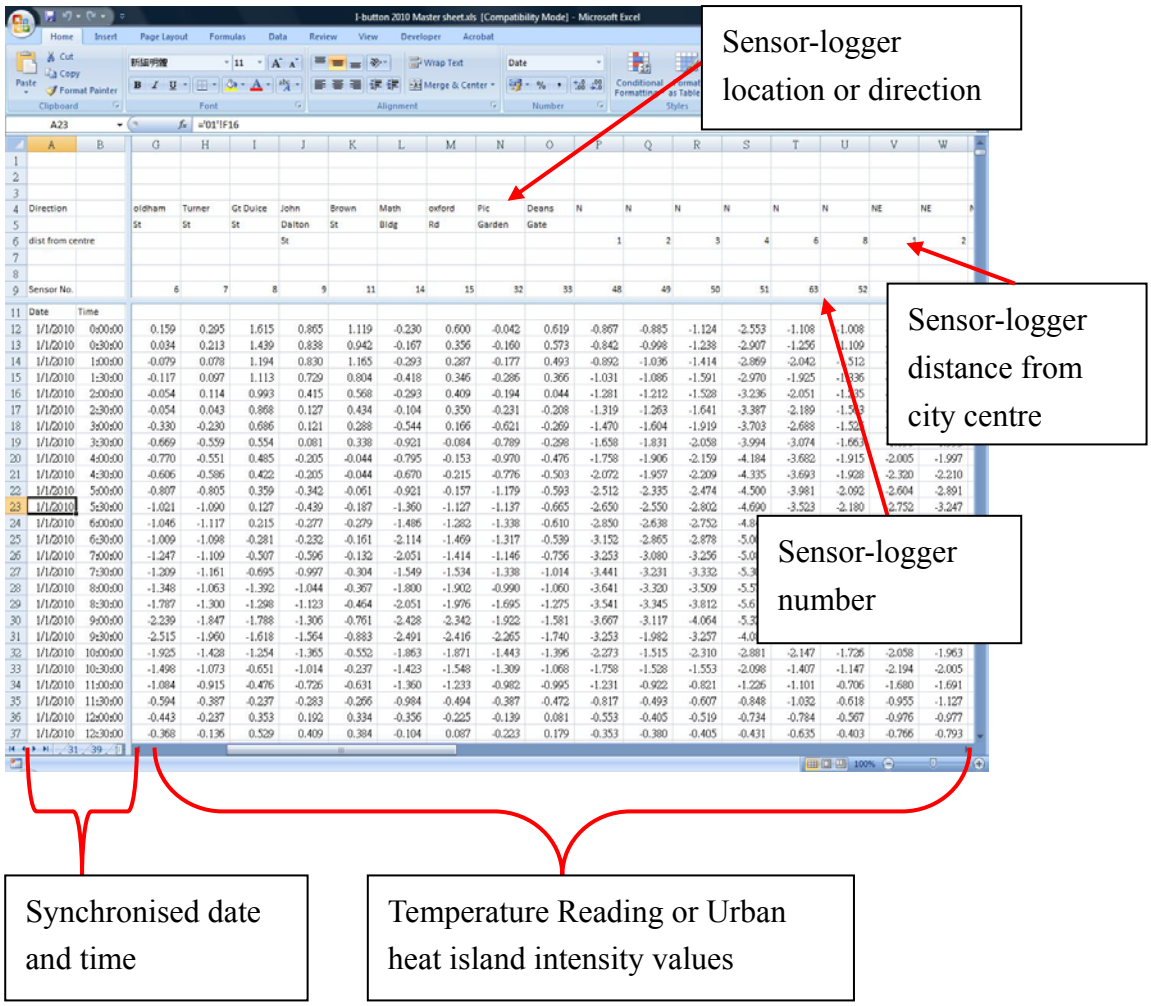

Figure 5.19 Master work sheet sample

During a later stage of the project, it was found that the clock recording the time in the sensor-logger was lagging from the actual time of the PC (the actual time of the PC was synchronized with the time server). The current time of the sensor-logger could be seen from the software as well as the time difference between the sensor-logger and the PC as shown in the figure 5.20. It was also noticed that this time difference tends to increase as the logging mission stays longer. In order to check if this is the problem due to the battery life time, a query email was sent to the manufacturer to investigate this. The manufacturer replied with the sensor-loggers' data sheet which shows that the battery could last for more than 3 years with a logging interval of 30

minutes. A shorter mission time was also recommended by the manufacturer. Nevertheless, a shorter mission time means a more frequent data collection period and a separate logging mission every time during data collection. The increase of data collection frequency would heavily increase the time the author would have to spend while a separate mission during each data collection would also increase synchronisation of the data for all sensors. Therefore, it was decided that sensor-logger would not be changed and logging mission would not be re-start every time. However, calculations would be taken to the procedure of organizing the data in excel in order to minimize the error.

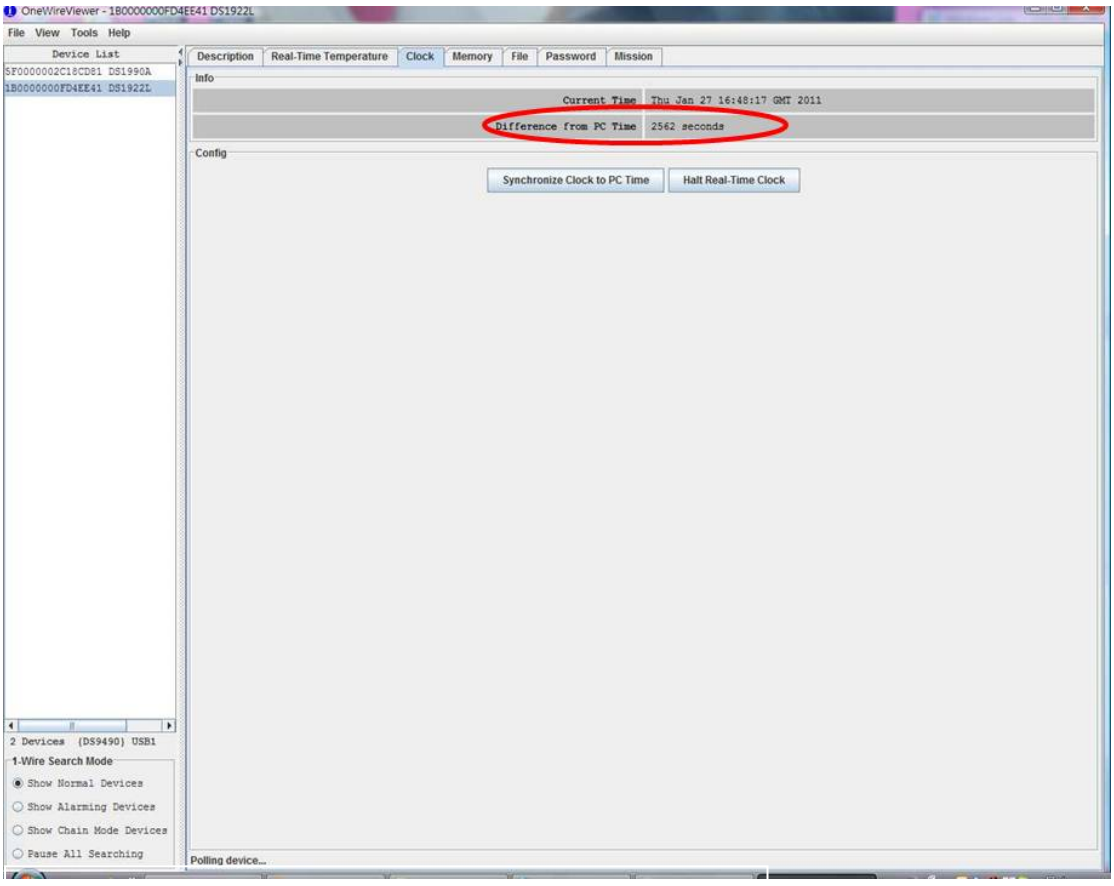

Figure 5.20 Time difference from sensor-logger against PC

In order to correct the time difference between the sensor and the PC, the time error

per day can be found using the following equation:

$$\text{Time difference per day} = \frac{\text{Time difference recorded on data collection}}{(\text{data collection date} - \text{sensor} - \text{logger first install date})}$$

The above equation was used twice for each sensor during the two data collection sessions to check if the time difference per day for each sensor is roughly the same. This ensures the relation between the time error and length of mission is linear.

Each sensor-logger worksheet mentioned earlier had to be changed slightly to adjust the time recorded in each set of reading. This could be done by using the time difference per day calculated in the equation above. Firstly, the temperature adjustment was made by using the adjustment value for each sensor-logger found from calibration experiments. Secondly, the total installed day was found at each set of reading. The time correction (in seconds) was then found by multiply the installed day with the time error per day. The unit of the total time correction was then converted from seconds to days and added onto the original recorded time. The sum would be the actual time each temperature reading was recorded. Finally, linear interpolation was performed to synchronise the time for each set of readings. Figure 5.21 indicates this refined data organizing procedure.

In order to check the accuracy of the temperature measurement over the duration of the project, two sensor-loggers (with the longest measurement period) were removed from the radiation shields and retested against the certified sensor-logger in a similar way as the calibration experiment. Only “cold test” were performed due to time limitation. Temperature measurement “missions” were not stopped so that any

temperature drift could be spotted easily (it was believed that both the time drift and temperature drift will be very small when new measurement "mission" starts). Table 5-4 shows the mean temperatures and the standard deviation of each sensor-logger. The average temperature difference between the certified sensor-logger and sensor-logger "1" is about 0.3^{o}C. Sensor-logger "15" had an average difference of 0.25 ^{o}C. These errors are very similar to those measured at the start of the project (see Table 5.4, which were corrected at the start of measurement) indicating that the sensor-loggers had not deteriorated significantly over the period of measurement. This is still acceptable according to the manufacturer's data sheet[108]. The calibrated sensor-logger had not been used since the last calibration.

Sensor-logger	A (certified)	01	15
Mean	6.694^{o}C	6.394 ^{o}C	6.446 ^{o}C
Standard Deviation	0.282 ^{o}C	0.267 ^{o}C	0.223 ^{o}C
Original Adjustment values		0.1756	0.1779

Table 5-4 Mean and standard deviations of two sensor-loggers.

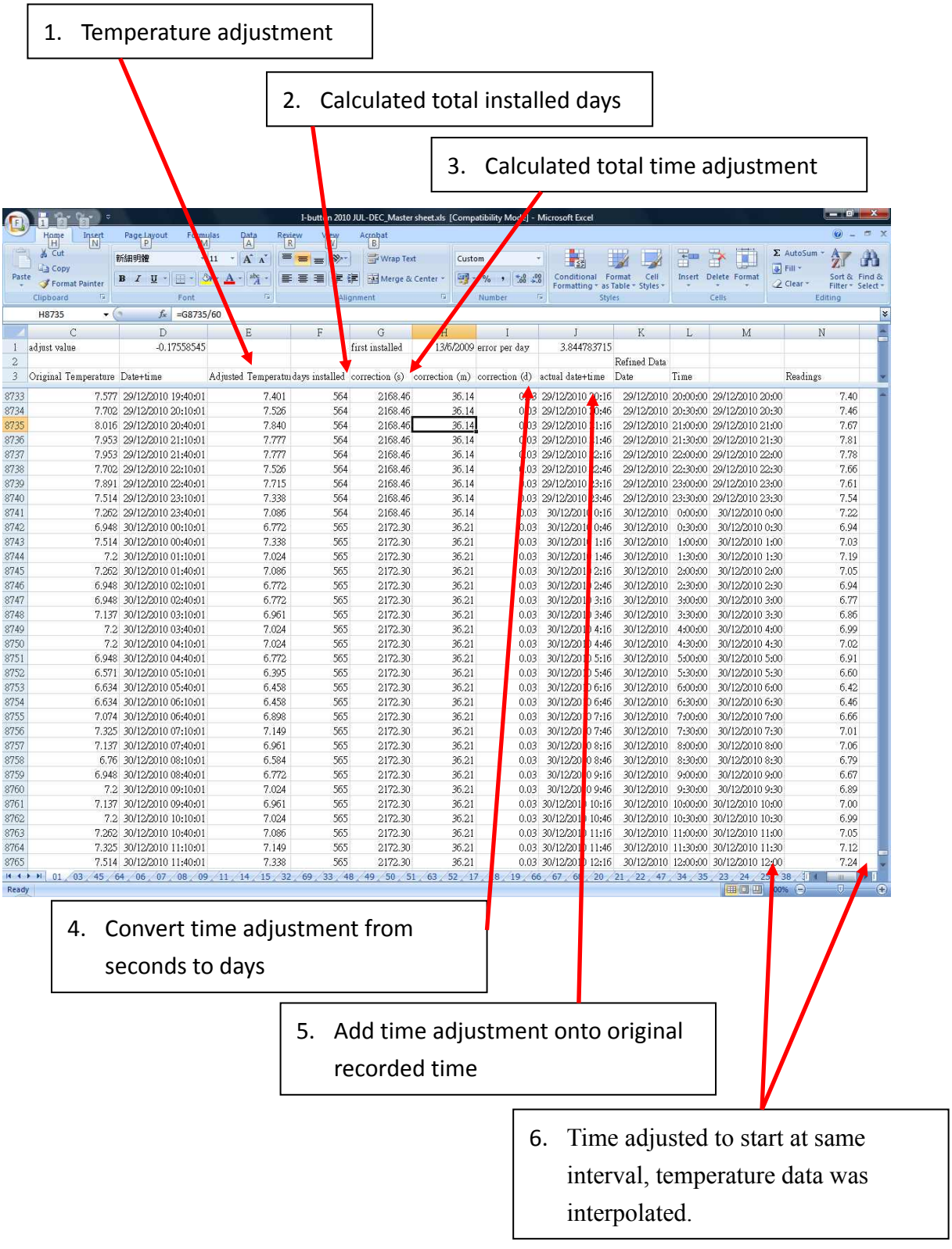

Figure 5.21 Additional modification on master spread sheet

5.8 Other weather data

Apart from the air temperature data obtained from Greater Manchester, there are other weather parameters which might affect the urban heat island effect as mentioned earlier in the literature review. These weather parameters include: solar irradiance, wind direction, wind speed and cloud cover. These data were also used in the Energy balance model described in Section 3. The procedures used to obtain and process these weather data are discussed within this section.

5.8.1 Solar irradiance data

It was not capable to find solar irradiance data from Met Office data in the beginning of this project. Therefore it was decided the solar irradiance data should be measured and recorded locally on the roof of a building in the university. A Delta-T BF3 Solarimeter and a Skye SKL-310 Lux meter were installed on the roof of Pariser Building, University of Manchester. Both total and diffuse solar irradiance in Wm^{-2} were measured every five seconds by the solarimeter while the lux level was measured at the same interval by the Lux meter. Both measurement devices come with calibration certificate from the supplier. The accuracy of the solarimeter is ±12% or $\pm 5 Wm^{-2}$ [109] and the accuracy of the Lux meter is ±5%[110] maximum according to the manufacturer data sheet. They were connected to a five Channel Skye DataHog 2 data logger on the floor below. The data logger averaged and recorded every ten minutes. The memory of the data logger was 1Mbyte which is capable of storing up to 20 days' worth of data at ten minute time intervals. The output from the data logger software produced a text file with data from relevant channels, and the relative date

and time. This text file could be accessed using Excel. The diffuse solar and light level data was then erased from Excel leaving data at 30 minutes interval. Finally, all the solar data was copied onto the same master Excel sheet along with the temperature data.

5.8.2 BADC data

The British Atmospheric Data Centre (BADC) releases weather data from Met Office Land Surface Observation stations. The BADC data used in this project were obtained by Dr John B. Parkinson[111]. There are three observation stations in Greater Manchester: Woodford, Ringway and Hulme (as shown in figure 5.22). Hourly data were obtained from these three stations. Hulme is located within the Manchester city area while Ringway and Woodford are at the outskirts of Greater Manchester. Woodford was selected to be the rural reference point because it was the most rural site (about 15 miles from Manchester city centre).

Figure 5.22 Location of three Met Office Ground Observation stations

Many different weather parameters are included in this hourly data. However, only the following parameters were useful to this project: cloud cover, dry bulb air temperature, wind speed, wind direction, rainfall and relative humidity. Details of other weather parameters could be found on the BADC website[112]. The original text format data could be accessed using Excel. Irrelevant data were erased leaving only the above mentioned parameters. Nevertheless, these data was still in hourly format. Linear interpolation was used to create data at 30 minute time intervals. The linear interpolation for wind direction was slightly different so that the bearing could be interpolated correctly when it is over 360^{o}. Finally this data was copied onto the master spread sheet containing all temperature readings obtained from sensor-loggers.

In order to set up fixed monitoring stations, the selection of temperature sensor-logger

was discussed in this chapter. The radiation shield was designed and fabricated so that the sensor-logger can be sheltered from rain and solar irradiance. The radiation shield was compared with a Stevenson Screen and the result indicates their performance were very similar. Two calibrations (one at 30^{o}C and one at 5^{o}C) were also performed for all sensor-loggers. Finally, the data collection and processing procedures were also discussed in this chapter.

CHAPTER 6

Urban heat island intensities

CHAPTER 6 Urban heat island intensities

6.1 Introduction

The existence of an urban heat island is determined by calculating the urban heat island intensity, defined below:

$$\text{UHI Intensity} = \text{Temperature}_{urban} - \text{Temperature}_{rural} \qquad \text{eq 6.1}$$

A positive value indicates the existence of an urban heat island, i.e. the urban temperature is higher than rural. A negative UHI intensity means that the urban temperature is lower than rural temperature and so indicates an urban cool island. The temperatures used in equation 6.1 can be air temperatures, radiant temperatures or surface temperatures. The UHI effect is commonly quoted based on air temperature with the radiant and surface temperature UHI effects being specifically identified, e.g. UHI(radiant) effect or UHI(surface temperature) effect. Air temperature in this project refers to dry bulb air temperature. It is measured easily with a thermometer. Air temperature is a result of the total energy exchange to or from the thermometer by convection, conduction and radiation [Oke[1] (1978)]. Radiant temperature is equal to the surface temperature if the surface forms part of a black body with emissivity equal to 1 [CIBSE[22] (2006)]. In general radiant temperature will be a function of surface temperature, the emissivity of the surface and the radiation from the surroundings reflected from the surface if the surface forms part of a grey body with emissivity less than 1 [CIBSE[22] (2006)]. Radiant temperature can be measured by a radiant thermometer, typically a thermometer in a black spherical enclosure. Surface temperature is the temperature of a surface adjacent to an air space [CIBSE[22] (2006)].

Surface temperatures is much more variable than air temperatures [Gartland[29] (2008)]. Also, it is very difficult to measure. Oke[1] (1978) suggested the true surface temperature is very similar to the surface radiant temperature which can be measured by an infra-red radiation thermometer. Air temperature can be very different from the surface temperature on a sunny day. Figure 6.1 [Stull R.B.[113] (1995)] below shows the temperature gradients within a few millimetres of the ground on a sunny day. This is because of the strong heat conduction fluxes from the hot surface of the ground. Often the radiant and surface temperature UHI effects are measured from satellites or aircraft (the latter as in the SCORCHIO project). However, these only refer to the ground and building surface as seen from above.

Only air temperature was measured and recorded in this project as it is the commonest measure of the UHI effect and the surface and radiant temperatures can be calculated from radiation exchanges and the emissivities.

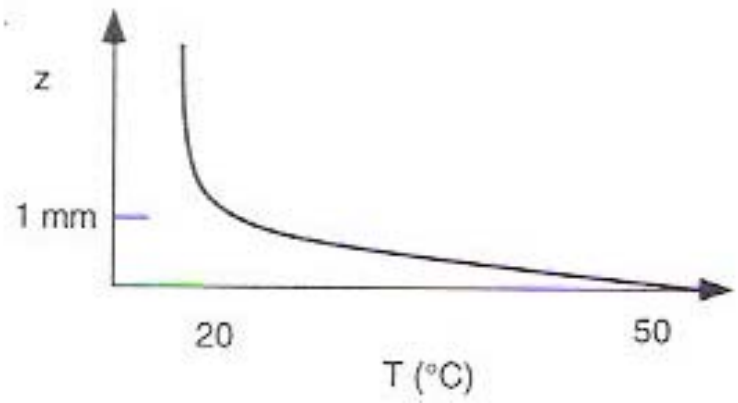

Figure 6.1 Temperature gradients within a few millimetres of the ground on a sunny day[113]

Air temperatures were measured at 59 different monitoring stations in Greater Manchester at an interval of 30 minutes for a year. 11 stations were located in different street canyons in Manchester city centre. The other monitoring stations were located at eight directions with equal radial distance as mentioned in an earlier chapter.

The Met Office ground observation station in Woodford was chosen to be the rural reference point. Urban heat island intensities were calculated for air temperature data obtained from sensor-loggers located in the Manchester city centre area and the air temperature from Woodford station. In this chapter, the urban heat island intensities are calculated to determine the existence of an urban heat island in Manchester.

In this section, the urban heat island intensity will be presented against percentage of total time of a season for both winter and summer of 2010. The mean UHI intensities daily profile will also be presented to show the variation of UHI intensities within a day.

Figure 6.2 shows the temperature variation at three different places on a clear day and night, from 12:00 on 30th Aug 2010 to 11:30 on 31st Aug 2010. This particular period is chosen because according to Oke[1], the urban heat island effect would be larger on clear and calm nights. The three measuring stations are Woodford, located 15 miles from Manchester city centre, Hulme Library, located about 0.75 miles from Manchester city centre and Brown Street (as shown in table 6-1), one of the monitoring stations located inside Manchester city centre having the deepest canyon (H/W=1.78). Woodford tends to have the lowest temperature during the night while Brown Street has the highest. This can be explained by the difference in long wave radiation loss and sky view factor (SVF) of each location. SVF is a ratio varies from 0 to 1 and is used to describe how much sky could be seen at a point (more details are given in section 7.2). Brown Street has a SVF value of 0.27 while Woodford has a SVF value close to 1. This means there is a lot more sky seen in Woodford compared to Brown Street. Thus, long wave radiation lost in Woodford will result in a quicker drop in temperature and a lower ultimate temperature than Brown Street. The

temperature difference between Woodford and Brown Street is the urban heat island intensity at Brown Street.

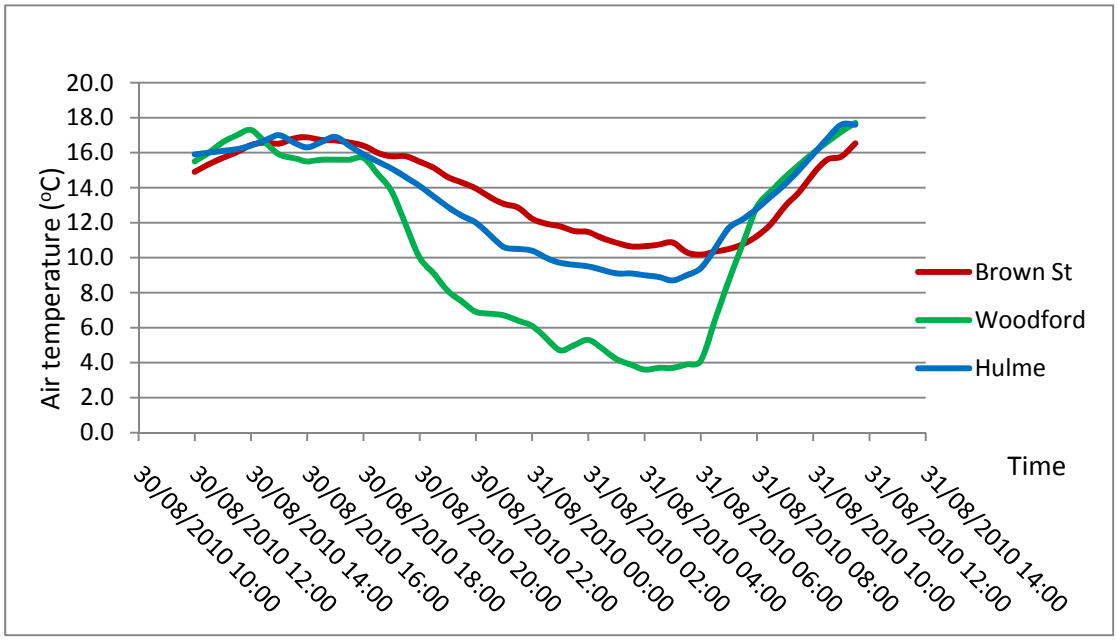

Figure 6.2 Air temperature variation over a clear and calm night

The air temperature measured at Hulme is also higher than Woodford, but about 2°C less than Brown Street. Figure 6.3 [Oke[1] (1978)] indicates a typical temperature profile for an urban heat island. The temperature gradient from the rural area to the suburban area forms a "cliff". The rest of the sub-urban area has a relatively gentle temperature gradient forming the "plateau". The thermal centre ("Peak") of an urban heat island is usually located in the central urban centre.

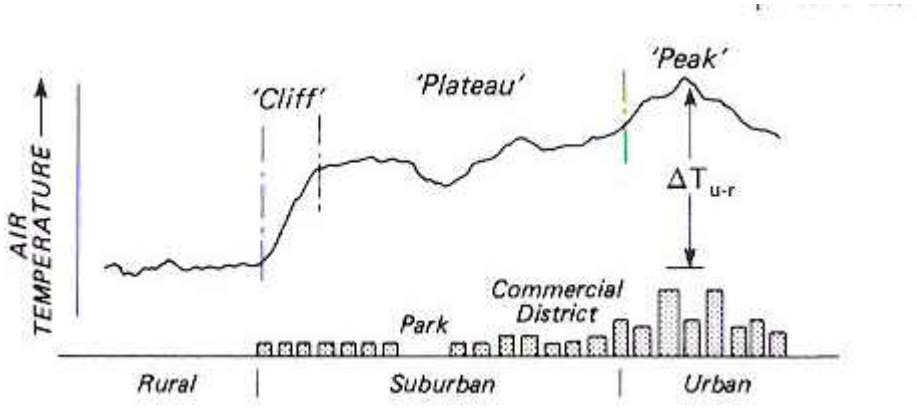

Figure 6.3 Typical temperature profile for urban heat island[1]

Hulme weather station is located about 0.75miles from Manchester city centre and it is on the roof of a two storey building. Therefore, the canyon effect cannot be seen by comparing only the Hulme air temperature with Woodford air temperature. The air temperature differences between Hulme and Brown Street are believed to be mainly caused by the street canyon characteristic, therefore known as the canyon effect. The Woodford temperature drops much quicker at night because it is more exposed to the clear sky than the other two locations. Meanwhile the air temperature difference between Woodford and Hulme is believed to be caused by distance into the suburban area and therefore is known in this project as the "distance effect". Therefore, the urban heat island effect is the sum of the distance effect and the canyon effect.

6.2 Calculation criteria

In order to determine the existence of urban heat island in Manchester area, the urban heat island intensity has to be measured. Table 6-1 indicates the locations of 11 monitoring stations located in the city centre of Manchester, their temperature logging periods and their sky view factor (sky view factors is an indication of the canyon geometry. This will be discussed in detail in the next chapter). These city centre locations were selected based on different canyon characteristics such as different height to width ratio or SVF. Piccadilly Gardens was selected as the geographical centre of all monitoring stations due to its location. However, it is not a street canyon, there is a lot of vegetation (grass and some trees) and a water fountain in the centre. Therefore the UHI intensity calculated from the sensor-logger here is expected to be a bit lower.

Air temperature data obtained from sensor-loggers were divided into four seasons as

below:

Spring: March, April and May

Summer: June, July and August

Autumn: September, October and November

Winter: December, January and February

Apart from the four seasons, data in each season were further divided into daytime data and nocturnal data. It would be very complicated and time consuming if the daytime and nocturnal data were separated according to the sun-set and sun-rise each day. Therefore, sun-rise and sun-set times on the 15th of each month were obtained from www.timeandday.com[114] and used to separate the original data into daytime data and nocturnal data.

The urban heat island intensities in this chapter were calculated for each sensor-logger logging at every 30 minutes using the measured air temperatures and Woodford rural temperatures. An average UHI intensity was then found for the 11 UHI sensor-loggers at every half hour. Average UHI intensity for each 30 minute interval was calculated with equation 6.2.

$$\text{Average UHI intensity} = \frac{\sum \text{UHI intensity from all sensor-logger within 30 minute}}{\text{number of sensor-loggers}} \qquad \text{eq 6.2}$$

The reason for calculating the average UHI intensity is to minimise the effect due to individual canyon characteristics, such as sky view factor, evapotranspiration fraction and anthropogenic heat (these factors are further discussed in the next chapter), and to show the overall canyon effect. The average UHI intensities are plotted against percentage of time as a histogram for each season, daytime and nocturnal, discussed later in this chapter. The mean values and standard deviations were also calculated.

Sensor-logger location	Logging period	Sky view factor
Pariser Building, University of Manchester	01/01/2010-31/12/2010	0.506
Faulkner Street	08/05/2010-31/12/2010	0.366
Oldham Street	01/01/2010-31/12/2010	0.328
Turner Street	01/01/2010-31/12/2010	0.297
Great Ducie Street	01/01/2010-31/12/2010	0.011
John Dalton Street	01/01/2010-31/12/2010	0.342
Brown Street	01/01/2010-31/12/2010	0.271
Deans Gate	01/01/2010-31/12/2010	0.437
Alan Turing Building, University of Manchester	01/01/2010-31/12/2010	0.706
Piccadilly Garden	01/01/2010-31/08/2010 21/11/2010-31/12/2010	0.878
Oxford Road	01/01/2010-31/12/2010	0.481

Table 6-1 Locations and logging periods of monitoring stations in city centre

Apart from the average UHI intensities, nocturnal UHI intensities for Brown Street and Piccadilly Garden were also selected for a similar histogram analysis. This was done because Brown Street has the smallest sky view factor (Great Ducie street has a much lower sky view factor, however, it is not a canyon, the monitoring station was located under a bridge) and Piccadilly Garden has the largest among the canyons. Only nocturnal UHI intensity histograms were shown because UHI intensity is larger on clear and calm nights according to Oke[1] (1978). Watkins[44] (2002) performed similar fixed point measurement to investigate the UHI effect in London in 2002.

Results from this project will also be compared with the UHI research performed in London.

6.3 Heat island intensities in different seasons

In this section, the frequency distribution histogram of UHI intensities for all the 11 sites is presented for summer and winter 2010. The reason of choosing only winter and summer is because urban heat island effect was believed to affect building energy use most during these two seasons. The overall urban heat island effect simulation will be discussed later in chapter 8.

6.3.1 Summer heat island intensities

Figures 6.4 and 6.5 show the daytime and nocturnal frequency distribution of UHI intensities in the summer respectively. The highest frequency of UHI intensity is 22% at 1.0^{o}C during daytime and 21% at 1.5^{o}C at night. Watkins *et al.,*[12](2002) found a very similar result found in London. Important factors to be noticed from these two graphs:

1. Nocturnal UHI intensity is higher and more frequent than daytime UHI intensity.
2. The occurrence of urban cool islands happened more during daytime than at night.
3. For the nocturnal data (Figure 6.5) the shape of the histogram is very skewed indicating that a mean and standard deviation of the UHI effect are poor descriptors.

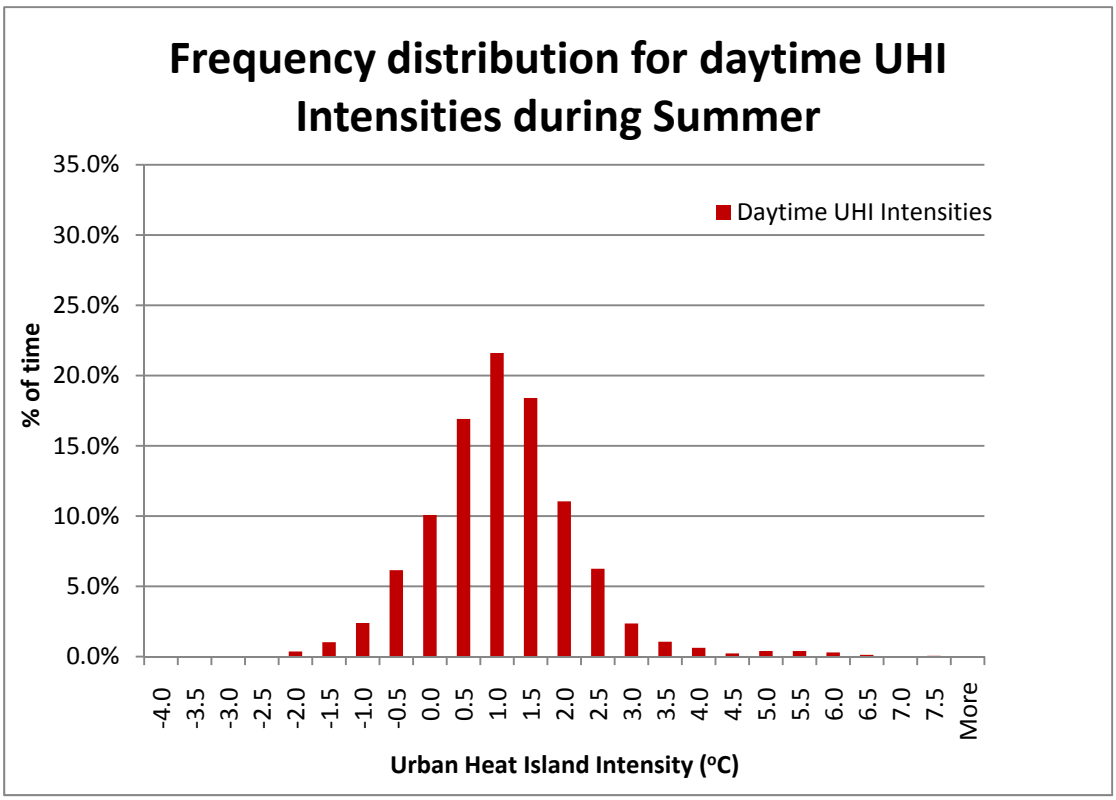

Figure 6.4 Frequency distribution of daytime UHI intensities during summer 2010, 11 city centre sites

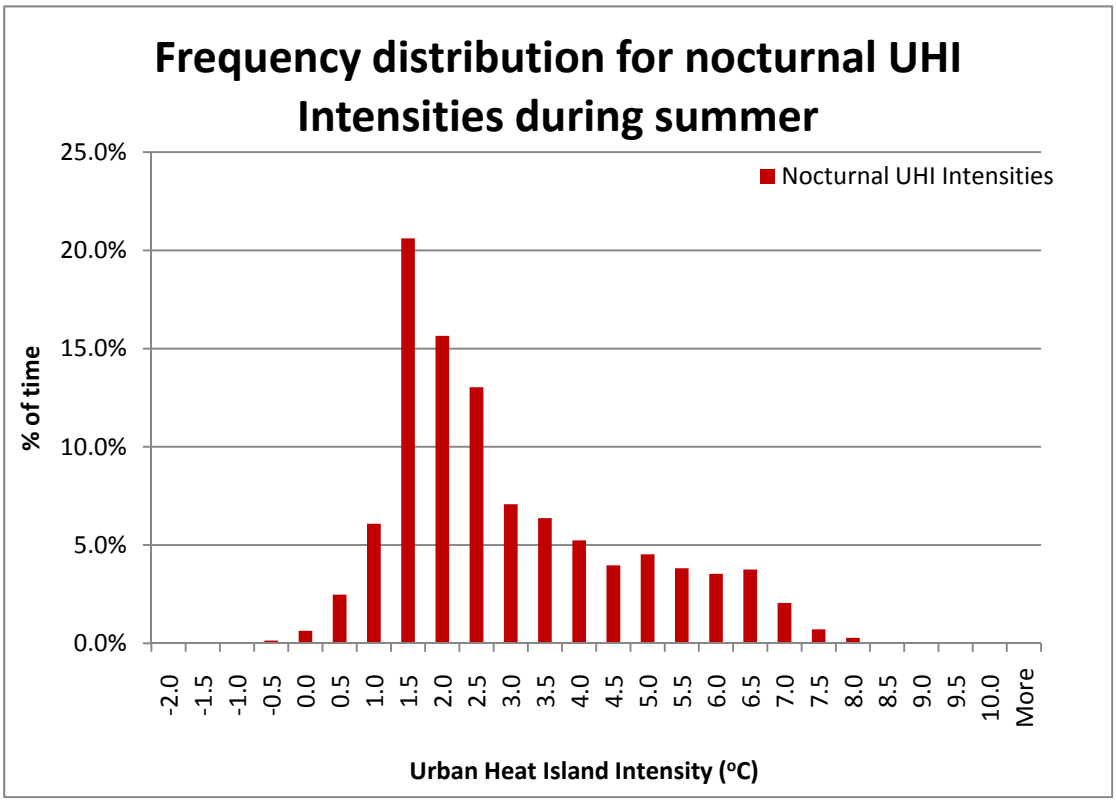

Figure 6.5 Frequency distribution of nocturnal UHI intensities during summer 2010, 11 city centre sites

Figure 6.6 and 6.7 show the frequency distribution of nocturnal UHI intensities for

Piccadilly Garden and Brown Street during the summer.

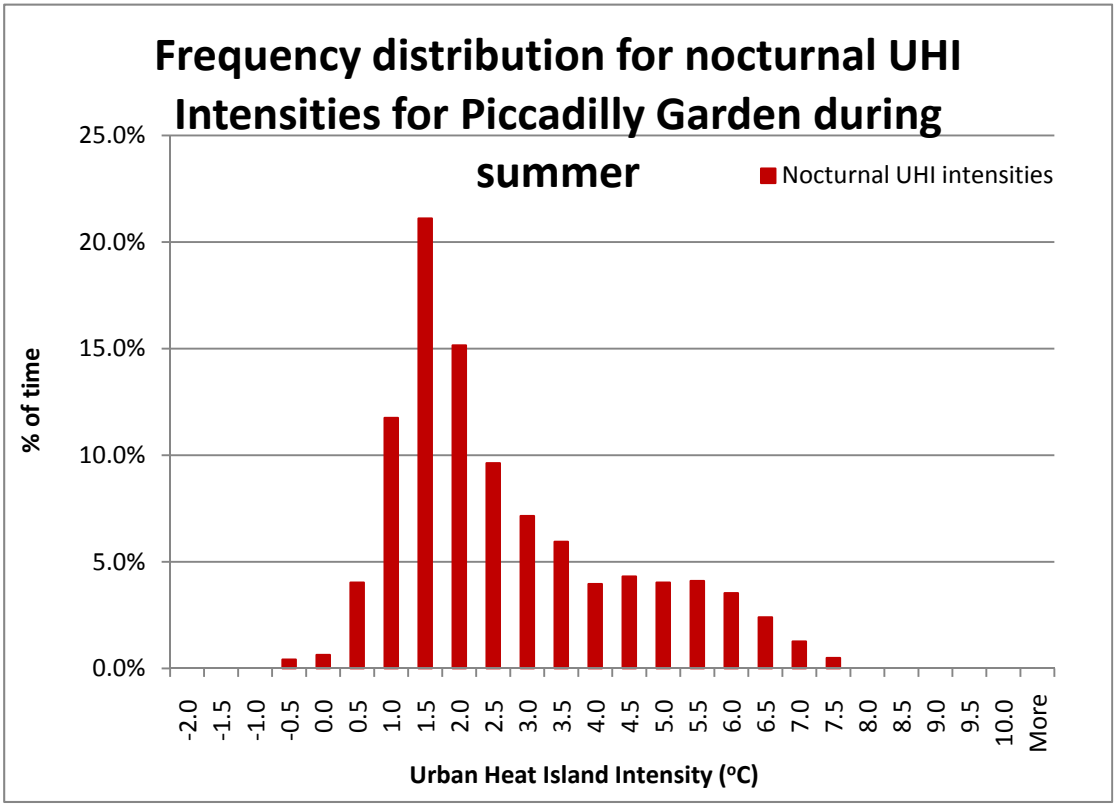

Figure 6.6 Frequency distribution of nocturnal UHI intensities for Piccadilly Garden during summer 2010, 1 city centre sites

A very similar pattern could be found between the two graphs. However, it can be seen that the maximum UHI intensity for Piccadilly Garden was at 7.5°C. It was 0.5°C smaller than that of Brown Street. Figure 6.8 indicates the mean daily profile of UHI intensities for all data collected during summer 2010. It can also be seen from this figure that the average UHI intensities during the day (from 06;00 to 20:00) is much lower than the night.

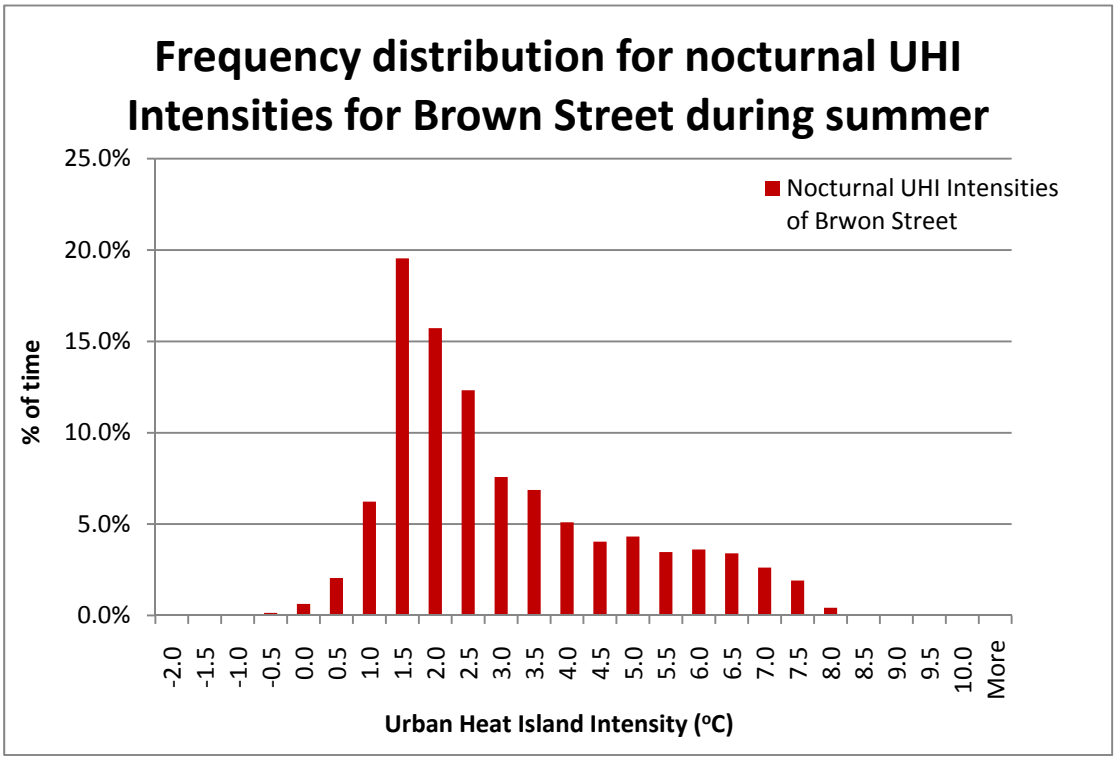

Figure 6.7 Frequency distribution of nocturnal UHI intensities for Brown Street during summer 2010, 1 city centre sites

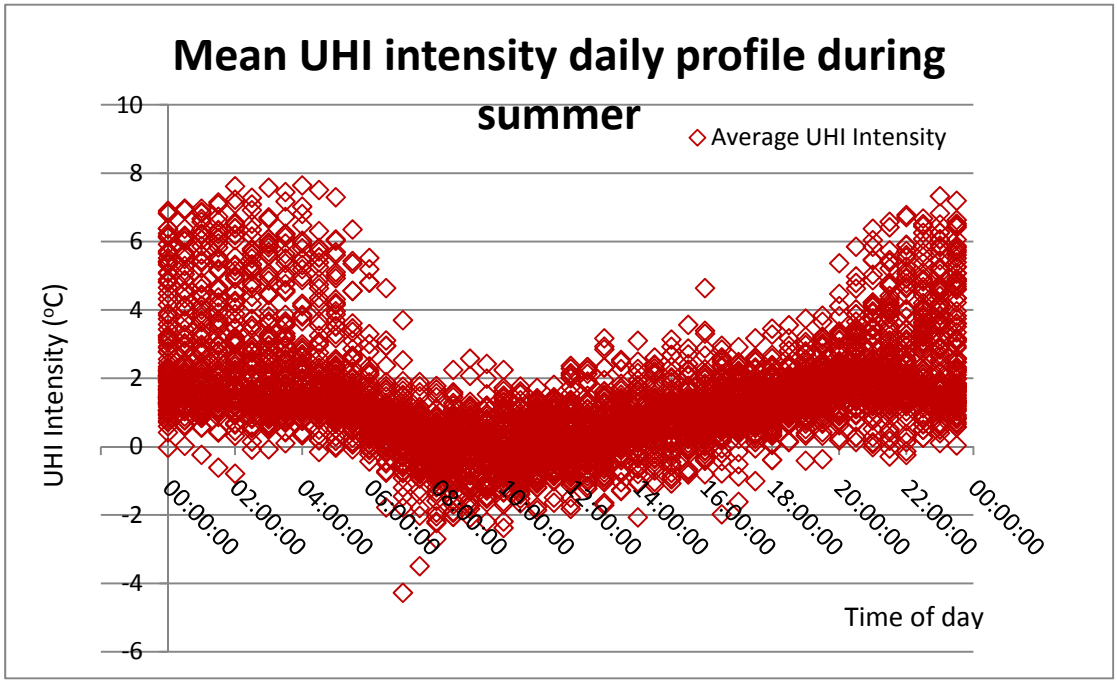

Figure 6.8 Mean UHI intensity daily profile 2010, 11 city centre sites 2010 11 city centre sites

In order to observe the maximum urban heat island intensity, air temperature data was filtered according to different weather parameters. The average UHI intensity is about

2°C. This is very similar to the findings in London from Watkins[44] (2002) who indicated a mean UHI intensity of 2.1°C in 1999. Literature has already suggested that the urban heat island would be a maximum under clear and calm nights [Oke[1], Landsberg (1981)[115], Tumanov *et al.,*[116] (1999)]. As a result, air temperature data was selected for clear and calm conditions with the following criteria:

1. Woodford wind speed less than or equal to 2.5 ms^{-1}
2. Woodford cloud level less than or equal to 2 oktas

Figure 6.9 shows the mean UHI intensity daily profile for 11 sites in city centre under clear and calm condition in summer 2010. Most of the data concentrated on the night period. Some hourly data are not included, such as 11:00 and 13:00. This is because it was not clear and calm during those hours. This could well be due to the solar radiation creating turbulent heat flux and upsetting the stable boundary layer [Stull R.B.[113] (1995)]. The maximum UHI intensity occurred at night time between 22:00 to 05:00 with a value of +7.8°C. The minimum UHI intensity was a single measurement of about -4°C which occurred during early morning about 07:00. It can be concluded that the summer UHI intensity at night is relatively higher than that of the daytime.

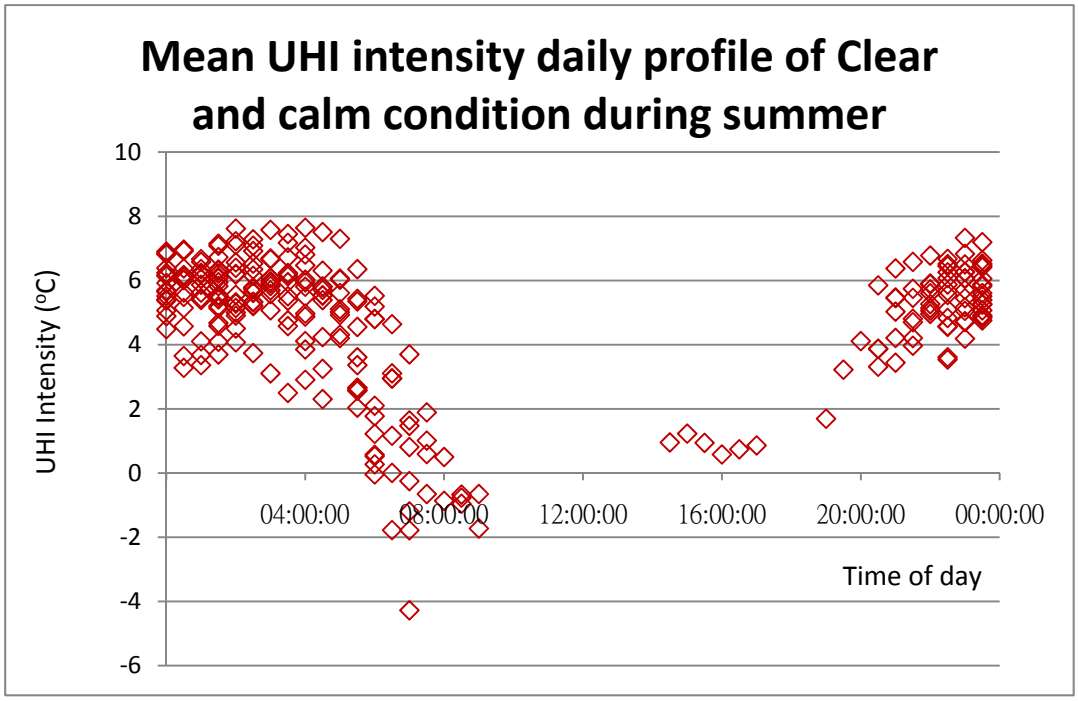

Figure 6.9 Mean UHI intensity daily profile for a clear and calm condition during summer 2010 11 city centre sites

6.3.2 Winter heat island intensities

Figure 6.10 and 6.11 shows the frequency distribution for daytime and nocturnal UHI intensities during winter respectively. The highest frequency of UHI intensity is at 1.0°C during the day and night. The following important points could be noticed:

1. Higher UHI intensities (greater than 2°C) tend to occur more frequently at night than daytime
2. Urban cool island tends to occur more during the day than night.

The maximum heat island intensity found during winter in Manchester is about 10°C which is slightly higher than the finding from Giridharan R and Kolokotroni M[43] (2009) for London. They indicated a maximum UHI intensity of 9°C in London during winter.

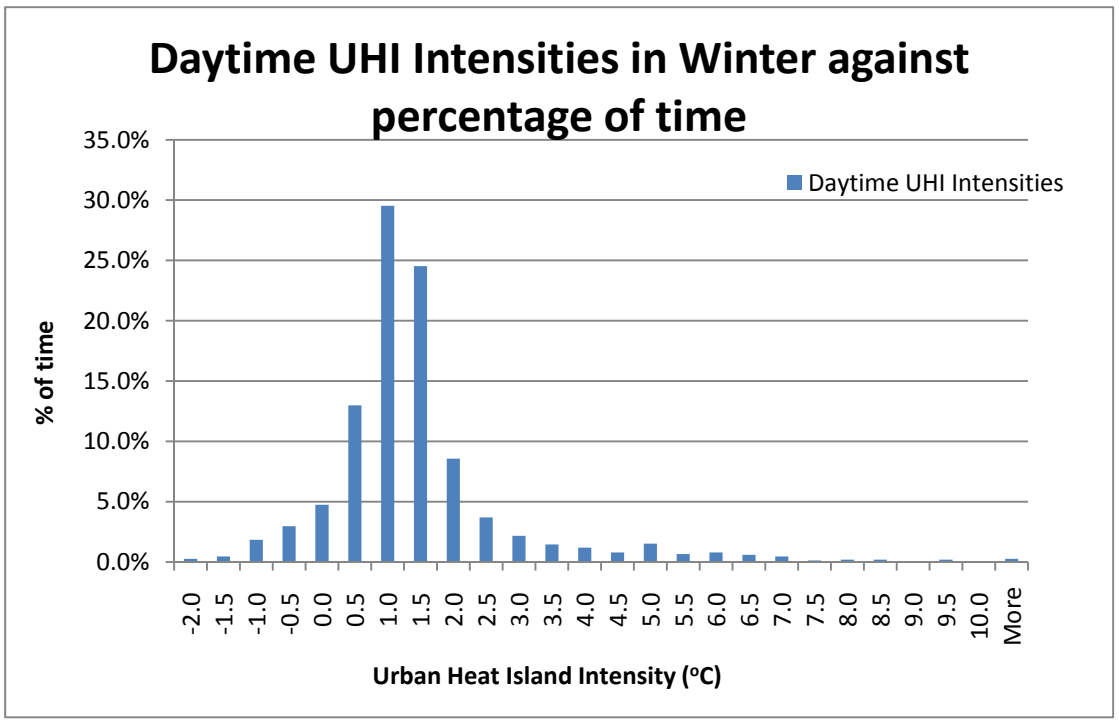

Figure 6.10 Frequency distribution for daytime UHI intensities during winter 2010, 11 sites in city centre

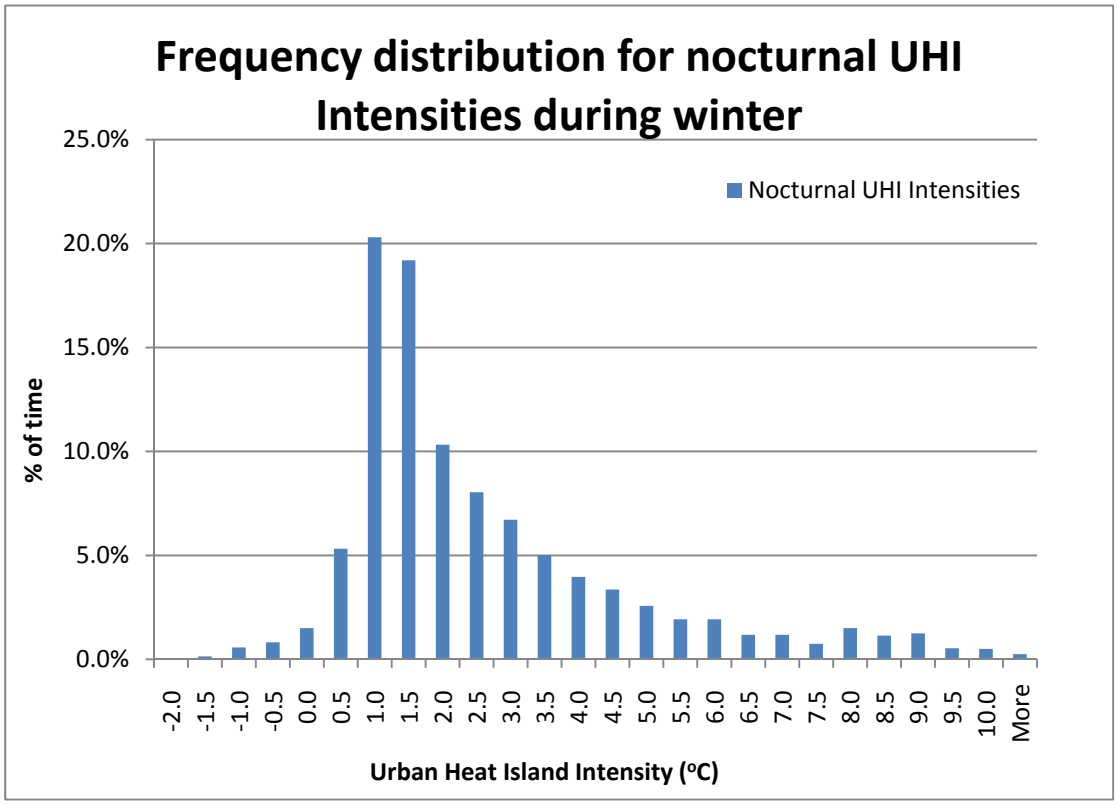

Figure 6.11 Frequency distribution for nocturnal UHI intensities during winter 2010, 11 sites in city centre

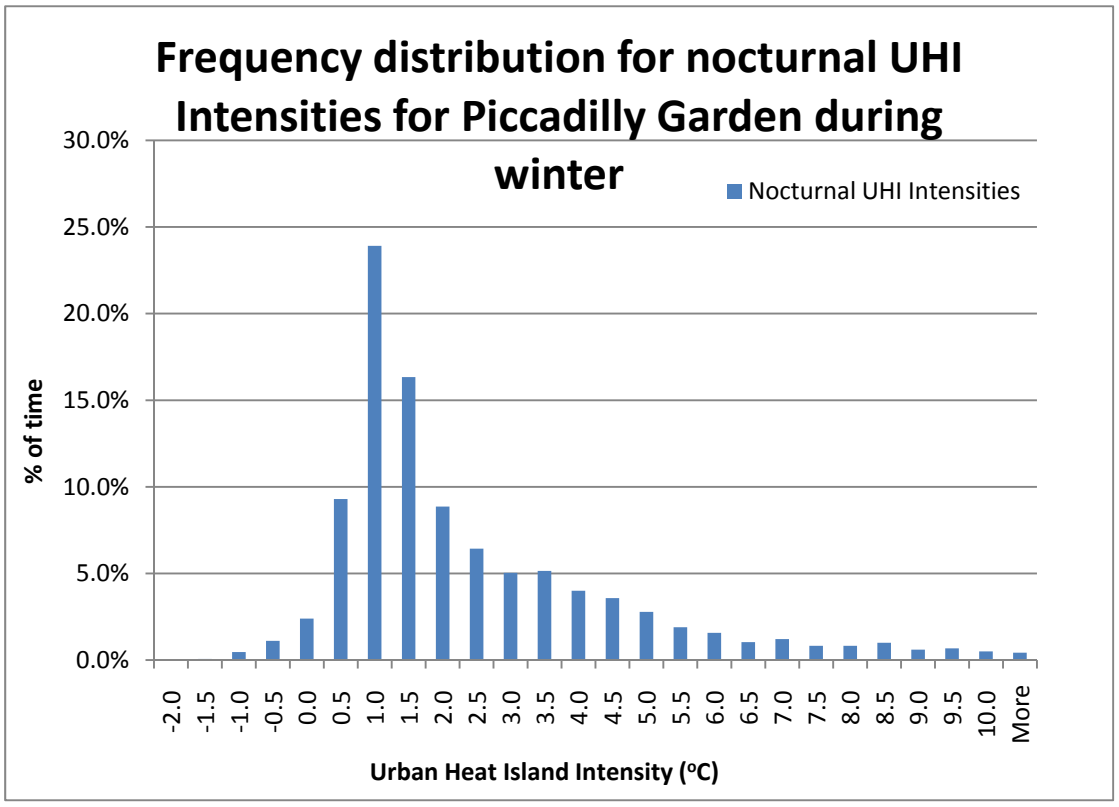

Figure 6.12 Frequency distribution for nocturnal UHI intensities for Piccadilly Garden during winter 2010, 1 sites in city centre

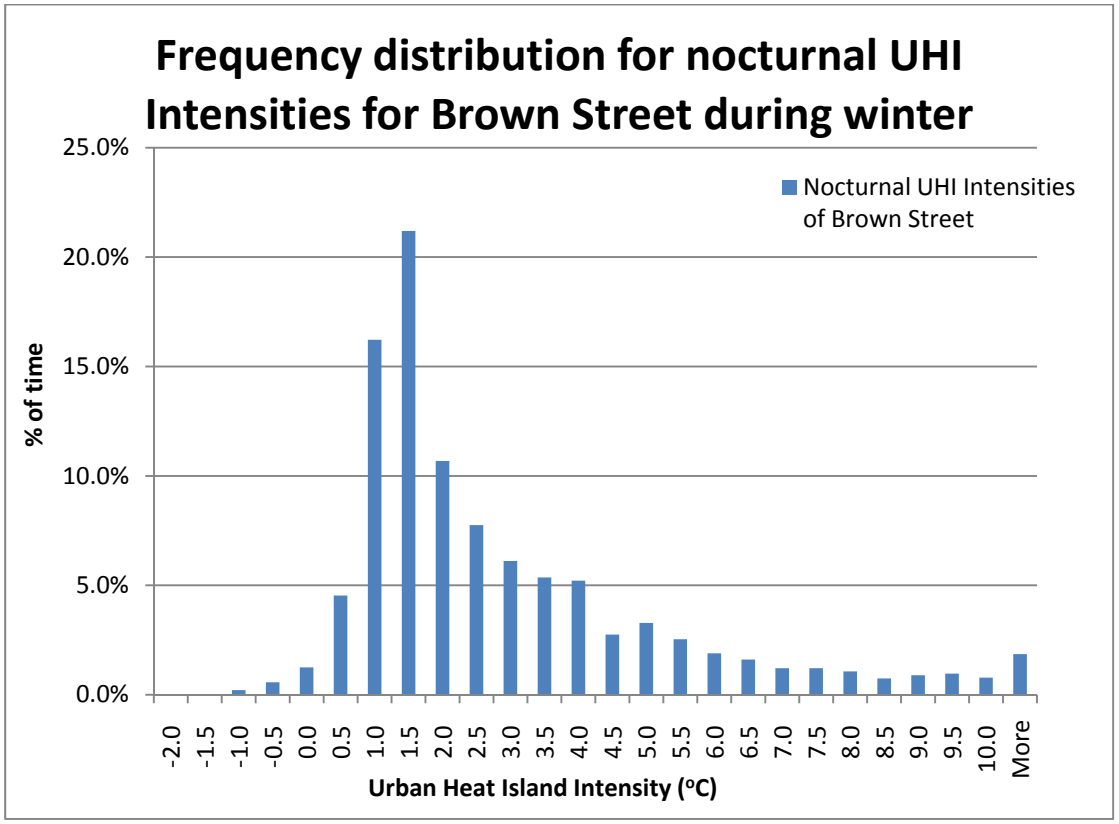

Figure 6.13 Frequency distribution for nocturnal UHI intensities for Brown Street during winter 2010, 1 sites in city centre

Figure 6.12 and 6.13 show similar frequencies for nocturnal UHI intensities for Piccadilly Garden and Brown Street. A similar UHI intensity pattern can be observed between Brown Street, Piccadilly Garden and the total average UHI intensities during winter. However, similar to the summer frequencies, Brown Street tends to have a higher maximum UHI intensity. High UHI intensities (UHI intensity greater than 6°C) also tend to occur more on Brown Street. Figure 6.14 shows the mean UHI intensity daily profile for winter 2010. It can be seen that the UHI intensities during the night (from 16:00 to 08:00) tend to be greater than that of the day.

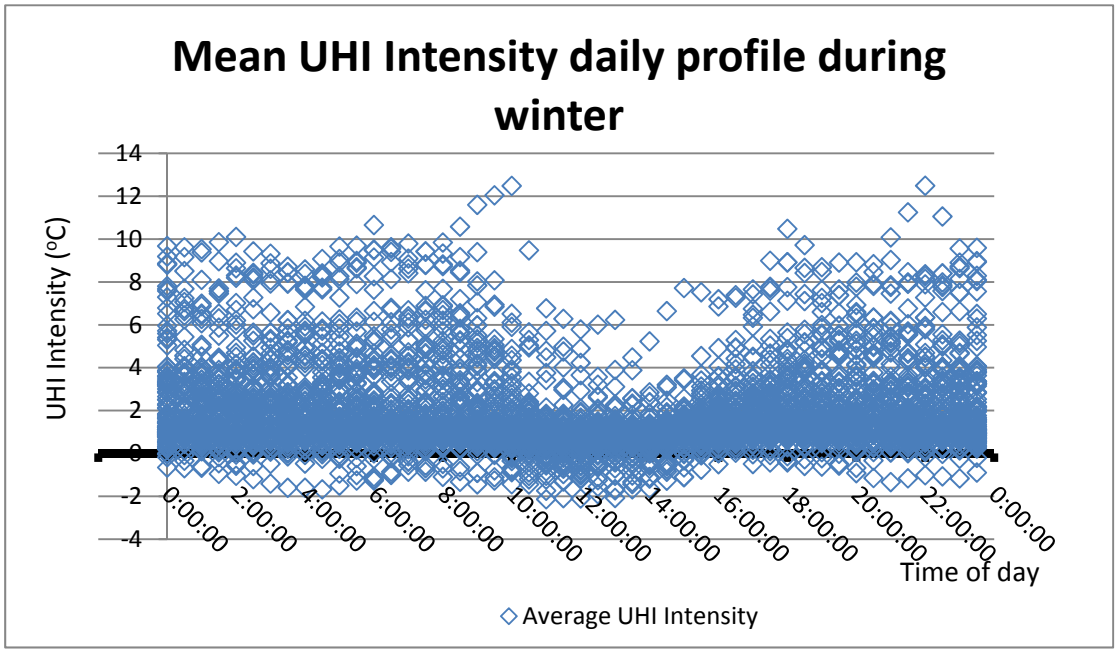

Figure 6.14 Mean UHI intensity daily profile in winter 2010, 11 sites in city centre

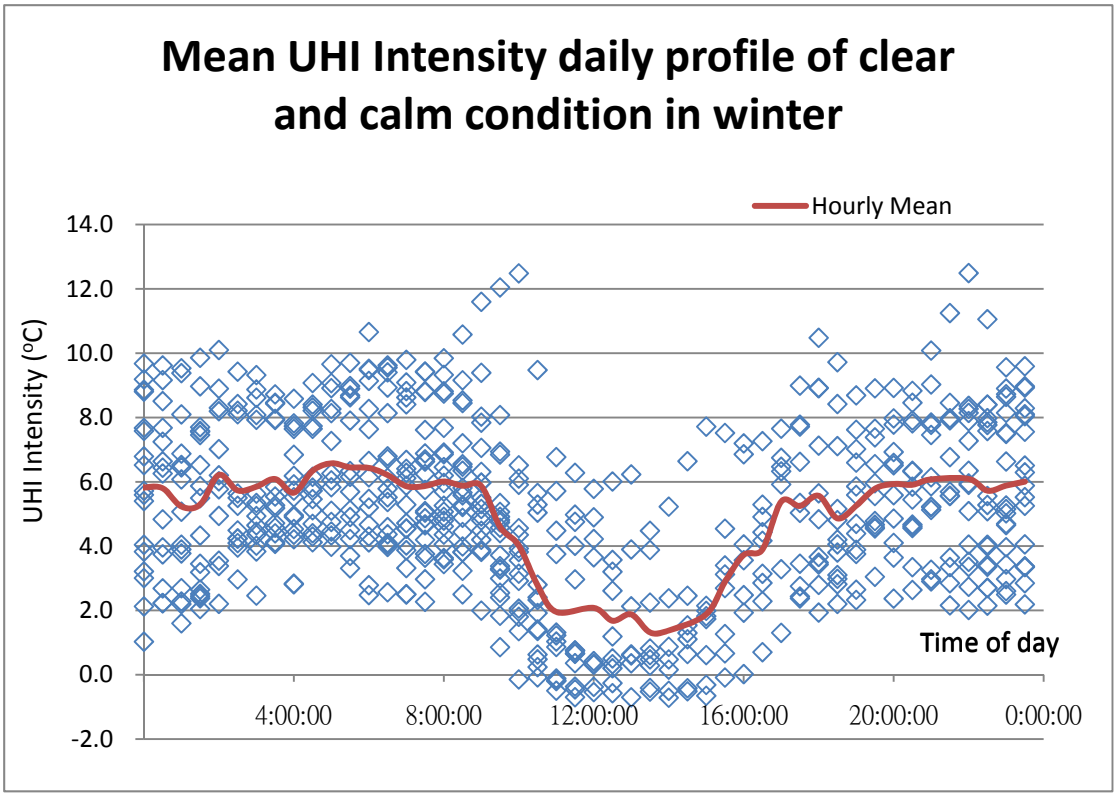

Figure 6.15 Mean UHI intensity daily profile for clear and calm period during winter 2010, 11 sites in city centre

Figure 6.15 indicates the Mean UHI intensity daily profile for clear and calm periods for winter 2010. The profile shows a maximum averaged UHI intensity, about 6°C although the data points go to abut 10°C, which occurs at around 22:00 to 09:00. The minimum averaged UHI intensity is about 0°C which occurs between 11:00 to 17:00. The hourly mean UHI intensity was about 6°C. The most negative averaged UHI intensity is about -1.5°C and occurs during the daytime. The average hourly mean UHI intensity is about 4°C for clear and calm days

6.4 Discussion

All the figures presented above indicate that there was an urban heat island effect in Greater Manchester during the winter and summer of 2010. Comparing the summer and winter urban heat island intensities, it can be seen that both the daytime and

nocturnal UHI intensity patterns were very similar in both seasons although the frequency of occurrence of the high UHI effects is more in summers. Nocturnal UHI intensity is always greater than that of the daytime. The occurrence time for maximum urban heat island agrees very well with Oke's[1] conclusion. Comparing the summer and winter nocturnal UHI intensities histogram (figures 6.5 and 6.11), there are two important findings:

1. The maximum UHI intensity is higher in winter than summer
2. The overall occurrence of strong urban heat island effect (indicated by UHI intensity larger than 3^{o}C) is more in summer than winter.

A higher maximum UHI intensity in winter has a positive impact on building energy consumption because less heating energy is required in winter. However, a high UHI intensity in winter might also be caused by anthropogenic heat released from poorly insulated buildings. In this case energy would be wasted. On the other hand, a higher occurrence of urban heat island in summer means comfort cooling might need to be introduced to some buildings. It is also important to note that since the urban heat island is largest at night, the use of building services systems such as night ventilation or thermal storage (Thermo deck) would be affected.

Table 6-2 below indicates the mean UHI intensities in day and night of each month in 2010 and their standard deviation. Monthly mean UHI intensities at night were always higher than that for the daytime. This indicates that there was a stronger urban heat island effect during the night than the day. The standard deviations of the daytime UHI intensities are always greater than the daytime mean values. This also indicates there is a higher possibility for a negative urban heat island effect (i.e. urban cool island effect). The overall heat island intensity for winter is higher than in summer nevertheless, the mean night time heat island intensity is highest in summer. The

yearly mean heat island intensity is 0.95°C for daytime and 2.62°C for nocturnal.

	Day		Night		Overall	
	Mean(°C)	SD(°C)	Mean(°C)	SD(°C)	Mean(°C)	SD(°C)
December	1.57	1.90	3.09	2.53	2.61	2.45
January	1.29	1.49	2.06	2.17	1.80	2.00
February	0.87	1.06	1.84	1.21	1.44	1.25
Seasonal Overall	1.22	1.52	2.37	2.17	1.97	2.04
March	0.80	1.02	2.27	1.55	1.53	1.51
April	0.71	1.19	3.27	1.98	1.78	2.01
May	0.97	1.17	3.26	1.83	1.73	1.79
Seasonal Overall	0.83	1.14	2.87	1.85	1.68	1.79
June	0.81	1.36	3.46	1.91	1.58	1.96
July	0.77	0.94	2.11	1.41	1.16	1.25
August	0.97	1.08	2.60	1.60	1.58	1.52
Seasonal Overall	0.85	1.14	2.71	1.73	1.44	1.61
September	0.84	1.21	2.49	1.56	1.63	1.62
October	0.81	1.30	2.57	1.85	1.80	1.85
November	1.03	1.30	2.38	1.78	1.87	1.74
Seasonal Overall	0.88	1.27	2.48	1.75	1.97	2.04
Yearly overall	0.95	0.25	2.62	0.54	1.71	0.35

Table 6-2 Monthly averaged UHI intensities in 2010

6.5 Conclusion

By comparing air temperatures measured in the city centre from a rural reference point, it was found that the urban heat island effect does exist in Greater Manchester. The urban heat island intensity varied between -4^{o}C to 7.8^{o}C in summer and -2^{o}C to 12^{o}C during winter in 2010. Kershaw *et al.,*[104] (2010) suggest mean UHI intensities of 2-3^{o}C in summer and 0.5-1.5^{o}C in winter. This agrees with results shown in table 6.2. The urban heat island intensity measured at night is always higher than that of the day. It was also found that the maximum heat island intensity during winter is higher than summer, however, the probability of the occurrence of a high urban heat island effect is higher during summer than winter.

After establishing the existence of an urban heat island effect in Greater Manchester, different causal factors contributing towards the heat island effect are investigated in the next chapter. These causal factors include distance from the city centre, sky view factor, wind speed, rural reference temperature, cloud level and evapotranspiration fraction.

CHAPTER 7

Urban heat island and causal factors

CHAPTER 7 Urban heat island and causal factors

7.1 Introduction

Urban heat island intensities were calculated for both summer and winter 2010 from temperature data collected from monitoring stations around Greater Manchester. It was found that an urban heat island does exist in Manchester. In this chapter, different causes of urban heat island will be investigated.

Factors causing urban heat island effect can be divided into two categories, canyon related factors and weather related factors. Canyon related factors include factors such as canyon width, building height in canyon, distance away from city centre, evapotranspiration fraction, sky view factor, road width, traffic etc. Weather related factors include wind speed, cloud level, total solar irradiation, rainfall, rural reference temperature. In this project, the following factors are investigated:

1. Sky view Factor
2. Distance and direction from city centre
3. Evapotranspiration fraction
4. Wind speed
5. Cloud level
6. Rural reference temperature
7. Wind direction and heat island centre

The relationship between different factors and the calculated urban heat island intensity will be investigated in this chapter. Correlation coefficients for each factor against UHI intensity will be shown and one tailed t-test will be performed to confirm

the significance of the data. Equation 7.1 was used to find the t-value for each case.

$$t = \sqrt{\frac{R^2(n-2)}{1-R^2}} \qquad \text{eq. 7.1}$$

Where R^2=coefficient of determination
n=number of samples

Similar to the previous chapter, the UHI intensities will be divided into daytime and nocturnal. The main focus will be upon winter and summer UHI intensity and causal factors' relations. Only UHI intensities calculated under clear and calm conditions will be used to so that the relations between UHI intensity and each factor will be seen more clearly.

7.2 Sky view factor (SVF)

7.2.1 Calculation of SVF

Sky view factor (SVF) is a fraction (varying between 0 and 1) used to describe how much sky could be seen at a point. It is the fraction of the total field of view which is visible sky.[117]. It is one method which is used to explain the geometrical characteristic of a street canyon. A low sky view factor means only a very small amount of sky can be seen at that point due to tall surrounding buildings. A high sky view factor (close to 1) is usually found in a rural area where a large area of sky can be seen. Johnson and Watson[118] (1983) defined that SVF is the ratio of long wave radiant flux reaching the sky vault from the flat floor of the canyon to that reaching the sky vault from an unobstructed flat surface. It is given by:

$$\psi s = \frac{1}{\pi R^2} \int_{Sv} \cos\varphi dS \qquad \text{eq.7.2}$$

Where ψs = the sky view factor [dimensionless]

φ = the angle between the canyon floor and the sky vault hemisphere radius to area dS [radians]

$dS = R^2 \sin(\varphi) d\varphi d\theta$ = the elemental area seen from the canyon floor [m^2]

θ= the azimuthal angle [radians]

R = nominal radius of the sky hemisphere [m]

Sv = the sky vault seen from the canyon floor

The SVF can be obtained from a hemispherical photograph. Hemispherical photographs can be made by using a fish eye lens to capture a 180^o image of the canyon. Supervision has been given to two undergraduate students, Danny Coles[119] (2010) and Daniel Reaney[120] (2009) on the how to take pictures with fish-eye lens (Nikon Coolpix 950 digital camera and Nikon FC-E8 fisheye lens) to obtain SVFs from the photos. Figure 7.1 shows a hemispherical photograph taken using a 180^o fish eye lens in one of the canyons in Manchester city centre.

Figure 7.1 Image captured by 180^{o} fish eye lens in street canyon of Manchester

The picture was processed with graphic software (Paint Shop Pro version 6.5) so that only black is left for all surrounding buildings and white for the sky (as shown in figure 7.2).

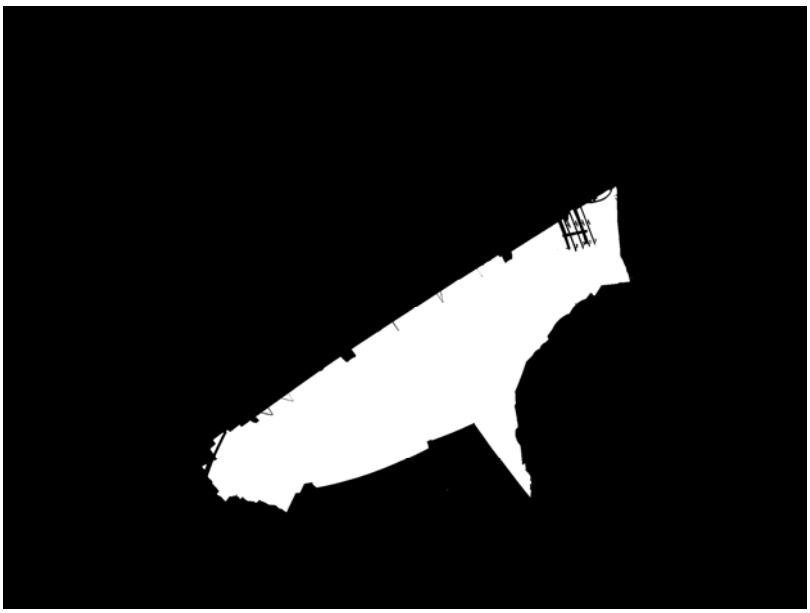

Figure 7.2 Black and white picture for analysing SVF

There are three calculation methods: Grimmond's Method[121], Chapman's method[122] and Coles' method[119] (using Matlab). The sky view factors for sensor-loggers in the

city centre for this project were also measured by Danny Coles[119]. The sky view factors used were calculated using the Coles' method which had higher resolution analysis, as well as using higher resolution (723823 pixels per image) photographs. This was because results from the other two methods have about 30% error as shown in figure 7.3. However, results found from Coles' method were in the middle of the other two methods for most of the cases. Both original equations used in Grimmond's and Chapman's methods were input into Matlab and it was found that an identical SVF result was found from both equations. Therefore it is believed that the 30% difference found between two methods was caused by using different number of annuli in their original programs. An annulus is the area between two different diameter concentric circles. A SVF program uses a number of these to calculate the SVF value. The more annuli a program uses, the higher the resolution and thus a better SVF value.

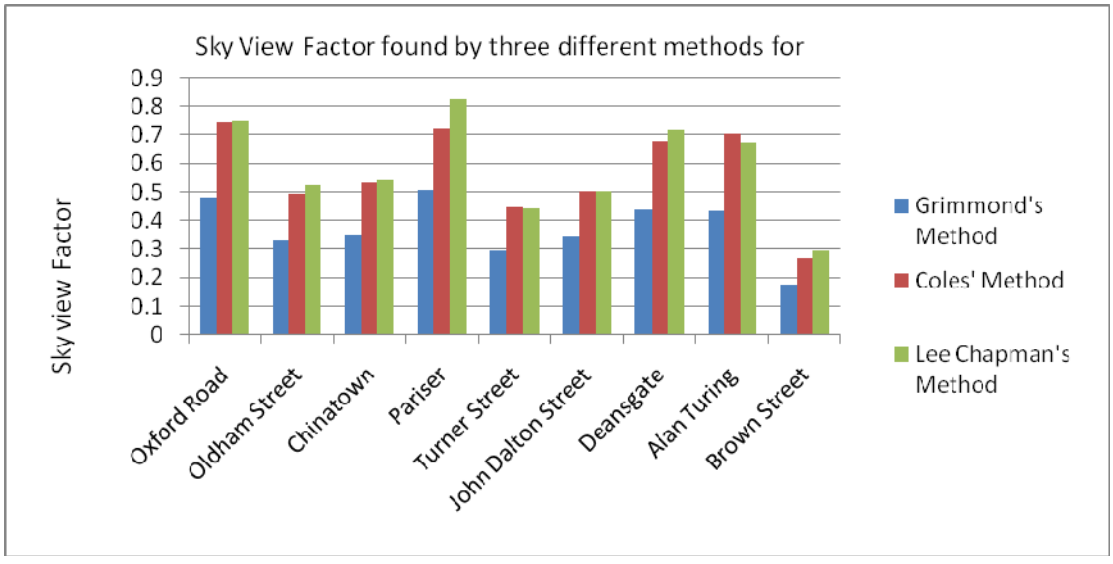

Figure 7.3 SVF found by three different methods for different street canyons[119]

A program written in Matlab software was then used to analyse the black and white

picture[123] and calculate the SVF.

Sky view factor is a very useful measure of the radiation exchange between the sky and canyon floor of a street canyon. Oke (1978)[1] provides data that shows a linear relationship between SVF and maximum UHI for a street canyon. He suggested the determination of SVF for a uniform street canyon is given by:

$$SVF = \cos\left[tan^{-1}\left(\frac{2H}{W}\right)\right] \quad \text{eq.7.3}$$

Where H=height of building in the canyon

W=Width of canyon

7.2.2 SVF and urban heat island

SVF values were found using the method mentioned in section 7.2.1 for all 59 monitoring stations. SVF was plotted against average UHI intensity for each site to investigate the correlation between them. T-tests were performed on each of the following graphs to prove the significance. Figures 7.4 and 7.5 indicate the relation between SVF and averaged UHI intensities for clear and calm summer days and nights.

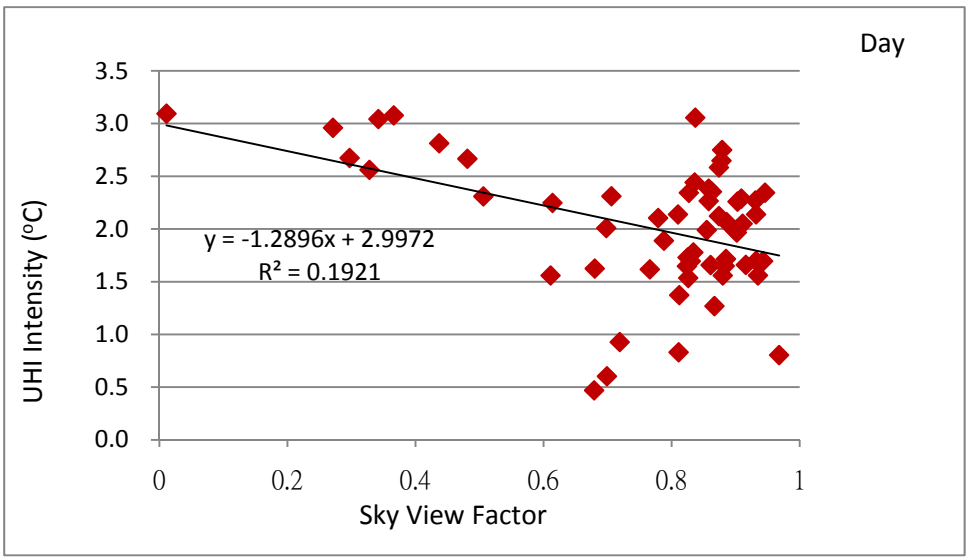

Figure 7.4 Averaged UHI intensity against SVF on clear and calm days during summer 2010 all 59 sites

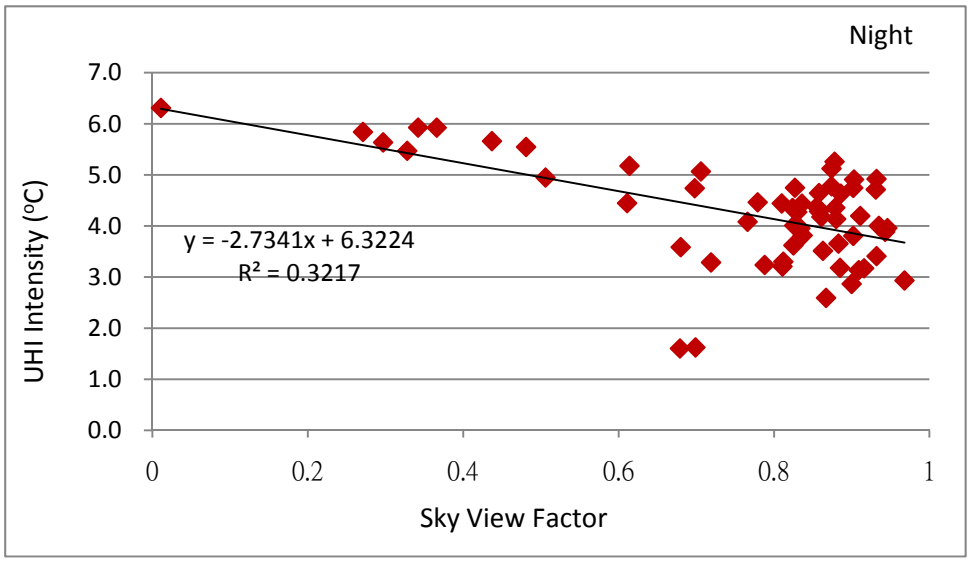

Figure 7.5 Averaged UHI intensity against SVF on clear and calm nights during summer 2010 all 59 sites

Figures 7.6 and 7.7 indicate the relation between SVF and averaged UHI intensity on clear and calm days and nights in winter.

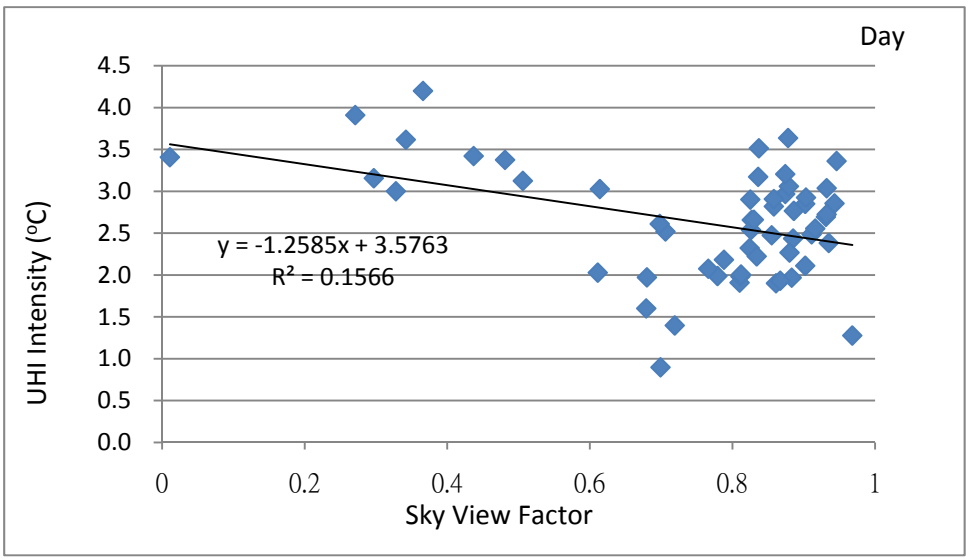

Figure 7.6 Averaged UHI intensity against SVF on clear and calm days during winter 2010 all 59 sites

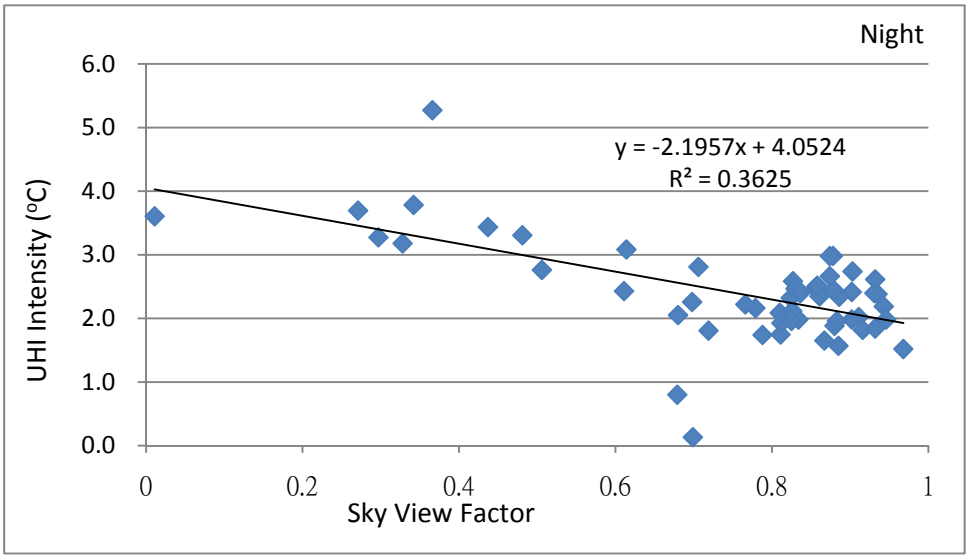

Figure 7.7 Averaged UHI intensity against SVF on clear and calm nights during winter 2010 all 59 sites

The following relations could be seen from the four graphs:

1. Urban heat island intensity reduces as SVF increases.
2. The correlation between SVF and UHI intensity was stronger for nocturnal than daytime.
3. The relations between SVF and UHI intensity were quite similar in winter and summer.
4. The relationships tend to be linear when SVF is smaller than 0.6.

5. UHI intensity does not go to zero when SVF=1.

Table 7.1 summarised the regression equations from figure 7.4 to 7.7.

Figure No	Season	Day/Night	Gradient	Intercept	R^2
7.4	Summer	Day	-1.29	2.997	0.192
7.5	Summer	Night	-2.73	6.322	0.322
7.6	Winter	Day	-1.26	3.576	0.157
7.7	Winter	Night	-2.20	4.052	0.362

Table 7-1 Summary of SVF regression equations from figure 7.4 to 7.7

7.2.3 Discussion

Negative relations were found in all four graphs. This suggests that the urban heat island intensity tends to increase when SVF decreases. A decrease in SVF means a reduction of visible sky area from the canyon. Therefore, less long wave radiation was lost to the sky. During daytime, short wave radiation entered the canyon dependent on the cloud level and other canyon property such as orientation. The effect of SVF was not dominant. This is the reason for a stronger relation between SVF and UHI intensity during the night than daytime. The UHI intensity does not go to zero when SVF=1. This is similar to the previous literature findings mentioned earlier in chapter 3 equations 3.1 to 3.6.

The relation between SVFs and the UHI intensity tend to be linear when the SVF is smaller than 0.6 as shown in figure 7.4 to figure 7.7. Data were reselected and SVFs smaller than 0.65 were plotted against UHI intensity as shown in figures 7.8 and 7.9 for clear and calm summer and winter nights 2010.

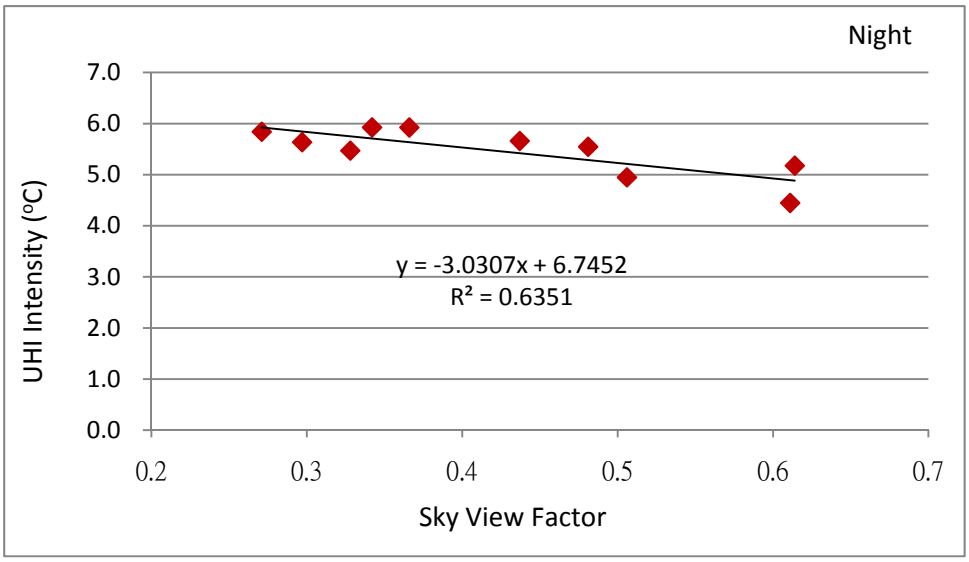

Figure 7.8 UHI intensity against SVF smaller than 0.65 on clear and calm nights during summer 2010 10 sites

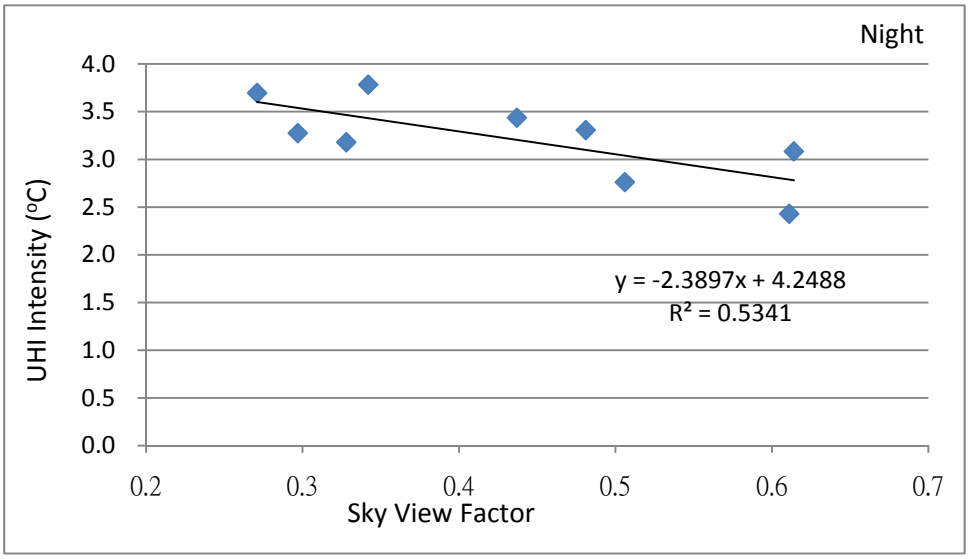

Figure 7.9 UHI intensity against SVF smaller than 0.65 on clear and calm nights during winter 2010 9 sites

There was data loss in the winter graph because one of the monitoring stations was not working in early winter of 2010. There was also a point with a low SVF because it was located under a railway bridge and data from this point was eliminated because it did not behave like a normal canyon. It can be seen from figures 7.8 and 7.9 that SVF has a better linear relationship (with higher R^2 values) on UHI intensity at night in both seasons inside the canyon. This suggests that for locations with larger SVF (more rural areas), the effect of SVF would be diminished and outweighed by other factors.

It can also be seen that the relationship between SVF and UHI intensity does not drop to zero if SVF is equal to 1. Literature mentioned previously in sections 3.3 (equation 3.2, 3.3, 3.5 and 3.6) also indicated a similar linear relationship. This is believed to be due to co-existing effects from other factors such as evapotranspiration fraction and anthropogenic heat.

Although a stronger relation could be seen for small SVF values against UHI intensity, there are also other factors affecting the UHI intensity at the same time during the measurement. It will be ideal if other factors such as distance away from city centre, evapotranspiration fraction etc were also controlled. This would require more data points installed in different canyons to obtain a greater range of SVFs for future investigation.

7.3 Distance and direction away from city centre

Distance is one of the important factors contributing towards urban heat island effect. The effect of direction is more dependent on local urban morphology type compared to distance. There are 48 sensor-loggers places at equally spaced radial distance over Greater Manchester. In this section, the distance and direction effect will be investigated.

7.3.1 Distance away from city centre

Similar to the analysis of SVF, only the data for clear and calm periods were used to minimise the influence caused by other weather parameters. The clear calm periods

were divided into daytime and nocturnal. T-tests were performed in each case to prove its significance at 95% level. Figures 7.10 and 7.11 show the relationship for the average heat island intensities against radial distance away from city centre during the summer. Figures 7.12 and 7.13 indicate a similar relation for clear and calm winter. It could be seen that the heat island intensity tends to reduce with increasing distance from city centre.

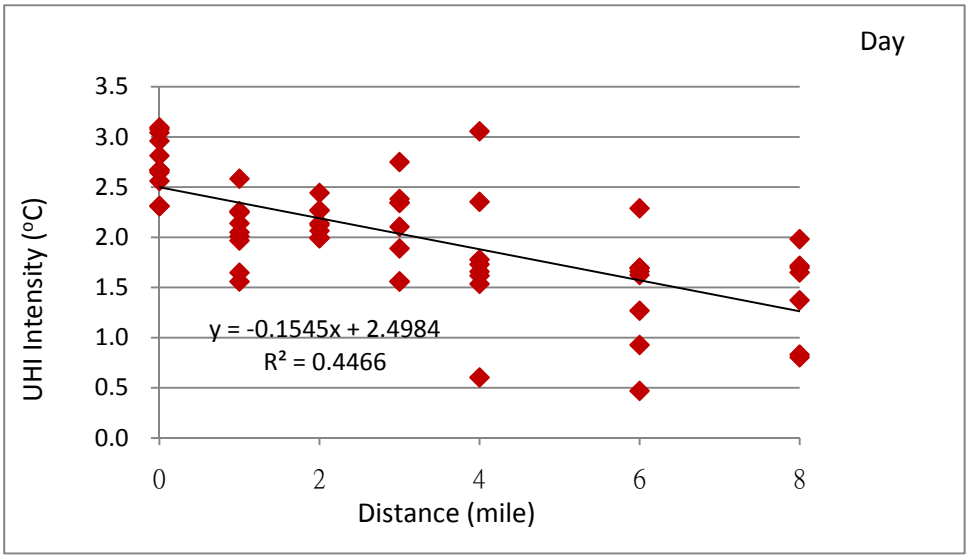

Figure 7.10 Averaged UHI intensity against distance from city centre on clear and calm days during summer 2010 all 59 sites

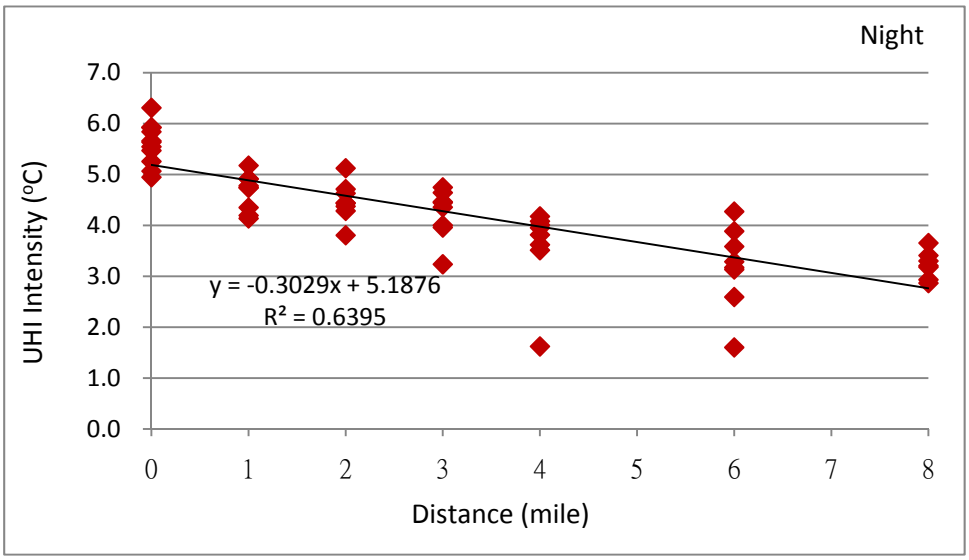

Figure 7.11 Averaged UHI intensity against distance from city centre on clear and calm nights during summer 2010 all 59 sites

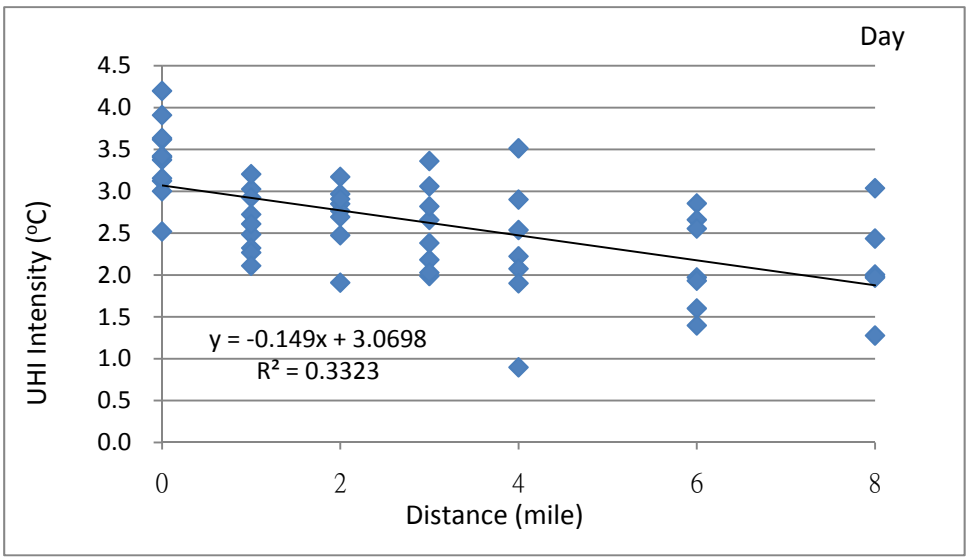

Figure 7.12 Averaged UHI intensity against distance from city centre on clear and calm days during winter 2010 all 59 sites

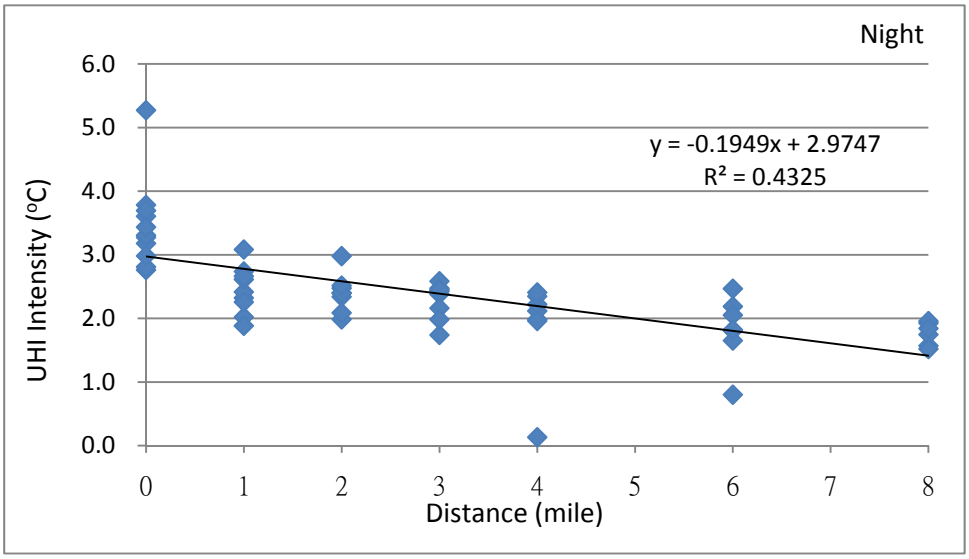

Figure 7.13 Averaged UHI intensity against distance from city centre on clear and calm nights during winter

The following relations could be observed from the graphs above:

1. Distance from city centre has a negative linear relation against UHI intensities.
2. The distance effect at night was stronger than daytime for both seasons.
3. The UHI effect does not disappear at the edge of the urban area, eight miles from the city centre.

A linear negative effect was found between distance from city centre and averaged UHI intensity. This indicates that the UHI intensity would decrease as one moves further away from city centre. These results agree with the distance decay function found by Smith *et al.,*[73] (2009). The distance effect is considered to be a combined effect of other factors. For example further from the city centre, there would be fewer canyons, so the SVF would reduce. The density of building would be different. The percentage of vegetation would also be different. It is also expected that there will be less traffic and lower occupancy density as the distance away from city centre increases. The correlation coefficient for nocturnal UHI intensity was stronger than the daytime. There is a similar relationship between SVF and UHI intensity as found in the earlier section. A very similar relationship between UHI intensity and distance away from city centre was also found by Watkins[44] (2002) in London. The UHI effect does not disappear at the eight mile from the city centre limit of the sensor-loggers probably because of the sub-urban sprawl, as Oke's[1] work showed (the "cliff" in figure 6.3).

7.3.2 Direction

Sensor-loggers were placed at eight different directions from city centre of Manchester. In this section, the effect of direction will be investigated. Direction from city centre can be a localised factor contributing towards urban heat island effect. The geographic characteristics in different directions might contribute towards different localised weather. Such geographic characteristics are very specific to the measurement locations.

Figures 7.14 and 7.15 show the averaged UHI intensity against distance away from the city centre in each direction for clear and calm summer and winter nights.

Daytime results are not presented here because there was no significant relation found. An averaged UHI intensity value from all city centre sensors was used on the graphs for zero distance. There were only five sensor-loggers long the West direction and there were only three sensor-loggers in northern east direction in winter. Therefore, there is no northern east direction shown on figure 7.15

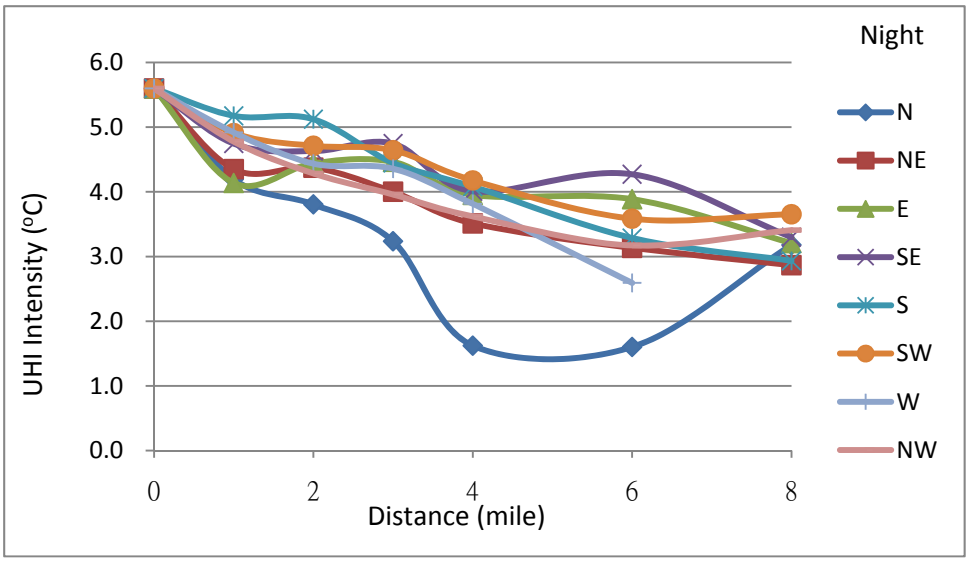

Figure 7.14 Averaged UHI intensity against distance from city centre in different direction on clear and calm nights during summer 2010 all 59 sites

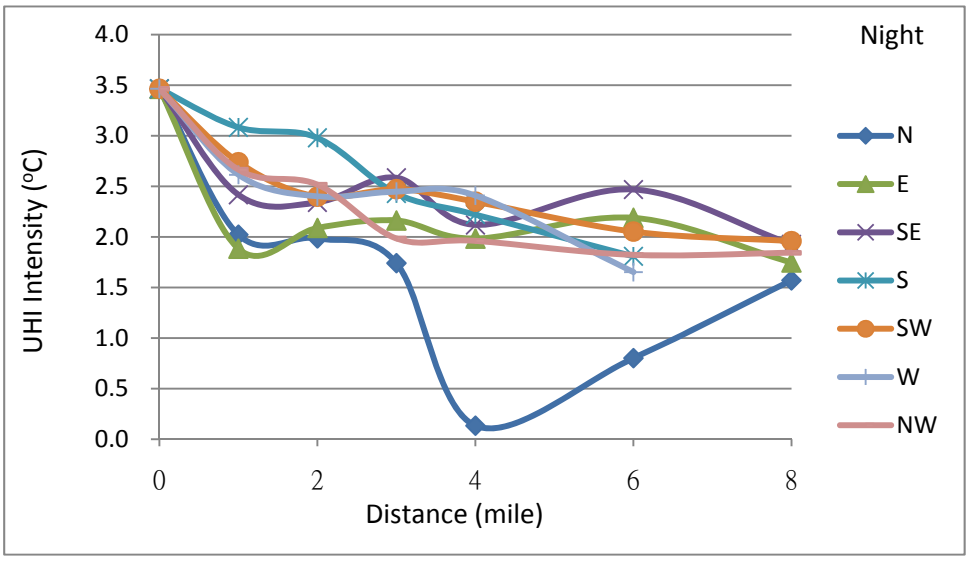

Figure 7.15 Averaged UHI intensity against distance from city centre in different direction on clear and calm nights during winter 2010 all 59 sites

Figures 7.14 and 7.15 have very similar patterns. UHI intensities show a general

pattern of dropping as the distance increase in almost all directions. However, a few points to be noticed are as follows:

1. There were large drops at four miles away from city centre on the Northern direction on both graphs. The UHI intensities then rose again thereafter.
2. UHI intensities were higher at six miles away from city centre on the southern east direction compared to the point at four miles away from city centre in the same direction.
3. UHI intensities were lower at one mile away from city centre on east direction compared readings thereafter.

In order to explain these anomalies, the actual types of land use have to be investigated. Evapotranspiration from vegetation can reduce temperature in the local area. Heaton Park is located about four miles North of Manchester city centre and is probably responsible for the large dip on the North graph in figure 7.15. This will be discussed in the next section. Six miles away from city centre on the southern direction is Stockport city centre. There are significant street canyons and a larger urban mass in Stockport town centre and this probably explains the higher UHI intensities shown at six miles in the south eastern direction. Finally, one mile from the city centre in the east is a large piece of un-used grass land. Similar to the effect of a park, the temperature here is slightly lower. The direction from the city centre affects the UHI intensities due to the local urban morphology. Watkins *et al,,*[12](2002) found similar differences between East and West London. Nevertheless it is generally true that the UHI effect drops with distance away from the city centre for all directions in Greater Manchester.

7.4 Urban morphology type (UMT) and evapotranspiration fraction

It was suggested in the last section that the type of land use might affect the UHI intensity reduction pattern over distance. In this section, the urban morphology type will be introduced. Investigation will be carried out on the evapotranspiration fraction (EF) of the urban morphology type around different sensor-loggers.

7.4.1 Urban morphology type (UMT)

There are 13 primary categories of urban morphology type (UMT) and 29 detailed categories identified initially by Land Use Consultants[124] (1993) and shown in figure 7.16. The UMTs used in this project were provided by S Gill (ASCCUE Project) in ArcGIS format. Figure 7.16 shows the Greater Manchester UMT map (originally developed by Susannah Gill[125]) used for this project.

Previous studies [V Whitford[102] (2001), S Gill[101] (2009)] indicated that green space areas had an important influence on the urban surface temperature. In this project, the relation between the averaged UHI intensity and the ratio of green areas will be investigated.

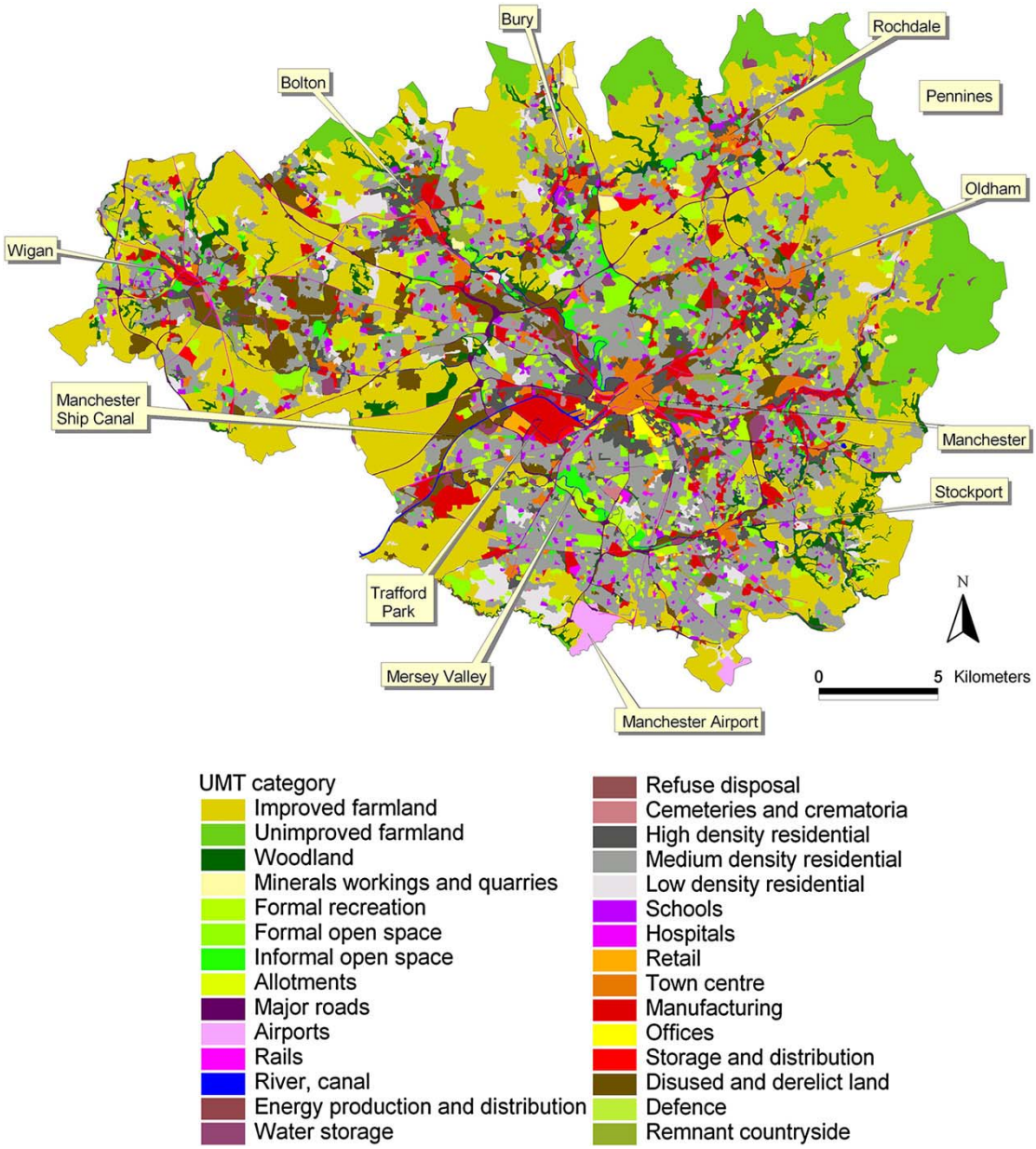

Figure 7.16 UMT map for Greater Manchester[101]

The detailed UMT category for each sensor-logger was first identified by over laying the sensor-logger location map with the UMT map in ArcGIS. The area ratio for four vegetation types (tree, shrub, meadow grass and rough grass) is calculated within each UMT category polygon. The total evapotranspiration fraction (EF) equals the sum of area ratios of all four vegetation types. Table 7-2 indicates all UMTs and their relative evapotranspiration fractions.

UMT	EF	UMT	EF
Town centre	0.2	Rail	0.47
Manufacturing	0.29	Medium Dense Residential	0.5
Storage and Distribution	0.3	Low Dense Residential	0.66
High Dense Residential	0.31	Formal Open space	0.9
Major Road	0.37	Informal open space	0.94
Office	0.45	Improved farmland	0.95

Table 7-2 UMT categories and their relative evapotranspiration fraction

Some of the sensor-loggers were located very close to another UMT on the map, therefore, in order to average the effect due to a different UMT, a 100 metre buffer zone was drawn around each sensor-logger on the map in ArcGIS as shown in figure 7.17.

Figure 7.17 100 meter buffer zone around each sensor-logger

An average EF value was calculated from all the UMTs included inside each 100 metre buffer zone. The elliptical shape of the buffer zone shown in figure 7.17 was due to the different national grid system used in GIS software. EF is only the sum of area ratios of all four vegetation types. It would be ideal if the area of the lands next to the sensor-logger was known for calculation purpose. Nevertheless, EF is the only parameter available for this project regarding vegetation.

The relationship of UHI intensities against EF values on clear and calm day and night for summer and winter were examined. Figures 7.18 to 7.21 show the averaged UHI intensity against EF on clear and calm day and night for summer and winter.

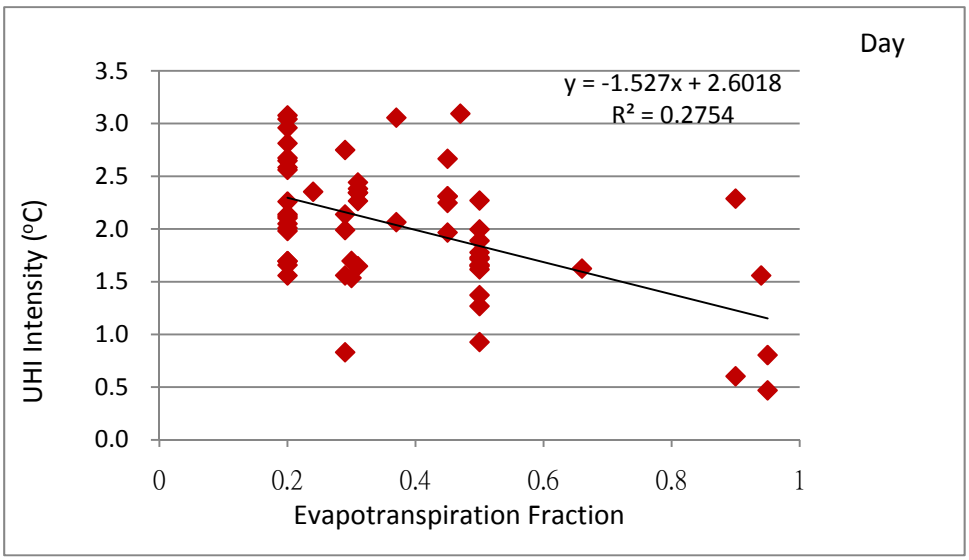

Figure 7.18 Averaged UHI intensity against evapotranspiration fraction on clear and calm summer days 2010 all 59 sites

It can be seen from the above figures that the relation between UHI intensity and EF is slightly stronger for night-time than daytime. This is similar to the relation mentioned in the earlier sections. A straight line of best fit was drawn, however, it does not show a high R^2 value although a t-test confirms the significance between UHI intensity and EF at the 95% confidence level. The heat island intensity reduces as the evapotranspiration fraction increases. This shows a similar trend to the previous studies done by Gill[125] and Whitford[101].

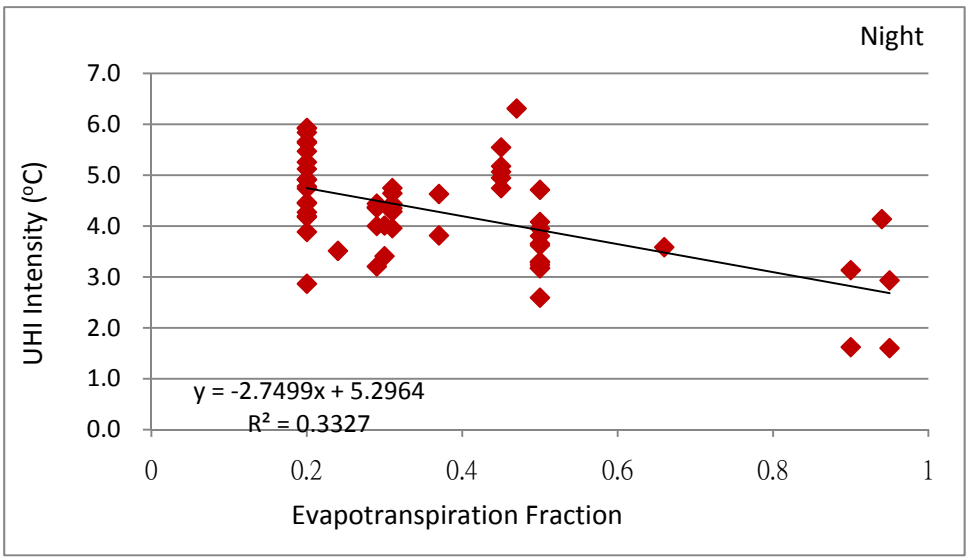

Figure 7.19 Averaged UHI intensity against evapotranspiration fraction on clear and calm summer nights 2010 all 59 sites 2010

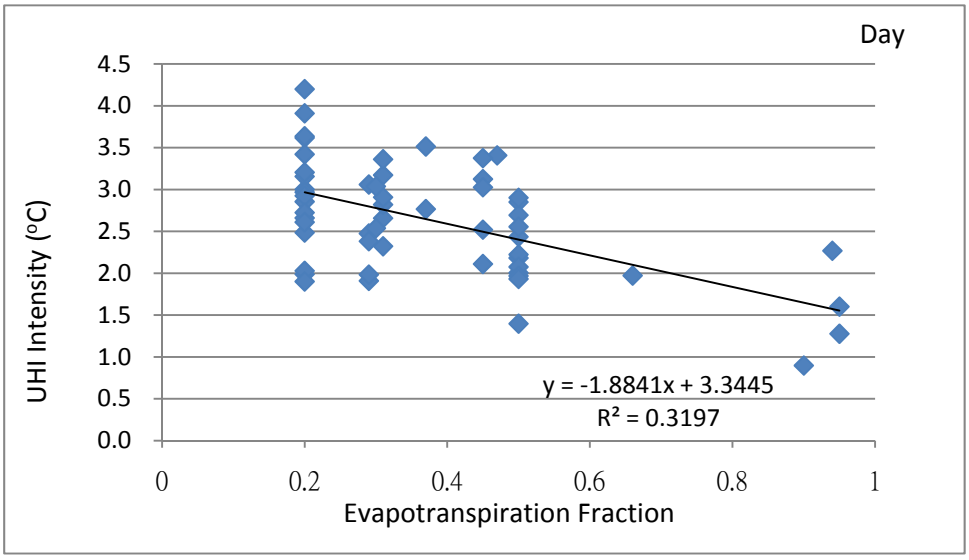

Figure 7.20 Averaged UHI intensity against evapotranspiration fraction on clear and calm winter days 2010 all 59 sites

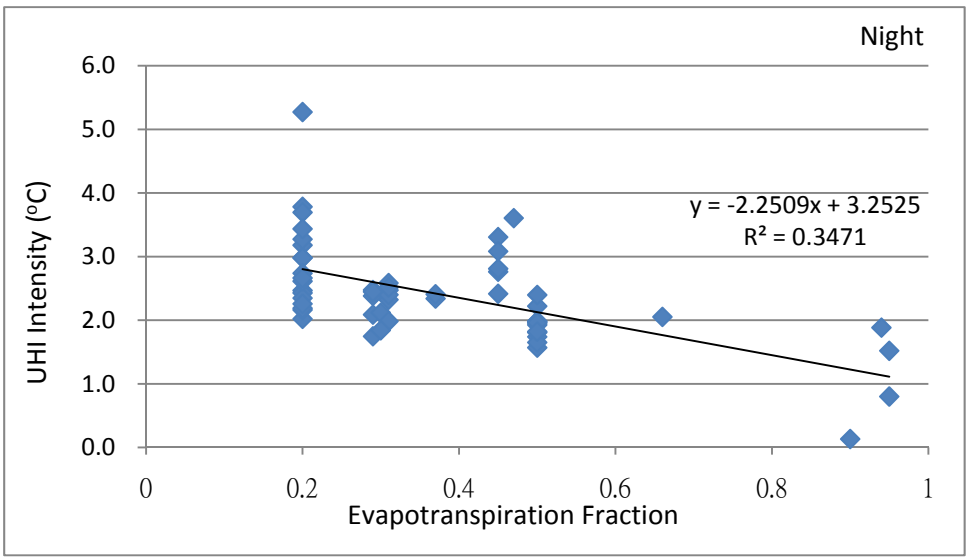

Figure 7.21 Averaged UHI intensity against evapotranpiration fraction on clear and calm winter nights 2010 all 59 sites

In their work, they studied the EF effect with the surface temperature rather than the air temperature. This might explain the relatively lower impact of EF on air temperature due to the fact that surface temperature tends to vary quicker than air temperature. Although evapotranspiration fraction has an impact on UHI intensity, compared to other causal factors, such as the distance from city centre and SVF, it does not correlate to UHI intensity as much as the other factors (indicated by the R^2 values). The evapotranspiration fraction has a negative relation to UHI intensity.

7.5 Wind speed

Wind speed data were obtained from three Met Office weather stations close to Manchester: Woodford, Ringway and Hulme. However, only Woodford station had the full set of weather data including cloud level and rainfall. Therefore, all the weather data used in this project was from Woodford station unless otherwise specified for consistency.

In the previous sections, urban heat island in Greater Manchester was analysed using clear and calm days so that the effect of wind could be minimised. However in this section, the relation between wind speed and UHI is examined. In order to eliminate the influence of other factors and maximise the UHI effect, clear periods were selected. The half hourly average temperatures for all sensor-loggers in the city centre were calculated, and the UHI intensities found. It was suggested from the previous section that nocturnal relation between weather parameters and UHI intensities were stronger than daytime. Therefore, only the nocturnal relation was investigated here. Figure 7.22 shows the heat island intensities against different wind speeds during clear summer nights. Figure 7.23 indicates the average heat island intensities against different wind speed on clear nights in winter.

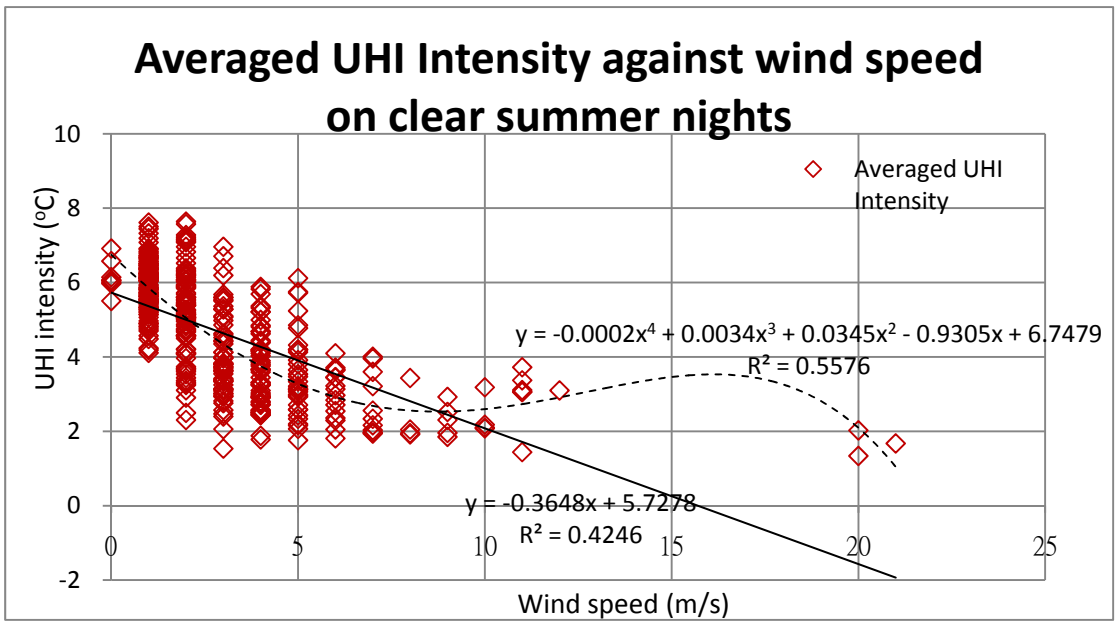

Figure 7.22 Averaged UHI intensity against wind speed on clear summer nights 2010 all 59 sites

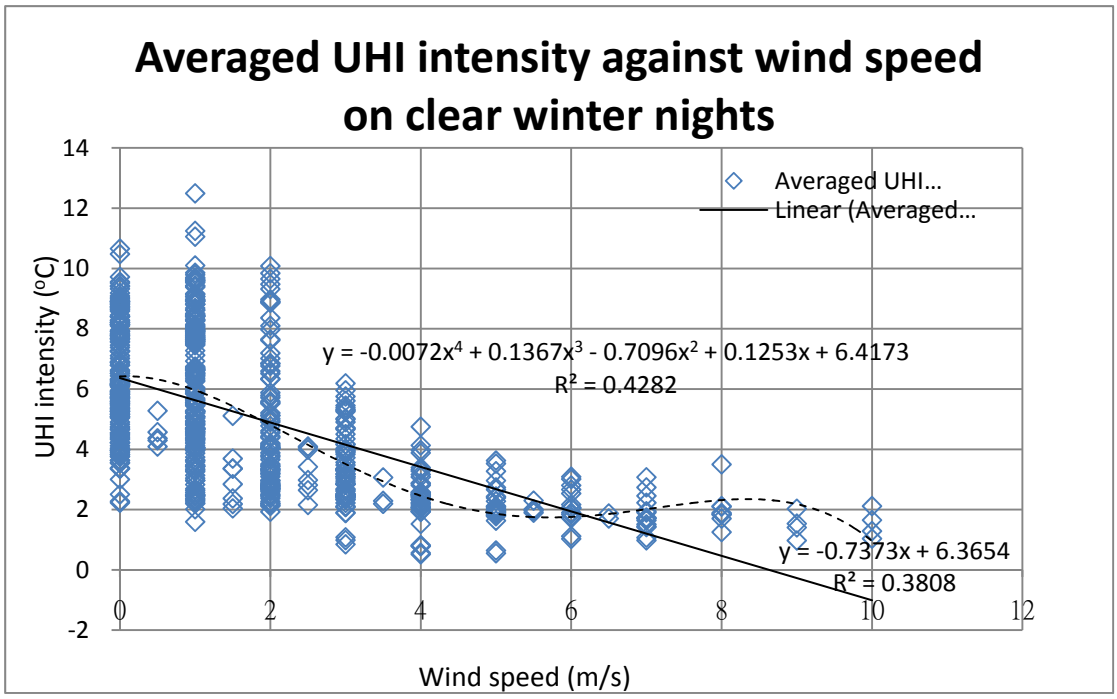

Figure 7.23 Averaged UHI intensity against wind speed on clear winter nights 2010 all 59 sites

It can be seen that the urban heat island intensity reduces as the wind speed increases. According to Erell *et al.,*[126] (2007), a UHI intensity of 2°C would rarely occur if the wind speed is higher than 2ms^{-1}. Nevertheless, heat island intensity higher than 4°C could still been seen in both figures for wind speeds higher than 2ms^{-1} in Greater Manchester. A polynomial regression line is the best fit with a variance of 55% in summer and 42% in winter. Such a finding is in line with the result from C Morris *et al.,*[30] (2001) who also suggested the UHI was inversely proportional to the fourth power of the wind speed and cloud cover. However, the secondary maxima that is located at a relatively high wind speed in both figures 7.22 and 7.23 does not seems to be accurate. Therefore a straight trend line was fitted to both graphs with a negative relationship with wind speed (less than 10ms^{-1}) was considered more appropriate. This relationship tends to become constant after 10ms^{-1} (this is discussed further in the next chapter of multiple regression model) reflecting the fact that the urban heat island effect tends to disappear as the wind speed increases (see Figure 7.24). Wind

promotes the removal of heat at a much quicker rate in comparison to calm conditions.

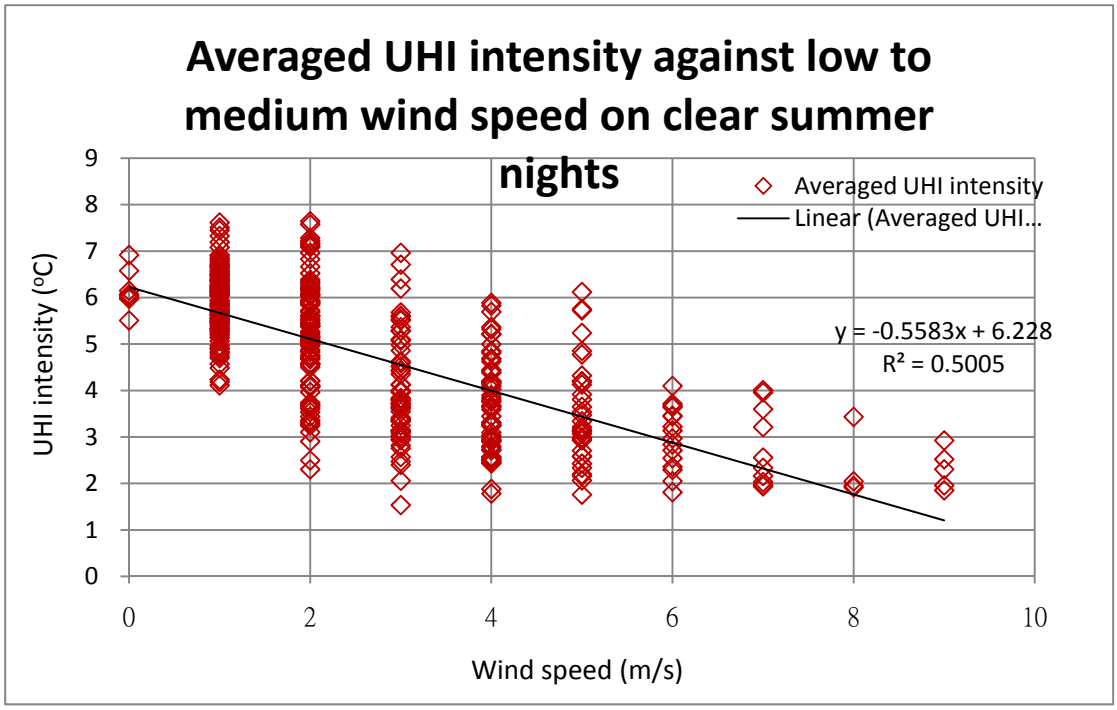

Figure 7.24 Averaged UHI intensity against low to medium wind speed 2010 all 59 sites

By comparing figures 7.22 and 7.24, it can be seen that the correlation coefficient increases from 42% to 50%. Unfortunately, the clear days in winter 2010 tended to be windless and there were no nights with high wind speed data for comparison. In conclusion UHI intensity tends to have a negative relation with low to medium wind speeds. The relation tends to constant at a high wind speed. Similar relationships were also found by Watkins[113] (2002). Giridharan and Kolokotroni[43] (2009) and Kolokotroni and Giridharan[42] (2008) divided wind speed into three sections, and their result also indicated urban heat island tends to be larger under low wind speed conditions.

7.6 Cloud cover level

Cloud level data was obtained from the Woodford Met Office observation station. It is

measured in oktas (eighths) varying from zero (clear) to eight (fully overcast). Only calm periods were used, to eliminate the influence of wind speed. Only nocturnal UHI intensities are shown for summer and winter because nocturnal UHI intensity are much larger than daytime values. Figures 7.25 and 7.26 show the averaged UHI intensities against cloud level on calm summer and winter nights respectively.

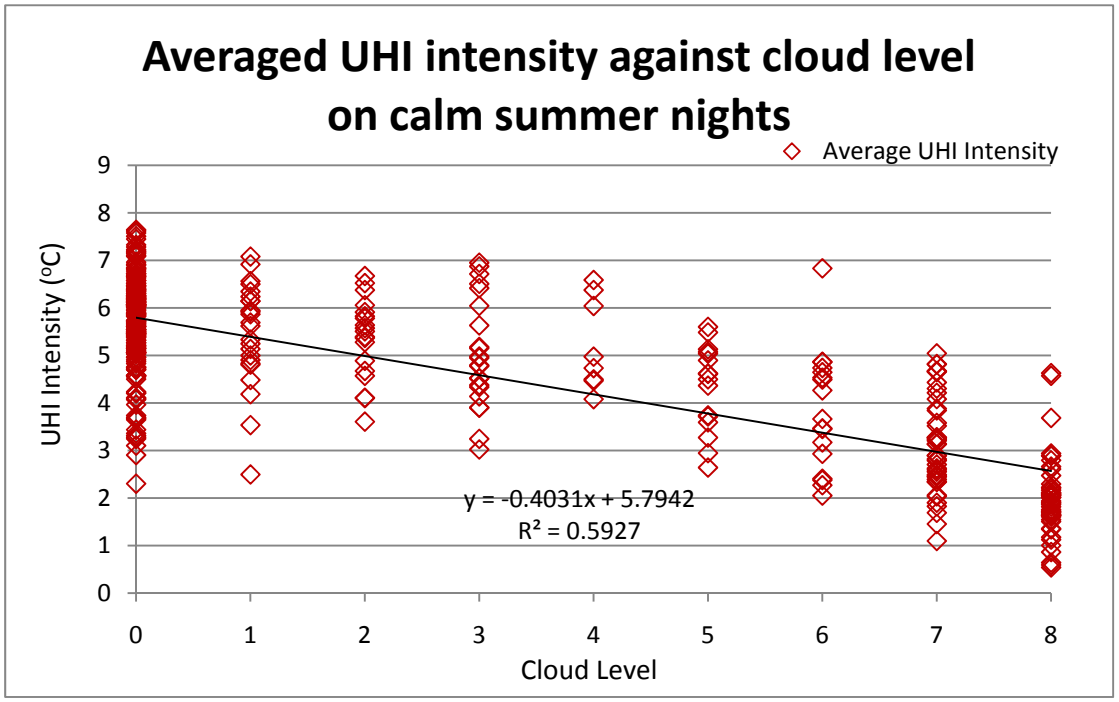

Figure 7.25 Averaged UHI intensity against cloud cover level on calm summer nights 2010 all 59 sites

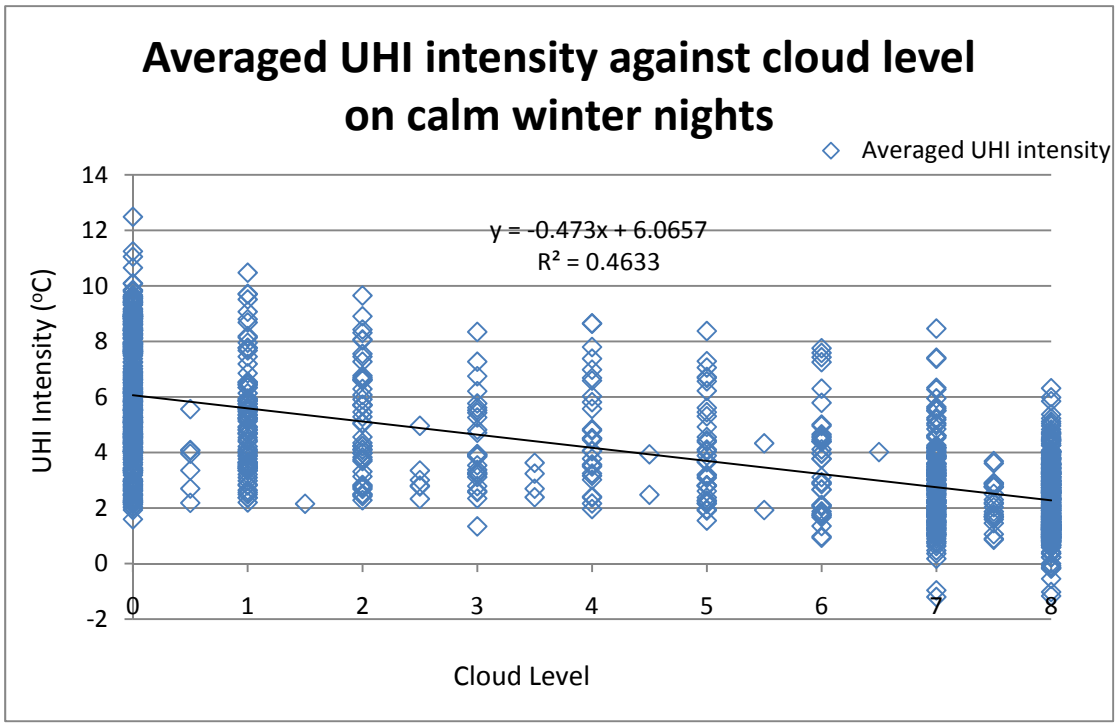

Figure 7.26 Averaged UHI intensity against cloud cover level on calm nights in winter 2010 all 59 sites

Both graphs indicate a negative linear relation between cloud level and UHI intensity on calm nights (R^2= 59% in summer and 46% in winter, significant at 95% level). The urban heat island effect tends to diminish as the cloud level increases during the night because the rural area does not cool so rapidly. A fourth power polynomial was suggested by C Morris *et al.,*[30] (2001) which is found to give a similar R^2 for the Manchester data. Giridharan and Kolokotroni[43] (2009) and Kolokotroni and Giridharan[42] (2008) divided cloud cover level into clear sky, partially cloudy and cloudy. Their results also show that urban heat island intensity is higher when there is a clear sky.

7.7 Rural reference temperature

The relation between averaged UHI intensity and rural reference temperature for clear and calm nights on summer and winter is shown in figures 7.27 and 7.28 respectively.

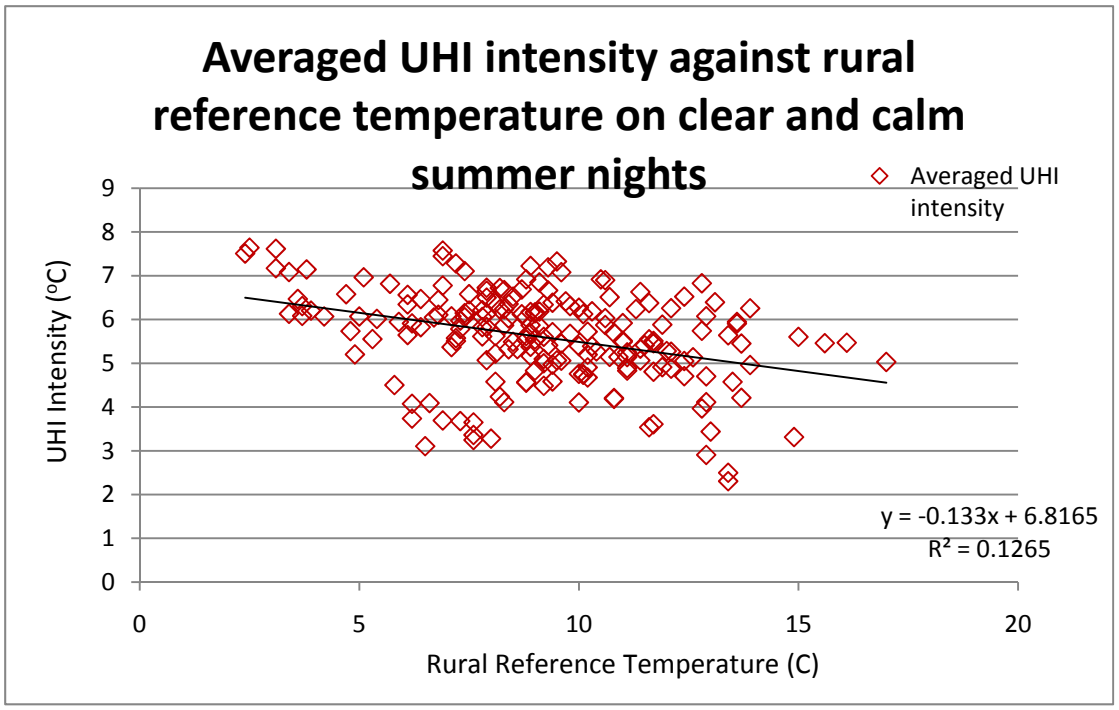

Figure 7.27 Averaged UHI intensity against rural reference temperature on clear and calm summer nights 2010 all 59 sites

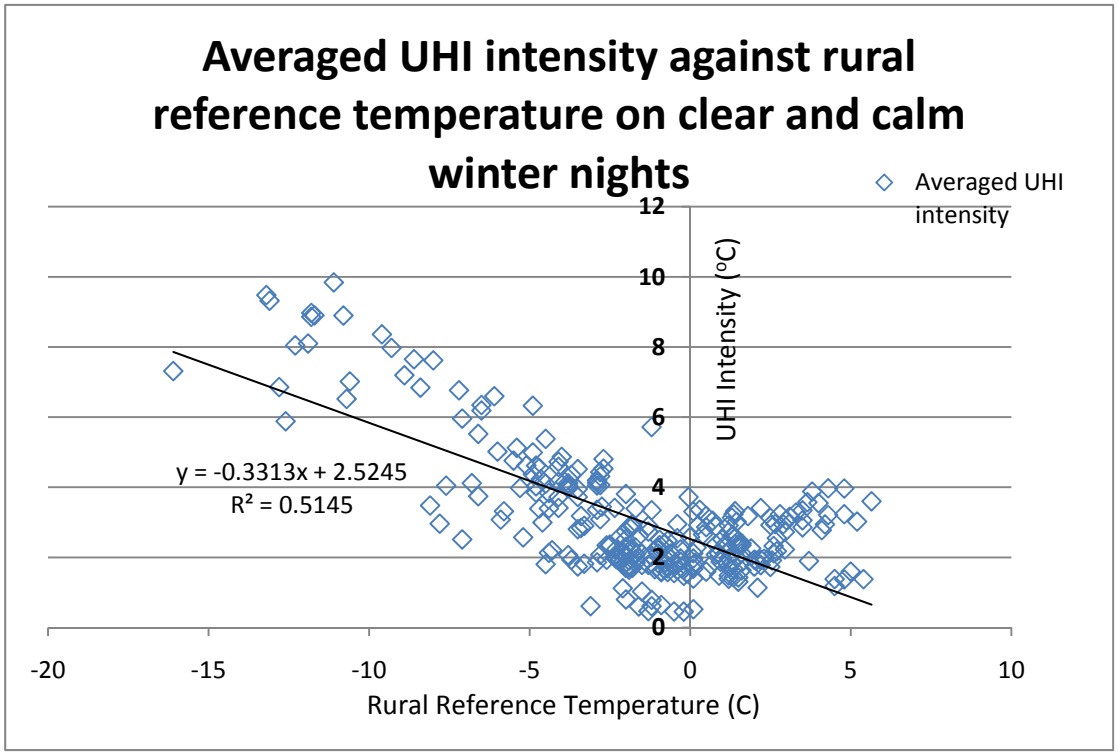

Figure 7.28 Averaged UHI intensity against rural reference temperature on clear and calm winter nights 2010 all 59 sites

It can be seen that the R^2 (12.7%, significant at 95% level) for the summer data is much lower than for the winter (51%, significant at 95% level). This means the

relation is stronger when the rural reference temperature is low. The relationship between rural air temperature and UHI intensity has a strong linear relation at very low rural reference temperature (smaller than 3°C) while the relation tends to be constant thereafter. Figure 7.29 shows a similar graph with a data from the lowest rural reference temperature up to 3°C. The R^2 is 62% in figure 7.29 which confirms the strong correlation at cold rural reference temperatures. One reason was believed to cause a strong relation between UHI intensity and low rural reference temperature is that the output of heating systems in buildings are all at maximum output when the air temperature is very cold. The anthropogenic heat flux therefore increases a lot under extremely cold weather and thus, urban heat island effects become more dominant.

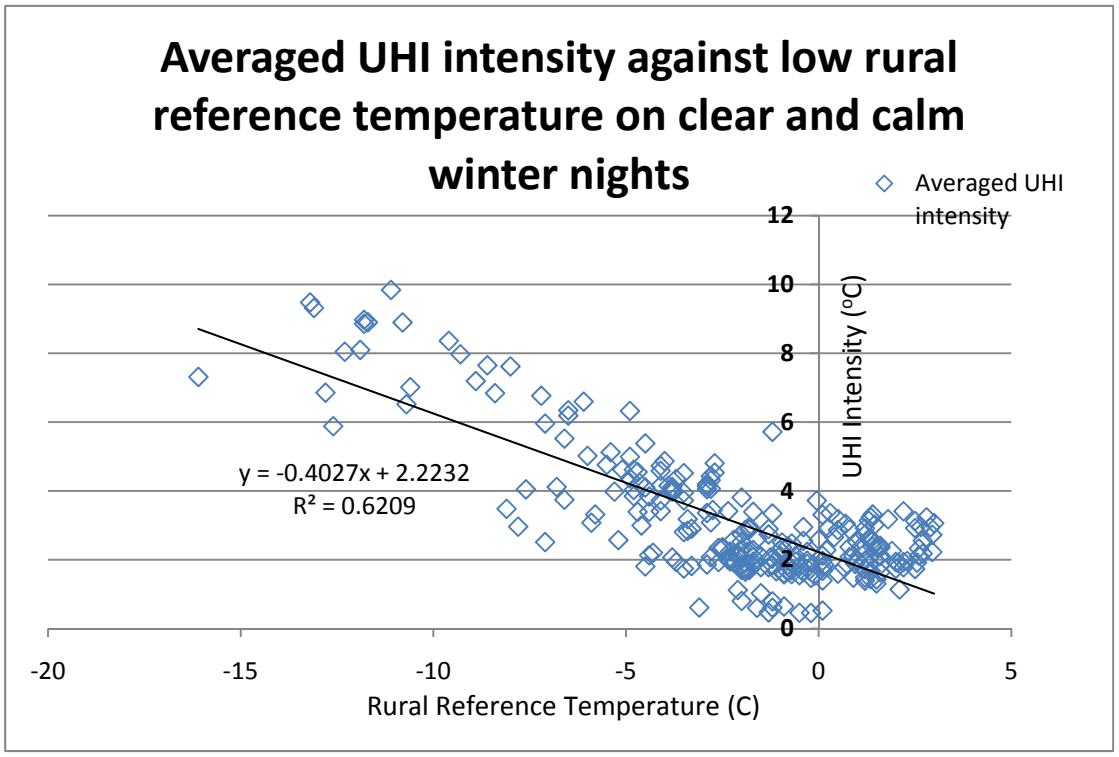

Figure 7.29 Averaged UHI intensity against low rural reference temperature (3°C) on clear and calm winter nights

7.8 Wind direction and heat island centre

In order to visualise the actual heat island effect, temperature / heat island intensity contours have been created. In this section, the process of creating the contours and the results are presented and discussed.

7.8.1 ArcGIS and Kriging

A Geographical Information System (GIS) is a system which can manage, analyse, access, store, manipulate and display geographic information[127]. This information could be spatial data which contain a position in space such as geographic location or non-spatial data such as temperature or population.

Temperature mapping was performed using GIS software so that the temperature / heat island intensity pattern over Greater Manchester could be seen. ArcGIS was selected because it was already purchased by the University of Manchester and could be used free of charge.

The latitude and longitude of each sensor-logger was already recorded by a GPS (Geko 310) device during data collection. A shape file which could be recognised by the GIS software was automatically created when spatial data was extracted from GPS to computer. Sensor-logger numbers were added into the shape file along with the spatial data. Maps of all the roads of Greater Manchester were obtained from Claire Smith[128]. The location of sensor-loggers could be seen after over-laying the map of the roads onto the sensor-logger shape file.

In order to create the temperature contours, temperature data had to be uploaded into the GIS software with reference to the sensor-logger numbers. Excel files of hourly temperature data was created with two columns, the sensor-logger number and the temperature at a particular hour. Temperature data for each hour had to be copied into separate excel file because the GIS software could only recognise excel files with no more than two columns. The Excel file was then joined into the sensor-logger shape file.

There were 44 sensor-loggers located in eight radial transect directions. Suitable interpolation had to be performed to find out the overall temperature pattern of Greater Manchester. Kriging, an interpolation method, was used here in the project as other interpolation methods, such as inversed distance weighting (IDW), only estimate based on the relation between the estimated point and other known points. However, Kriging also takes account of the relation between all known points (see Appendix J based on communication from Dr. J Parkinson[111]).

All of the above procedures were performed automatically within the GIS software which produced a temperature mapping output with different colours indicating the temperature differences. Finally contour lines were added with a relative temperature scale. The colour pattern was then removed because the temperature scale of the colour pattern was estimated by the maximum and minimum values of each map (each hour) and the 24 maps for one day would have 24 different temperature colour scales. The temperature/UHI intensity can be read off from the contour lines directly. The map was exported in JPG format. In addition, weather data such as wind direction, average wind speed and cloud cover were added onto the contour diagram to provide

more information.

Figure 7.30 shows an example of the temperature contour map. Due to the irregular sensor-logger location pattern in the city centre, all the readings from city centre sensor-loggers were removed so that the contour pattern would be more regular to ease analysis.

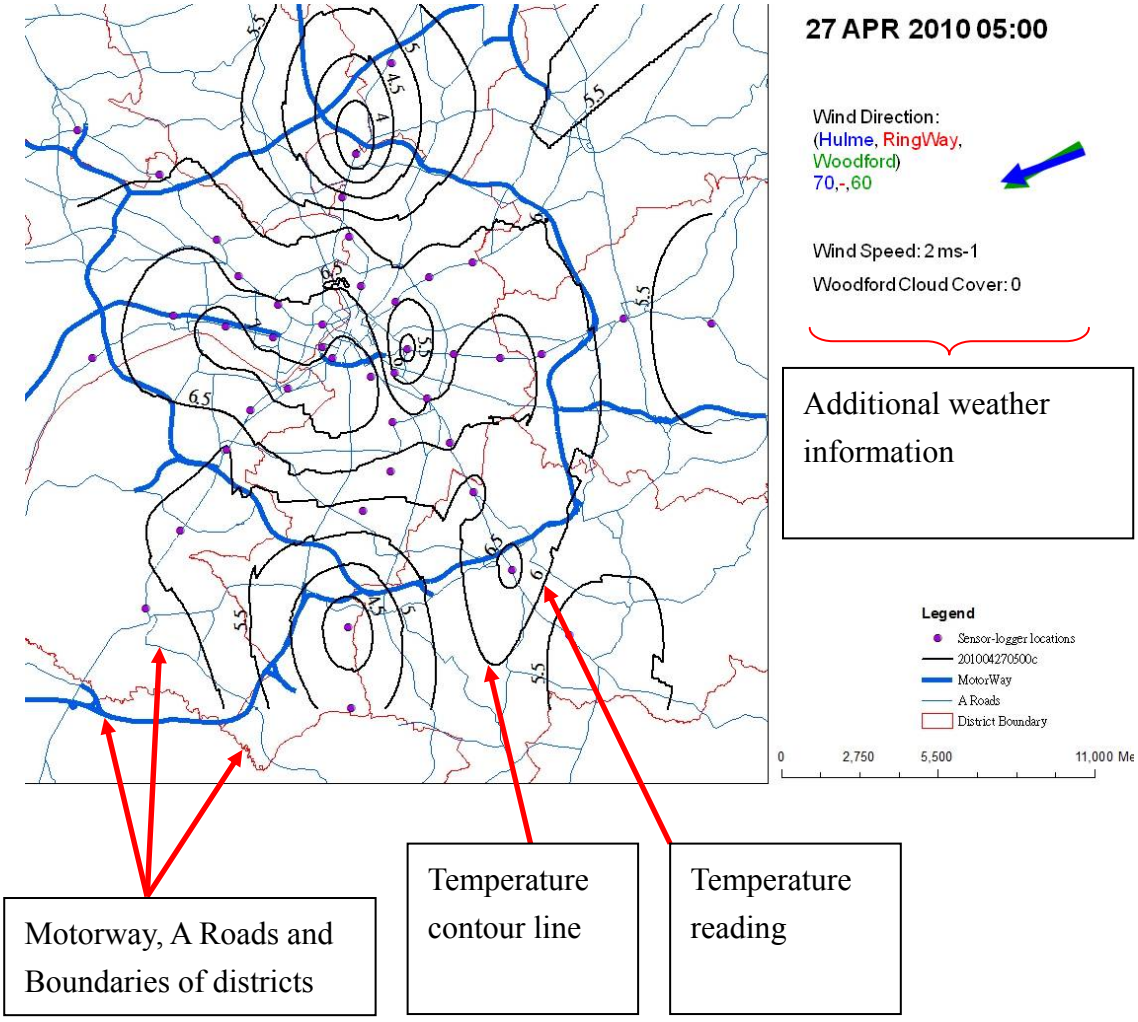

Figure 7.30 Example of temperature contour map

7.8.2 Results and discussion

Before creating temperature/UHI intensity contours from the actual data, the accuracy of the Kriging ability in the GIS software had to be validated. Figure 7.31 shows UHI

intensity contours created from dummy data. It can be seen that one sensor-logger (at three mile from city centre on SW direction) was missing. All sensor-loggers were reset with dummy temperature data, so that, all sensor-loggers at the same radial distance from city centre had the same temperature, starting with 6°C for all sensor-loggers one mile from city centre. Sensor-loggers one mile further out were set at 5°C and so on. Kriging was then performed in GIS software and it could be seen that regular circular contours were produced. It can also be seen that the contour line passing the missing sensor-logger was of 4°C which is exactly the correct temperature for this location. In conclusion, the Kriging calculation performed in the GIS software has been confirmed to be working correctly.

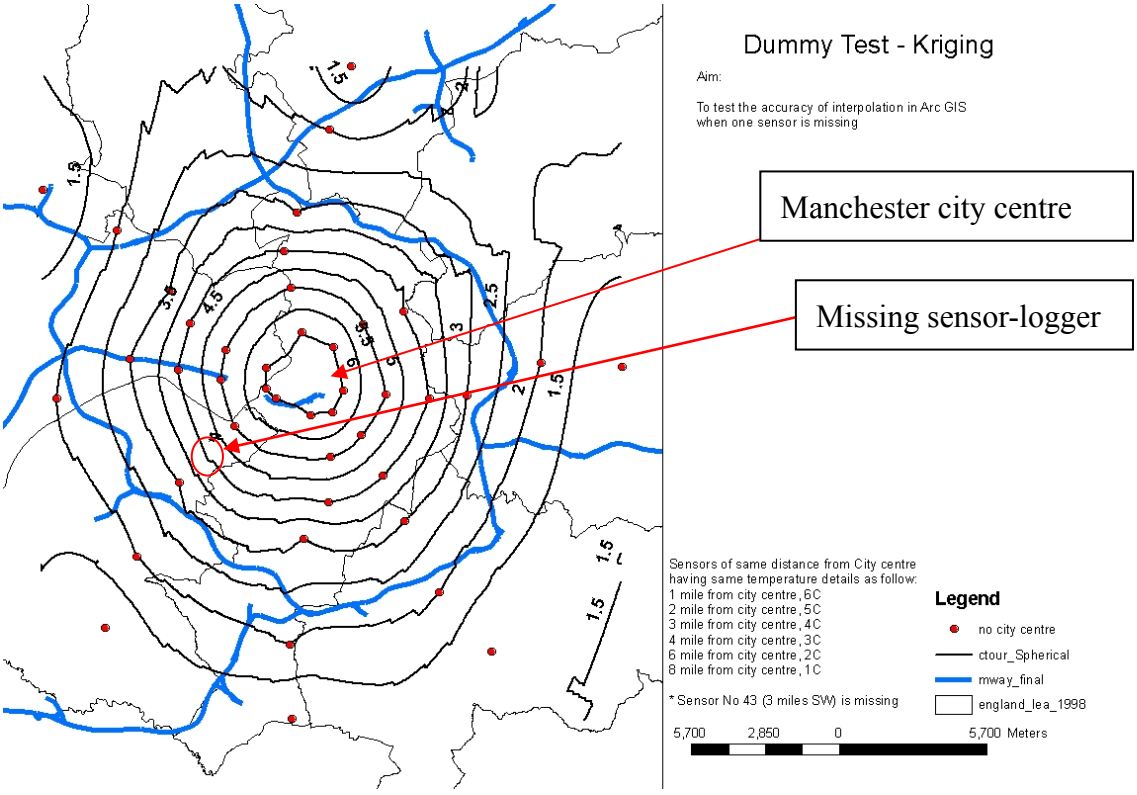

Figure 7.31 Temperature contour with dummy result

Figure 7.32 shows a day time temperature contour of 12:00pm on 7th Mar 2010. It can be seen that the overall temperature pattern is very irregular and complicated. Therefore only clear and calm, nocturnal period data were used to create contours in

order to maximise the urban heat island effect.

A nocturnal UHI intensity contour map can be seen in figure 7.33. This UHI intensity contour was created from data at 2:00am on 8th Mar 2010. An urban heat island centre with UHI intensity of 3°C was located to the south west of Manchester city centre. At this time, the wind direction recorded from all three weather observation stations (Hulme, Woodford and Ringway) indicated a wind direction from 70° (east-north-east). Note also the relatively cooler area located four miles north of Manchester city centre. This is Heaton Park mentioned earlier in section 7.3. The effect of this on the whole urban heat island can be seen from the contours.

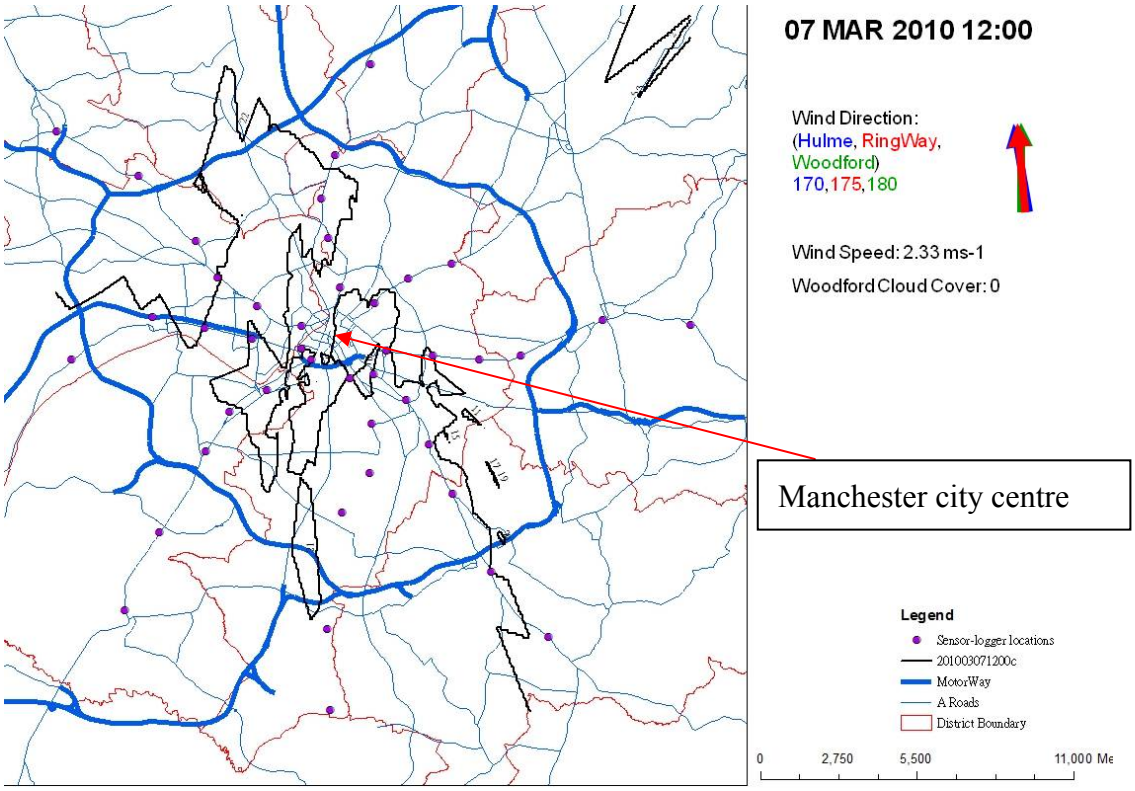

Figure 7.32 Example of daytime temperature contour

Figure 7.34 shows another UHI intensity contour map at 2:00a.m. on 21st Apr 2010. It can be seen that an urban heat island centre was located south east of Manchester city centre. Wind direction records from three observation stations indicated that there was

a west wind although the Hulme station recorded a north-west-north wind.

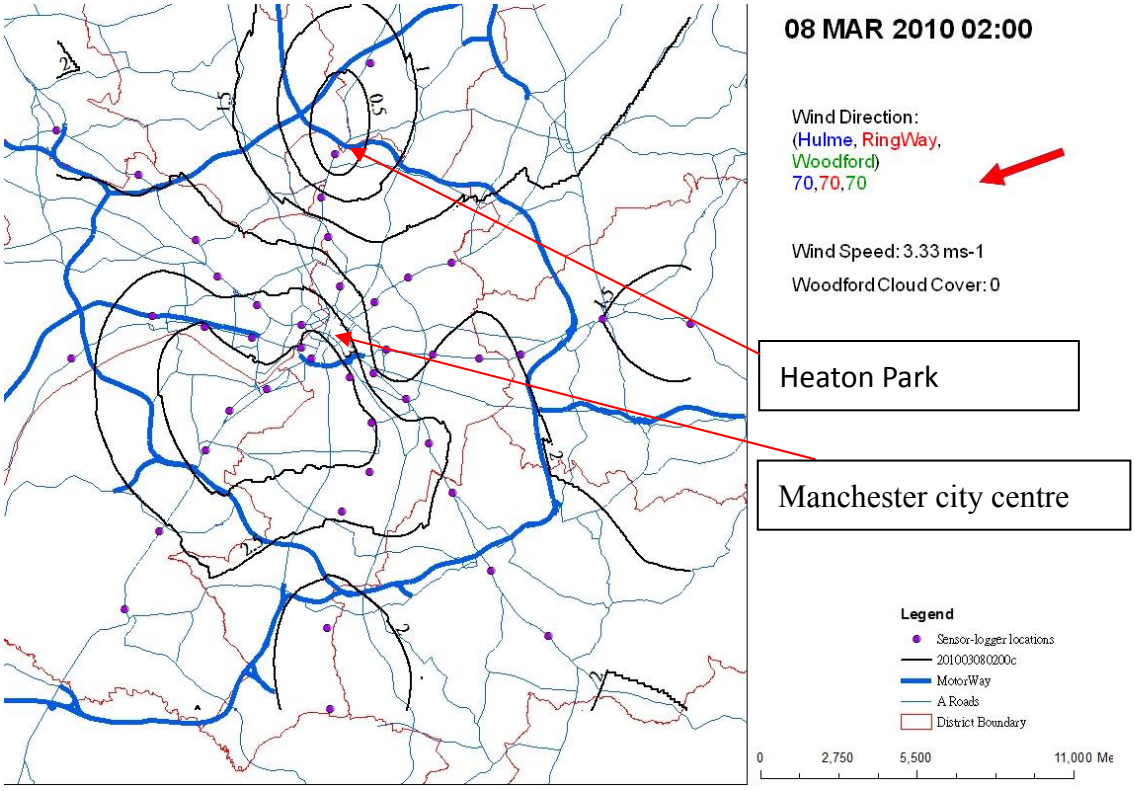

Figure 7.33 UHI intensity contour at 2:00a.m. of 8th Mar 2010

Looking at both figures 7.32 and 7.33, it was believed that there is a relationship between the wind direction and the urban heat island centre. The wind tends to push the thermal centre of the urban heat island towards different directions in a city when wind direction is changing. Watkins[44] (2002) also indicated a similar finding.

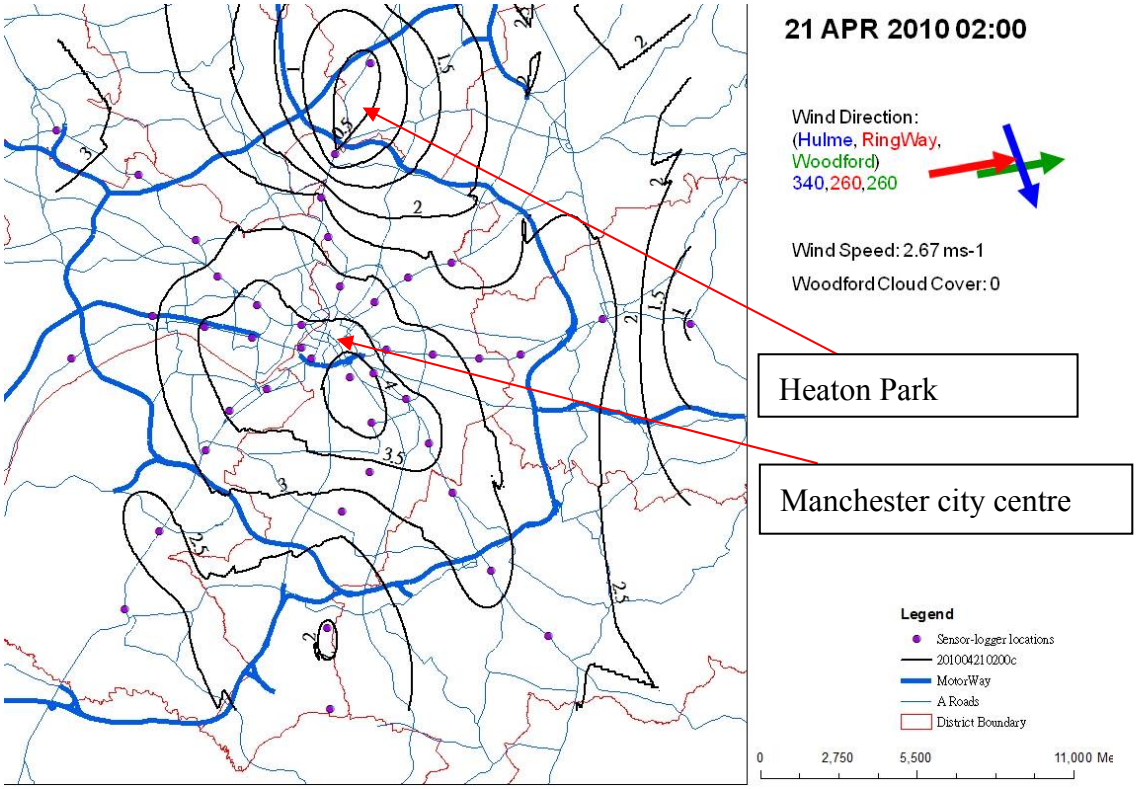

Figure 7.34 UHI intensity contour at 2:00a.m. of 21st Apr 2010

7.9 Conclusion

After demonstrating the existence of an urban heat island in Greater Manchester in the previous chapter, the relations between different factors contributing towards the urban heat island effect have been investigated in this chapter.

The SVF has a negative linear relation with urban heat island intensity as do distance and cloud cover. Evapotranspiration fraction also has a negative linear correlation with UHI intensity. Wind speed has a negative linear correlation with UHI intensity when it is less than $10ms^{-1}$ but above this speed, the UHI effect is small and the relation becomes constant. The rural reference temperature also has a negative linear relation with UHI intensity only when it is less than $3^{o}C$. Above this temperature, the UHI effect is smaller and the relation becomes constant..

Although different causal factors were investigated, the R^2 values for most of the factors were low. The speculative reason of this is because the effects of other factors were not controlled when analysis was performed between UHI intensity and one factor. For instance, when the relation between SVF and UHI intensity were investigated, the sensor-loggers selected have different evapotranspiration fractions and were located at different distances from city centre. It would be very difficult to control other factors unless many more monitoring stations were set-up. This project is only the first step of investigating the UHI effect in Manchester.

After understanding the basic relations between UHI intensity and different factors, it is important to create a model to combine all these factors. Multiple regression models were created and are discussed in the next chapter using a statistical software package.

CHAPTER 8

Multiple regression model

CHAPTER 8 Multiple regression model

8.1 Introduction

The main objective of this project is to develop a mechanism or a model so that the urban heat island effect could be predicted from weather data (either historical or future). Such weather data could then be very localised and specific towards a particular building site or a street canyon. This model should be capable to modify weather data which can be used by engineers in the dynamic building simulation to reflect the impact of urban heat island effect on building performance. In order to achieve this model, all factors that contribute significantly towards the urban heat island effect must be included. The independent effects between different factors and UHI intensity in both summer and winter were investigated in the last chapter. In this chapter, multiple regression models will be created to investigate their combined effect on UHI intensity. Giridharan and Kolokotroni[43] (2009) produced a multiple regression model with six different variables including: Surface albedo, aspect ratio, thermal mass, green density ratio, plan density ratio and fabric density ratio. However their model does not indicate the influence of other weather parameters. Thus, new models will be developed for this project.

8.2 Methodology and data used

SPSS[129] version 16 was used to analyse the main effect of different factors on urban heat island intensity (except for the interactions between different factors). Due to the different software layout between Microsoft Excel and SPSS, the UHI intensity data originally stored in Excel format must be modified first . All UHI intensities data were stored in columns for each sensor-logger as shown in figure 5.18 with each weather

data in a single column. However in SPSS, each variable had to be in one column only, therefore all UHI intensities for the different sensor-loggers were placed in one single column with the concomitant weather and location parameters duplicated alongside so to match the corresponding UHI intensity. Linear relationships found between various factors and UHI intensity as discussed in the previous chapter were utilised in a univariate general linear model fitted using SPSS. This means there will be only one predicted variable (namely UHI), with multiple weather and location predictors. UHI intensities calculated from every sensor-logger in 2010 were used to develop the model.

The air temperature data used are the same as those mentioned in the previous chapters. They were obtained from the 62 monitoring stations mounted at four metres above ground on street lamp posts located around Greater Manchester. Rural air temperature and other weather parameters such as wind speed, wind direction, cloud level and rainfall were obtained from Met Office Woodford Observation station. Total solar radiation was measured by BF3 solarimeter installed on the roof of the Pariser Building, University of Manchester (about 30 meters above ground). Sky view factors (SVF) were obtained by analysing photographs taken in street canyons using fish-eye lens as mentioned in section 8.2. Evapotranspiration fraction (EF) was found from the urban morphology type file in ArcGIS format provided by Sarah Lindley[130].

8.3 Models

8.3.1 Model criteria

12 models were created based on the factors mentioned below. They could be divided into two main categories:

1. City centre model
2. Non-city centre model

Different factors were analysed in each of these categories as listed below in table 8-1:

Factors	City Centre model	Non-city centre model
Sky View Factor (SVF)	Y	Y
Evapotranspiration fraction (EF)	N	Y
Distance from city centre	N	Y
Direction from city centre	N	Y
Canyon orientation	Y	N
Total solar irradiance	Y	Y
Rural cloud level	Y	Y
Rural Rainfall	Y	Y
Rural Wind speed	Y	Y
Rural Wind direction	Y	Y
Time	Y	Y
Rural air temperature	Y	Y

Table 8-1 Factors included in the two categories

Most of the weather parameters used in this model was obtained from Met Office's ground observation stations. Although some of the factors lack accuracy for local weather prediction for the city centre, the main purpose of this model is to predict local micro climate from readily available data that can be easily obtained from Met Office.

No evapotranspiration fraction has been included in the city centre models because all these evapotranspiration fractions were the same for city centre location. The direction and distance were also eliminated from the city centre model because all sites were at very close proximity to each other.

No canyon orientation information were included in the non-city centre model because most of the sensor-loggers were on the main roads. The effect due to canyon orientation was assumed to be minimal for all non-city centre sensor-loggers.

There are six sub-categories based on the type of data set used:

1. Daytime data
2. Nocturnal data
3. All data
4. Clear and calm daytime data
5. Clear and calm nocturnal data
6. Clear and calm all data

The sun-rise and sun-set times on the 15th of each month were used to determine the daytime and night time for each month. A period is defined as clear and calm if:

1. Wind speed smaller than or equal to 2.5ms^{-1}, And
2. Cloud level smaller than or equal to 2 oktas

The main purpose of using the statistic package is to develop a statistical multiple regression model for forecasting future urban heat island effect using all calculated UHI intensities, street and weather parameters. It is most preferred that all data points

were used in this model, unlike the last chapter which only used clear and calm weather data. In the following section, the city centre model and non city centre model (combined day and night) will be discussed in detail. This is because these two models are expected to be general enough to suit most engineering applications. It would be very complicated if models generated from selected data where chosen. Before using this model, the user must filter their data in a way similar to the model in order to get similar condition.

8.3.2 City centre model

The city centre model only used data from ten sensor-loggers which were located within Manchester city centre. UHI intensities have already been calculated in Microsoft Excel before imported into SPSS. Before any analysis was performed, it is important that the data set was validated. This was principally done by plotting the mean UHI intensity against each month for each sensor-logger as shown in figure 8.1. The “Marginal Means” shown on the axes label is simply an SPSS expression for the means that occur in the matrix margins. It can be seen that the UHI variation patterns of each sensor-logger were similar (i.e. the actual data had small variations). This similarity suggests there should be no gross abnormality in the data set and thus it can be concluded that the data are valid to use for analysis purposes.

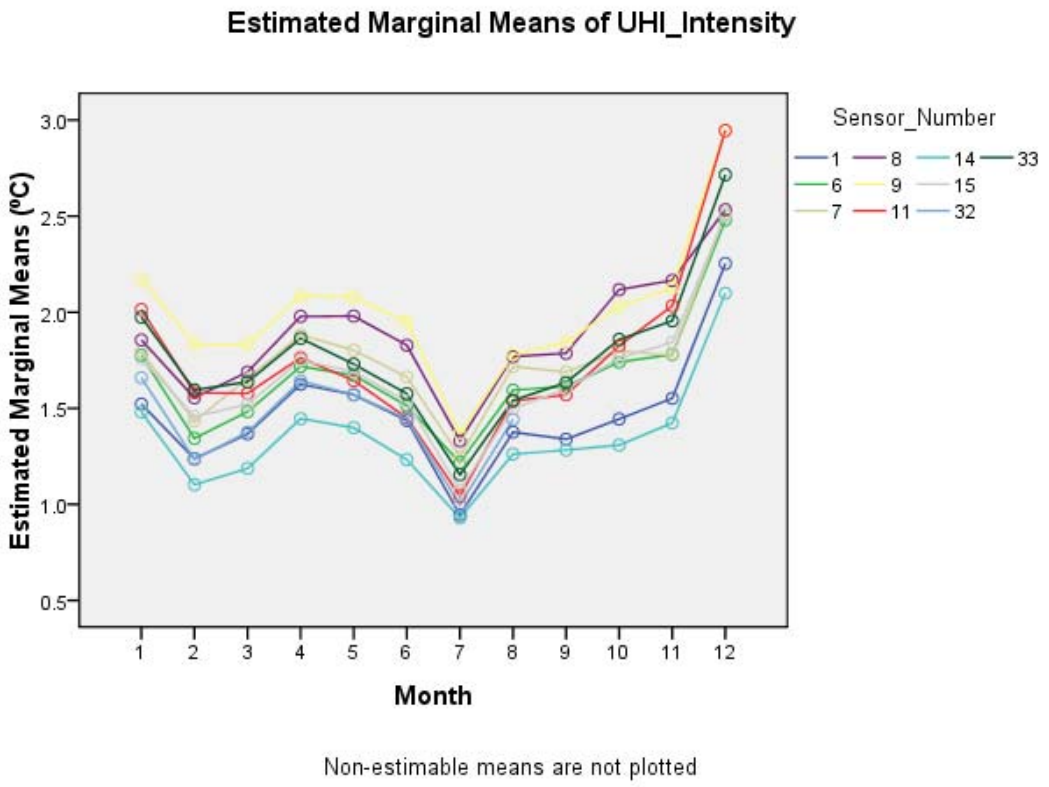

Figure 8.1 Mean UHI intensities against month for each sensor-logger

Before combining all factors into a model, each of the factors had to be investigated separately to ensure a linear relation could be seen. Figure 8.2 indicates the relation between wind speed and mean UHI intensity. Similar to the findings in section 7.5, wind speed had a linear relation when it is below $10ms^{-1}$. When wind speed exceeds $10ms^{-1}$ the relationship tends to be roughly constant. Therefore, all wind speed data above were truncated to $10ms^{-1}$ for modelling purposes. A similar plot is shown in figure 8.3. By comparing figures 8.2 and 8.3, it could be seen that the correlation coefficient has improved.

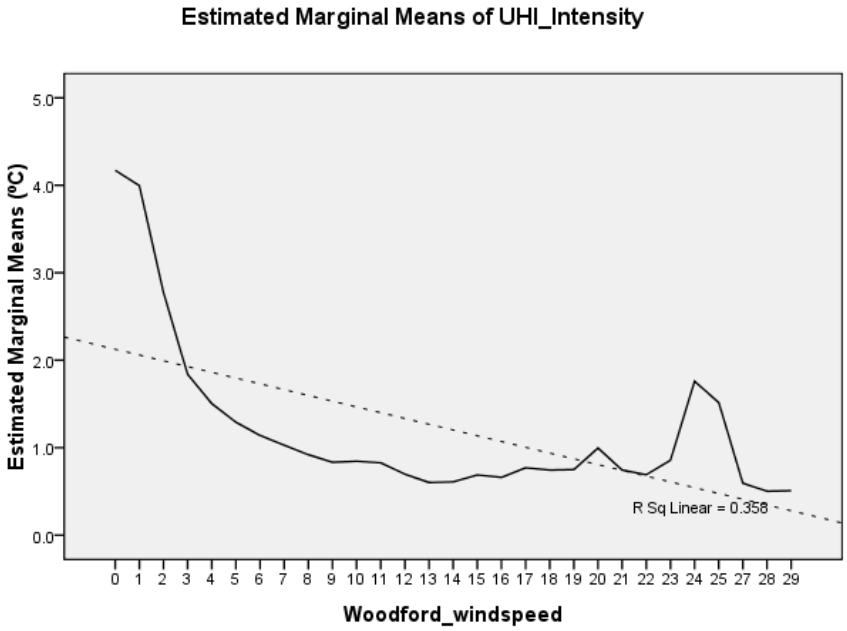

Figure 8.2 Mean UHI intensity against wind speed

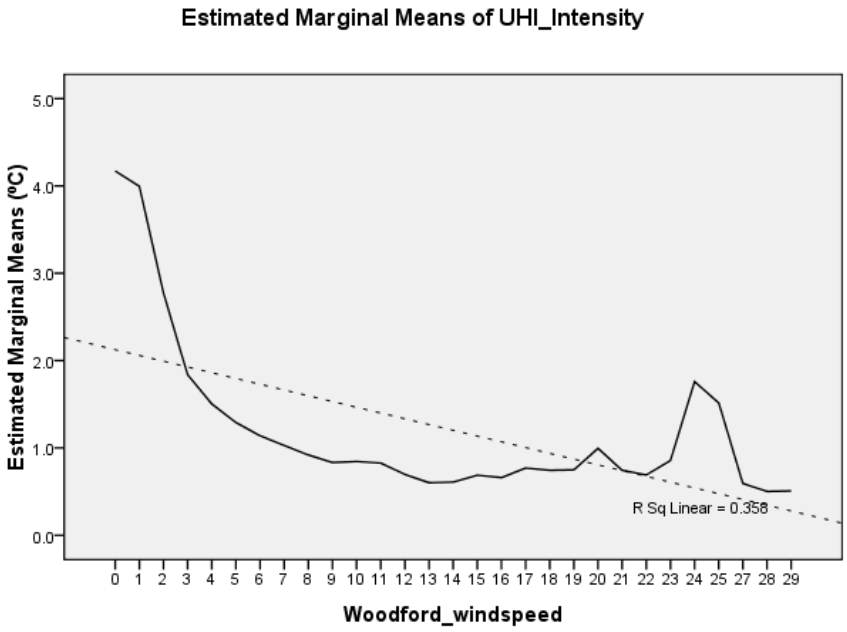

Figure 8.3 Mean UHI intensity against truncated wind speed

Figure 8.4 shows the relation between mean UHI intensity and Sky view factor (SVF). A similar negative relation could be seen with a R^2 of 58%. There is a peak in the SVF of 0.342. It is believed to be caused by the heavy traffic (anthropogenic heat) on this particular site (John Dalton Street, which is in the centre of Manchester and is a

main arterial road).

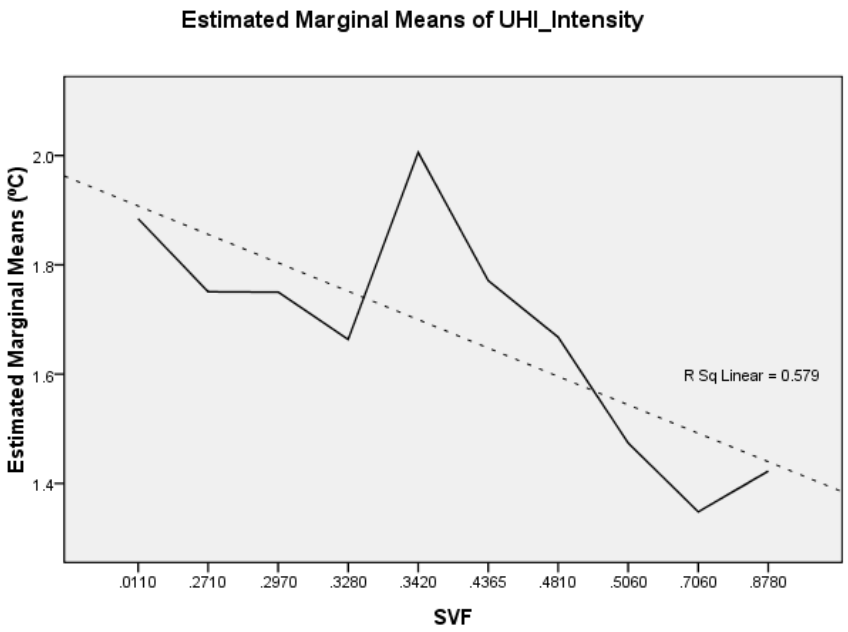

Figure 8.4 Mean UHI intensity against SVF

Figure 8.5 below shows the relationship between mean UHI intensity and cloud level in oktas (Cloud8 scale). A very high correlation coefficient of 90% was found as was found for clear and calm nights in the previous section 7.6.

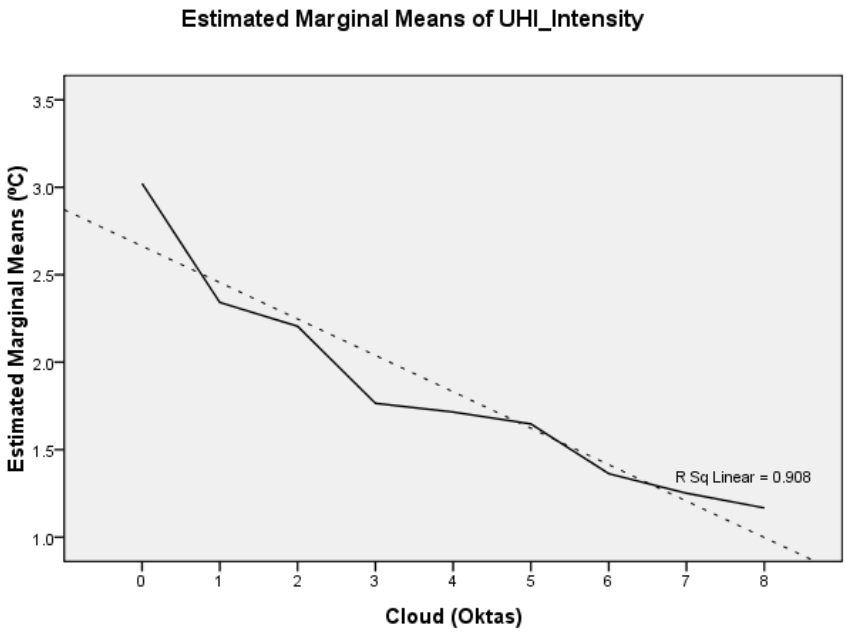

Figure 8.5 Mean UHI intensity against cloud level

Figure 8.6 shows the relationship between mean UHI intensity and rainfall. Rainfall was not investigated in the previous chapter; however it could be reflected by the cloud level. High rainfall implies significant cloud level. In theory, UHI intensity should be highest if there is no rainfall and reduce as the rainfall increases. However no significant relation could be seen from figure 8.6. Nevertheless, the evapotranspiration rate of the urban and rural surfaces will increase at different rates due to absorption after raining. Therefore, the UHI intensity will change as mentioned earlier in chapter 7 section 4. Therefore, rainfall was included in the model.

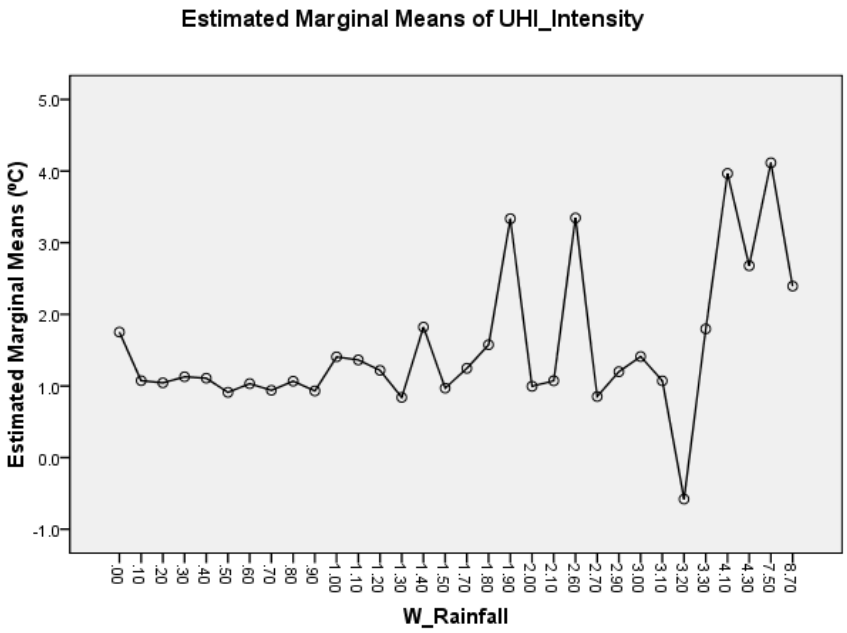

Figure 8.6 Mean UHI intensity against rainfall

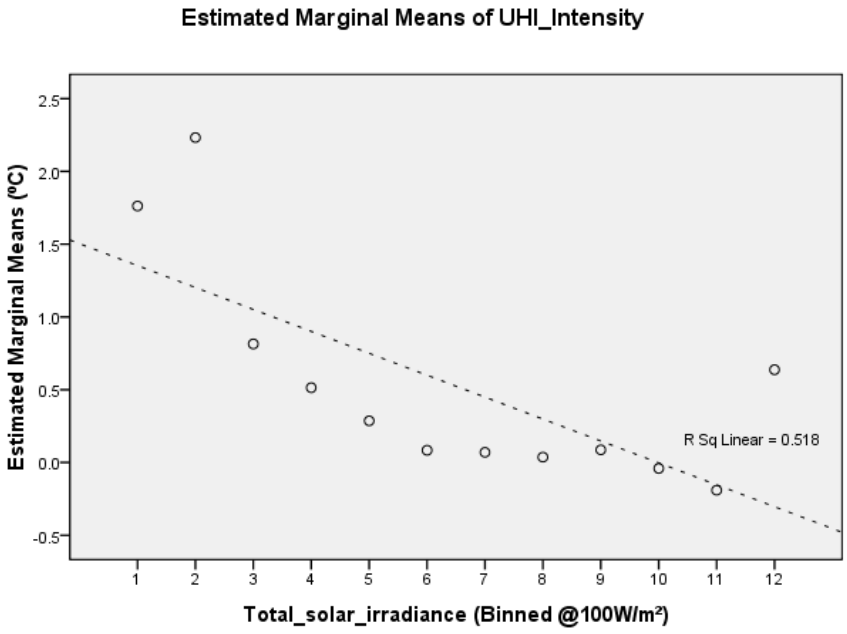

Figure 8.7 Mean UHI intensity against total solar irradiance binned to 100Wm^{-2}

Figure 8.7 above shows the relation between mean UHI intensity and total solar irradiance binned to 100Wm^{-2} per step. Due to similar reasons to rainfall as mentioned previously, total solar was not investigated previously because clear and calm nights were primarily of interest and also solar irradiation can also be approximately

represented by cloud coverage level. The total solar irradiance should be high where there is no cloud, and vice versa. An R^2 value of 52% was obtained which indicates a fairly high relation between total solar irradiance and mean UHI intensity.

Figure 8.8 shows the relation between mean UHI intensity and rural reference temperature. A relatively high R^2 was found (80%). It could also be seen that there was a better correlation at lower rural reference temperature. The relationship tends to become horizontal when the rural temperature is higher. A similar graph was plotted for all temperatures smaller than 3^{o}C as shown in figure 8.9. Conclusively, the R-square value increased to 95% which indicates a very strong relationship between the UHI intensity and the low rural reference temperature.

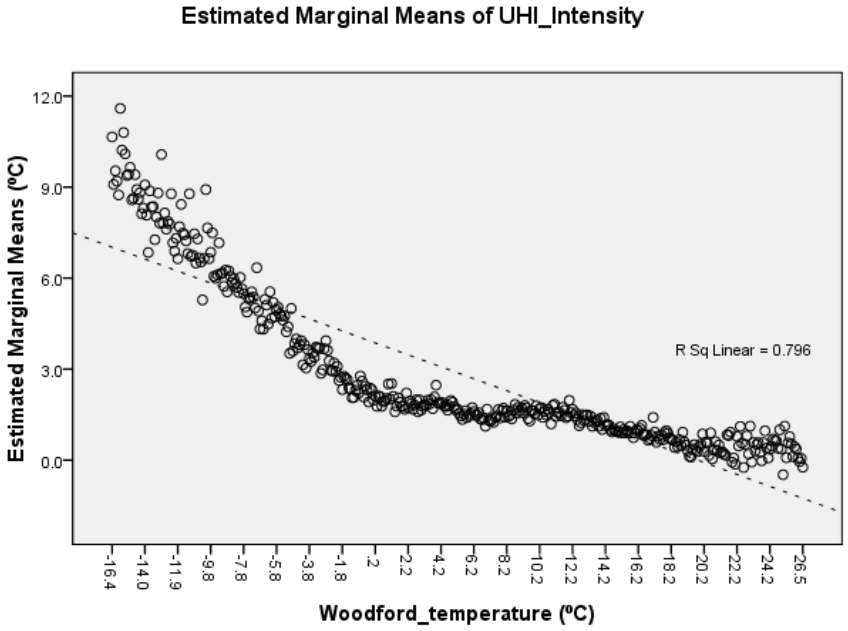

Figure 8.8 Mean UHI intensity against rural reference temperature

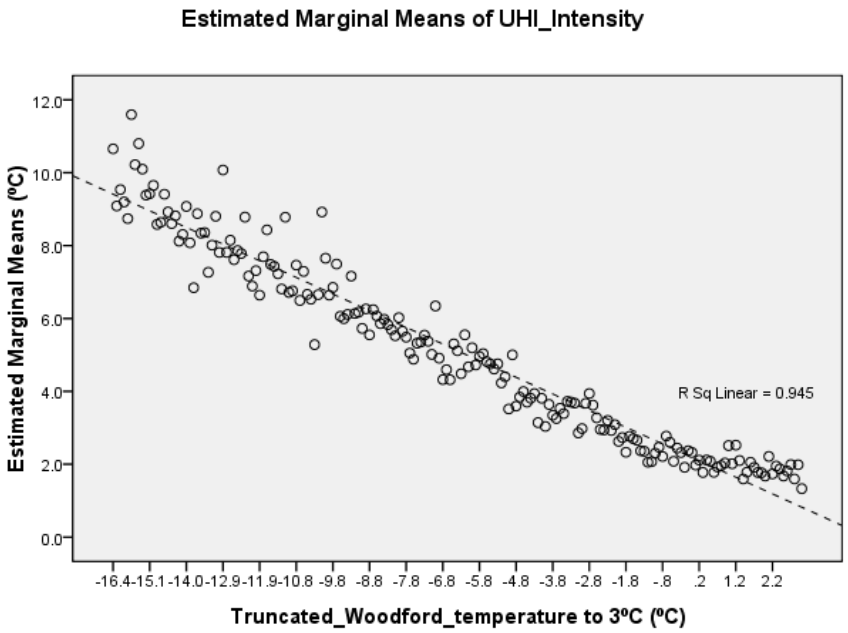

Figure 8.9 Mean UHI intensity against rural reference temperature truncated to 3^{o}C

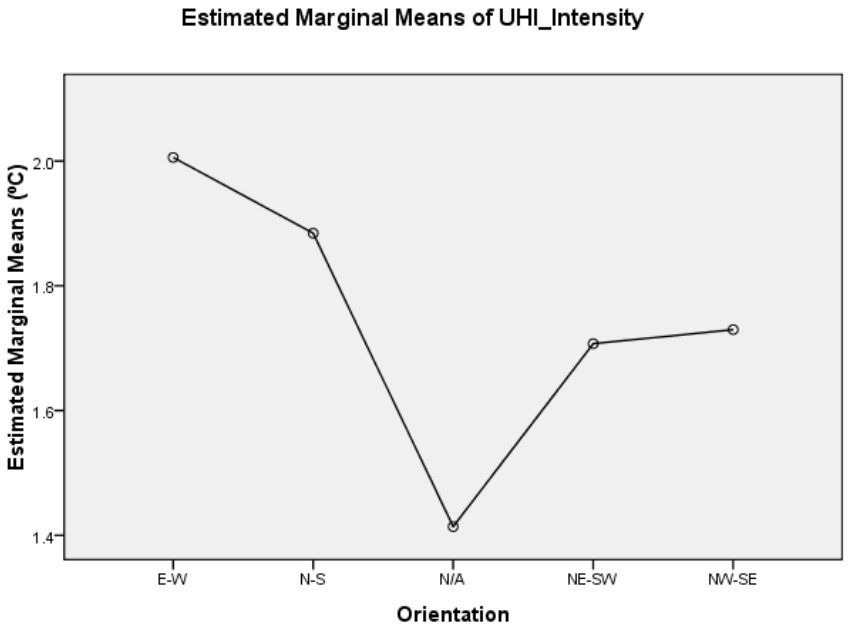

Figure 8.10 Mean UHI intensity against orientation of different canyons

Figure 8.10 shows the relationship between mean UHI intensity and different canyon orientations. “N/A” means the sensor-loggers were located in large area such as Piccadilly Garden which is not a street canyon. Figure 8.10 shows the lowest means UHI was resulted in “N/A” orientation. It was believed that a large open area would

have much more vegetation than a normal street canyon resulting in a lower UHI intensity (Such as Piccadilly Gardens and Pariser Building). Canyon orientation was regarded as a fixed factor rather than covariate in the model. As a result, a unique coefficient could be generated for each orientation in the final model.

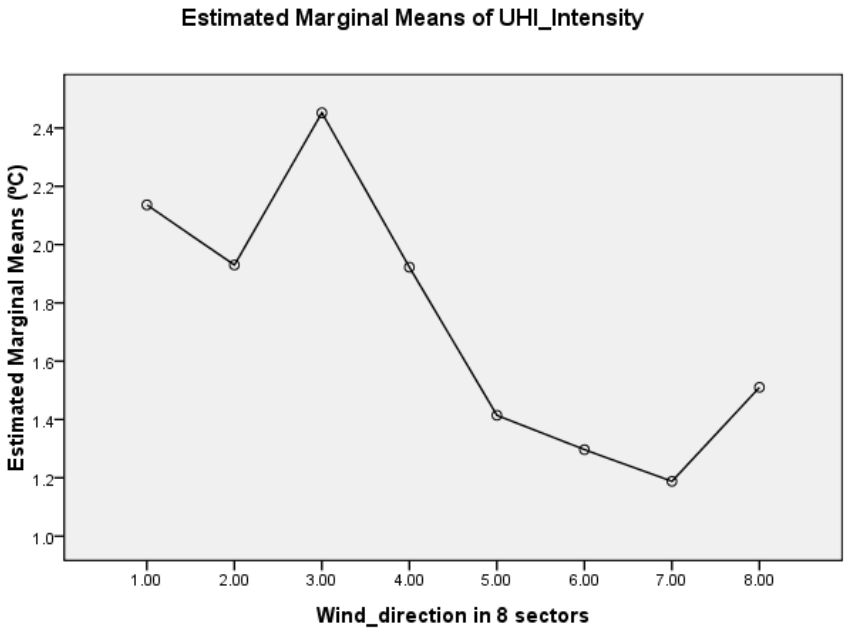

Figure 8.11 Mean UHI intensity against wind direction in eight quadrants

Figure 8.11 shows the relation between mean UHI intensity and wind directions. The wind direction was measured from Woodford ground observation station. Eight sectors (named 1 to 8) were defined to cover wind direction from 0^o to 360^o with each sector covering a 45^o section. Sector 1 means wind direction from 0^o to 45^o, sector 2 mean 46^o to 90^o and so on. Wind direction has two effects on the urban heat island effect. The first effect is the interaction between wind direction and canyon orientation. If wind direction is parallel towards the canyon orientation, heat inside the canyon could be removed by the wind. The other effect depends on the compass direction of the wind. Wind from the north tends to be cooler whilst wind from the south tends to be warmer due to the location of UK on the globe. It was mentioned

earlier in the chapter that this thesis will only focus upon the main effects of different factors rather than their interaction. The interacting effect between wind direction and canyon orientation are therefore not investigated. Figure 8.11 shows that the wind direction from northern directions (sectors 7.3) tends to result a higher mean UHI intensities than the other sectors. In order to simplify the calculation, a linear relationship was assumed for wind directions.

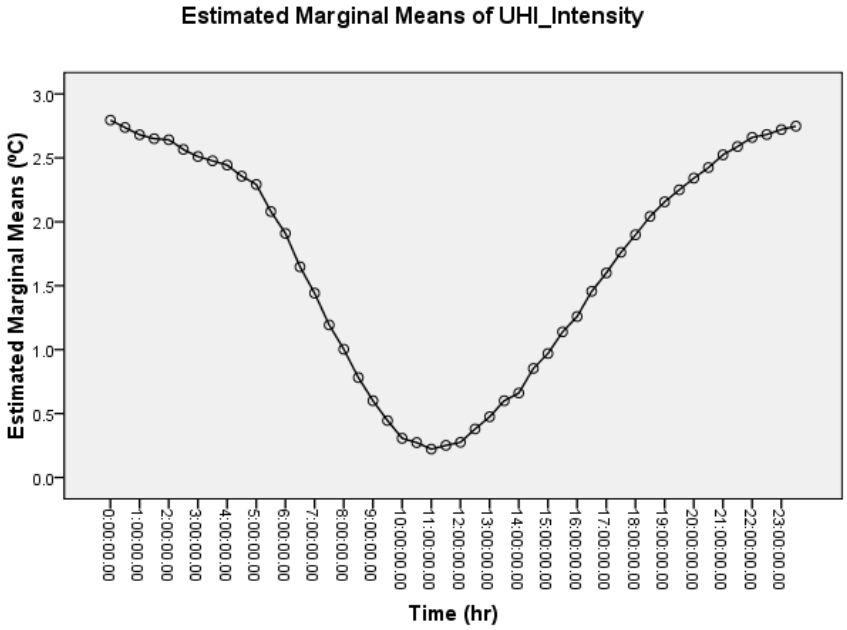

Figure 8.12 Mean UHI intensity against time

The relationship between mean UHI intensity and the time of a day is shown in figure 8.12. Compared with the clear and calm winter and summer daily profiles, shown in figures 6.9 and 6.15, they all have similar shapes. However, the averaged UHI intensities shown in clear and calm periods are much higher instead of a linear relation, a quadratic relation or trigonometric relation could be seen here. In order to model the diurnal variation, a trigonometric function was adopted with both sine and cosine (both to account for any phase shift). Apart from the diurnal variation, the yearly variation was also adopted using a similar trigonometric function. The diurnal

variation was believed to be caused by the anthropogenic activities, while the yearly variation was believed to be caused by the seasonal monthly mean temperature difference. Monthly and weekly variation was not included in this model for simplicity (different days in a month for monthly variation and different holidays over a year for weekly variation).

Tables 8-2 and 8-3 indicate the results of the model which have been extracted directly from the software. It could be seen from table 8-2 that the residual variance for this model is 1.443^{o}C. By taking the square root of this, a standard error of 1.2^{o}C is found. Type I sum of squares is the residual sum of squares for regression of UHI on that particular term. "df" means the degrees of freedom, they are the number of fitted coefficients for that particular term. Mean square equals the residual sum of the squares divided by df. The significance is the probability of getting a value at least as large as the one calculated for the term if the term is redundant[131]. The usual cut off points are 0.1% as "highly significant", 1% is "strongly significant", 5% is "significant", 10% is "weakly significant". All factors have shown their significance in the model. The standard error term in table 8-3 is the square-root of variance used instead of standard deviation when it refers to residual variance at the end of a model. "t" is the ratio of the "B" to its own standard error. The 95% confidence interval is an interval which is 95% likely to contain the true value of the Beta ("B") coefficient.

Dependent Variable:UHI_Intensity

Source	Type I Sum of Squares ($^oC^2$)	df	Mean Square ($^oC^2$)	Sig.
Corrected Model	352931.944[a]	11	32084.722	.000
Intercept	479322.485	1	479322.485	.000
SVF	3897.907	1	3897.907	.000
Total solar	104008.104	1	104008.104	.000
Rainfall	2009.612	1	2009.612	.000
Wind Speed	103634.516	1	103634.516	.000
Rural Temperature	55350.392	1	55350.392	.000
Cloud	41374.977	1	41374.977	.000
Wind direction in 8 sec	40.110	1	40.110	.000
sin_hr_2pi_24_rad	5890.144	1	5890.144	.000
cos_hr_2pi_24_rad	19401.436	1	19401.436	.000
sin_hr_2pr_8760	146.989	1	146.989	.000
cos_hr_2pr_8760	17177.758	1	17177.758	.000
Error	223379.810	169323	1.319	
Total	1055634.239	169335		
Corrected Total	576311.754	169334		

a. R Squared = .612 (Adjusted R Squared = .612)

Table 8-2 Regression model result showing the residual variance

Table 8-3 shows the coefficients for each factor as summarised in equation 8.1 shown below:

$$\text{UHI Intensity for city canyon} \sim N(\mu, 1.148) \qquad \text{eq 8.1}$$

where $\mu \equiv 4.421 — 0.2887 \times \sin\left(\frac{2\pi \times \text{hr}}{24}\right) + 0.4454 \times \cos\left(\frac{2\pi \times \text{hr}}{24}\right) - 0.6461 \times \text{SVF} - 0.003205 \times \text{Solar} + 0.1552 \times \text{Rainfall} - 0.1248 \times \text{wind speed} - 0.2855 \times \text{rural temperature} - 0.1479 \times \text{cloud} - 0.02082 \times \text{wind direction} - 0.01634 \times \sin\left(\frac{2\pi \times \text{hr}}{8760}\right) - 0.5597 \times \cos\left(\frac{2\pi \times \text{hr}}{8760}\right)$

Dependent Variable:UHI_Intensity

Parameter	B	Std. Error (°C)	t	Sig.	95% Confidence Interval	
					Lower Bound	Upper Bound
Intercept	4.421	.011	414.721	.000	4.400	4.442
SVF	-0.6461	.013	-49.805	.000	-.672	-.621
Total solar	-0.003205	.000	-133.708	.000	-.003	-.003
Rainfall	0.1552	.013	12.053	.000	.130	.180
Wind Speed	-0.1248	.001	-121.324	.000	-.127	-.123
Rural Temperature	-0.2855	.001	-205.739	.000	-.288	-.283
Cloud	-0.1479	.001	-144.476	.000	-.150	-.146
Wind direction	-0.02082	.001	-14.847	.000	-.024	-.018
sin_hr_2pi_24_rad	-0.2887	.004	-71.491	.000	-.297	-.281
cos_hr_2pi_24_rad	0.4454	.006	80.980	.000	.435	.456
sin_hr_2pr_8760	-0.01634	.004	-4.050	.000	-.024	-.008
cos_hr_2pr_8760	-0.5597	.005	-114.109	.000	-.569	-.550

Table 8-3 Model result corrected to four significant figures

Equation 8.1 can be explained as the UHI intensity is a normal distribution with the mean equal to the function of all factors and a standard error of 1.319.

After developing the general model equation, it was essential to identify the model's dominant factors. Table 8-4 indicates the maximum and minimum values which can be put in for each factor in the model as well as the maximum and minimum value after multiplying by their own coefficients. "B" in table 8-4 is the coefficient found for each variable from the model. It is the same as the "B" shown in table 8-3. The "difference" in table 8-4 refers to the difference between "B*max(x)" and "B*min(x)" The difference between the products of their maximum and minimum values shows

the factors' dominance. It could be seen that rural temperature is the most important factor followed by solar irradiance and rainfall.

	B	max (x)	min (x)	B*max(x)	B*min(x)	difference
Intercept	4.421					
SVF	-0.6461	1	0	-0.6461	0	-0.6461
Total solar (W/m^2)	-0.003205	1000	0	-3.205	0	-3.205
Rainfall (mm)	0.1552	10	0	1.552	0	1.552
Wind speed trun.10 (m/s)	-0.1248	10	0	-1.248	0	-1.248
Rural Temperature trun. 3 (^oC)	-0.2855	3	-20	-0.8565	5.71	-6.5665
Cloud	-0.1479	8	0	-1.1832	0	-1.1832
Wind direction 8sec(^{o})	-0.02082	8	1	-0.16656	-0.02082	-0.14574
Sin(2pi*hr/24)	-0.2887	1	-1	-0.2887	0.2887	-0.5774
Cos(2pi*hr/24)	0.4454	1	-1	0.4454	-0.4454	0.8908
Sin(2pi*hr/8760)	-0.01634	1	-1	-0.01634	0.01634	-0.03268
Cos(2pi*hr/8760)	-0.5597	1	-1	-0.5597	0.5597	-1.1194

Table 8-4 Dominance of different factors in city centre model

8.3.3 Non-city centre model

Non-city centre model was generated using air-temperature data measured from 48 non city centre sensor-loggers. Additional factors such as the evapotranspiration value and the distance away from the city centre were included in the non-city centre model. Similar to the city centre model, the relation between each factor was investigated first before combining them to generate a model. Due to the significant similarity with city centre model, only the relationships between new factors and mean UHI intensity will be discussed in this section.

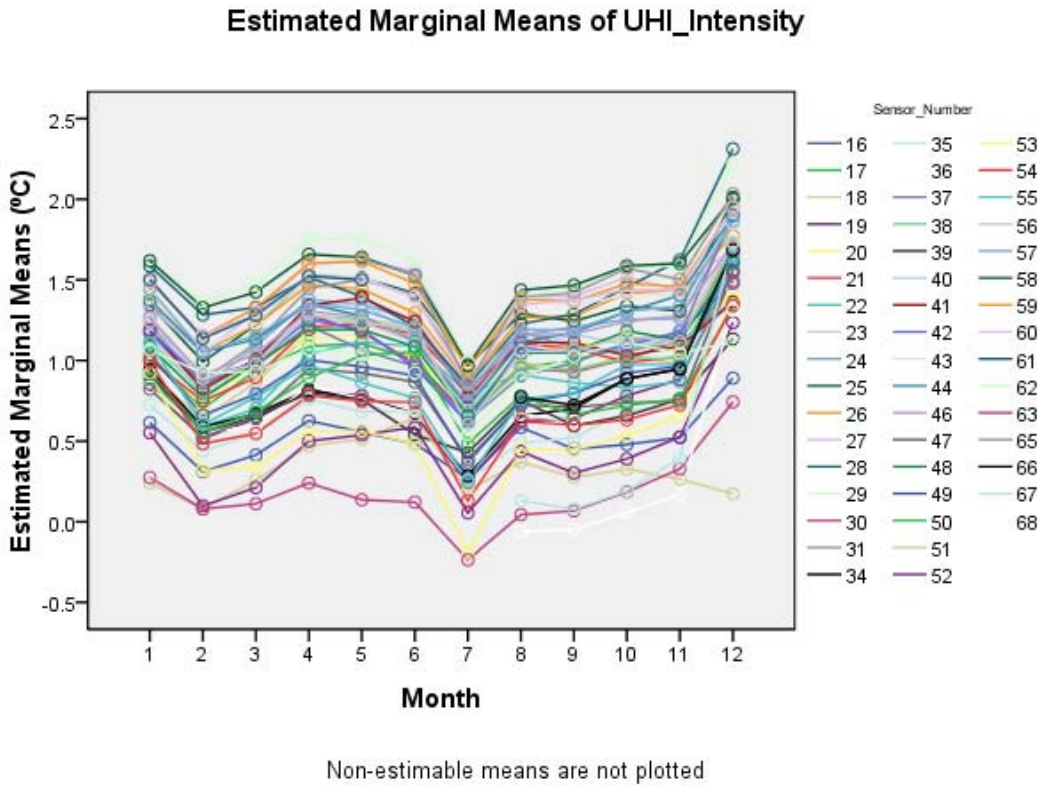

Figure 8.13 Mean UHI intensity variation against month for each sensor-logger

In order to perform the correct calculations, it is important to check if all data sets are entered correctly into SPSS. This could be performed by looking at the temperature variation pattern of data from each sensor-logger. It can be seen that data set from all sensor-loggers shows a relatively uniform pattern over the 12 month period. There is no abnormality shown in the graph and therefore, it suggests that all data sets were correctly entered into SPSS.

Evapotranspiration fraction (EF) is a reflection of the amount of vegetation as mentioned earlier in section 7.4. EF values vary from 0 to 1 which indicates the area ratio for four vegetation types. Figure 8.14 shows the relation between EF values and UHI intensities over a year. R-square value was similar to the value which was found for seasonal variation in section 7.4.

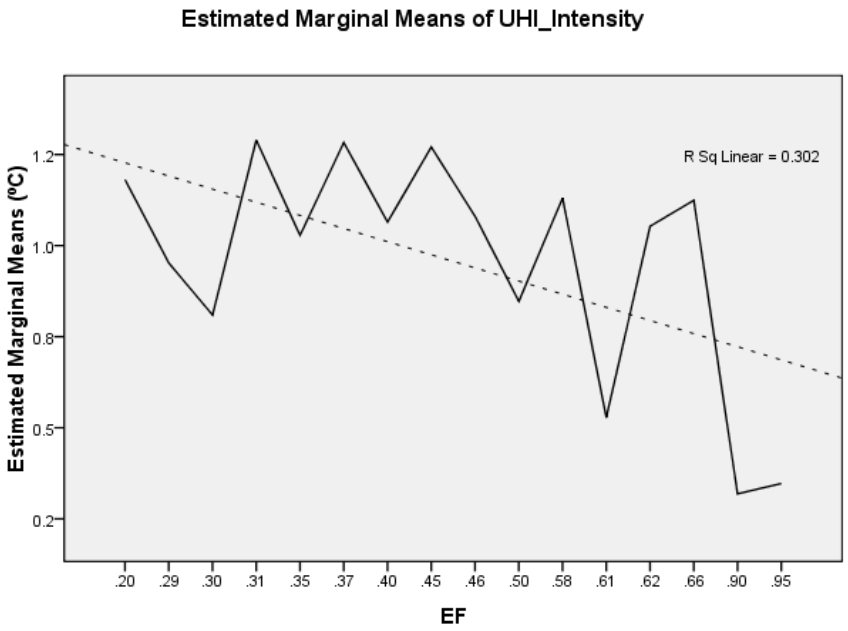

Figure 8.14 Mean UHI intensity against EF

Distance was another factor which was not included in the city centre model. Figure 8.15 shows the relation between mean UHI intensity and distance away from city centre. It could be seen that the relation was linear with a high correlation coefficient value of 96%.

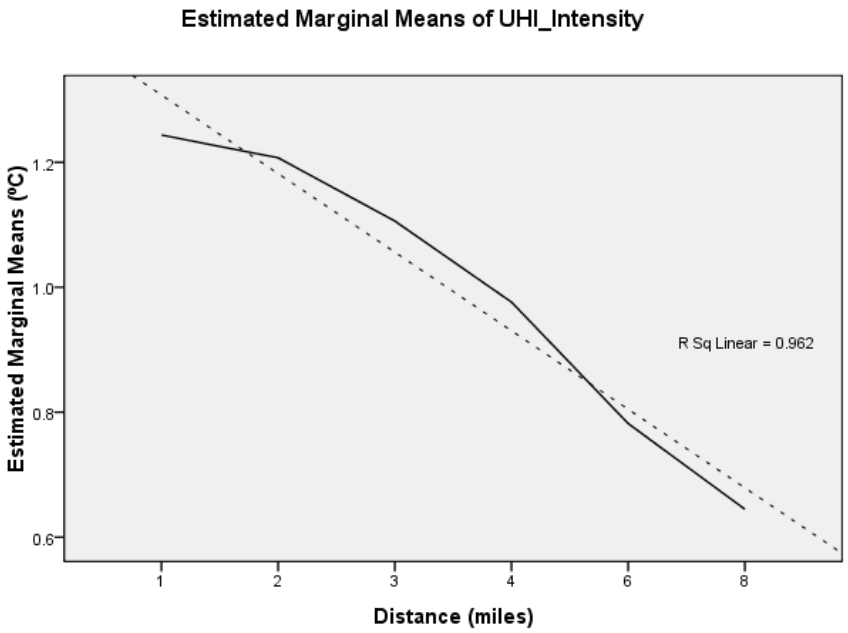

Figure 8.15 Mean UHI intensity against distance away from city centre

Direction from the city centre was also a factor excluded from the city centre model. Figure 8.16 shows the relation between mean UHI intensity and direction from city centre. The relation is fairly linear with a R^2 value of 72%. Although directions from city centre were shown in angular bearing, there should not be too much correlation between each direction. Therefore, directions were decided to be included in the model as a fixed factor.

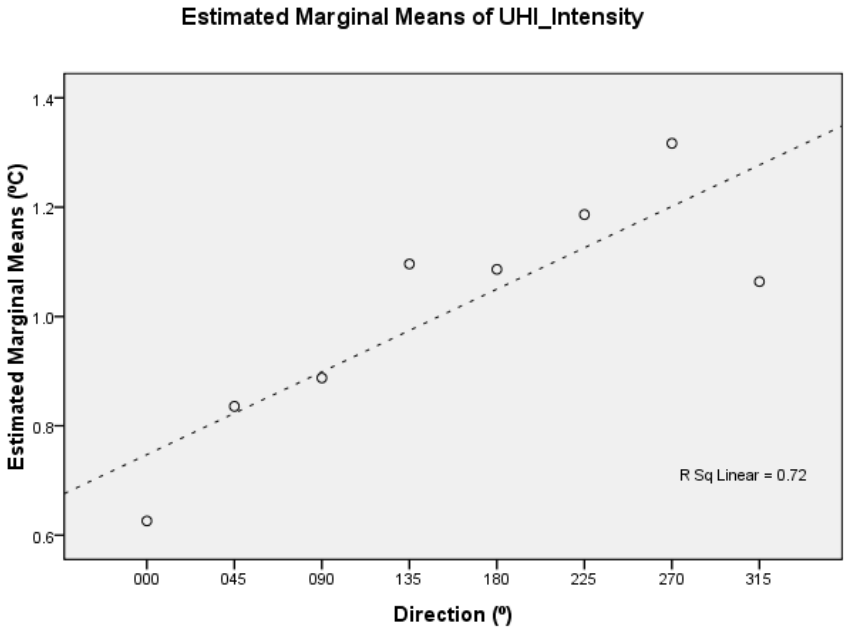

Figure 8.16 Mean UHI intensity against direction

Equation 8.3 summarised the model to 4 significant figures:

$$\text{UHI Intensity for non city centre} \sim N(\mu, 1.052) \qquad \text{eq 8.3}$$

$$\begin{aligned}\text{where } \mu \equiv\ & 3.490 - 0.3262 \times \sin\left(\frac{2\pi \times \text{hr}}{24}\right) + 0.2329 \times \cos\left(\frac{2\pi \times \text{hr}}{24}\right) - 0.09016 \\ & \times \text{SVF} - 0.4939 \times \text{EF} - 0.07731 \times \text{Distance} - 0.002054 \times \text{Solar} \\ & + 0.1530 \times \text{Rainfall} - 0.09610 \times \text{wind speed} - 0.2160 \\ & \times \text{rural temperature} - 0.1198 \times \text{cloud} - 0.01861 \times \text{wind direction} \\ & + 0.0002598 \times \sin\left(\frac{2\pi \times \text{hr}}{8760}\right) + 0.4531 \times \cos\left(\frac{2\pi \times \text{hr}}{8760}\right) \\ & + \begin{bmatrix} -0.3124 \times (\text{N}) \\ -0.3029 \times (\text{NE}) \\ -0.1466 \times (\text{E}) \\ 0.07753 \times (\text{SE}) \\ 0.09382 \times (\text{S}) \\ 0.1672 \times (\text{SW}) \\ 0.2071 \times (\text{W}) \\ 0 \times (\text{NW}) \end{bmatrix}\end{aligned}$$

It could be seen that the coefficients for all the direction is larger than the coefficient

of SVF. To compare all the sensor-logger data at different directions from the city centre, direction was taken out of the equation so that the model could be more generalized. Equation 8.4 shows the refined equation corrected to four significant figures.

$$\text{UHI Intensity for non city centre} \sim N(\mu, 1.068) \qquad \text{eq 8.4}$$

$$\text{where } \mu \equiv 3.559 - 0.322 \times \sin\left(\frac{2\pi \times \text{hr}}{24}\right) + 0.2327 \times \cos\left(\frac{2\pi \times \text{hr}}{24}\right) - 0.1429 \times \text{SVF} - 0.6575 \times \text{EF} - 0.07200 \times \text{Distance} - 0.002056 \times \text{Solar} + 0.1526 \times \text{Rainfall} - 0.09602 \times \text{wind speed} - 0.2161 \times \text{rural temperature} - 0.1197 \times \text{cloud} - 0.01858 \times \text{wind direction} + 0.01119 \times \sin\left(\frac{2\pi \times \text{hr}}{24}\right) - 0.4570 \times \cos\left(\frac{2\pi \times \text{hr}}{24}\right)$$

Table 8-5 indicates the dominance of each factor for the non-city centre model. Similar to the city centre model, the rural temperature is the most dominant factor followed by rainfall and total solar irradiance.

	B	max (x)	min (x)	B*max(x)	B*min(x)	difference
Intercept	3.559					
SVF	-0.1429	1	0	-0.1429	0	-0.143
EF	-0.6575	1	0	-0.6575	0	-0.658
Distance	-0.072	8	0	-0.576	0	-0.576
Total_solar (W/m^2)	-0.002056	1000	0	-2.056	0	-2.056
Rainfall (mm)	0.1526	10	0	1.526	0	1.526
Wind Speed(m/s)	-0.09601	10	0	-0.9601	0	-0.960
Rural Temperature(^{o}C)	-0.2161	3	-20	-0.6483	4.322	-4.970
Wind direction (^{o})	-0.01858	8	0	-0.14864	0	-0.149
Cloud	-0.1197	8	1	-0.9576	-0.1197	-0.838
Sin(2pi*hr/24)	-0.3262	1	-1	-0.3262	0.3262	-0.652
Cos(2pi*hr/24)	0.2327	1	-1	0.2327	-0.2327	0.465
Sin(2pi*hr/8760)	0.01119	1	-1	0.01119	-0.01119	0.022
Cos(2pi*hr/8760)	-0.457	1	-1	-0.457	0.457	-0.914

Table 8-5 Dominance of different factors in non-city centre model

8.4 Validation of model

In order to ensure the accuracy of both models, model validations were performed. The entire validation processes was developed into two stages:

1. Testing using 2010 data (data used to develop the model)
2. Validation using 2009 data

The first stage of the validation was done by comparing the model's data with the actual UHI intensity measured from sensor-loggers in 2010. In other words, part of the data used to create the model was extracted and compared with the simulation result. This procedure is important so that the model could be checked for any major errors. The model's UHI intensities should be in phase with the actual UHI intensities which was measured and calculated. UHI intensities calculated from four sensor-loggers were chosen in random for the comparison in each model (i.e. four for city centre model and four for non-city centre model). Data from July and December 2010 were used for the validation.

The second stage of the model validation process tests the general prediction ability of the model on "new" weather data not used before or in the main data set used for the model derivation. A set of new data which were not used for the development of the model was used. Due to the late release of Met Office weather data in 2011, there were no complete data available for validation at this stage, therefore, only old 2009 data was used instead. Data measurement for sensor-loggers started in Nov 2009. As a result, only Dec 2009 data was available for the second stage validation process.

8.4.1 City centre model validation

UHI intensities data calculated from the four sensor-loggers chosen in random were used for the city- centre model validation process. In this case, summer data (July) and winter data (December) were used. Due to the similarity in the validation result, only one summer and one winter validation will be discussed in this section.

Figure 8.17 and figure 8.18 show the actual UHI intensities variation for sensor-logger data and UHI intensities from the model for in July and December respectively.

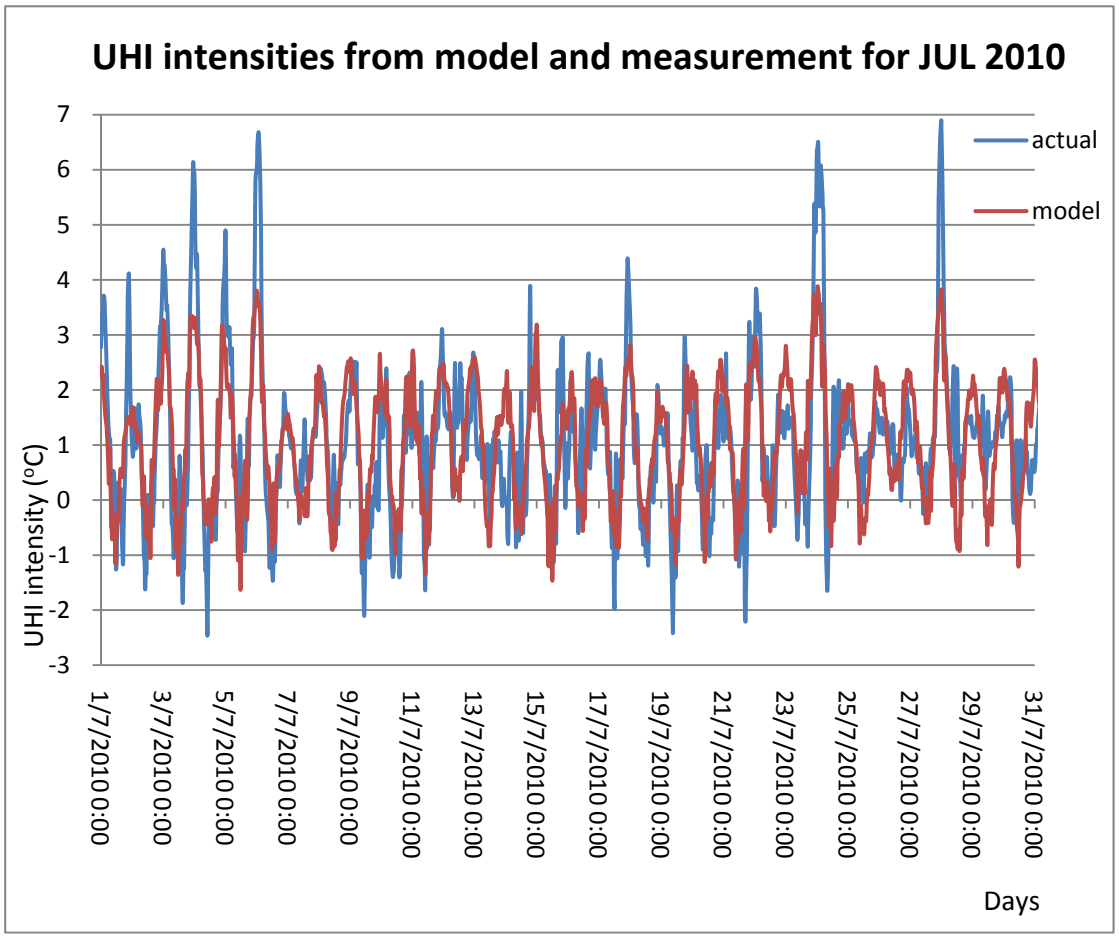

Figure 8.17 UHI intensities from model and measured for JUL 2010

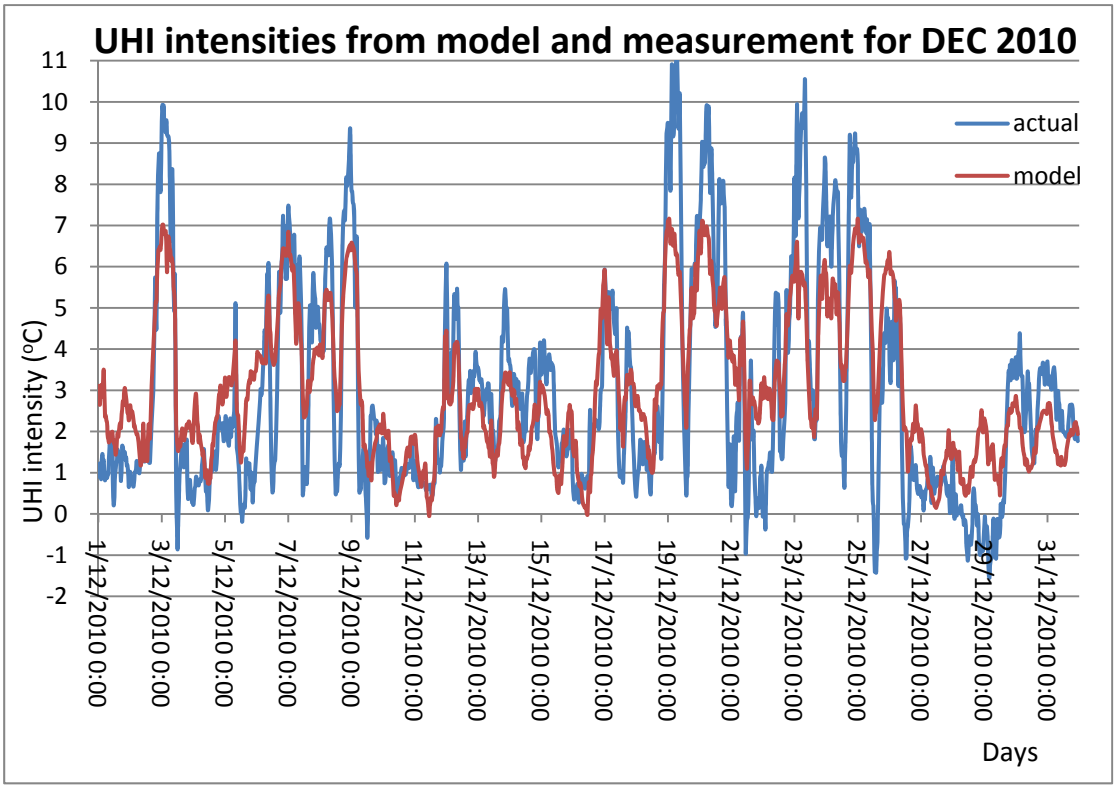

Figure 8.18 UHI intensities from model and measured for DEC 2010

It could be seen from both graphs that the modelled UHI intensities are generally in line with the calculated UHI intensity. However, the modelled UHI intensities do not reach the measured maximum and the minimum UHI intensities. Figures 8.19 and 8.20 show the actual UHI intensities against the UHI intensities obtained from the model for both months respectively.

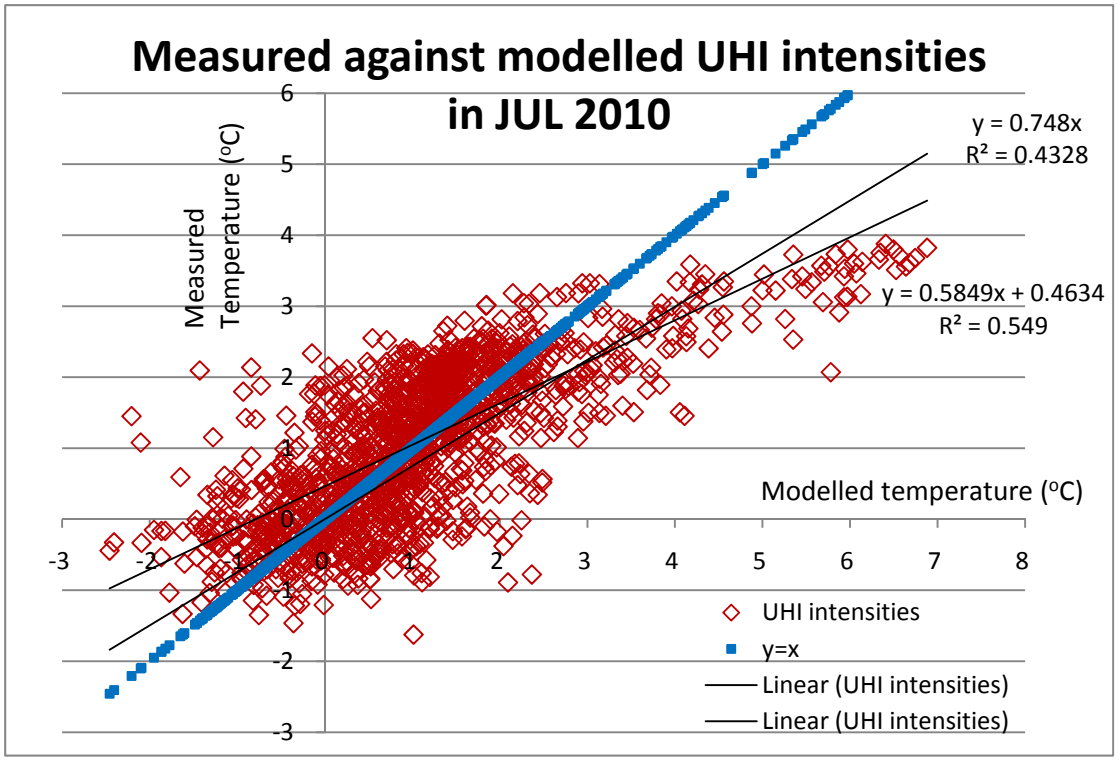

Figure 8.19 Measured UHI intensities against modelled UHI intensities in JUL 2010

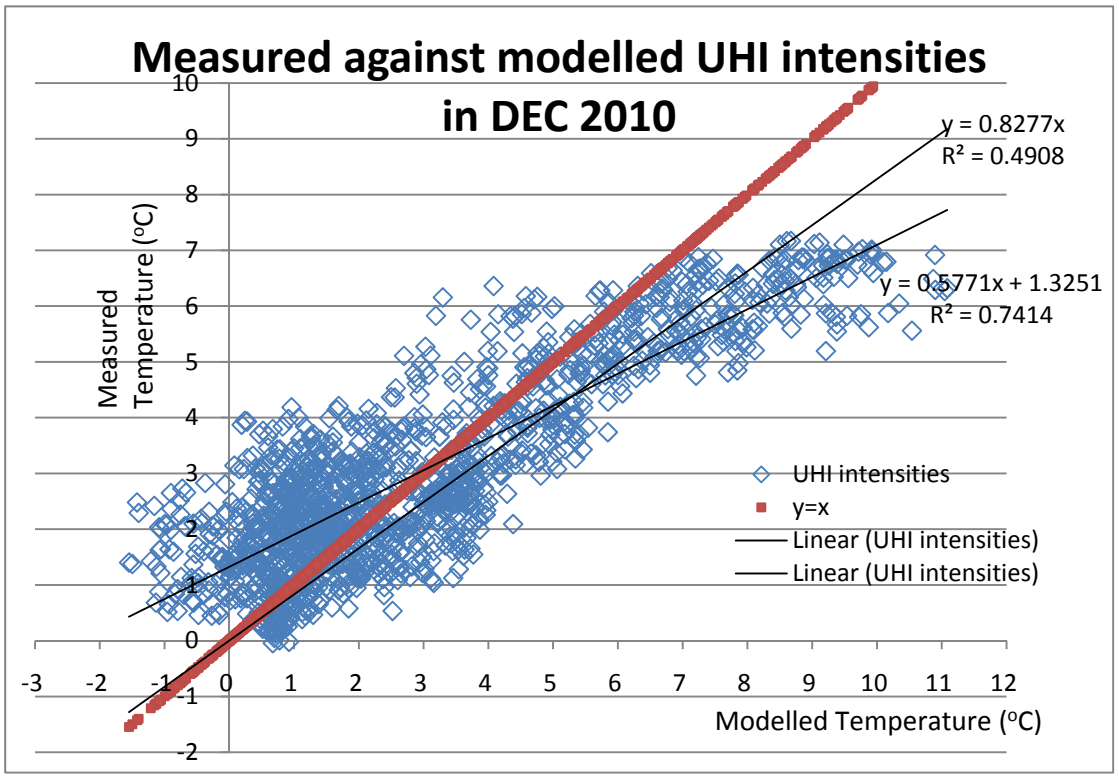

Figure 8.20 Measured UHI intensities against modelled UHI intensities in DEC 2010

Two trend lines have been drawn on each graph. The trend line with a higher R^2 value represents the best fit trend line. The other trend line was drawn to pass through the

origin to show the effect of the offset of the data and its effect on the accuracy. In theory, the model's data should be same as the actual UHI intensities and the line of best fit should have a gradient of 1 and passes through origin. The lines through the origin have R^2 values of 43% to 49% whereas the offset lines have R^2 of 55% and 74%. The higher R^2 values are for winter than summer which means the model predicts winter UHI intensities better. A t-test was also performed to confirm the significance of the result between the measured and modeled UHI intensities. One of the reasons for the different between modeled and measured UHI intensities in both summer and winter is due to the difference in local weather compared with rural weather. All the weather parameters used in this model were obtained from Met Office ground observation station for rural areas. However, the simulation's weather parameter for local area (where the street canyon was located) might be different. For example, the wind speed in the rural area might be strong at a time but the urban wind speed could be very low. This might result in a high UHI intensity in the city centre. Furthermore, anthropogenic effect was not included in the model. This might also enhance the heat island effect.

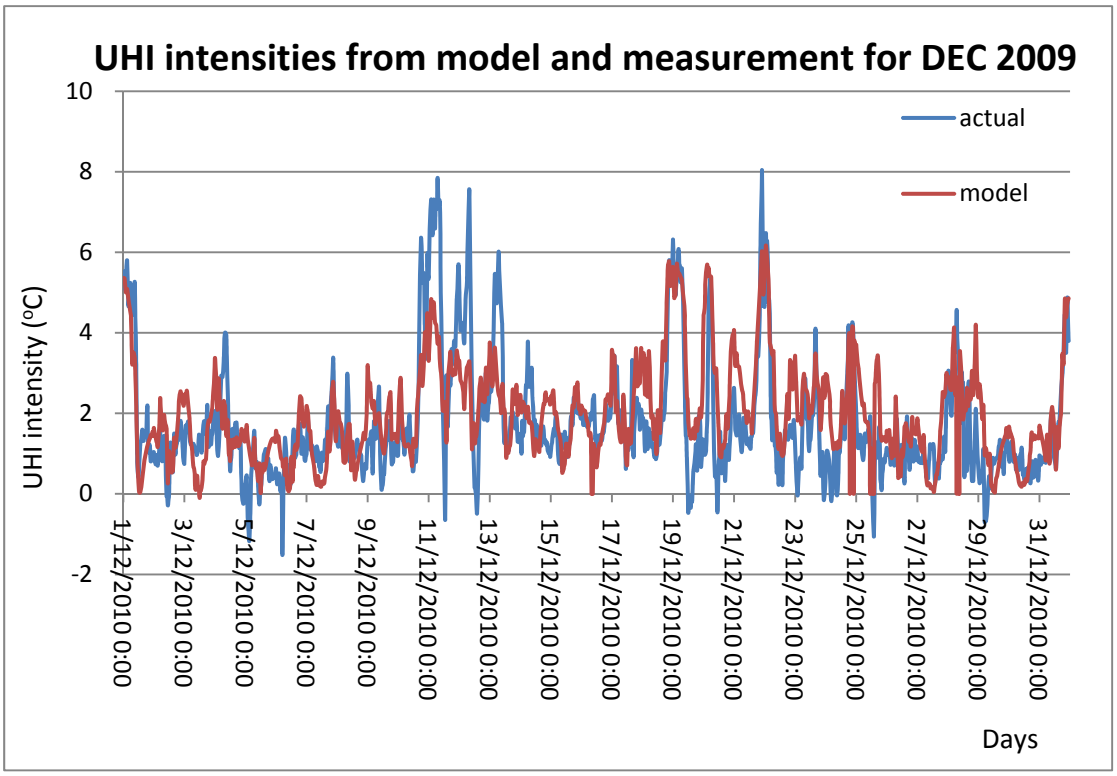

Figure 8.21 UHI intensities from model and measurement for DEC 2009

Figure 8.21 shows the graphical output of the second stage validation using Dec 2009 data which was not used in the development of the model. Similar to the first stage validation process, the model should be in phase with the calculated UHI intensity and less accurate in predicting the maximum and minimum values. Figure 8.22 shows the actual UHI intensity against the UHI intensity from the model. The R^2 value for the trend line which passes through origin dropped is 24% . This is expected to be lower than the previous result as these data were not used to create the model. Due to the limitation in time, further investigation on the model was infeasible. Nevertheless, this gives rise to a further research direction which will be discussed later in the future work section.

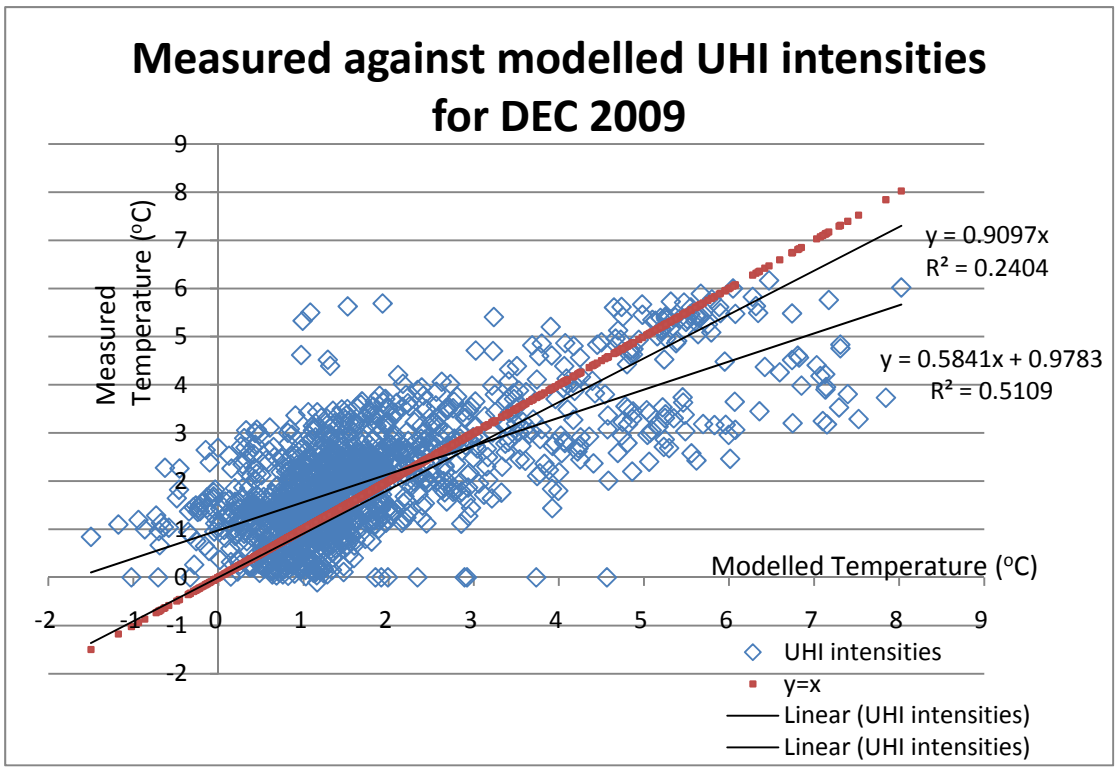

Figure 8.22 Measured against UHI intensities from model for DEC 2009

8.4.2 Non-city centre model validation

Similar to the city centre model, the non-city centre model was validated in the same way. Figure 8.23 and 8.24 shows the first stage validation result using the actual UHI intensity from one sensor-logger for JUL and DEC 2010.

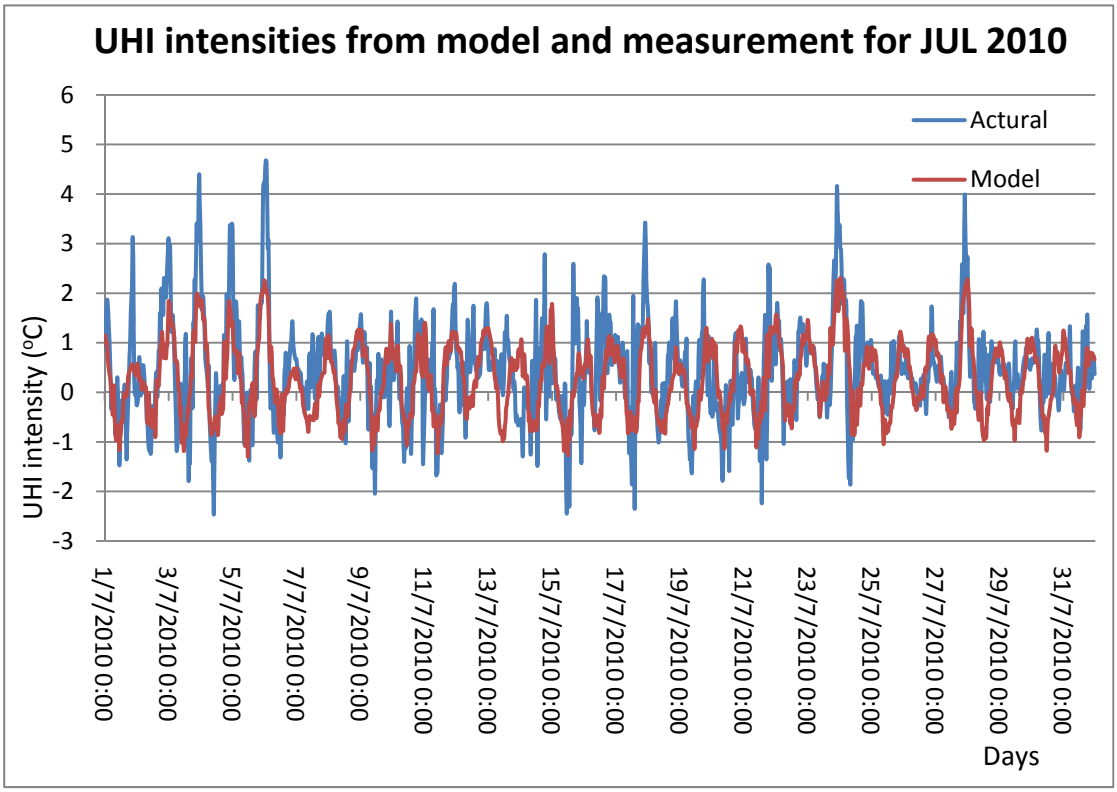

Figure 8.23 UHI intensities from model and measurement for JUL 2010

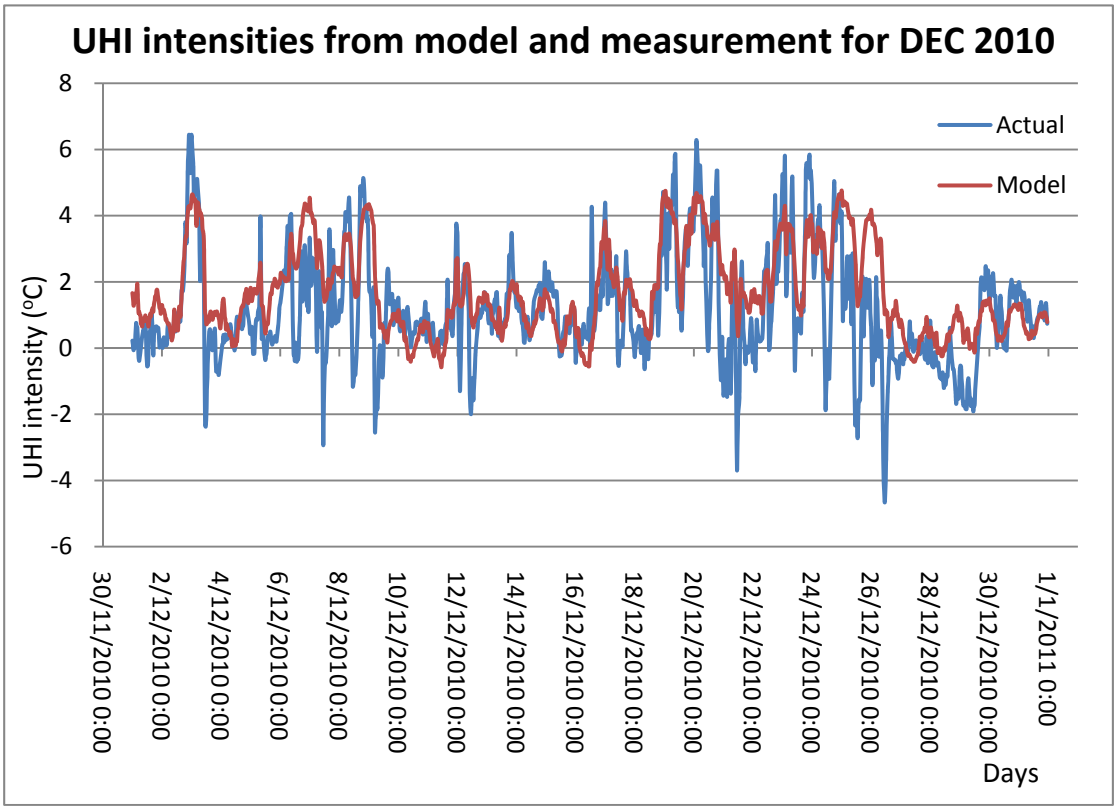

Figure 8.24 UHI intensities from model and measurement for DEC 2010

It can be seen from both figures 8.23 and 8.24 that the modelled data are in phase with the measured UHI intensities. However, the modelled data cannot predict the maximum and minimum correctly. Figures 8.25 and 8.26 show the corresponding graphs for actual against modelled UHI intensities.

The R^2 value for summer is 40% and for winter is 45%. They are lower than the values found in the city centre model. This is reflecting the larger variation in the non-city centre sensor-logger sites. December tends to have a larger UHI intensity as well as larger negative heat island intensities compared to July in both the city centre and non-city centre models. It can therefore be deduced that the model predicts better for winter than summer when the heat island intensities are usually larger.

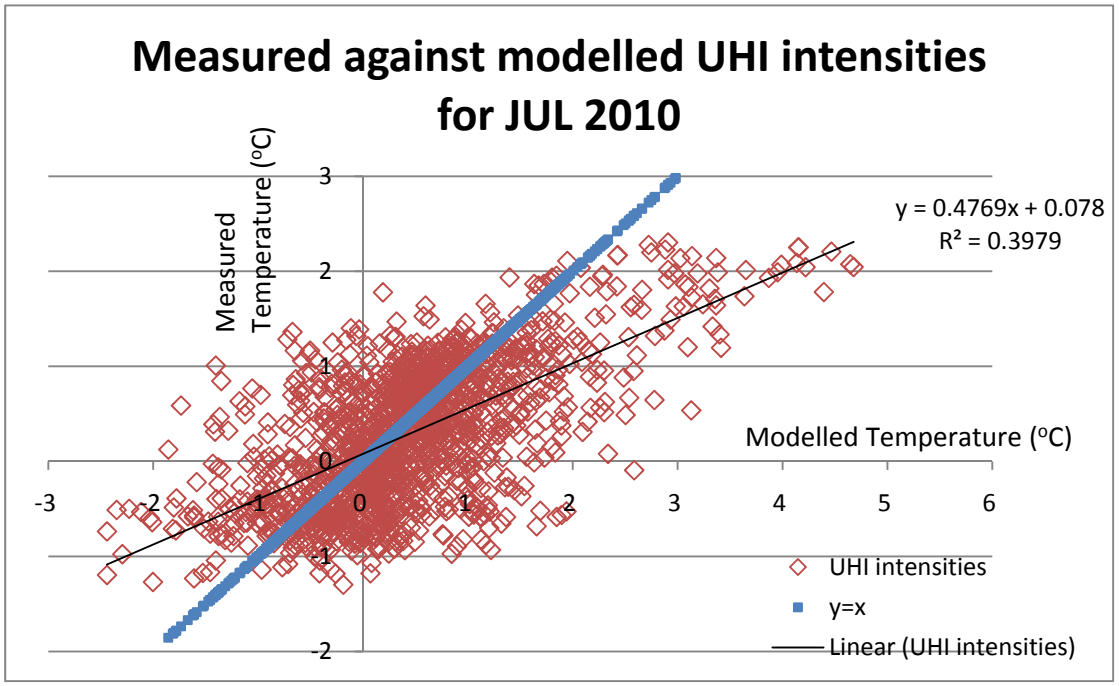

Figure 8.25 Measured against modelled UHI intensities for JUL 2010

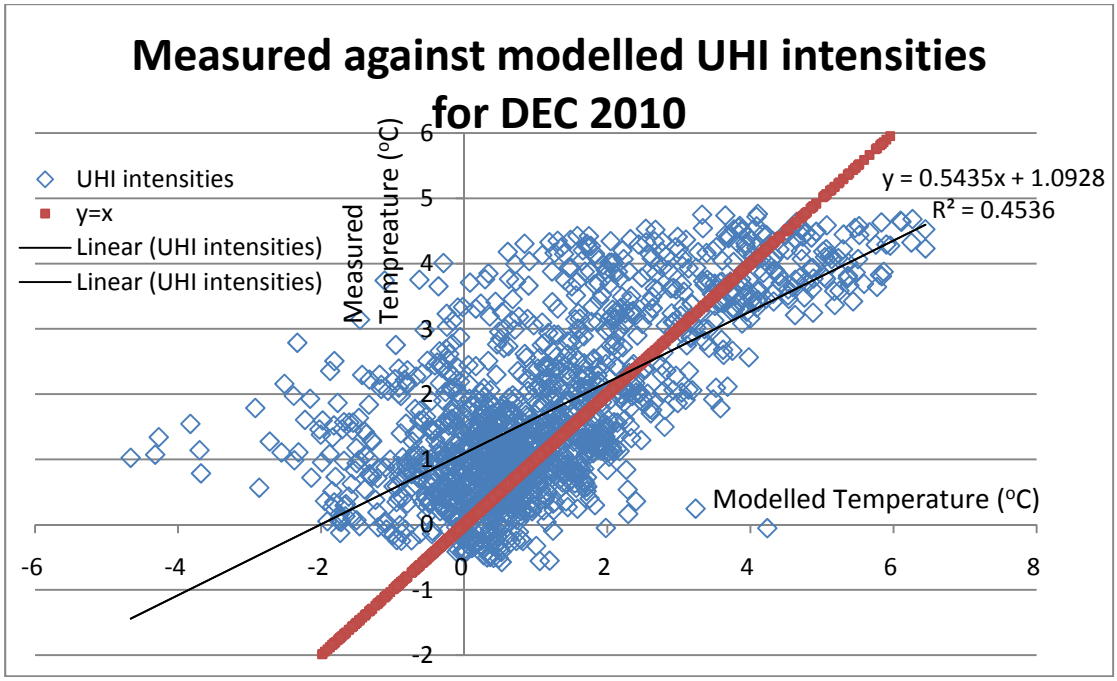

Figure 8.26 Measured against modelled UHI intensities for DEC 2010

Figure 8.27 shows the second stage validation result using DEC 2009 data. Figure 8.28 shows the actual against measured UHI intensity for the same period of time. The results are overall quite good compared to the city centre model, but the maximum and minimum values arte not modeled so accurately. R^2 is 30% of the DEC 2009 data as shown in figure 8.27. This is lower than the first stage result as expected for the same reason as explained in the city centre model.

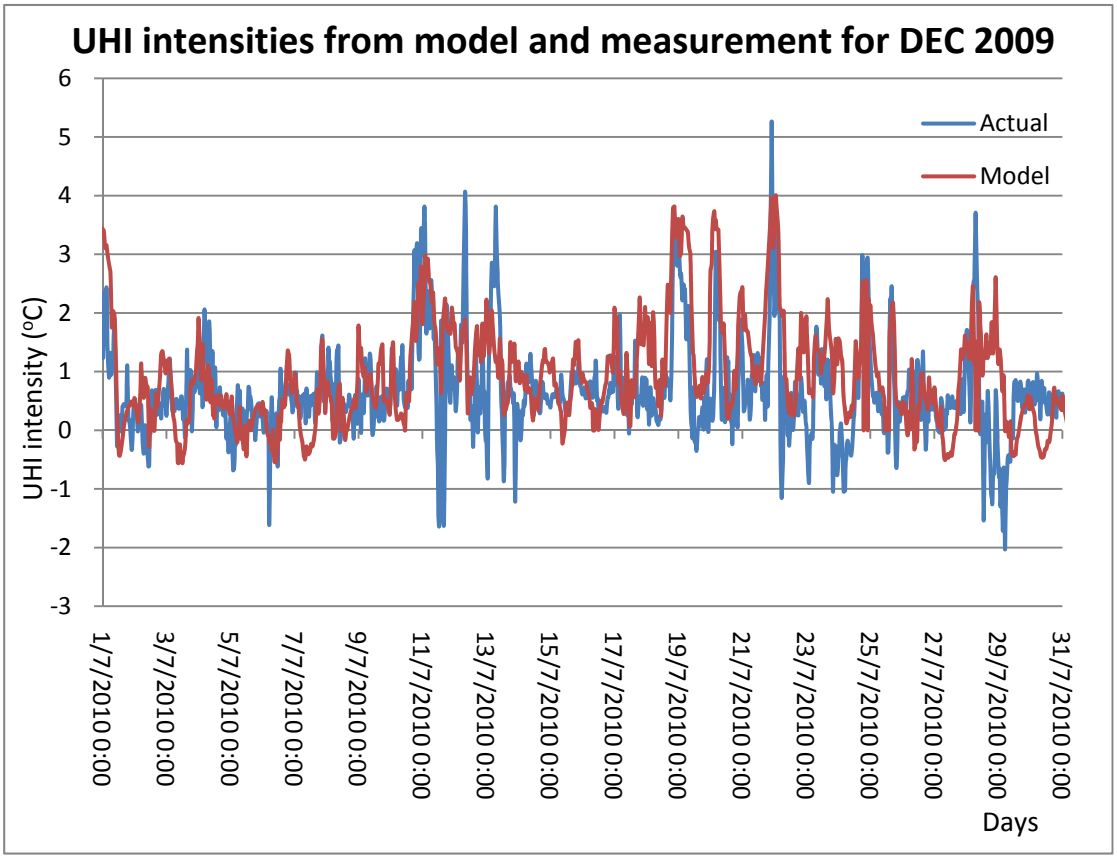

Figure 8.27 UHI intensities from model and measurement for DEC 2009

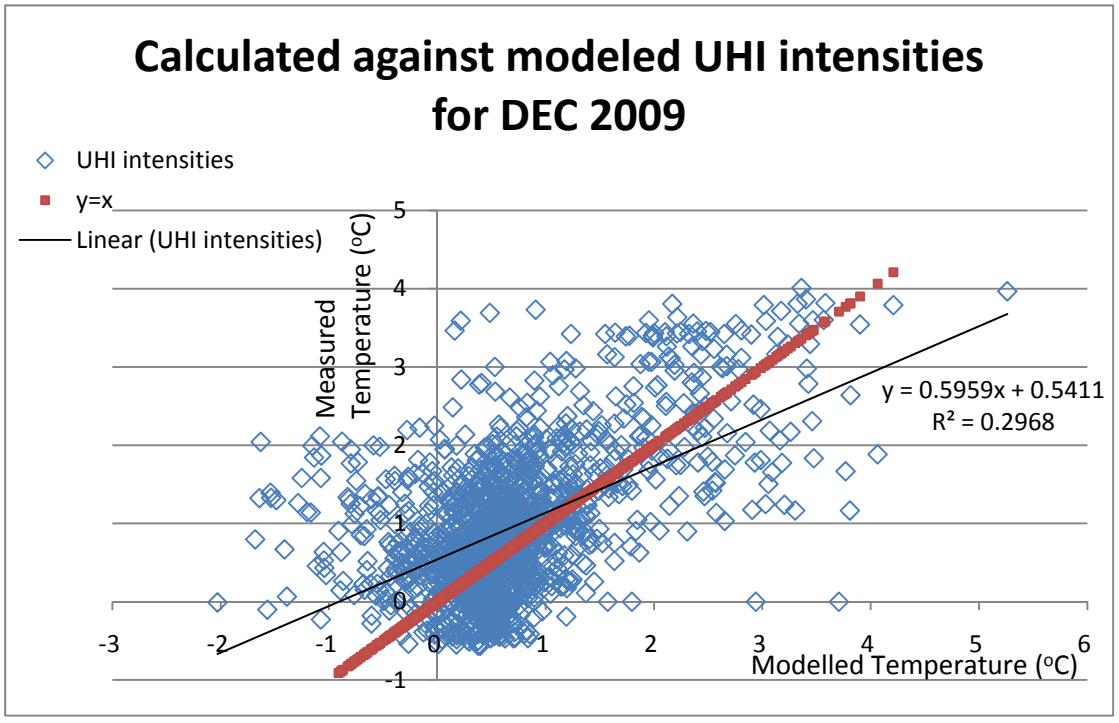

Figure 8.28 Measured against modelled UHI intensities for DEC 2009

8.5 Conclusion

Air temperature data collected from 59 sensor-loggers around Greater Manchester in 2010 were used to develop statistical models which can be used to estimate the urban heat island intensity of a canyon. Two models were developed: the city centre model and the non-city centre model. The input parameters were slightly different for these two models. Six sub-categories were also created based on the variation in data filtering. Nevertheless, only models with complete data sets were used. These models can be used with quite reasonable accuracy with Met Office hourly weather data to reflect the impact of urban heat island.

Initial analyses were performed in Excel on the UHI intensity and its key contributing factors. All factors considered were shown to have linear relationships with reasonable correlations with the UHI intensity. Thus, a general linear model was used in SPSS to generate two more general and detailed statistical models using all the parameters. From the SPSS analysis, each factor was plotted against UHI intensity to recheck the linear relationships. The linear relationships were very similar to the excel relationships. It was found from the SPSS analysis that the wind speed could be truncated to a maximum of $10ms^{-1}$ as higher wind speeds had no influence to UHI intensity (see figures 8.2 and 8.3). It was also found that the rural reference temperature could be truncated to $3^{o}C$ as heat island intensities tends to become constant with any further increase in rural reference temperature, see figures 8.8 and 8.9. This is probably due to the fact that the UHI intensity can be higher in the winter although there are more frequent occurrences of high UHI intensity values in the summer. Furthermore, the diurnal UHI intensity variation was shown to be a "squashed" sine wave. Finally, in order to simplify the calculation, the wind

directions were transformed into eight sectors. Compared with Kolokotroni and Giridharan[42] (2008) the significance levels of every parameter in the two models here in the thesis are much higher. This is probably due to the larger data sets used in the latter two models.

After generating the two models, a sensitivity calculation was performed. It was found that rural temperature was the most dominant factor followed by rainfall and total solar irradiance.

Error testes and validations process were performed on each model. Data used to develop the model was the first input. Results from the error testing suggest that both models can predict some features of the UHI intensity variations reasonably accurately. Also, the modelled UHI intensity variations are in phase with the actual intensity variation. However, the models were less able to predict the maximum and minimum UHI intensities. The validation process used a month of data not used in developing the models. These produced a lower R^2 than for first stage but still reasonably good accuracy, the t-tests showed they were significantly correlated to the 95% confident level.

To conclude, both the city centre and the non-city centre model can predict average UHI intensity for a reasonable accuracy, but the accuracy dropped in predicting the maximum and minimum UHI intensities. Nevertheless, the equation in the model could be used to modify hourly weather data, for example in Excel, to reflect the urban heat island effect. Further investigation of the model will be discussed later in the future work section. In order to predict the maximum urban heat island intensity, an analytical model was developed and will be discussed in the next chapter.

CHAPTER 9

Analytical canyon model

CHAPTER 9 Analytical canyon model

9.1 Introduction

A statistical model was developed in the previous chapter; however the model at the moment, does not predict the peak UHI intensities as accurately as the overall UHI intensities. The statistical model can be added on hourly weather data used for dynamic simulation. However, engineers will mainly be interested in the maximum UHI intensities for their building services design (steady state plant sizing[22]). Therefore, an analytical model was developed which is discussed in this chapter. A number of canyon models were briefly discussed in Chapter 3.4. Tso's model[96,97] was first considered to be suitable. Sensitivity tests performed on the evapotranspiration fraction and mass of concrete indicated that the model was capable of handling these variations. However, no canyon property is included in the model. Although the model might be capable of producing the heat island effect based on the difference in concrete mass or evapotranspriation fraction. It cannot predict the effect due to canyon specification such as SVF. Apart from Tso's model, other models have also been reviewed as mentioned in section 3.1. Nevertheless, most of these models needed more data than was available from a standard Met Office weather station and were considered more complicated than required for our engineering requirements. Therefore, a new model was developed for these purposes to calculate the maximum urban heat island effect.

9.2 Concept of canyon model

A paper has been published by the author on this model[132]. More details are given

here for completeness than are in the paper. The basic concept of the new model uses the energy balance equations based on basic CIBSE equation where possible. Short wave irradiation arrives from the sun. Part of it is reflected, the rest absorbed by the Earth. Long wave radiation was also considered. In the rural area which sees the most of, or the complete, hemispherical sky (SVF = 1.0), the upward long wave radiation from the surfaces is unrestricted as there are no obstructions blocking it. In contrast, long wave radiation is blocked to an extent by the buildings in the canyon so that not all of long wave radiation escapes to the sky. Figure 9.1 below illustrates both situations. This new model compares a rural slab of concrete with similar slabs making up a canyon so that the air temperature in the rural area and inside the canyon can be compared. The heat island can then be calculated from the subtraction of them. As concrete slabs are considered there is no consideration of evapotranspiration as the effect of the canyon shape is investigated. The details are discussed below.

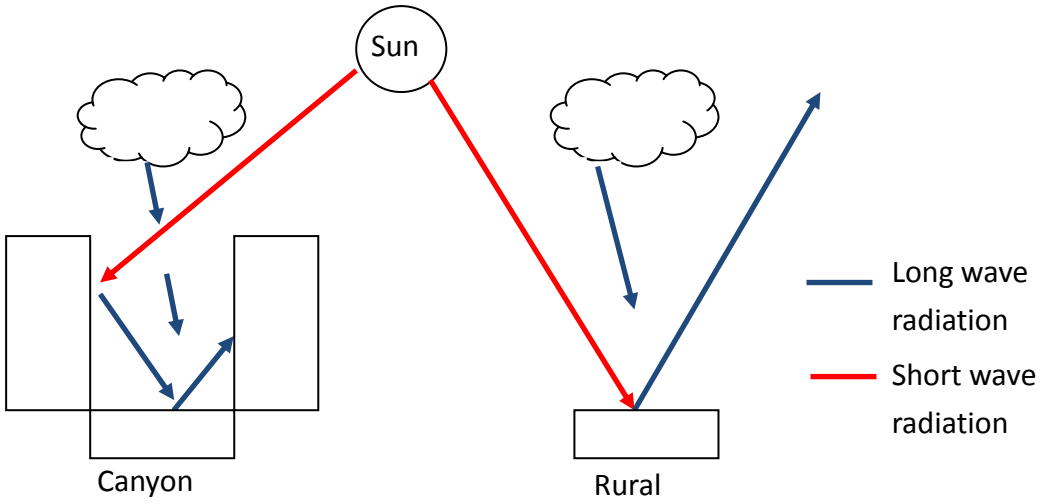

Figure 9.1 Difference in long wave radiation loss in canyon and slab condition

9.3 Rural slab model

Consider a canyon of length L metre, width W metre and height of H metre, a slab of

similar dimension should be compared. The energy balance of the slab could be found below in equation (9.1).

$$\alpha Q_{\mathrm{s}} = Q_{\mathrm{slab}} + Q_{\mathrm{l}} + Q_{\mathrm{ac}} \qquad \text{eq. 9.1}$$

Where

Q_{s} = Horizontal global solar irradiance [W]

Q_{slab} = Heat into the slab [W]

Q_{l} = Long wave irradiance emitted from slab surface [W]

Q_{ac} = Convective heat loss to the air above slab [W]

α = Absorption of solar irradiance into the slab

Given the width [W]m and length [L]m for a slab, the heat transferred into the slab was stored in its mass and part of it is lost to earth. This could be expressed by equation 9.2:

$$Q_{\mathrm{slab}} = Q_{\mathrm{e}} + \rho LW\mathrm{x}C_{\mathrm{p}}\frac{dt_{\mathrm{s}}}{dT} \qquad \text{eq. 9.2}$$

Where

ρ = The density of the slab [kgm^3]

C_{p} = The specific heat capacity of the slab [Jm^{-3}K^{-1}]

t_{s} = Temperature of the middle of the slab [$^{\mathrm{o}}$C]

x = Thickness of the slab [m]

Q_{e} = Heat lost from slab to earth [W] equation 9.3

Equation 9.3 was used to calculate the heat lost to earth

$$Q_{\mathrm{e}} = \frac{2\mathrm{k}LW(t_{\mathrm{s}} - t_{\mathrm{e}})}{\mathrm{x}} \qquad \text{eq. 9.3}$$

Where

t_{e} = Temperature of earth [$^{\mathrm{o}}$C]

k = Conductivity of slab [$\mathrm{Wm^{-1}K^{-1}}$]

The temperature of the earth varies depending on the depth of measurement. In comparison to the air temperature, this variation is much smaller during a day. It was assumed earth temperature is constant in the model. The earth temperature at 0.5m depth was found to be 6.5$^{\mathrm{o}}$C[133] above year average. In this instance for Manchester, the year average was 10$^{\mathrm{o}}$C[134], thus, the earth temperature used in this model was assumed to be 16.5$^{\mathrm{o}}$C. The temperature of the slab is heated by solar radiation during the day and becomes hotter than the air temperature. The air close to the slab will then be heated up by conduction. The warm air starts to rise due to its lighter density. In contrast, the slab is cooler at night than air temperature as long wave radiation is lost to the cold sky. Convection heat flow stops. Maximum urban heat island occurs on a clear and calm night according to Oke[1] which has also been confirmed by the temperature measurements mentioned in earlier chapters. Consequently, the advection heat (Q_{as}) in equation 9.1 could be ignored in the model.

Solar irradiance could be found from weather data. Long wave radiation loss depends on cloud cover level. Equation 9.4 below was obtained from CIBSE guide A[22] determining the long wave radiation lost.

$$Q_{\mathrm{l}} = LW(93 - 79C) \qquad \text{eq. 9.4}$$

Where

$$C = \text{Cloud cover } (0 \leq \mathrm{C} \leq 1)$$

Substituting into equation 9.1, the slab differential equation becomes:

$$\alpha q_{\mathrm{s}} = \frac{2\mathrm{k}(t_{\mathrm{s}} - t_{\mathrm{e}})}{\mathrm{x}} + \rho \mathrm{x} C_{\mathrm{p}} \frac{dt_{\mathrm{s}}}{dT} + (93 - 79C) \qquad \text{eq. 9.4a}$$

Equation 9.4a was then rearranged and becomes equation 9.5

$$\left[\frac{\mathrm{x}}{\mathrm{k}}\right]\{\alpha q_{\mathrm{s}} - (93 - 79C) - 2(t_{\mathrm{s}} - t_{\mathrm{e}}) = \tau \frac{dt_{\mathrm{s}}}{dT} \qquad \text{eq. 9.5}$$

Where

$$\tau = \frac{\rho \mathrm{x}^2 C_{\mathrm{p}}}{\mathrm{k}}$$

τ is the time constant of the slab, the differential equation 9.5 has the solution as equation 9.6 below:

$$t_{\mathrm{s2}} - t_{\mathrm{s1}} = (\beta - t_{\mathrm{s1}})\{1 - \exp[\frac{-2(T_2 - T_1)}{\tau}]\} \qquad \text{eq. 9.6}$$

Where

$$\beta = (\frac{\mathrm{x}}{2\mathrm{k}})[\alpha q_{\mathrm{s}} - (93 - 79\mathrm{C})] + t_{\mathrm{e}}$$

9.3 Canyon model

The canyon model was also created based on the same energy balance equation (eq. 9.1) Nevertheless, some modifications were made to the equations of irradiance absorption and reflection. Figure 9.2 indicates a typical street canyon. The opening on top of the canyon has the same area as a slab. This is to ensure that the same amount of solar irradiance was received as to the slab model. In order to simplify the model,

the canyon was considered as three slabs. The two vertical slabs represent the external surface of a building facing the canyon.

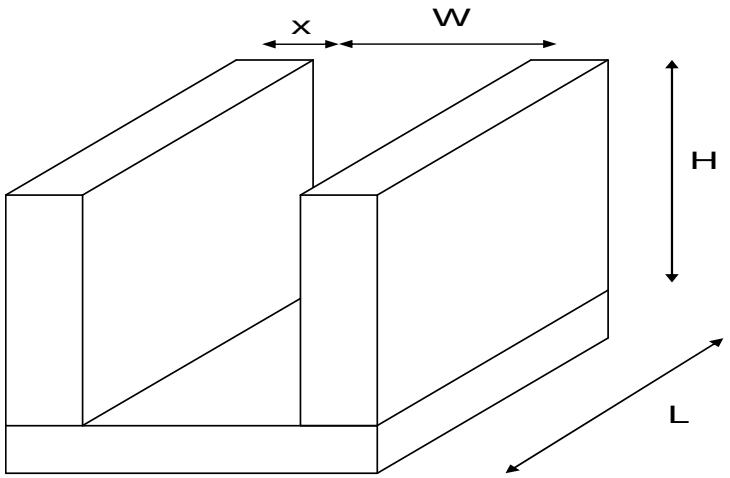

Figure 9.2 A street canyon

Equation 9.10 was the canyon exchange equation.

$$Q_{\text{sabc}} = Q_{\text{canyon}} + Q_{\text{lc}} + Q_{\text{ac}} \qquad \text{eq. 9.10}$$

Where

Q_{sabc} = Solar irradiance absorbed by the inside of the canyon [W]

Q_{canyon} = The heat conduction at the canyon's inside surface [W]

Q_{lc} = Long wave radiation from canyon [W]

Q_{ac} = Convective heat exchange between the air within the canyon and the inside canyon surface [W]

Equation 9.11 shows the conduction effect in the canyon. Only surfaces inside the canyon would be considered. The heat inside the canyon is stored in the mass of the canyon surfaces. Heat flows from the slabs to (or from) the earth and the interiors of buildings. Figure 9.3 indicates all the temperature abbreviations used.

$$Q_{\text{canyon}} = Q_{\text{cie}} + \rho L(2H + W)\text{x}C_{\text{p}}\frac{dt_{\text{c}}}{dT} \qquad \text{eq. 9.11}$$

Where

Q_{cie} = Heat flow to (or from) slabs into earth or building interior [W] (see eq. 10.12)

t_{c} = Temperature of middle of the canyon slab [$^{\text{o}}$C] (see figure 9.3)

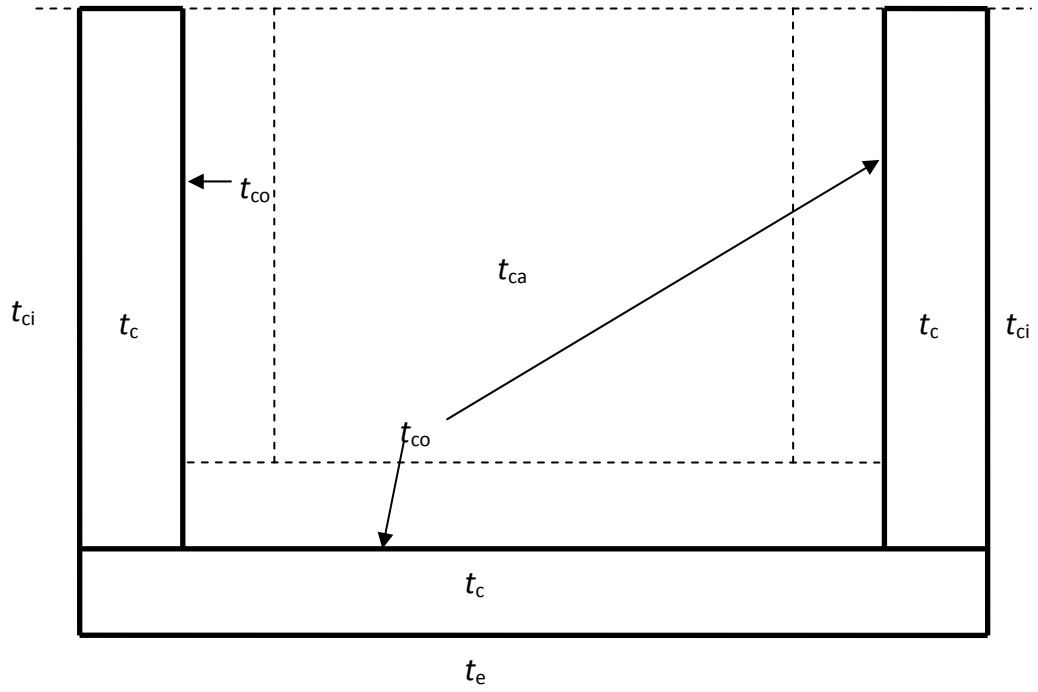

Figure 9.3 Temperature abbreviations used in canyon model

Equation 9.12 indicates the calculation of Q_{cie}, which is the heat flow from the canyon slabs into earth or building interior. In order to simplify the model calculation, an area weighted "outer" canyon surface temperature was derived from the building interior temperature t_{ci} (which is assumed to constant all the time) and the earth temperature t_{e} as shown in equation 9.13

$$Q_{\text{cie}} = \frac{2\text{k}L(2H+W)(t_{\text{c}}-t_{\text{cie}})}{\text{x}} \qquad \text{eq. 9.12}$$

$$t_{\text{cie}} = \frac{2LHt_{\text{ci}}+WLt_{\text{e}}}{2HL+WL} = \frac{2Ht_{\text{ci}}+Wt_{\text{e}}}{2H+W} \qquad \text{eq. 9.13}$$

Similar to the slab model, the advection heat transfer would not be considered because

this model is aimed to predict maximum urban heat island effect which occurred on clear and calm nights. Convection heat transfer would also be ignored due to similar reasons as described in the slab model.

Substituting into the energy exchange equation (eq 9.10), the canyon model become:

$$\left[\frac{\mathrm{x}}{kL(2H+W)}\right](Q_{\mathrm{sabc}} - Q_{\mathrm{lc}}) - 2(t_{\mathrm{c}} - t_{\mathrm{cie}}) = \tau\frac{dt_{\mathrm{c}}}{dT} \qquad \text{eq. 9.14}$$

This could be solved similarly to equation 9.5.

9.4 Maximum UHI effect

The purpose of this model is to look at the maximum urban heat island effect which will occur under clear and calm night conditions. The differential term will tend to zero in both slab model (eq. 9.5) and canyon model (eq. 9.14). In addition, the solar irradiance in both equations was ignored as well because maximum urban heat island always occurs at night. In the steady state for slab:

$$2(t_{\mathrm{s}} - t_{\mathrm{e}}) = (t_{\mathrm{so}} - t_{\mathrm{e}}) \qquad \text{eq. 9.15}$$

Similarly for the canyon,

$$2(t_{\mathrm{c}} - t_{\mathrm{cie}}) = (t_{\mathrm{co}} - t_{\mathrm{cie}}) \qquad \text{eq. 9.16}$$

The slab equation (eq. 9.5) will then become:

$$\left[\frac{\mathrm{x}}{\mathrm{k}}\right]\{-(93 - 79C)\} + t_{\mathrm{e}} = t_{\mathrm{so}} \qquad \text{eq. 9.17}$$

Similarly, the canyon equation (eq. 9.14) becomes:

$$\left[\frac{\mathrm{x}}{\mathrm{k}L(2H+W)}\right]\{-(93-79C)\}+t_{\mathrm{cie}}=t_{\mathrm{co}} \qquad \text{eq. 9.18}$$

The UHI intensity could be found by subtracting equation 9.17 from equation 9.18:

$$t_{\mathrm{co}}-t_{\mathrm{so}}=\left[\frac{\mathrm{x}}{\mathrm{k}L(2H+W)}\right][-Q_{\mathrm{lc}}]+t_{\mathrm{cie}}-t_{\mathrm{e}}-\left[\frac{\mathrm{x}}{\mathrm{k}}\right][-93] \qquad \text{eq. 9.19}$$

The long wave losses from the inside walls and floor of the canyon were assumed to be similar to the slab, therefore, equation 9.19 becomes:

$$t_{\mathrm{co}}-t_{\mathrm{so}}=\left[\frac{\mathrm{x}}{\mathrm{k}L(2H+W)}\right][-93]+t_{\mathrm{cie}}-t_{\mathrm{e}}-\left[\frac{\mathrm{x}}{\mathrm{k}}\right][-93] \qquad \text{eq. 9.19}$$

Rearrange equation 9.19 becomes equation 10.20

$$t_{\mathrm{co}}-t_{\mathrm{so}}=\left[\frac{\mathrm{x}}{\mathrm{k}}\right]\left[\frac{2H}{(2H+W)}\right][93]+t_{\mathrm{cie}}-t_{\mathrm{e}} \qquad \text{eq. 9.20}$$

Finally substituting the calculation of t_{cie} from equation 9.13:

$$t_{\mathrm{co}}-t_{\mathrm{so}}=\left[\frac{2H}{(2H+W)}\right]\left[93\left[\frac{\mathrm{x}}{\mathrm{k}}\right]+t_{\mathrm{ci}}-t_{\mathrm{e}}\right] \qquad \text{eq. 9.21}$$

Equation 9.21 can be used to calculate the maximum heat island intensity. The factors included in equation are:

1. Height and Width of canyon,
2. Conductivity of the concrete
3. Thickness of the concrete
4. Building interior temperature
5. Earth temperature

The earth temperature was assumed to be constant at 16.5^{o}C and the building interior

temperature was assumed as 21°C. UHI intensity calculated from equation 10.21 would be validated in the next section by comparing with the calculated UHI intensity from measured air temperature in the canyon.

9.5 Validation of model

UHI intensity calculated from equation 9.21 is validated to confirm the accuracy of the model. Similar to chapter 7, only the winter UHI intensity and the summer UHI intensity could be used to validate the model because winter and summer are the extreme cases.

SVF instead of height and width of canyon was measured and calculated in this project. Therefore, equation 9.21 was transformed slightly to cope with SVF. The relationship between SVF and height to width ratio was mentioned by Oke[1] in equation 9.22 below.

$$SVF = \cos\{\tan^{-1}\left(\frac{2H}{W}\right)\} \qquad \text{eq. 9.22}$$

After substituting into equation 9.21, it becomes:

$$t_{co} - t_{so} = \{\frac{\tan(\cos^{-1}[\text{SVF}])}{1+\tan(\cos^{-1}[\text{SVF}])}\}\left[93\left[\frac{x}{k}\right] + t_{ci} - t_{e}\right] \qquad \text{eq. 9.23}$$

The trigonometric term (tan/(1+tan)) is almost linear. As the term in square brackets is a constant, the maximum urban heat island effect ($t_{co} - t_{so}$) is a linear function of SVF. Figure 9.4 shows the model and measured UHI intensities for nine canyons in Manchester city centre during summer. The measured UHI intensities were average values for all clear and calm nights (same condition criteria as stated in chapter 6.3,

100 hours over 36 nights.) The model fits the best when $\left[93\left[\frac{x}{k}\right]+t_{ci}-t_{e}\right]$ has a value of 7.98 and a slop of 5.0. This implies a low value of x with a typical conductivity of k at 1.13. The best fit line to the data is:

$$UHI_{\text{effectmax}} = 6.43 - 2.12SVF \qquad \text{eq. 9.24}$$

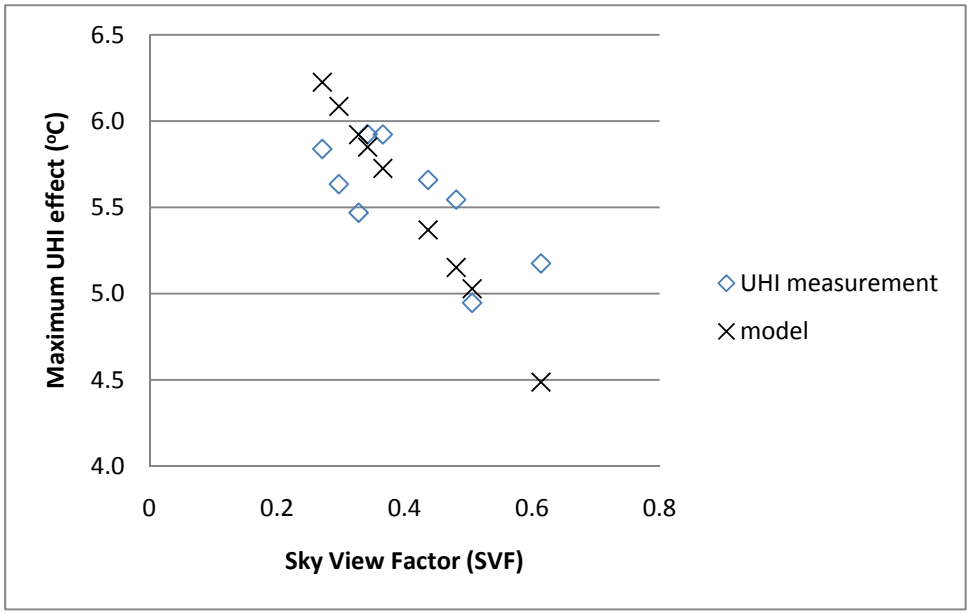

Figure 9.4 Model vs canyon measurements in Manchester City centre during the summer

The model has a reasonable fit to the data but it is interesting that the maximum UHI intensity would be 6.43°C when SVF is 0 which means the sky is completely blocked with no long wave radiation escape. This agrees well with figures 6.4 and 6.5. Also the urban heat island does not disappear when SVF=1. This is believed to be caused by the urban and suburban sprawl. In this project the most remote sensor-logger is still located in the suburban area. Also, some of the suburban areas also have their own canyon which might contribute towards the UHI effect.

Figure 9.5 shows the model and measured UHI intensities for nine canyons in Manchester city centre during winter. The measured UHI intensities were average UHI intensity for all clear and calm nights (same condition criteria as stated in section

7.3, 140 hours over 45 nights.) The model fit the best when $\left[93\left[\frac{x}{k}\right]+t_{ci}-t_{e}\right]$ has a value of 4.82 and a slope of 3.1. This also implies a low value of x similar to the summer equation with a typical conductivity of k at 1.13. The best fit line to the data is:

$$UHI_{\text{effectmax}} = 4.0 - 1.68SVF \qquad \text{eq. 9.25}$$

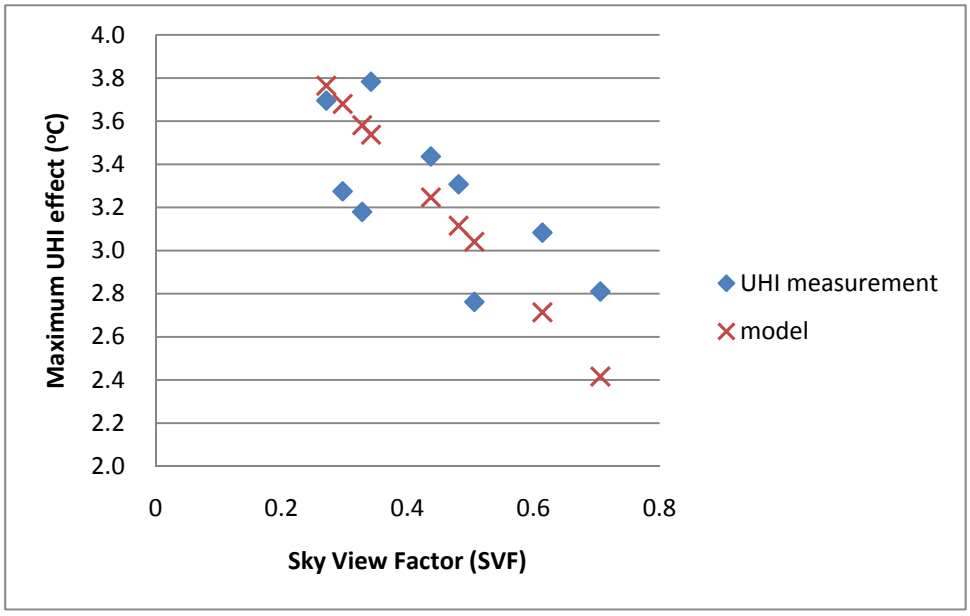

Figure 9.5 Model vs canyon measurements in Manchester City centre during the winter

The model fits the winter data better than the summer data and it indicates a maximum UHI intensity from equation 9.25, is 4°C when the SVF is 0. Similarly to the summer urban heat island, the UHI effect does not disappear when SVF is equal to 1. This is could well be the "cliff" effect mentioned in chapter 6.1 and shown in figure 6.3. However, both the fitted model and the measured data show that the canyon only provides part of the UHI effect. This is confirmed by the measurement shown in figure 6.2 that the canyon contributes about a third of the maximum UHI effect and that the "urban sprawl" beyond the canyon contributes about two thirds.

9.6 Conclusion

An analytical model was developed using energy balance equations to calculate the maximum urban heat island intensities at clear and calm nights. The equation includes canyon characteristics such as height and width or SVF, earth temperature and building interior temperature. Initial validation indicates the model is in-line with averaged measured UHI intensities in summer. The comparison seems slightly lower in winter however; the R^2 indicates a better fit in winter than in summer. This is believed to be the reason of urban and sub-urban sprawl. Further improvement on the model is required. Please refer to future work for detailed further research section.

CHAPTER 10

Conclusion and future work

CHAPTER 10 Conclusion and future work

10.1 Conclusion

Air temperature measurements were performed in 59 fixed point monitoring station over Greater Manchester at 30 minutes intervals. All sensor-loggers were calibrated with a certified device. The radiation shields used were also tested against a Stevenson Screen to compare performances. The urban heat island intensity for each monitoring station was found by subtracting from it the rural reference air temperature at Woodford.

Positive UHI intensities were found during most of the nights indicating the existence of urban heat island effect in Greater Manchester. Negative UHI intensities were found on some clear and calm mornings after sun-rise showing an urban cool island.

Clear and calm nocturnal UHI intensities were used to analyse against the different factors that causes the heat island effect. These factors includes: Sky view factor, distance away from city centre, evapotranspiration fraction, wind speed, cloud level and rural reference temperature. Negative linear relationships were found for all the factors against UHI intensities. However, it was found that the effect tends to become constant as wind speed is greater than $10ms^{-1}$ and rural reference temperature is greater than $3^{o}C$. UHI intensity contours were also created for a few clear and calm nights. It was found that the urban heat island centre could be shifting according to the wind direction.

All UHI intensities data were input into statistical software. General linear

multi-regression models were produced. Validation proved that these models were capable of predicting the average UHI effect, but not the maximum and minimum. It was believed that this is due to some missing factors in the model. The equation of this model could then be used to modify hourly air temperature weather data.

An analytical model was created using energy balance equations to calculate the maximum urban heat island intensity. Input parameters includes: earth temperature, indoor temperature, SVF (or height and width of canyon), and thickness of concrete. Validation shows that this model can predict maximum urban heat island intensity in summer but the model does not perform very well for winter predictions. One of the reasons for this is speculatively because the averaged winter UHI intensities used to validate the model are lower than that of summer.

The hypotheses were:

1. There is an urban heat island effect in Greater Manchester.
2. Urban geometry contributes towards urban heat island
3. This urban heat island effect can be modelled statistically or empirically and reasonably simply.
4. Weather data can be used with the model to reflect urban heat island effect.

The heat island intensity varied from 4^{o}C to 7.8^{o}C during summer and -2^{o}C to 12^{o}C during winter in 2010 indicating the existence of urban heat island effect in Greater Manchester (hypothesis 1). The average UHI intensity was found to be 1.97^{o}C during winter and 1.44^{o}C during summer. This agrees with the result from Watkins[44] (2002) and Kershaw[104] *et al.,* (2010). The maximum UHI intensity was higher in winter than

that of summer but the occurrence of high urban heat island was more frequent in summer than in winter.

UHI intensities on clear and calm nights were selected and compared with different causal factors of urban heat island effect because the UHI effect is maximum under clear and calm conditions [Oke[1] (1978)]. UHI intensity was found to drop as SVF increases. It was found that the R^2 of SVF and UHI intensity is 32% in clear and calm summer nights and 36% in clear and calm winter nights. The R^2 values for the UHI intensity against SVF smaller than 0.65 was 64% in summer and 63% in winter. This indicates a strong relationship between small SVFs and the UHI intensity. The UHI intensity also reduced when the distance from city centre increased. R^2 values equalled 64% and 43% for relationships between the UHI intensity and the distance from city centre in summer and winter respectively. The evapotranspiration fraction was also found to have a negative linear relationship with UHI intensity. R^2 values for the relationship between EF and UHI intensity in the summer was 33% and in the winter was 35%. The UHI intensity was also found to have a relationship with low wind speed (less than 10 ms^{-1}). The R^2 value for the summer was 59% and for the winter was 46%. The rural reference temperature was also found to be correlated to the UHI intensity. The relationship was stronger in the winter (R^2 of 51%) than in the summer (R^2 of 13%).

Hypothesis 2 was proved because urban geometry (represent by SVF) was found to have about 2^oC contribution towards the overall urban heat island effect on a clear and calm night by temperature monitoring. The analytical model also found that the influence of SVF towards the urban heat island varies from 1.68^oC in winter to 2.12^oC in summer.

Regarding hypothesis 3, the temperature data obtained from all the sensor-loggers in 2010 were used to develop two multiple regression models, the city centre model and the non-city centre model. These models can be expressed by an equation consisting of different causal factors of the UHI effect with different coefficients. They could be used to modify the hourly weather data from the Met Office. Both models were validated against the 2009 data. The city centre model had an R^2 of 24% and the non-city centre model had an R^2 of 30% when comparing the model prediction with the measured UHI intensity in 2009. Both models could be used with hourly weather data (hypothesis 3) to reflect the impact of the urban heat island, although the accuracy dropped in predicting the maximum and minimum UHI intensities.

An analytical model (hypothesis 3) was also created by using energy balance equations to predict the maximum urban heat island effect. This model was also validated with measured UHI intensity data. Results indicated a good fit with summer measured UHI intensities but a lower fit with the winter UHI intensities. Further improvement of the model is required and other parameter, such as wind, included.

Although the statistical model can be used with weather data, hypothesis 4 is not fully completed because the peak heat island intensities cannot be predicted accurately with the model. The analytical model created can only predict maximum urban heat island intensities. Therefore it cannot be used with hourly weather data at the moment. However, the concept of modifying weather data to reflect urban heat island has been demonstrated in this thesis. Future works on the model is required.

10.2 Future work

Considering the output so far, the following work is recommended in the future.

10.2.1 Temperature monitoring

1. The temperature monitoring process should continue so that more data could be collected for future model development. Clear and calm data is especially required as it is when the maximum UHI often occurs.
2. Additional monitoring points should be set up in small canyons with low SVFs
3. Additional monitoring points should be set up to cover further positions (outside Greater Manchester) right up to the rural reference point to estimate, more accurately, the urban "cliff".
4. Further measurement of the evapotranspiration effect would provide more data for Greater Manchester especially around the parks and green areas. Dry bulb and RH sensor-loggers are now available.
5. Additional sensor-loggers should be set up to measure other weather parameters in canyons such as the relative humidity and wind speed. Wind speed data in canyons would be especially useful for developing better canyon models, but the stand-alone wind sensor-loggers are not currently available.

10.2.2 Statistical model

1. Additional factors such as anthropogenic heat should be covered in the model.
2. It would be interesting to modify the model with the dependent variable as y=ln (UHI+5) so that this might model the peak data better.

10.2.3 Analytical canyon model

1. Modify the model to cover additional weather and canyon criteria, such as wind effect, solar irradiance, anthropogenic heat etc, so that it can be used to predict hourly heat island intensity rather than just the maximum.
2. It should be investigated further whether the canyon model can be combined with the statistical model into a single model.

Apart from the fine-tuning of the existing work, there are also other future research directions. Both the statistical model and the analytical model need to be assessed for use in other cities. However, there is no other data readily available, even from London to test and fine tune the models. But as a first step in assessing the UHI effect in other towns and cities in the UK the models detailed in this thesis are useful. Finally, weather data modified with these models should be used for building simulation and plant sizing so that the energy consumption of a building under the effect of an urban heat island can be investigated.

Related publications

Journal Papers:

Cheung, H., Levermore, G., Watkins, R. (2010) A low cost, easily fabricated radiation shield for temperature measurements to monitor dry bulb air temperature in built up urban areas. *Building Services Engineering Research and Technology* (31)4, 371-380

Levermore, G., Cheung, H. (2011) A low order canyon model to estimate the influence of canyon shape on the maximum urban heat island effect. *Building Services Engineering Research and Technology* Submitted in March 2011

Conference Paper:

Cheung. H. and Levermore, G. - *Urban Heat island in Manchester, UK* LCCA 2010：1st China-UK Forum on the theme of Low Carbon Cities and Architecture

Leveremore. G., Watkins. R., Cheung. H., Hill. F., Lindy. S. and Webb.A - *Low carbon cities and the urban heat island effect; a UK perspective* LCCA 2010：1st China-UK Forum on the theme of Low Carbon Cities and Architecture

Appendix A – Temperature sensor selection experiment

Introduction

Air temperature is one of the most important factors for Urban Heat Island (UHI). In order to measure and log temperature correctly, a suitable temperature sensor with reasonable response time need to be selected. The purpose of this experiment is to test the response time of three different temperature sensors, I-button, Rotronic and Tinytag using a HVAC unit in the laboratory. The actual temperature in the HVAC unit will also be measured with a thermometer. All the readings will be plotted into graphs for comparison.

A suitable temperature sensor will be recommended for measuring air temperature in Manchester based on the result of this experiment. 50 temperature sensors are proposing to be mounted on street lamp posts around Manchester with a radiation shield.

This experiment is carried out further to the previous similar experiment but with a longer heating period to ensure all temperature sensors reach their maximum reading during the single step change.

Aim:

- To find out the response time of 3 different temperature sensors, I-button, Rotronic and Tinytag using HVAC unit.

Methodology and Procedure

HVAC unit (Fig 1) is used in the experiment. There are two separate 1kW air heaters inside the unit. 3 temperature sensors with a thermometer are placed inside in the section just after the air heater. The whole HVAC unit was left non-operation for 1 hour to stabilize the temperature sensors. The fan was then switched on for 10 minutes, both air heaters was then switched on for 2 hours. The fan was still left in operation for 30 minutes after the heater was switched off. The settings of three temperature sensors are shown in table 1

The thermometer reading was taken manually every 1 minute. Excel was used then to interpolate the results into five seconds intervals for I-button and thermometer

readings. Rotronic readings are recorded every 5 seconds and will be used as the reference time interval. Tinytag readings will also be interpolated to the same time interval for comparison.

(Fig 1)

Temperature Sensor	Logging interval
I-Button	1 minutes
Tiny-tag	5 seconds
Rotronic	5 seconds

Table 1: Temperature sensor setting

The thermometer used in this experiment has been calibrated before. However, the accuracy of the three temperature sensors is uncertain. Solver is Excel is used to optimize the results from all sensors. A bid was add on the results and solver is used to minimize the sum of all error difference squares.

The time constant of a sensor is the defined by the sensor time for the sensor temperature to rise to 63.2% of its full temperature rise [1]. The time constant of all 3 sensors and the thermometer will also be calculated and shown.

$$t_s - t_{s\,initial} = \{ t_{final} - t_{s\,initial} \}[1 - exp\,(-T/\tau)] \qquad \text{----} \qquad [1]$$

From equation 1 [1], the difference between the maximum (final) temperature and the

temperature at any point is an exponential equation. Therefore, if we take natural log, this should become a linear equation.

The linearity of a first order system will also be checked by plotting the natural log of the differences between the max temperature and the temperature reading at each time interval. Regression Test from Excel Add-in tool will also be performed to check the R^2 of the readings against time.

Results and Discussion:

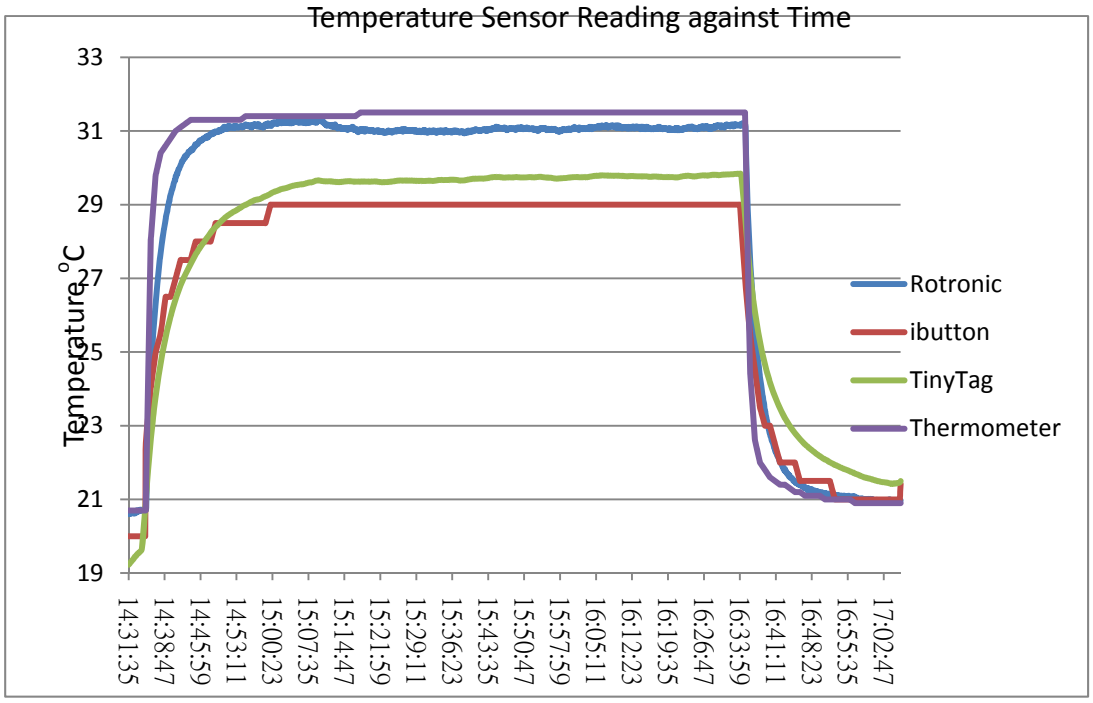

Fig 2 – Original Temperature Reading Against Time

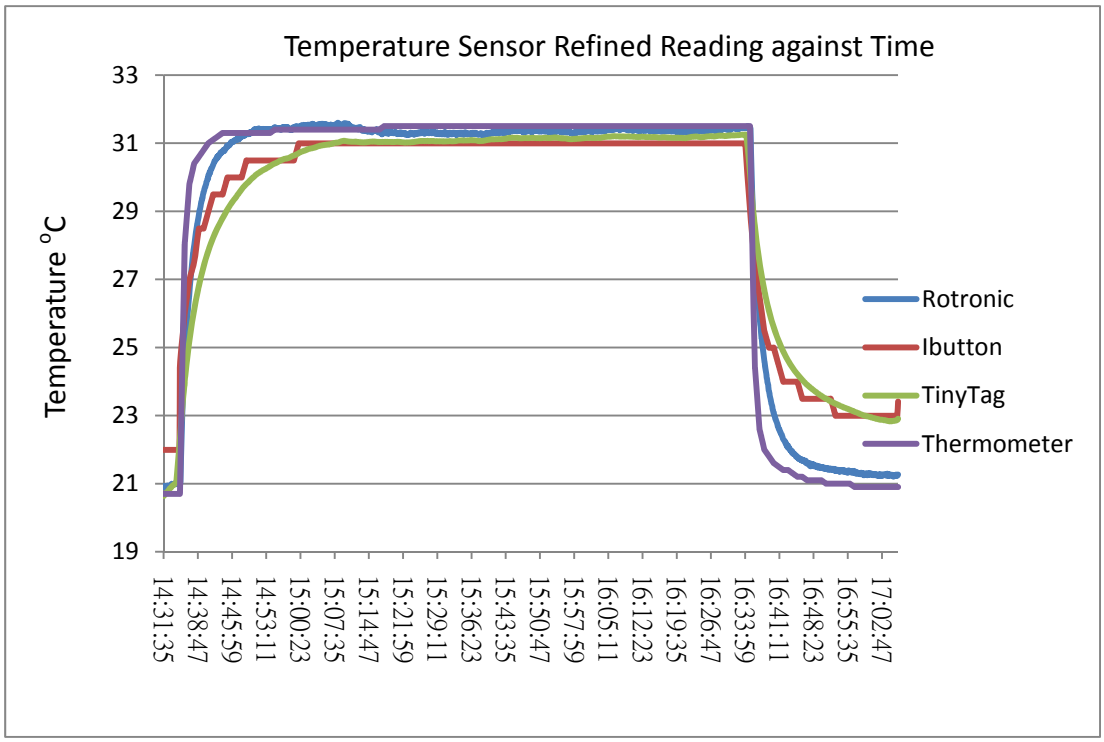

Fig3 – Optimized Temperautre Reading against Time

Hand Calculation of Time constant

Time constant of temperature sensor is the time for the sensor to reach 63.2% of its maximum value in one step change

The table below shows the calculation of the time constant of all 3 temperature sensors

Starting time: 14:35:00

	Thermometer	Rotronic	I-button	TinyTag
T_{Max}	31.5	31.309	29	29.844
$T_{Initial}$	20.7	20.719	20	20.9294
$T_{max} - T_{initial}$	10.8	10.59	9	8.9146
at 63.2%	6.8256	6.69288	5.688	5.6340272
Plus $T_{initial}$	27.5256	27.41188	25.688	26.5634272
Time this occurs	14:35:55	14:37:44	14:38:11	14:41:19
Time Constant	0:00:55	0:02:44	0:03:11	0:06:19

The difference between T_{max} and $T_{initial}$ is the same as same bias were add on all temperature readings.

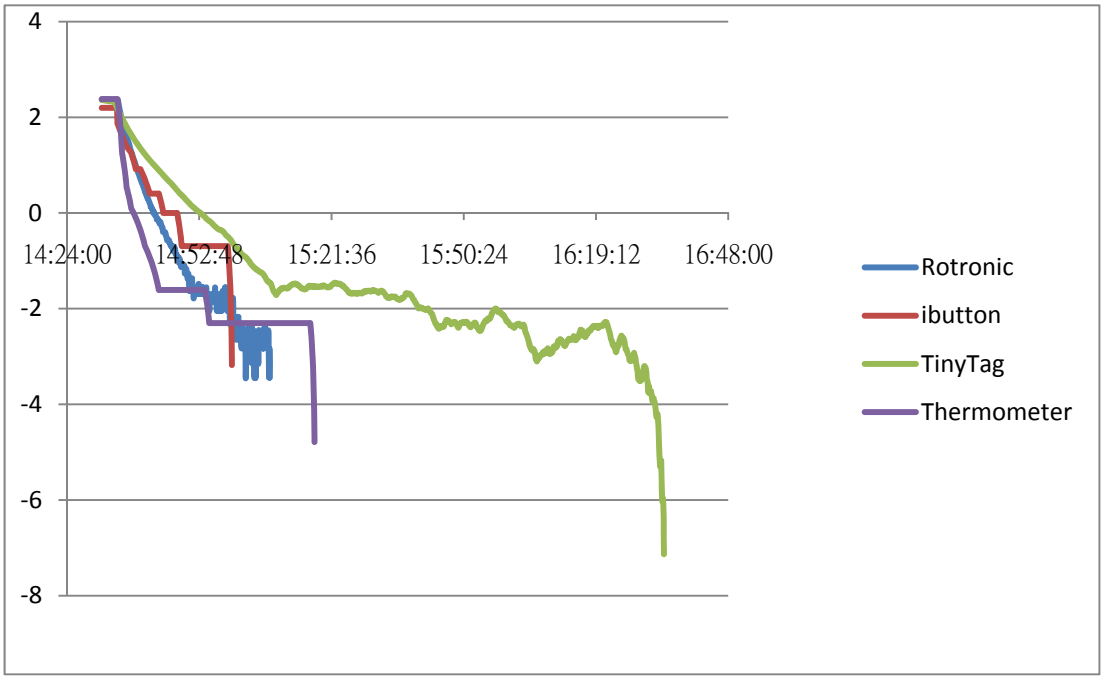

Fig 4 – Natual log of temperautre difference between maximum and each time interval (original data)

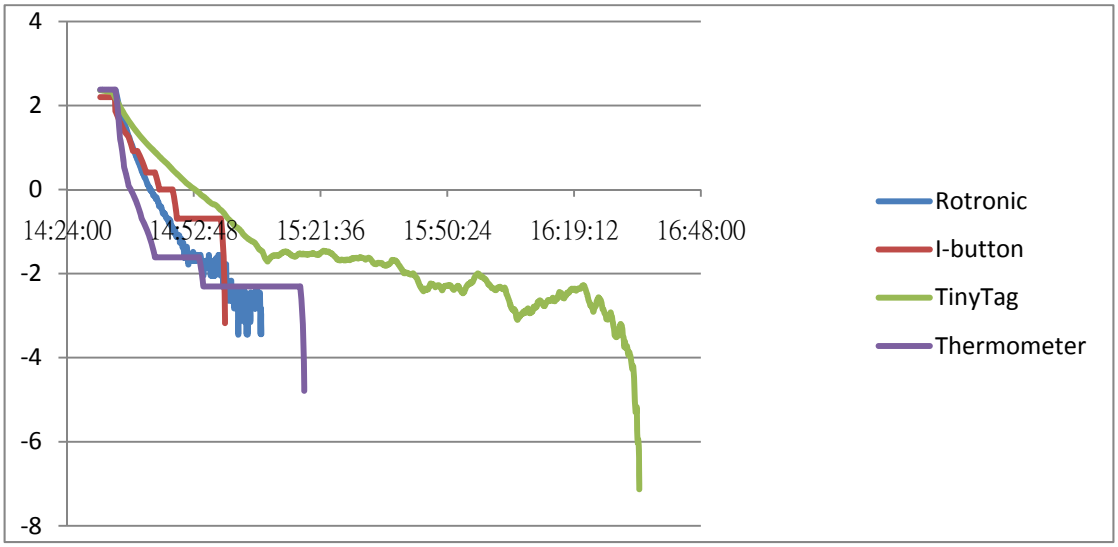

Fig 5 – Natual log of temperautre difference between maximum and each time interval (Solved data)

Thermometer can always give the most accurate instantaneous temperature reading because of its extremely low thermal mass. It can also be seen that Rotronic is the best in terms of response time among all three temperature sensors in the case of rising

temperature.

The advantage of Rotronic sensor is its accuracy, however, the size is not small enough which make it impossible for mounted on lamp post. Furthermore, the price of Rotronic sensor is the highest among 3. It is therefore not suggested to be used in setting measuring point around the city.

I-button is the cheapest and smallest among 3 temperature sensors. However, i-button used in this experiment can only log up to 2046 data. This might caused a problem of download data in future. Furthermore, i-button can only measure up to $0.5^{o}C$ of temperature compare to the other sensors. Further investigation is required for the usage of i-button.

Although Tiny-tag is the slowest response time temperature sensor, it seems to be the best sensor for measuring temperatures in city. The size of the sensor is reasonably small, and can be fitted into a radiation shield. It can also collect much more data than I-button.

The purpose of this experiment is to choose the best sensors for measuring Urban Heating Island in a constant location with a continuous measurement. The time that a sensor responds to a sudden single change is not the most important factor.

Further Researches

Further researches and experiments need to be performed on Tiny-tag and I-button. Different types of I-buttons needed to be looked at to solve the problems mentioned above.

The same experiment should be performed again with all sensors mounted inside radiation shield. Different methods of manufacturing radiation shield should also be investigated.

Temperature sensors might also be sensitive to magnet which might be used as a tool for handling the sensors. The possible inference should also be investigated.

Reference

1. *Building Energy Management Systems Applications to Low-Energy HVAC and Natural Ventilation Control.* 2nd Edition. G. J. Levermore

Appendix B – Design drawing for radiation shield

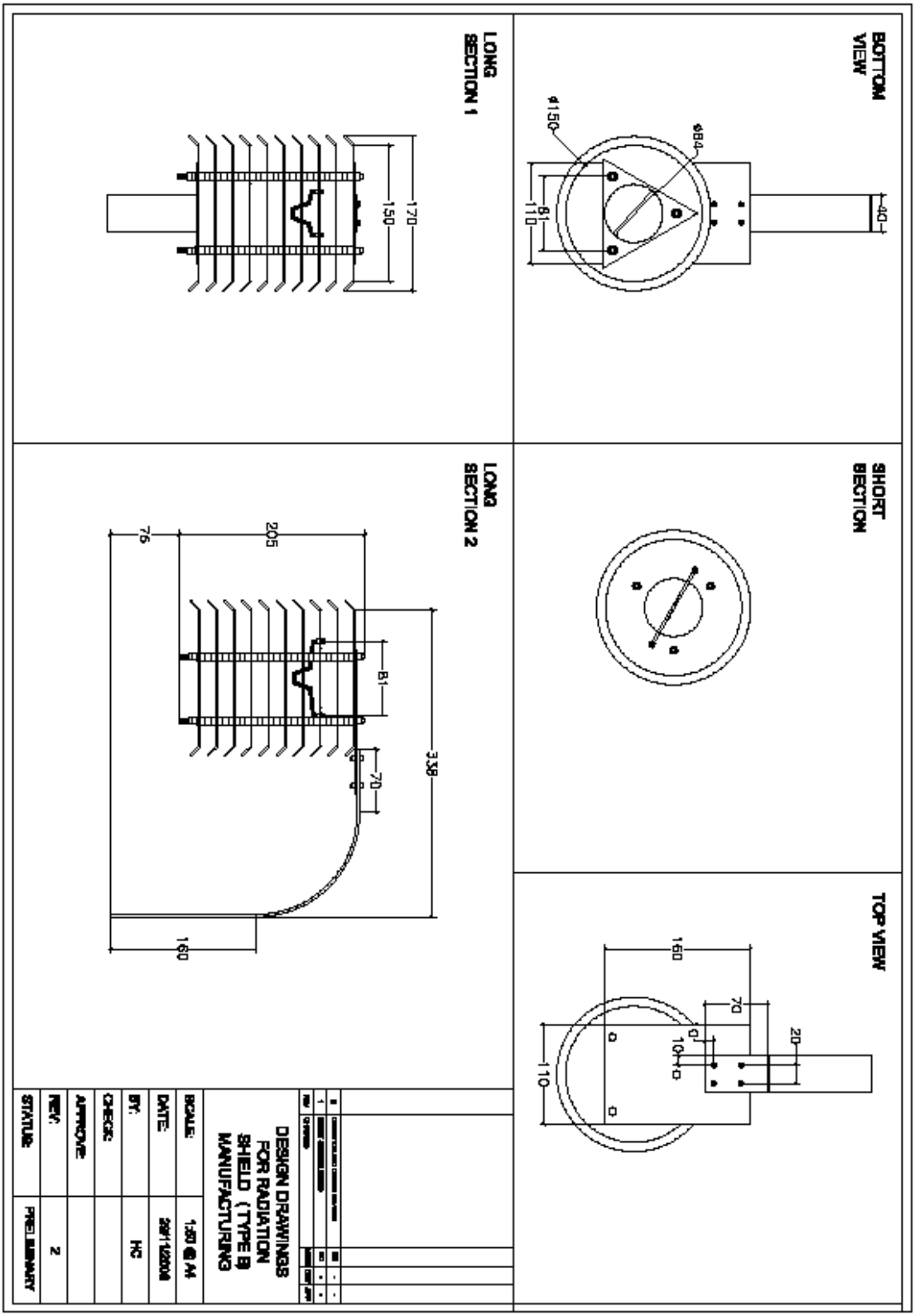

Appendix C – Components drawing for radiation shield

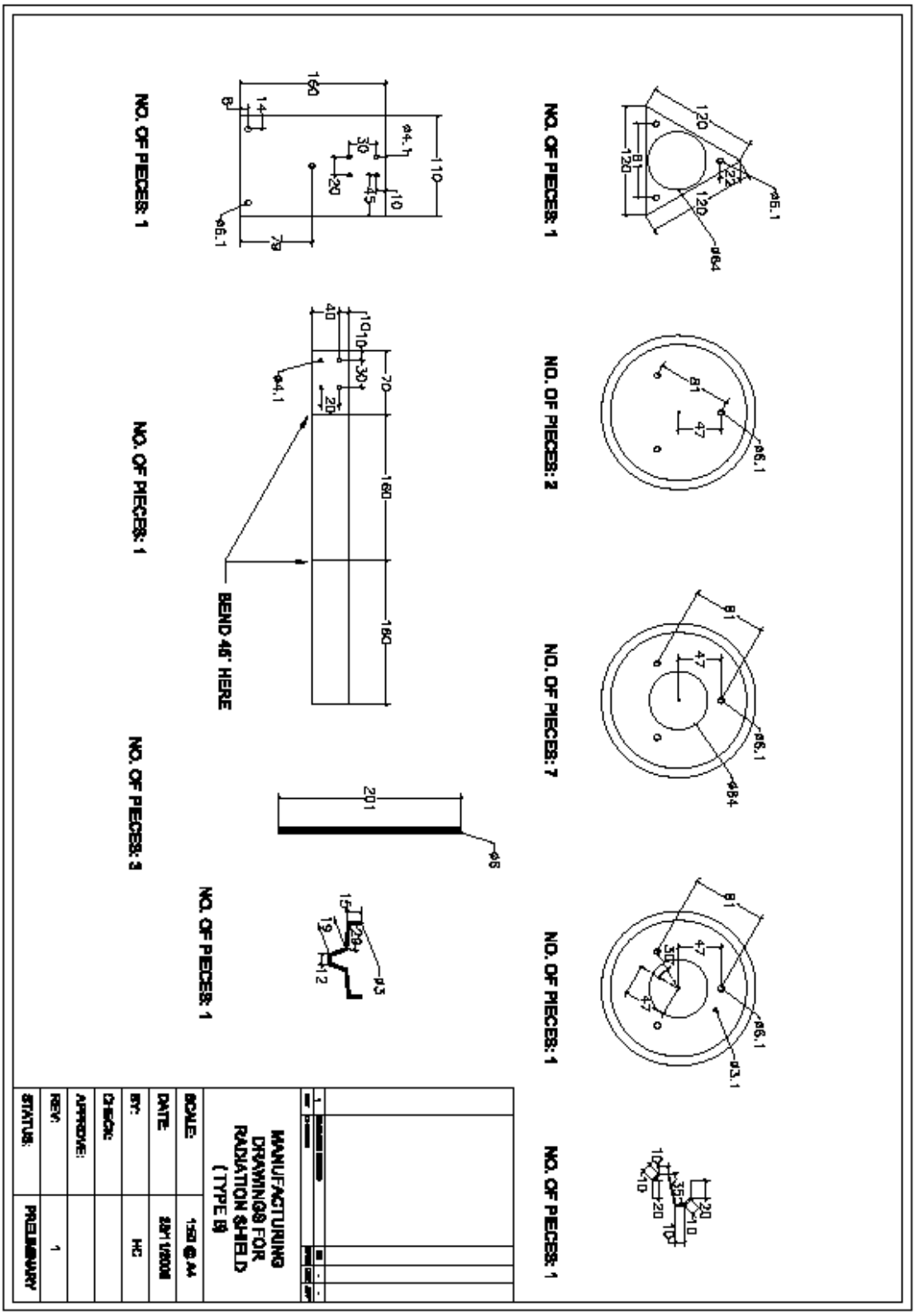

Appendix D - Radiation shield and Accessories Specification

Radiation Shield

Saucers

10 Saucers were required for each radiation shield. 15cm colormatt saucer (product code: 5030) from Sankey (Tel: 0115 9739 328) should be used. Saucers came in a pack of 18 cost £6.64 + VAT per pack (quoted in Mar 2009).

There were 3 sets of holes need to be drilled on saucers. They could be standardised as follow (also refer to manufacturing drawing):

1. Three numbers of Ø6.1mm holes 47mm from centre of saucers spaced at 81mm from each other
2. Two numbers of Ø3.1mm holes 47mm from centre of saucers opposite to each other. These holes should not be too close to any of the three holes in set 1, 10mm or more is recommended
3. One Ø64mm hole at centre of saucers.

Numbers of saucers with different holes arrangement for making a radiation shield could be found in the table below. Please also refer to manufacturing drawings

Hole set arrangement required	No of Saucers
1	2
1,2,3	1
1,3	7

Top Rectangular metal

A rectangular metal of either 1.5mm thick stainless steel or 1.5mm thick aluminium should be created with the size of 110mm x 160mm. Set 1 holes should be drilled in the correct positions as indicated in the drawing. Four Ø4.1mm holes should also be drilled for attaching the “arm” in the later stage.

Bottom Triangular metal

A triangular metal with length of 120mm on each side should be cut from either a 3mm thick stainless steel or a 3mm thick aluminium. Set 1 and 3 holes should be drilled in the relevant positions according to the drawing.

Arm

The “arm” of the radiation shield was made of 3mm thick aluminium or 3mm thick stainless steel. It should be cut to size as indicated in the drawing and rolled to the indicated radius. Four extra Ø4.1mm holes should be drilled at one end for attaching the “arm” to the “Top rectangular metal” by M4 stainless steel bolts and nuts.

Gate

The “gate” of the shield was used to prevent the sensor from dropping in case it falls off in strong wind. The “gate” was made from 1mm stainless steel cut into size described in the drawing. Holes should be drilled on the bended side so that the gate will not opened by strong wind blowing to it. The sizes and number of these holes were not critical.

**Please note that all edges of finished metal work should be smoothened for health and safety reasons.

Studdings

M3 studding

M3 studding should be bended to the distance described on the drawing; however, the exact bending angle should be adjusted manually when producing every single piece. This M3 bended studding should then be mounted on saucers with set 2 holes by double polystyrene nuts and washers on both sides. It will be used for hanging the sensors.

M6 studding

M6 Studding should be cut into 200mm long as indicated in drawing.

Assembly procedure:

Three M6 studs were threaded through the saucers and a rectangular metal plate on top. This rectangular metal plate should be attached to the “arm” by suitable stainless steel bolts and nuts. Polystyrene dome nuts were then placed on the studs above the bracket. The ten saucers were stacked onto the studdings with two M10 nuts as spacers between each pair of saucers. A triangular aluminium plate, also with a large hole was placed at the bottom of the shield to provide strength. The “gate” was then placed in one of the three studdings with 2 polystyrene washer on top and bottom of it.

All three studs were secured at the bottom by double M6 nuts and “Locktite”.

Hooks

Hooks consist of a shower curtain rail holder and a painted mild steel plate (1mm thick). They were connected using two pairs of nuts and bolts with “Locktite”.

Curtain Rail holder

The curtain rail used for making the hook can be order from Rothley (Tel: 01902 756461). The produce code is Q661XW and cost £1.52 each. The minimum order from Rothley is £100.00, therefore, this product can also be found in some of the B&Q if small numbers need to be purchased.

An opening of length about 12mm should be created near the bottom of the oval ring (refer to manufacturing drawing) this distance is not critical but should not be too big. Recommended length is about 10 to 12mm. Please also note that it is essential for this opening to be created close to the bottom of the oval.

Mild Steel Plate

Mild steel plate of 4mm x 4mm should be prepared first. The plate should then be cut into shape shown in the drawing. Two Ø4.1 holes should be drilled with the same spacing as the holes on the curtain rail holder.

Telescopic Pole and magnet

The telescopic pole is used to mount and un-mount sensor from the shield at four metre high. A piece should be attached at the top to attach the bottom mild steel plate of the hook.

The telescopic pole is usually been modified from a Studio Lighting Tripod. The pole itself must be able to reach a height of three meter to enable user mount and un-mount sensor at four metre. There is no standard supply of poles. A 3.5 metre studio lighting tripod is recommended.

Three tripod legs should be taken off first, this will leave just the telescopic pole. Depending on the different sizes of the screw tip, an adaptor should be made to

connect the pole with a magnet. A red button magnet with 3.2kg pull force was used by the author. Magnets can be found of this website:
http://e-magnetsuk.com/
Please note the pull force of the magnet should not be too strong as this may damage the whole radiation shield. Pull force between 2kg to 4 kg is recommended.

Appendix E – Experimental report of radiation test for the radiation shield

Background

The objective of the COPSE project is to measure the Urban Heating Island in Great Manchester areas and to develop a set of local weather data for engineering usage. Temperature sensors are required to be placed on street lamp post around Greater Manchester to record air temperature continuously. A radiation shield has to be designed to accommodate the temperature sensor so that the sensor measure the accurate air temperature and will not be affected by the direct sun shine.

A radiation shield has been designed using plant saucers and metal structures. Refer to Appendix 1 for design details and dimensions. In order to test the efficiency of the shield, this experiment is thus performed using two 60W Tungsten lamps as two heat sources.

Objectives and Hypothesis

The reading of a temperature sensor will be affected when it is directly exposed under a heat source such as sunshine. The main function of a radiation shield is to prevent direct sun shine to the temperature sensor so that it can measure the actual air temperature in the area. Sufficient ventilation is also essential to the sensor inside a shield as hot air will not be trapped.

The main objective of these experiments is to find out what will be the behaviour of the I-button when it is exposed compared to been accommodated inside a radiation shield.

Methodology

In order to similar a direct heat source, two 60W Tungsten lamps have been used as the heat sources. Two I-button sensors have be placed close together at the same horizontal level. However, one of them was accommodated inside a radiation shield (as shown in Fig 1-4). Wooden surface has been chosen so that the reflection of the heat from the lamps was minimised. A third I-button sensor was placed few meters away from the heat source. This I-buttons was used as control to measure the room air

temperature.

The whole experiment set up was then left for 20 minutes for the sensors to stabilise to room temperature. Both lamps were then been turned on. There was no air movement inside the room and therefore, a fan in the HVAC laboratory unit was been switched on to create some air movement after the lamps were on for an hour.

Each I-button sensor has a different adjustment value according to the calibration experiment performed previously (refer to appendix F and G for details). Therefore each individual value is adjusted and all values were plotted onto graph.

Table 1 below shows the individual adjustment of all 3 I-button used in the experiment:

I-button Ref	I-button 14	I-button 15	I-button 16
Adjustment (^{o}C)	0.1182	0.0996	0.1151

Table 1: Individual adjustment values of three I-buttons used.

Results

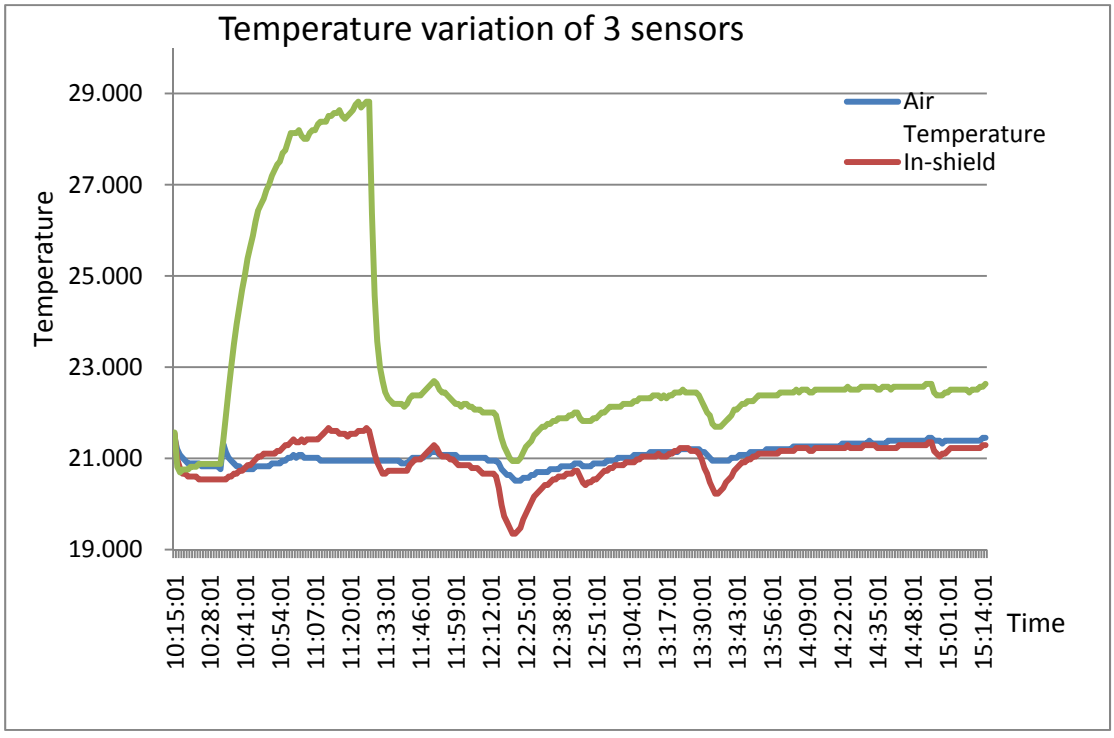

Fig 1: Temperature variation of 3 sensors

Discussion

Sensor	I-button No 33	Rotronic
Difference (^{o}C)	0.124	-0.3

Table 2: Difference of I-button No.33 and Rotronic against Certified I-button

Table 2 shows the mean temperature of I-button sensors No. 33 and Rotronic sensor against the standard mean tempearture measured by the certified I-button A. It can be seen that the difference is less than 0.2^{o}C, the average difference from last calbration experiment. This is far better than ±0.5^{o}C stated in the I-button data sheet.

By considering the new difference value found on Sensor No. 33, adjustment to each sensor was re-calculated and can be found in the table 3 below:

Sensor	Adjustment	Sensor	Adjustment	Sensor	Adjustment	Sensor	Adjustment
1	0.101947	15	0.099627	29	0.143859	43	0.146979
2	0.102577	16	0.115057	30	0.076017	44	0.081457
3	0.122097	17	0.168873	31	0.192178	45	0.099077
4	0.114387	18	0.099747	32	0.115767	46	0.074157
5	0.170175	19	0.121097	33	0.123967	47	0.126775
6	0.155755	20	0.15852	34	0.152721	48	0.081757
7	0.146243	21	0.120317	35	0.193762	49	0.128693
8	0.136362	22	0.103697	36	0.079917	50	0.163461
9	0.114857	23	0.094727	37	0.108357	51	0.128862
10	0.140362	24	0.118797	38	0.060627	52	0.135758
11	0.132714	25	0.132384	39	0.145222	53	0.140311
12	0.088177	26	0.141279	40	0.143052		
13	0.120547	27	0.106657	41	0.116527		
14	0.118217	28	0.150028	42	0.119887		

Table 3: Revised Tolerance of each sensor

Conclusion

A certified I-button was used to perform the calibration this time. By using a certified device, the result will be much more convincing. It can be seen that the maximum difference is about 0.194 found on I-button No.35. The validation period of the certificate is a year, it is suggested that similar calibration should be performed each year to ensure the accuracies of all I-button sensors.

Appendix F – Sensor-logger calibration report 1

Background

The objective of the COPSE project is to measure the Urban Heating Island in Great Manchester areas and to develop a set of local weather data for engineering usage. 3 kinds of temperature sensors, Rotronic, Tinytag and I-button were compared before. I-button temperature sensors are agreed to be used to measure and log air temperatures around Manchester. Each I-button sensor will be accommodated by a radiation shield which will then be mounted on the street lamp post.

53 I-button sensors was calibrated using HVAC laboratory unit as well as leaving in warm and cold environment (refer to calibration report 1). However, it was suggested a more stable thermal environment (such as an environmental chamber) is required for more precise calibration.

Objectives and Hypothesis

All I-buttons have an accuracy of ±0.5^{o}C according to the manufacturer data sheet. However the actual device accuracy will be difference from device to device.

The main objective of these experiments is to find out the accuracies of all 53 I-button sensor so that adjustment can be made when measurement carried out in future.

Methodology

All I-button sensors were placed on a cardboard as shown in figure 1. The whole cardboard was then placed into the 30^{o}C oven over night (as shown in fig 2 and fig 3).

A period of 19:00-0900 was taken and the mean temperature of each sensor was then calculated and plotted on to graph. The same experiment was carried out three times with different I-button arrangement on cardboard. Mean value was taken for all three experiments for each sensor and then they were compared to the mean of ALL sensors to find out the tolerance of each sensor. The error due to the arrangement of the I-button can then be reduced. The sampling time for each sensor is one minute.

Fig 1: I-button on cardboard

Fig 2 & 3: 30^{o}C oven

Mean and Standard Deviation will then be calculated. The lower the standard deviation, the more reliable the test is, this is because sensors should have a maximum error of 0.5^{o}C according to the manufacturer.

Results

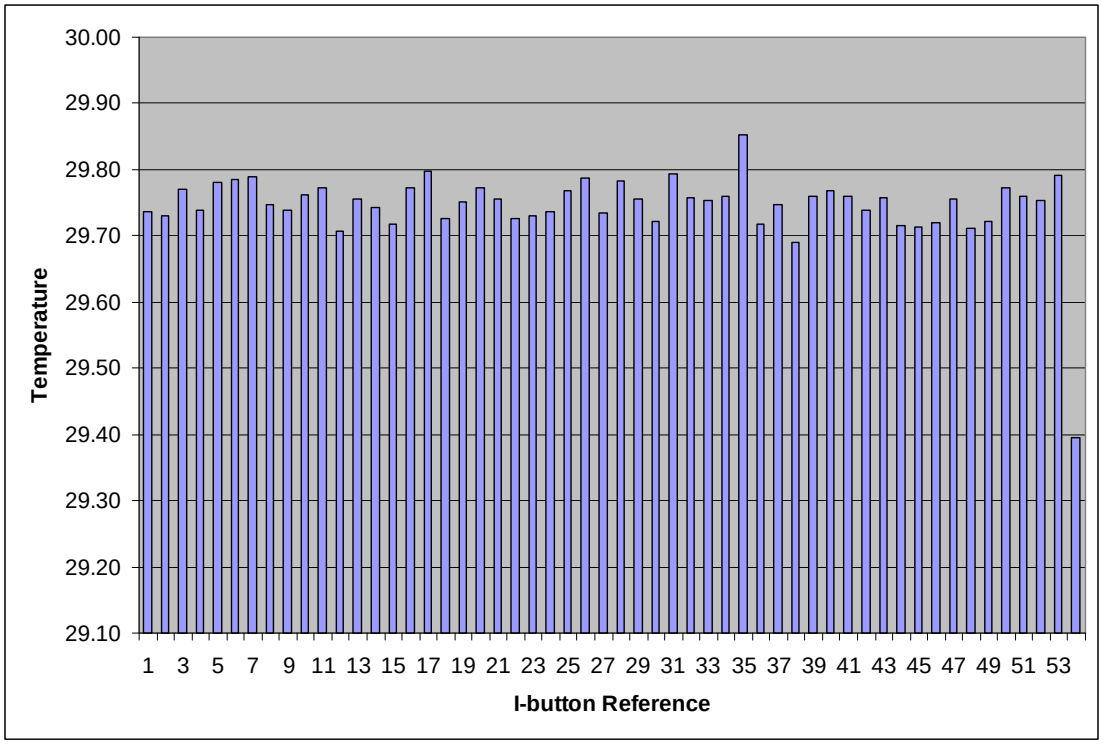

Fig 4: Average temperature against each sensor for Test 6 – No. 54 is the Rotronic sensor

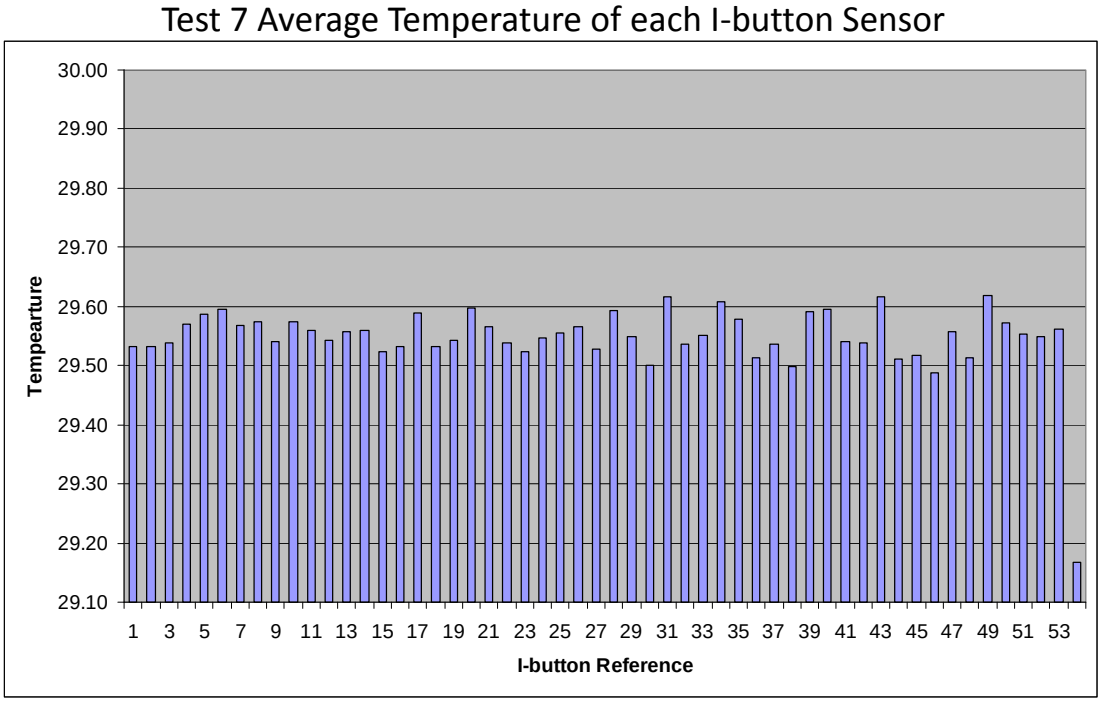

Fig 5: Average temperature against each sensor for Test 7 – No. 54 is Rotronic sensor

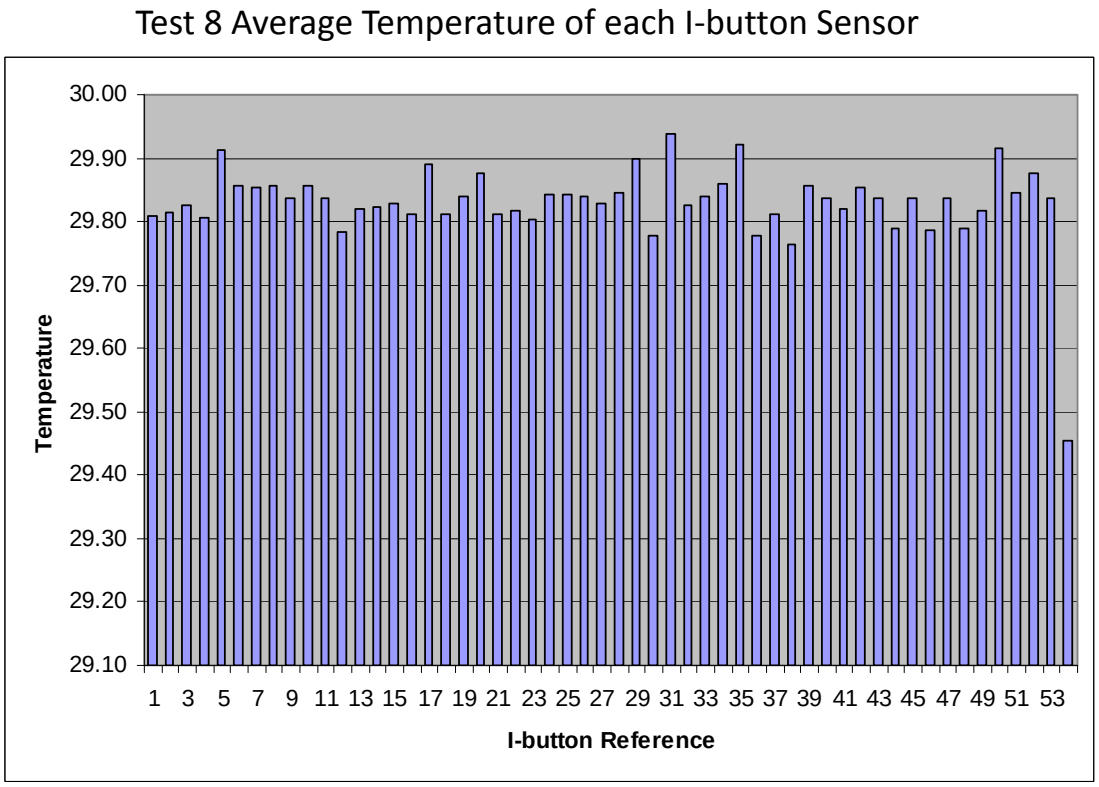

Fig 6: Average temperature against each sensor for Test 8 – No. 54 is Rotronic sensor

Discussion

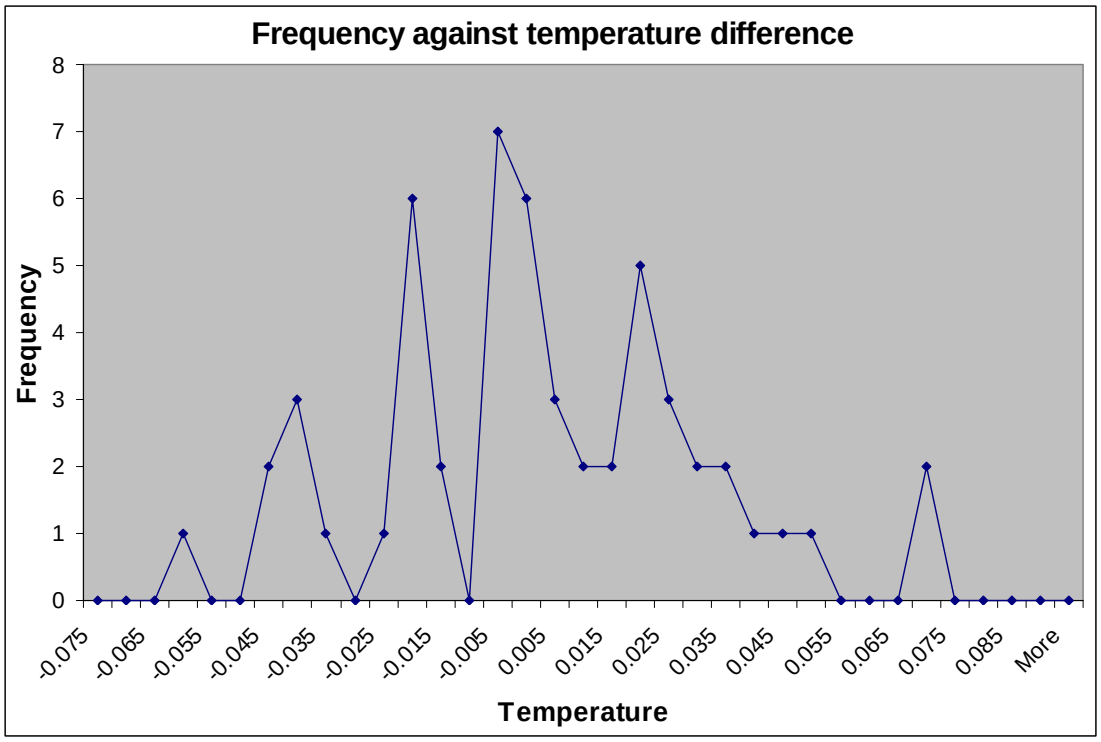

Fig 7: Frequency of temperature difference against temperature difference

	Test 6	Test 7	Test 8	All 3
Mean	29.752	29.554	29.836	29.714
Standard Deviation	0.029	0.031	0.037	0.029

Figure 4 to 6 show the mean temperature of all I-button sensors in three tests. It can be seen that the maximum difference is less than 0.2^{o}C. This is far better than ±0.5^{o}C stated in the I-button data sheet. There is also no special pattern shown which means all the sensors are in the evenly distributed thermal environement.

By comparing the standard deviation in this set of experiment with the one in the last set, it can be seen that the standard deviation drop from about 0.11 lat time to 0.03. This is a great improvement and can give confidence to the result.

Instead choosing the mean value for calibrating sensors, an actually mean temperature reading is used as the standard value. Tolerances of all other sensors are adjusted to this one. By doing this, the next calibration can be done with the mean sensor on its own against any other certified sensors.

Sensor 33 was chosen to be the mean sensor as the individual mean of sensor 33 is 29.714^{o}C. Adjustment to each sensor can be found in the table 2 below:

Sensor	Adjustment	Sensor	Adjustment	Sensor	Adjustment	Sensor	Adjustment
1	-0.02202	15	-0.02434	29	0.019892	43	0.023012
2	-0.02139	16	-0.00891	30	-0.04795	44	-0.04251
3	-0.00187	17	0.044906	31	0.068211	45	-0.02489
4	-0.00958	18	-0.02422	32	-0.0082	46	-0.04981
5	0.046208	19	-0.00287	33	0	47	0.002808
6	0.031788	20	0.034553	34	0.028754	48	-0.04221
7	0.022276	21	-0.00365	35	0.069795	49	0.004726
8	0.012395	22	-0.02027	36	-0.04405	50	0.039494
9	-0.00911	23	-0.02924	37	-0.01561	51	0.004895
10	0.016395	24	-0.00517	38	-0.06334	52	0.011791
11	0.008747	25	0.008417	39	0.021255	53	0.016344
12	-0.03579	26	0.017312	40	0.019085		
13	-0.00342	27	-0.01731	41	-0.00744		
14	-0.00575	28	0.026061	42	-0.00408		

Table 2: Tolerance of each sensor

Conclusion and further work

The result from 3 tests has improved a lot when comparing with last set of test, however, it is still uncertain that if these reading are confident due to the lack of a certified temperature measurement device. It is suggested that one more calibration between the mean I-button sensor against a certified temperature logging device should be performed to ensure all the exercises performed were meaningful.

Appendix G – Sensor-logger calibration report 2

Background

The objective of the COPSE project is to measure the Urban Heating Island in Great Manchester areas and to develop a set of local weather data for engineering usage. 3 kinds of temperature sensors, Rotronic, Tinytag and I-button were compared before. I-button temperature sensors are agreed to be used to measure and log air temperatures around Manchester. Each I-button sensor will be accommodated by a radiation shield which will then be mounted on the street lamp post.

I-button sensor No. 33 was calibrated under 2 conditions, using Environmental Chamber of 30^{o}C (refer to calibration report 2) and left in fridge (about 5^{o}C) over night against the certified I-button Sensor A, as well as the Rotronic sensor.

Objectives and Hypothesis

All I-buttons have an accuracy of ±0.5^{o}C according to the manufacturer data sheet. However the actual device accuracy will be different from device to device.

The main objective of these experiments is to find out the accuracies of I-button No. 33 as it has been used as the mean value among other 53 I-button sensors.

Methodology

I-button sensors No 33 and certified I-button A were placed on a piece of cardboard. The whole cardboard was then placed into environmental chambers for several hours. The same Rotronic temperature sensor is also placed for calibration. Table 1 below shows the 5 test temperature of I-button A with their corresponding difference:

Reference Temperature	Read Temperature	Difference
-35.64	-35.68	-0.04
-15.07	-15.04	0.03
0.01	0.04	0.03
40.15	40.28	0.13
80.2	80.24	0.04

Table 1: Certified I-button A data

A period from 10:15-15:15 was taken for 30°C situation and 02:00-09:00 was taken for 5°C situation. The mean temperature of each sensor was then calculated. Interpolation is used to find the difference of I-button A at 30°C and 5°C. All the temperature values from I-button A were then adjusted and the mean of this particular time period is found. The mean of I-button No. 33 and Rotronic in the same period were also found. All 3 means were than plotted on graph. Mean difference can then be calculated.

Results

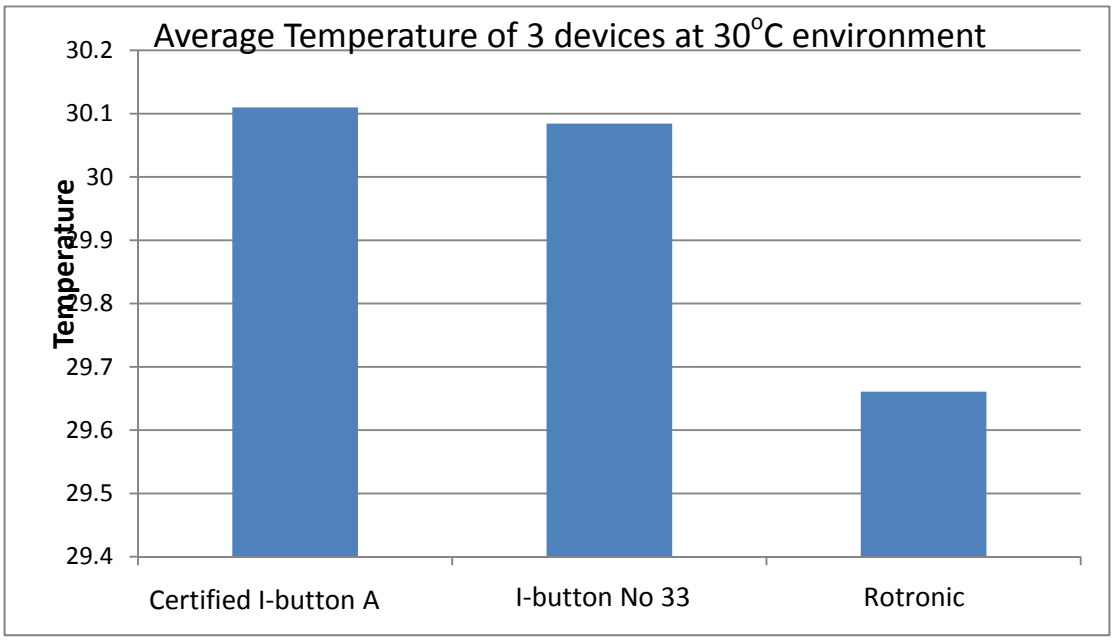

Fig 1: Average temperature against each sensor at 30°C

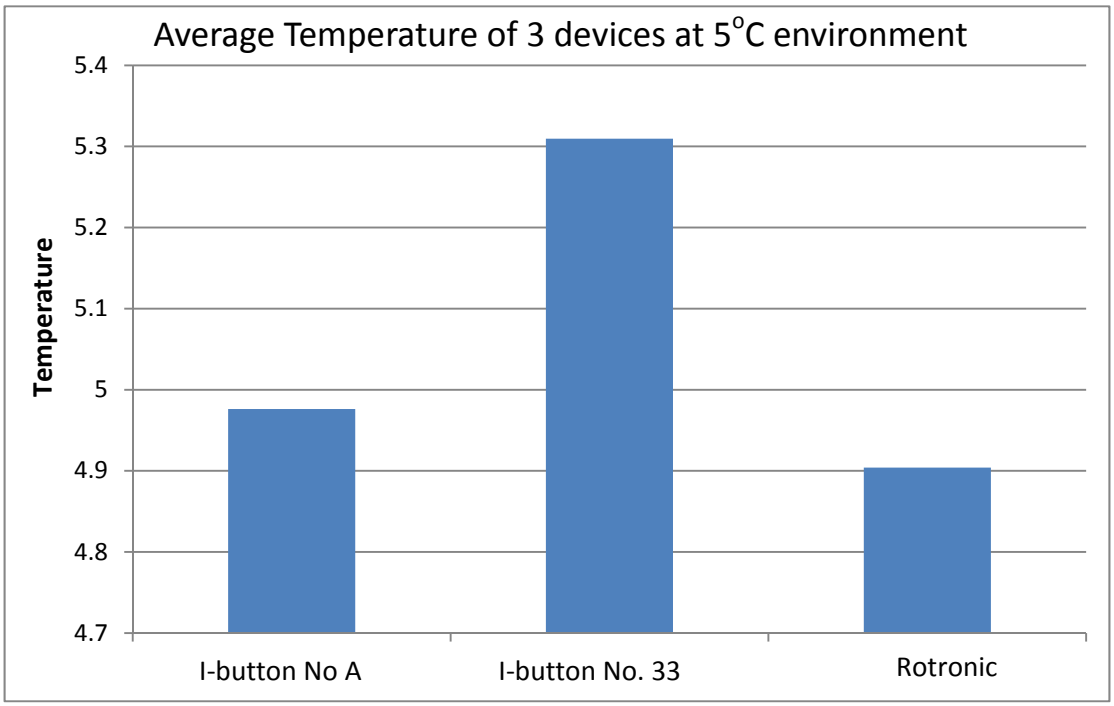

Fig 2: Average temperature against each sensor at 5°C

Discussion

Sensor	I-button No 33	Rotronic
Difference at 30°C(°C)	0.026	+0.449
Difference at 5°C(°C)	-0.333	+0.072

Table 2: Difference of I-button No.33 and Rotronic against Certified I-button

Table 2 shows the mean temperature of I-button sensors No. 33 and Rotronic sensor against the standard mean tempearture measured by the certified I-button A. It can be seen that the average difference is about 0.2°C. This is far better than ±0.5°C stated in the I-button data sheet. For the simplicity of future calculation an average value of -0.2162 is used as the adjustment for I-button No. 33

By considering the new difference value found on Sensor No.33, adjustment to each sensor was re-calculated and can be found in the table 3 below:

Sensor	Adjustment	Sensor	Adjustment	Sensor	Adjustment	Sensor	Adjustment
1	-0.17559	15	-0.17791	29	-0.13368	43	-0.13056
2	-0.17496	16	-0.16248	30	-0.20152	44	-0.19608
3	-0.15544	17	-0.10866	31	-0.08536	45	-0.17846
4	-0.16315	18	-0.17779	32	-0.16177	46	-0.20338
5	-0.10736	19	-0.15644	33	-0.15357	47	-0.15076
6	-0.12178	20	-0.11902	34	-0.12482	48	-0.19578
7	-0.13129	21	-0.15722	35	-0.08378	49	-0.14884
8	-0.14117	22	-0.17384	36	-0.19762	50	-0.11408
9	-0.16268	23	-0.18281	37	-0.16918	51	-0.14868
10	-0.13717	24	-0.15874	38	-0.21691	52	-0.14178
11	-0.14482	25	-0.14515	39	-0.13232	53	-0.13723
12	-0.18936	26	-0.13626	40	-0.13449		
13	-0.15699	27	-0.17088	41	-0.16101		
14	-0.15932	28	-0.12751	42	-0.15765		

Table 3: Revised tolerance of each sensor

Conclusion

A certified I-button was used to perform the calibration this time. By using a certified device, the result will be much more convincing. It can be seen that the maximum difference of is about -0.266 found on I-button No. 46. The validation period of the certificate is a year, it is suggested that similar calibration should be performed each year to ensure the accuracies of all I-button sensors.

Appendix H – Data collection software installation and user guide

All I-button sensor-logger can be access on a PC with software "OneWireViewer (Driver)" released by Maxima (manufacturer of I-button). Before installing the OneWireViewer, please ensure Java has been installed on PC. Java can be downloaded from www.java.com for free.

Installation

OneWireViewer can be downloaded from the following link:

http://www.maxim-ic.com/products/ibutton/software/resources.cfm

Select ***1 wire Drivers*** and select ***Click to go to download page*** on the other page

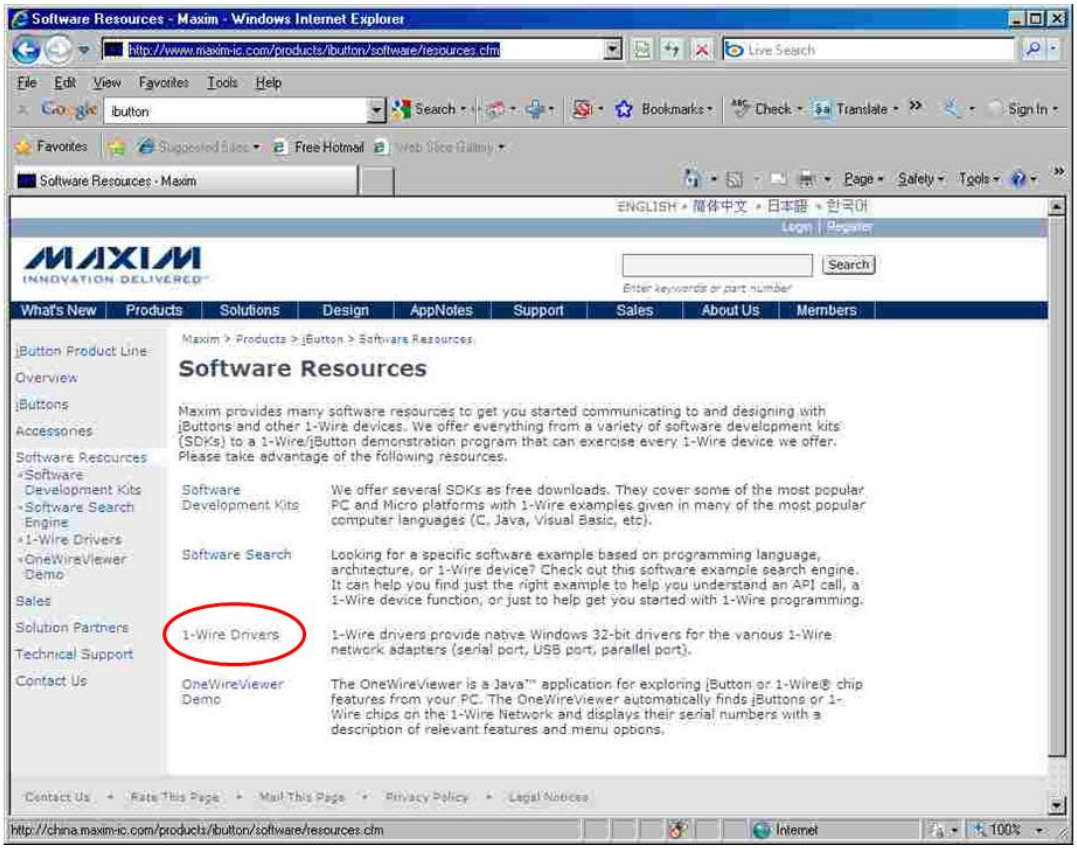

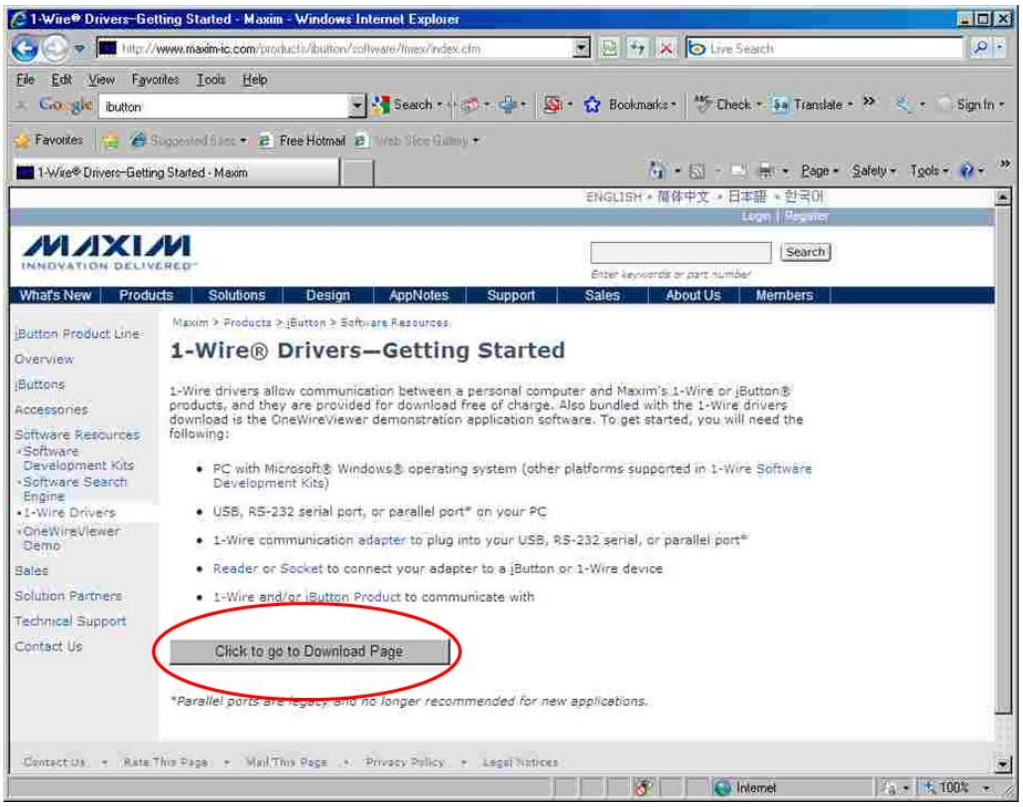

This will then bring you to another page to select the operation system of your PC

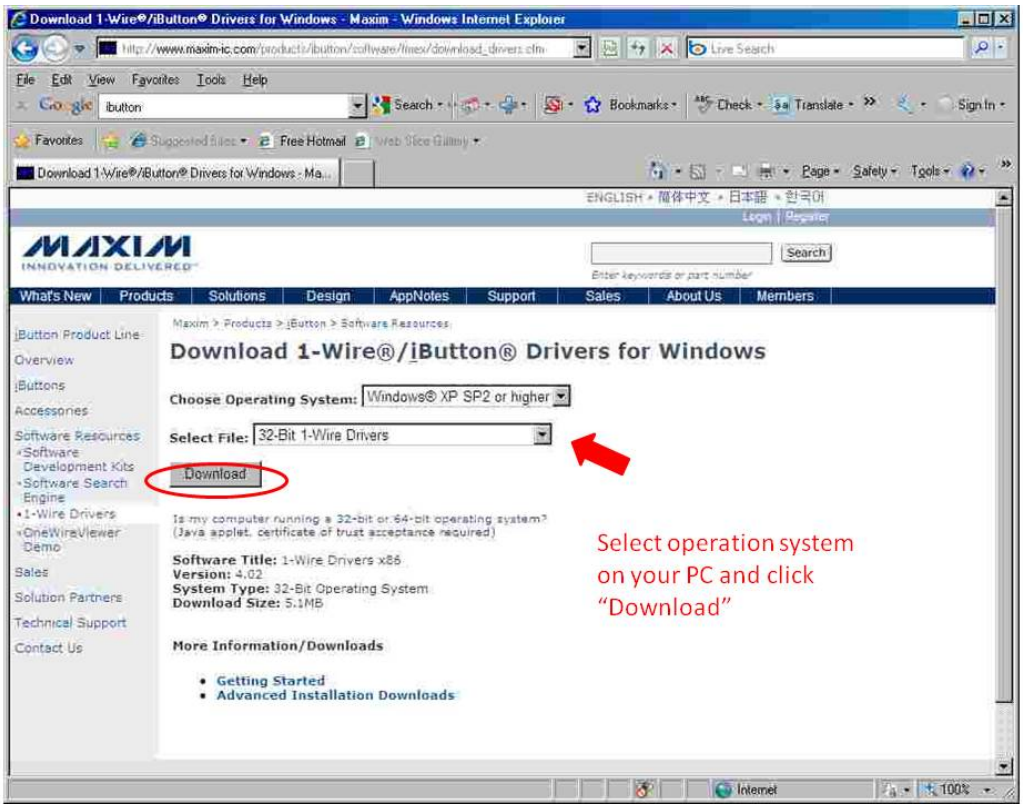

Click ***Save*** and save the file on your PC. Double click on the downloaded file to start installation. Click Run if there is a Security window opened:

This will then bring you to the setup manual, click on the accept license agreement and then click ***Install***

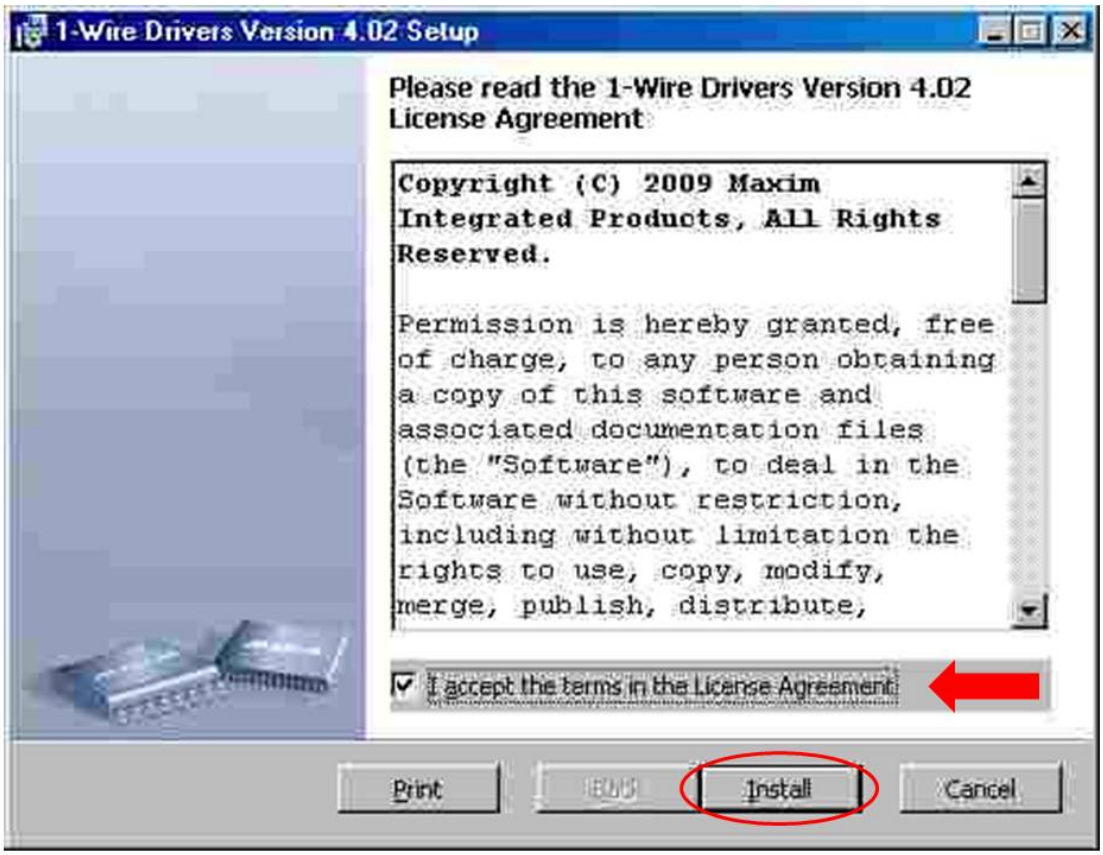

Click ***Finish*** once it is finished installation


1-Wire Drivers Version 4.02 Setup
Completed the 1-Wire Drivers Version 4.02 Setup Wizard
Click the Finish button to exit the Setup Wizard.
Finish

Plug in the USB adaptor and install drivers

Drivers needed to be installed when the USB adaptor was plug into a USB port for the first time. Once the OneWireViewer is installed, all the drivers should have been copied into your PC. Please follow the following instructions for installation of drivers. Please also note, drivers are required to be installed again if another USB port was used next time.

In this "Found New Hardware Wizard", select ***No, not this time*** to skip the searching of driver process as all drivers were already copied into your PC when you install the OneWireViwer software.

Select ***Install the software automatically (recommended)*** and then click on ***Next***

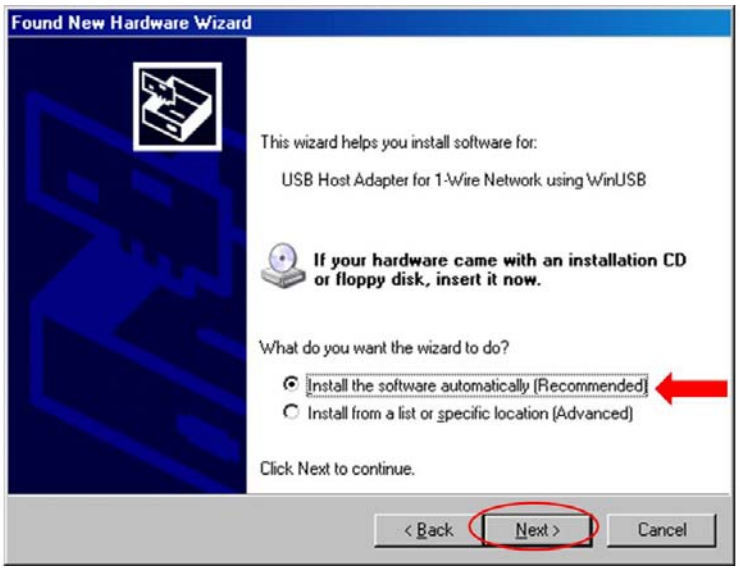

Drivers will then be installed automatically:

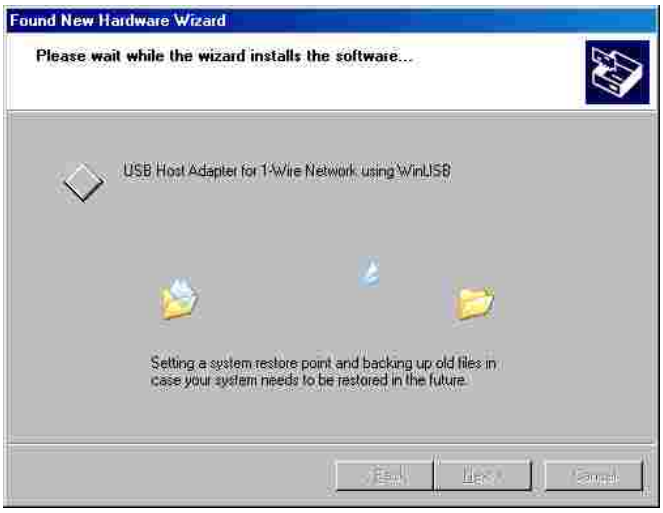

Click on ***Finish*** once driver has been installed

**Please note there might be several drivers to be installed and this installation procedure will be repeated several time.

Using OneWireViewer

Once both the software and all drivers has been installed, OneWireViewer can be found in program file:

Click on the ***OneWireViewer.exe*** inside the default folder *"1-Wire Drivers x86"*

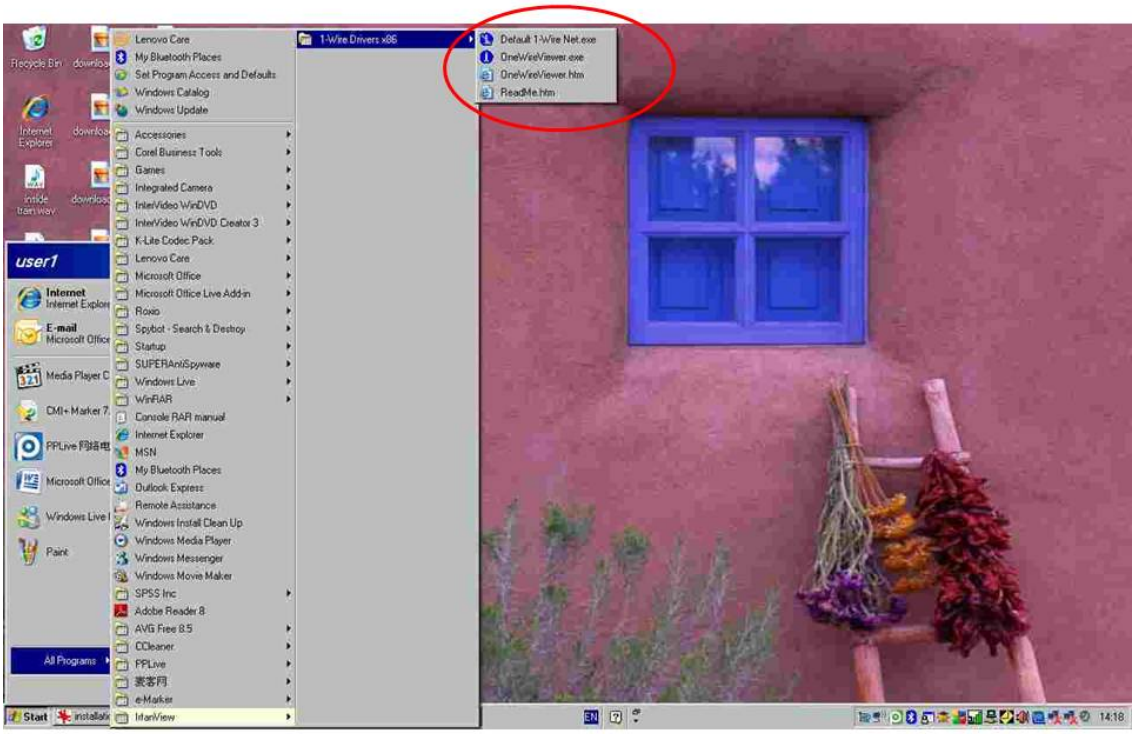

Once the software is opened, the software window is divided into 2 parts, the left part shows the device list and the right part shows the description. There should be one row of numbers under the device list. This is the serial number of the USB adaptor.

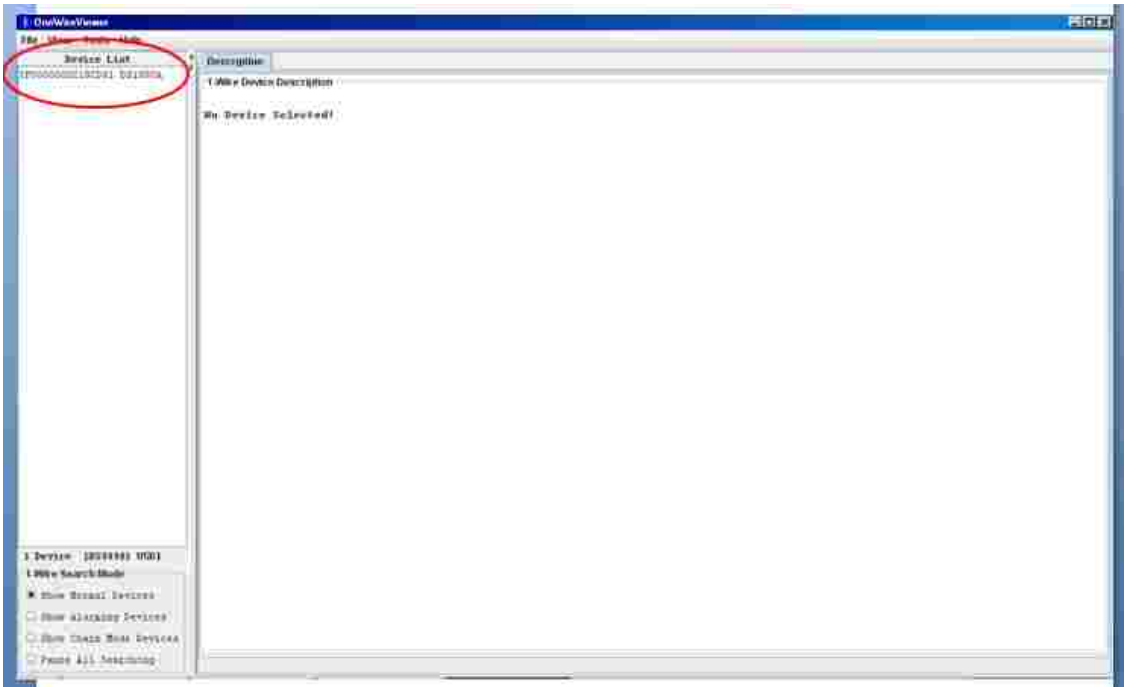

I-button Sensor-logger can be read by the software once it is clipped into the USB adaptor. Nevertheless, it will be quite difficult to unclip it. During data collection, it is always a good practice to have the I-button touching the adaptor rather than clip it in entirely. There is spring at the back of the contact surface of the adaptor. Once the I-button is push down slightly, the continuous contact with the adaptor will enable data been recorded onto PC.

Once the I-button is connected, there should be another serial number appear on the device list on the left hand side. Click on the new serial number on the left and new tabs labelled “Temperature”, “Clock”, “Memory”, “File” and “Mission” will appear on the right:

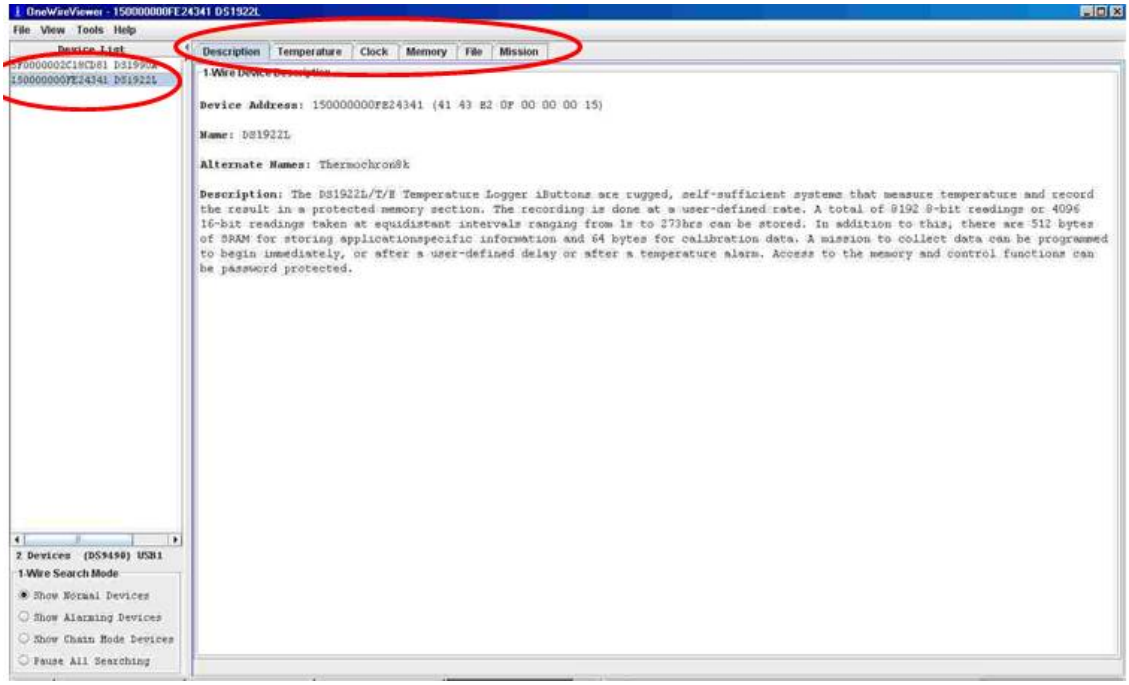

Once these new tabs appeared, click on "***Mission***" on the right hand side. This will display the current status of the I-button.

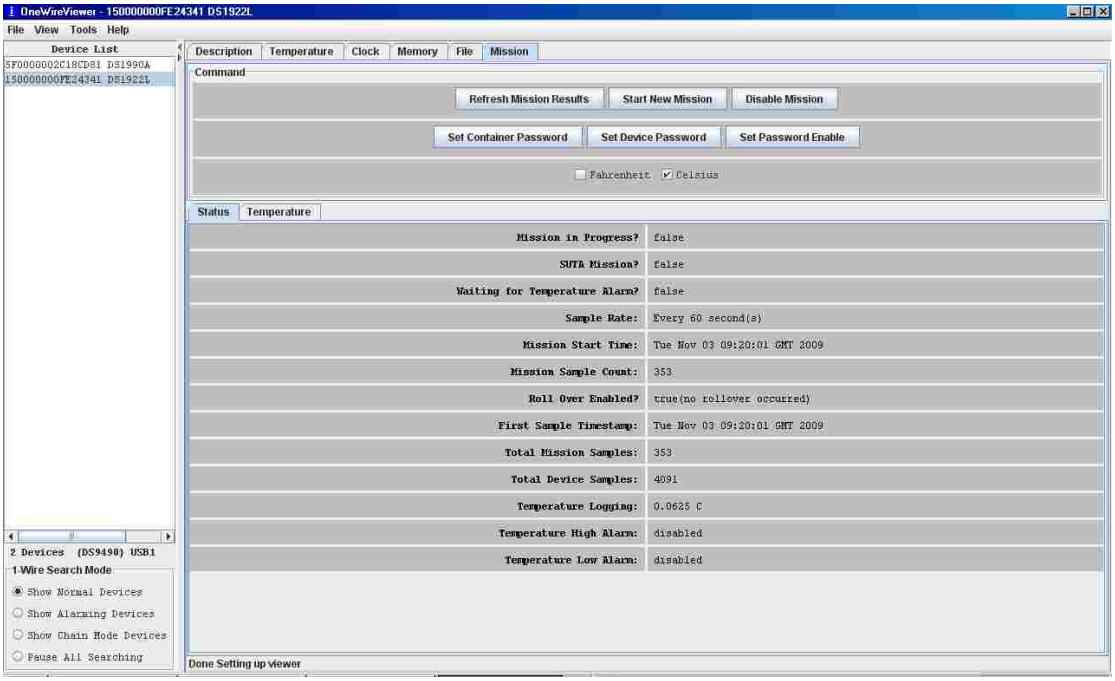

Start a mission

Click on "***Start New Mission***" under the "*Mission*" tab on the right and a new setup window will appear.

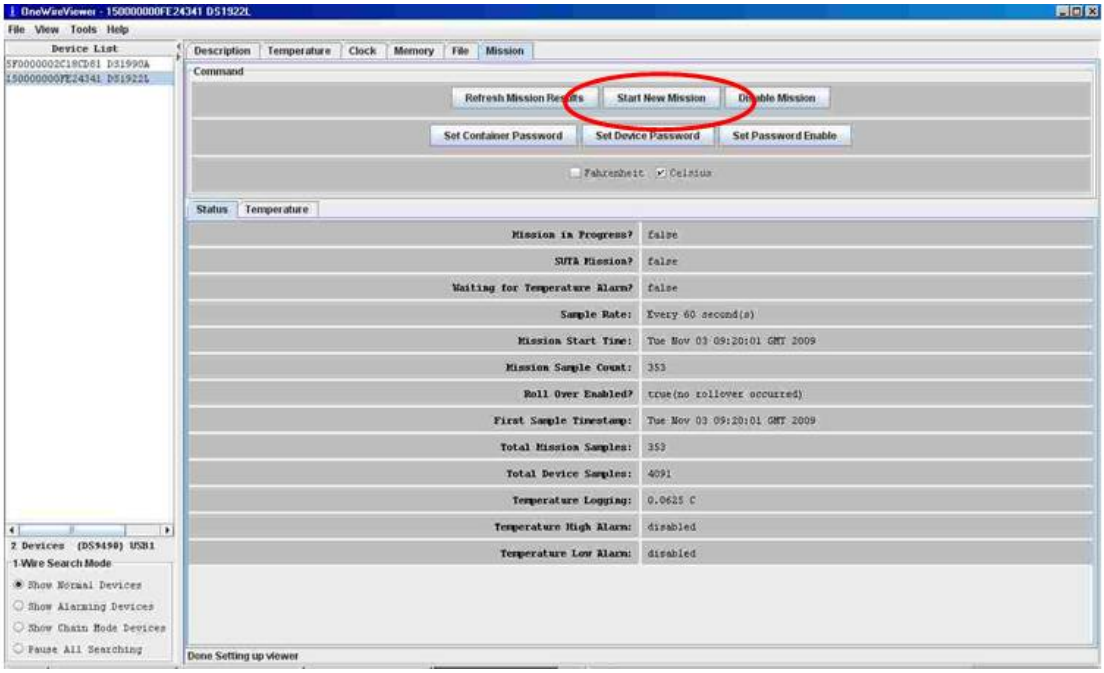

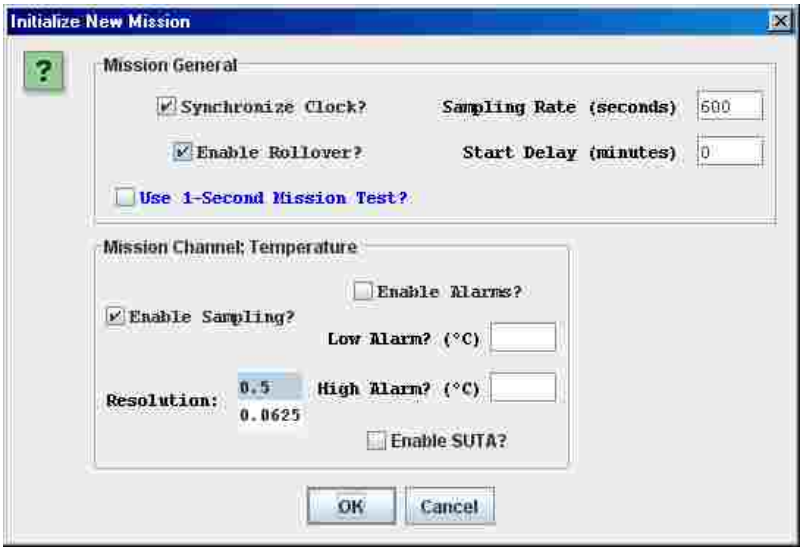

All criteria can be set here for the measurement. Note that the "*Sampling rate*" is in seconds while the "*Start delay*" is in minutes. Alarm is not required for normal temperature measurements. It is also suggested to click "*Synchronize clock*". It is also suggested to choose a high resolution, i.e. 0.0625 for air temperature measurement.

** For long term temperature monitoring, it is very important to ensure the clock of

the PC is in GMT (untick “Automatic ally adjust daylight clock for daylight saving changes” in the clock setting of PC) when start AND stop the missions in I-button

Once set up everything, Click on ***“OK”*** and this will return to the I-button status window. Check all status of the I-button, especially the first status “*Mission in Progress*”. This should read “*True*” when a mission is started even where there is a delay value. Once everything looks ok, unclip the I-button.

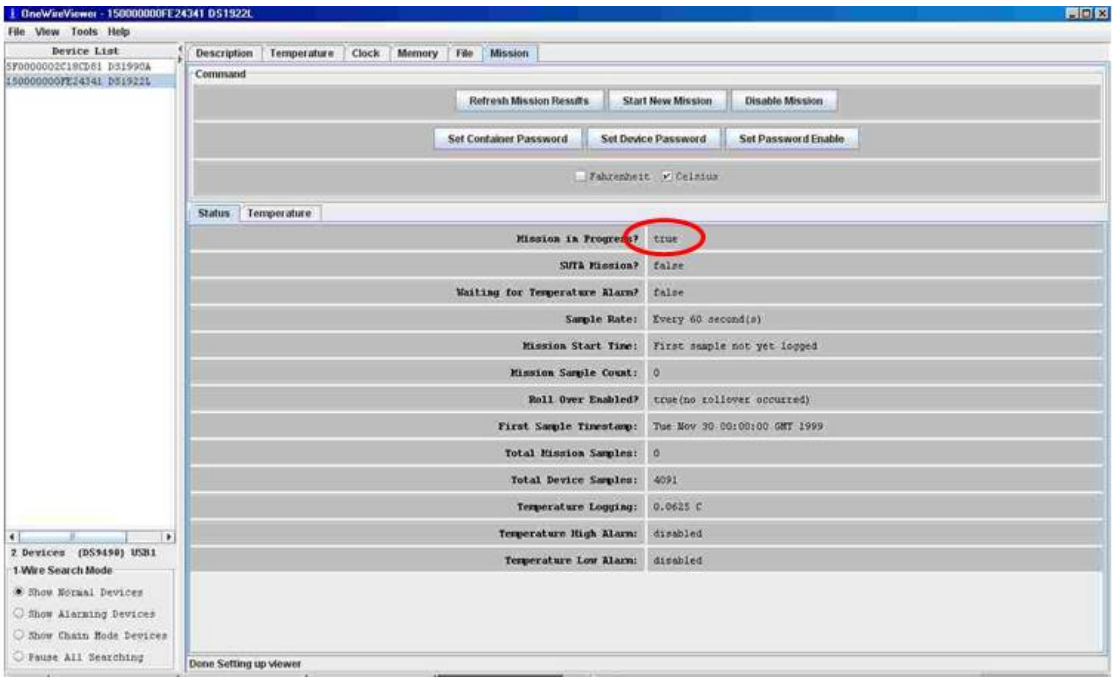

Stop a mission

Simply click on "**Disable mission**" to stop a mission. Once a mission is disabled, check the "*Mission in Progress*" and this should read "False".

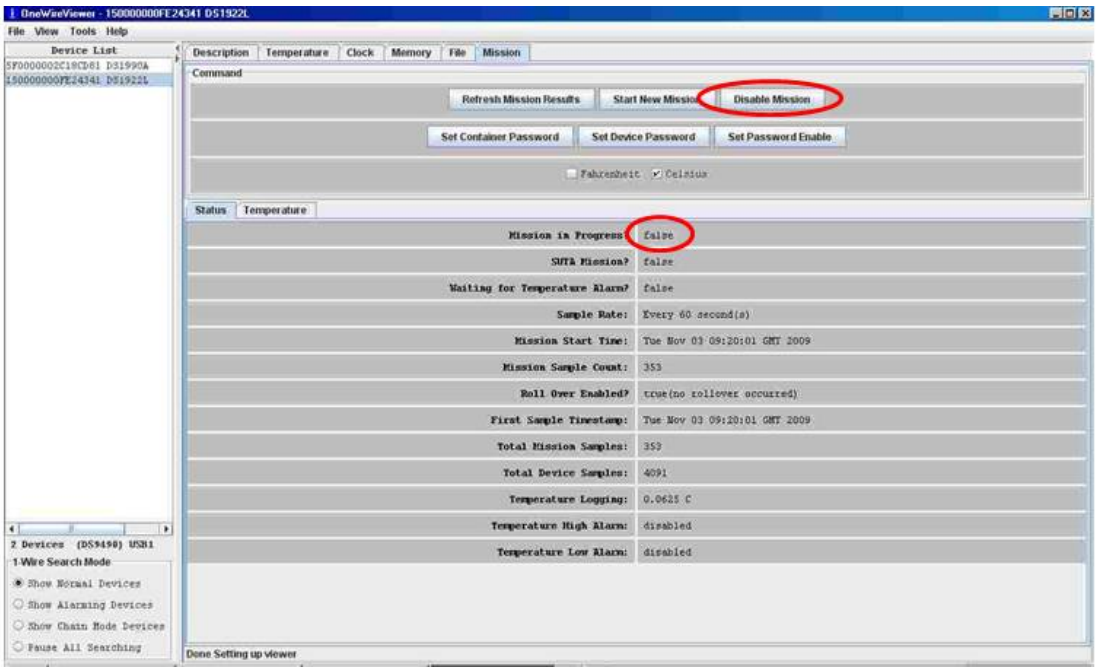

Take readings

Click on the sub-tab "*Temperature*" and the bottom half of the screen should display a graph of the temperature variation.

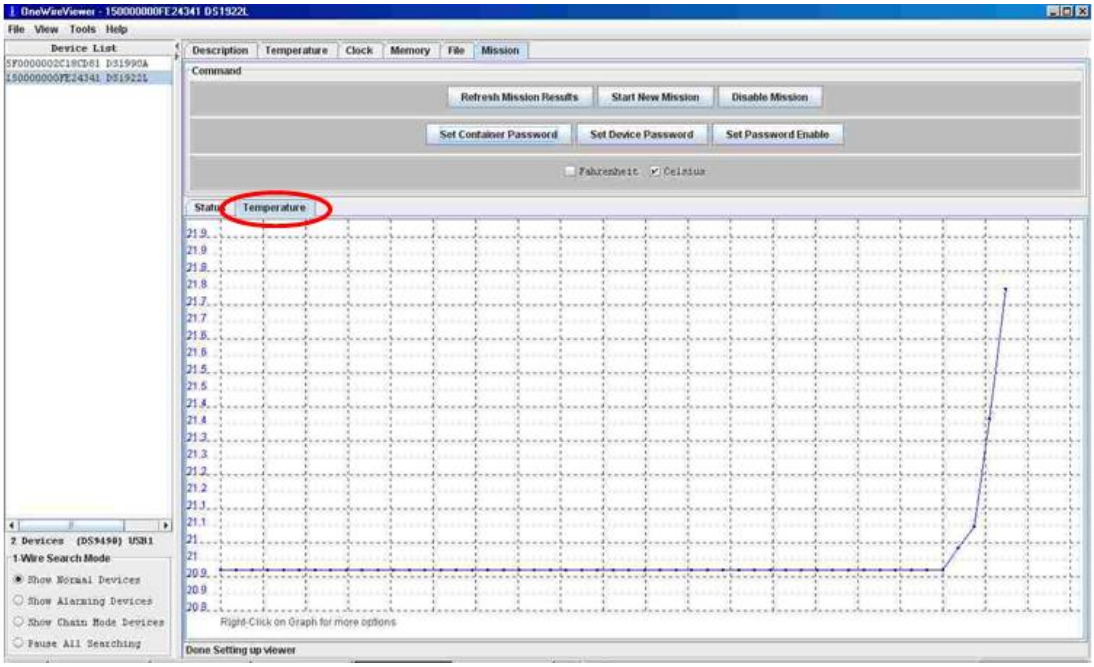

"*Right Click*" on the graph below and select "**Copy Data to Clipboard with Labels**". Open you notepad and simply paste all the copied data into the notepad and save as a *.Txt file. Excel can then be used to open the *.Txt file and sort out the data.

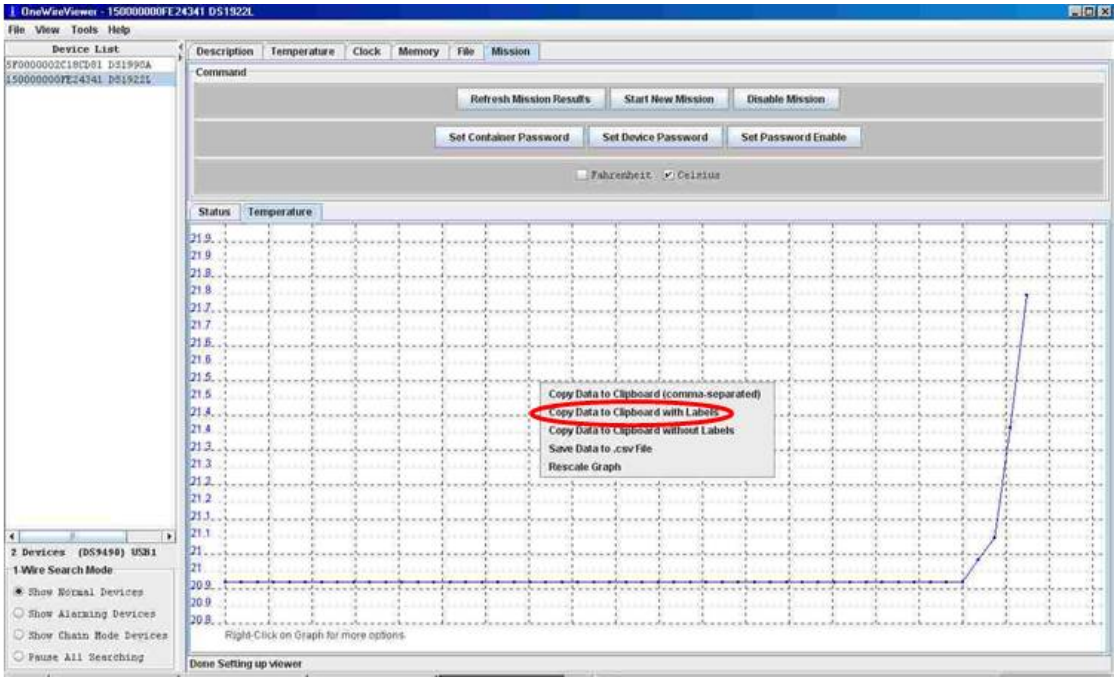

It is not necessary to disable a mission for data collection. It is always good to copy the data over WITHOUT disabling the mission. This can allow continuous measure.

** please note I-button can only hold data for one mission. Once a new mission started, all data from the previous mission will be erased. It is usually a good practice to copy the data over first before disabling the mission.

Appendix J - Notes on Kriging

Interpolation method Kriging was named after a mining engineer D. G. Kringe in the gold fields of South Africa in 1966[1]. This interpretation method improved the precision in estimating gold concentration at that time. Kriging was used to interpolate values of variables for an unknown point by looking the relations between other known points. These known point do not have to be regularly spaced. This method could be performed in 1-dimension, 2-dimension or even 3-Dimension. The following equation (A.1) was used to found the estimated value of an unknown point.

$$\hat{f} \approx \sum_{i=1}^{N} w_i f_i \qquad \text{(A.1)}$$

Where: f_0 = *estimated value of unknown point*

w_i = *weighting factors of know points*

f_i = *values of known points*

Further to equation (A.1) the sum of all weighting factors should also satisfy equation (A.2):

$$\sum_{i=1}^{N} w_i = 1 \qquad \text{(A.2)}$$

There are two stages of Kriging:

1. A Semivariogram was constructed from variation and difference in distance of all known data points. A smooth best fitted curve (usually three or four types only)

was found from the semivariogram.

2. Calculate the weighting factors by solving a set of linear simultaneous equation. Coefficients used in these liner equations were usually obtained from the smoothed curve on the semivariogram.

Appendix K – Draft SKV paper

1.0 Introduction

Urban Heat Island (UHI) is becoming a common known consequence due to rapid urbanisation. Urban Heat island intensity, calculated by subtracting urban air temperature by rural air temperature, can easily reflect the urban heat island effect.

One important factor contributing towards urban heat island is the urban geometry as mentioned by Oke (1981). He used a hardware model to show the decreased of net long wave radiation was related to the reduced (SVF) under clear calm conditions.

There are different methods of calculating SVF. With knowledge of the canyon geometry such as street width and building heights it is possible to calculate the SVF by hand. However, this assumes the canyon is symmetrical, meaning the buildings are the same height on both sides. The calculations become more complicated for unsymmetrical canyons so it is time consuming to obtain results.

As defined by Johnson and Watson (1983) is the ratio of long wave radinnt flux reaching the sky vault from the flat floor of the canyon to that reaching the sky vault from an unobstructed flat surface. It is given by:

$$\psi s = \frac{1}{\pi R^2} \int_{Sv} cos\varphi dS \qquad \text{eq.1}$$

Where ψs = the sky view factor [dimensionless]
φ = the angle between the canyon floor and the sky vault hemisphere radius to area dS [radians]
dS = the elemental area seen from the canyon floor [m^2]
R = radius of the sky hemisphere [m]
Sv = the sky vault seen from the canyon floor

The SVF is dimensionless and can vary from zero to one. A zero sky view factor indicates no sky is visible due to the obstruction of buildings or bridges while a sky view factor approaching one would be found in a very open space with very little obstructions.

SVF can also be obtained from hemispherical photography. Hemispherical photography can be achieved using a fish eye lens to capture a 180^{o} image of the canyon.

Figure 1 Hemispherical image of John Dalton Street, Manchester,

The advantage of SVF derived from hemispherical photography is that estimation is made from a 3-D perspective, as opposed to a 2-D point specific view factor calculated from the height to width ratio of the canyon.
Additionally, 2-D view factors become inaccurate in asymmetric canyons, so the solution is to segment the hemisphere and calculate the sum of the different height to width ratios in each segment to produce a SVF value. Another advantage of using photography is that by reducing the time for manual intervention there becomes a greater potential to increase the number of images taken in the field, hence more data can be obtained.

Recently fast methods have been developed to calculate SVF using fish eye photography. By utilising available software such as the Grimmond (2001) and Chapman (2001) programs photographs can be processed quickly.

To calculate SVF Grimmond uses the Johnson and Watson equation (1983):

$$\psi_{sky} = \frac{1}{2\pi}\sin\left(\frac{\pi}{2n}\right)\sum_{i=1}^{n}\sin\left[\frac{\pi(2i-1)}{2n}\right]\alpha_i$$

n = number of annuli

i=annulus index

α_i = width of each annulus, this is amount of degrees that sky is visible in each annulus

Chapman's method for calculating SVF is similar to the Grimmond method. Chapman used FORTRAN to split the image into 33 annuli of equal width and then equation 2.3 is used to calculate SVF which takes into consideration the weighting of each annulus:

Chapman method uses low resolution images (75x75 pixels per image) because it is used for real time SVF calculations, so computational time has to be very low and it is assumed that relative errors in calculations will be negligible[135]. Image resolution describes the detail an image contains, hence a greater amount of detail is given if a larger amount of pixels are used [Wiki (2010)]. This low image resolution allows images to be processed quicker, however, by comparing the two images below of John Dalton Street, Manchester, it is evident that the error will probably be significant:

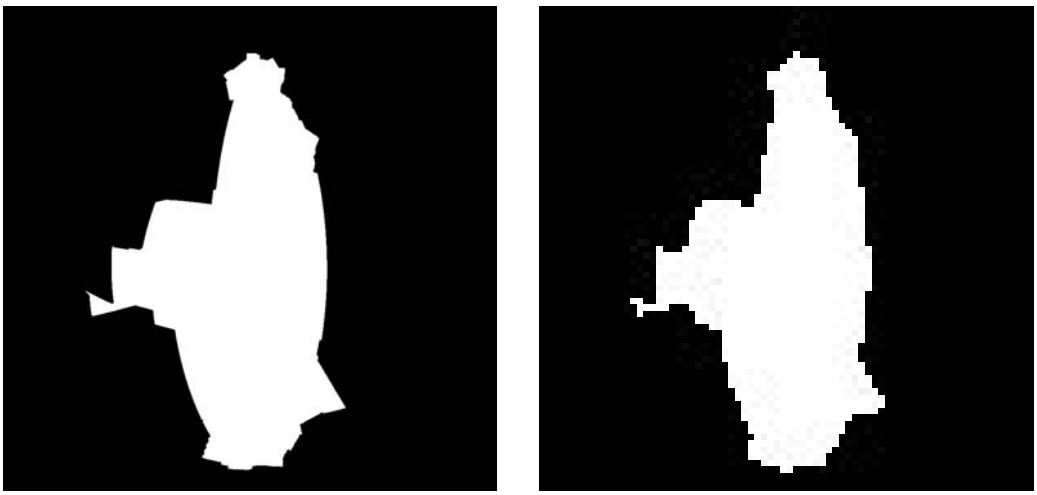

(a) (b)

Figure 2 John Dalton Street at a resolution of (a) 960x960 pixels (b)76x76 pixels

It can be seen that both methods have their advantages and disadvantages. It is also important to note there are other methods in use as well:

- 3D-GIS Extension – uses 3D Sky View Extension algorithm written in Avenue to work with Arc view GIS 3.2 to transform coordinates of polygons into stereographic and orthographic coordinates to allow SVF estimation.[136]
- LI – COR LAI - 2000 Plant Canopy Analyzer – measures diffuse non interceptance light using a fisheye optical sensor.
  The method has two main sources of error, being that the instrument's full field of view is only 148^{o}, which is much less than 180^{o} which needed for accurate SVF measurement. Also any radiation reflected off buildings in the

urban canyon will result in error because diffusion is calculated by measuring radiation penetrating the canyon, so over estimation will occur[4].

- Calculation Sheet – AI fish eye Nicole auto 8mm lens and F2.8 camera made by Nippon Kogaku used to obtain canyon photographs at a height of 1.2m. Then a calculation chart is used with the photo to obtain SVF.[137]

In this paper, a new package was developed in Matlab which can calculate SVFs from photos taken with a fisheye lens. These SVF values were validated with both packages developed by Grimmond[3] and Chapman[4]. The SVF values found were then analysed against air temperature data obtained from different temperature sensors in these case study areas in Greater Manchester.

2.0 Methodology

Nine case study areas in the city centre of Greater Manchester UK were selected for the analysis of SVF against urban heat island intensities.

Photos taken with the fisheye lens of all nine case study areas were first analysed using both Grimmond's[3] and Chapman's[4] methods. Figure 4 and Table 1 indicate that there was an average error ratio of 1.5 for all 9 venues between two methods.

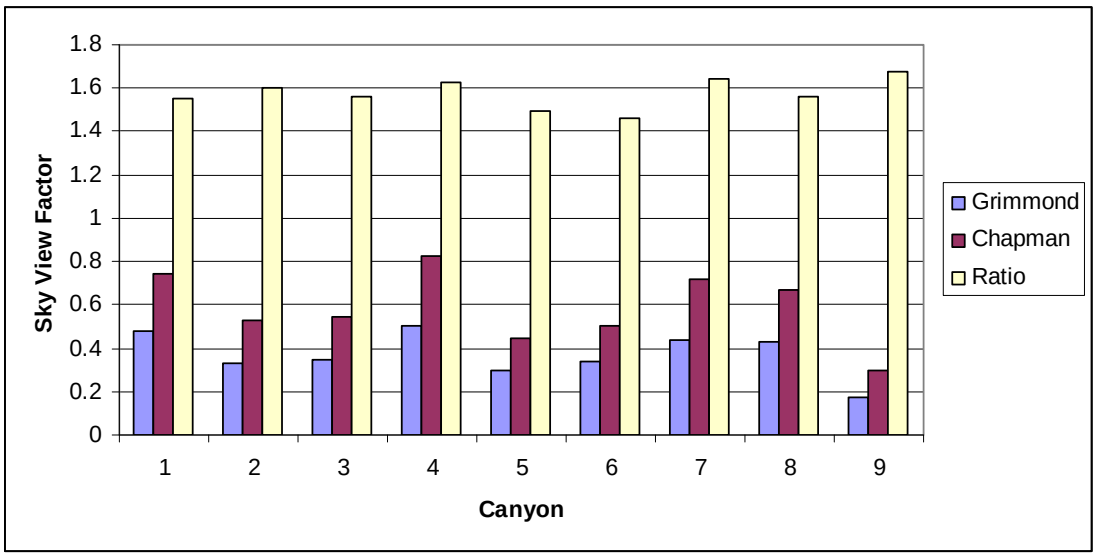

Figure 3 Sky View Factor results using Grimmond and Lee Chapman method.

	Canyon	Grimmond	Chapman	Ratio
1	Oxford Road	0.481	0.746	1.551
2	Oldham Street	0.328	0.525	1.601
3	Chinatown	0.347	0.541	1.559
4	Pariser	0.507	0.826	1.629
5	Turner Street	0.297	0.443	1.492
6	John Dalton Street	0.342	0.501	1.465
7	Deansgate	0.437	0.717	1.641
8	Alan Turing	0.431	0.672	1.559
9	Brown Street	0.177	0.297	1.678

Table 1 SVF found by both methods at the nine case study areas

Matlab Method

To improve on the accuracy of results for SVF, a package for calculating SVF in Matlab was written. This uses a similar method to the Grimmond and Chapman methods but has several advantages. It has higher accuracy as it splits photographs into more annuli, hence giving a converged solution. Accuracy is improved further by using high resolution images (723823 pixels per image). Additionally computational time is decreased because Matlab handles a matrix as a single unit, which is not the case in Fortran. Finally the program interface is simple to use.

The Matlab method uses a Nikon Coolpix 950 digital camera and Nikon FC-E8 fisheye lens mounted on a Sony VCT-R640 tripod to capture images of urban canyons. Once images have been captured, they are processed using Paint Shop Pro Version 6 or 7 to convert them to black and white so that they only contain two pixel values. Black pixels represent buildings whilst white pixels represent the sky. The image is then read into Matlab. User can then specify the number of annulus (up to 24 annulus) to be used for analysing the picture. The pixel distribution in each annuli is counted to input into an equation to calculate SVF.

Due to the nature of fisheye photography, when an image is displayed as a 2-D circular image, the area it is representing has been reduced.

Consider a hemisphere which has an area of $2\pi r^2$ where r is its radius, this is the area a fisheye photo represents, however it is displayed as a circular 2-D image of area πr^2, therefore the ratio of the two areas is equal to 2. So each pixel in the 2-D circular image represents an area greater than it takes up, and it is the position of the

pixel that determines the amount of area it represents. The image is split up into annular sections and weighting functions for each annulus are applied to take this into consideration.

Both equations used by Grimmond and Chapman were input into Matlab and it was found that an identical SVF result was found from both equations.

Because of the high resolution of the photos, the maximum amount of annuli that the image can be split into is 27 because by exceeding this value the computer runs out of memory. However, because accuracy is maintained in the photo itself, by using high resolution photographs, it is shown that accuracy of the SVF data is significantly improved when compared to the Chapman and Grimmond methods.

SVF photos were taken in different positions (including different height and different horizontal position in a canyon) of the canyons in Greater Manchester were then compared.

Air temperature sensors-loggers were installed at all nine case study areas. All sensor-loggers were accommodated in a radiation shield. Both the radiation shields and the sensor-loggers were tested and calibrated[138] (Cheung 2010). Sensor-loggers were located at four metres above ground on street lamp columns. All sensor-loggers were set to be logged at every 30 minutes. Linear interpolation was performed on the data collected so that all data could be synchronised to the same 30 minutes for comparison. The logging period started at the beginning of February 2010 and finished at the end of April. The rural reference data was obtained from the British Atmospheric Data Centre (BADC) by Dr John B. Parkinson[139].

3.0 Sky view factor measurements

Validation of Matlab method

As with the Grimmond and Chapman method, it is necessary to perform test runs to validate the accuracy of the Coles' Matlab method. Test runs were performed with four standard pictures: full black (theoretical SVF=0), full white (theoretical SVF=1.0), half black and half white (theoretical SVF=0.5) and quarter white (theoretical SVF=0.25). Four runs were then performed with each standard picture with different number of annuli. All test run results can be found in table 2.

Photograph	Number of Annuli	Matlab	Theoretical SVF	Error (%)
Black	3	6.78E-05	0	0
	6	5.65E-05	0	0
	12	5.11E-05	0	0
	24	5.56E-05	0	0
White	3	1.047	1	4.72
	6	1.012	1	1.15
	12	1.003	1	0.29
	24	1.001	1	0.07
Half White Half Black	3	0.524	0.5	4.84
	6	0.506	0.5	1.22
	12	0.502	0.5	0.36
	24	0.501	0.5	0.12
Quarter White	3	0.261	0.25	4.32
	6	0.252	0.25	0.76
	12	0.250	0.25	0.12
	24	0.249	0.25	0.32

Table 2 Test results obtained using the Matlab method.

From Table 2 it can be seen accuracy is sufficiently high to conclude that the Matlab method is a more accurate method than Grimmond and Chapman method. Therefore the analysis of SVF data is performed using data obtained from the Matlab method.
The test results also prove that using the Chapman equation for each annulus is valid due to the high accuracy obtained.

Additionally, from table 2 it can be seen that by increasing the number of annuli the image is split up into, the accuracy increases, however this increase in accuracy is only significant when the number of annuli is below 6.
Therefore during the remainder of the analysis 12 annuli are used because accuracy is sufficiently high and computational time is reduced. (From 2 minutes per image for 24 annuli to 20 seconds per image for 12 annuli).

To emphasise this last point the convergence of results for SVFs for different canyons can be shown:

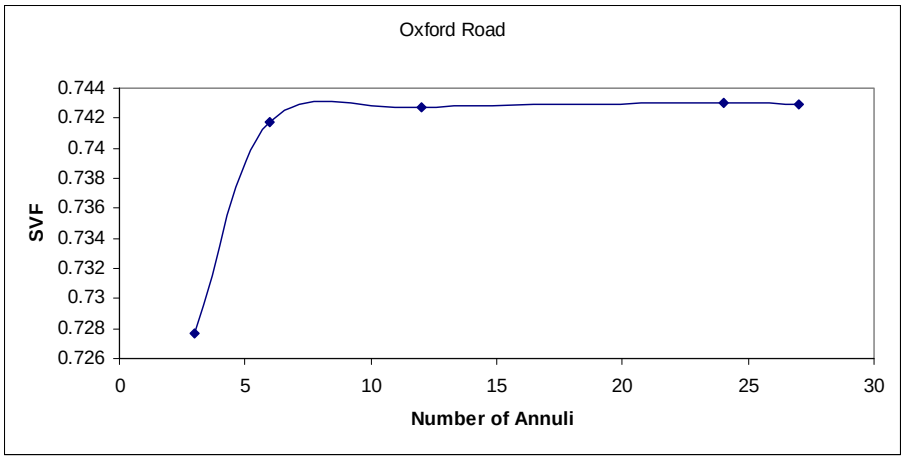

(a)

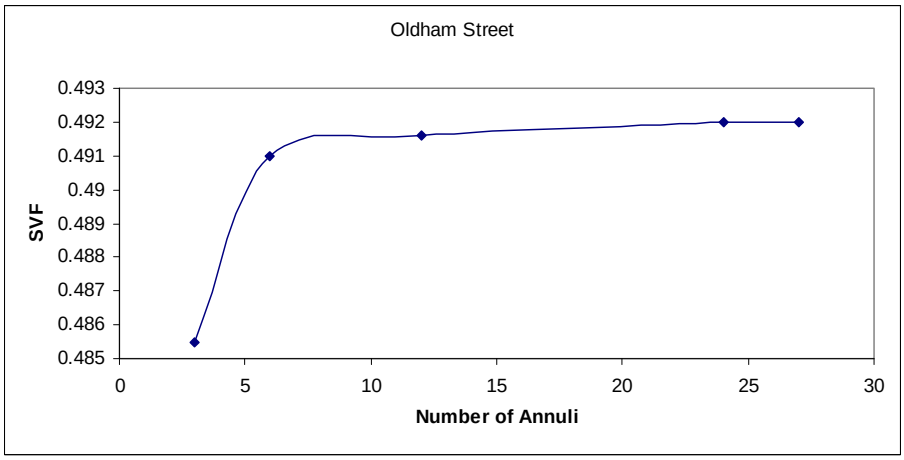

(b)

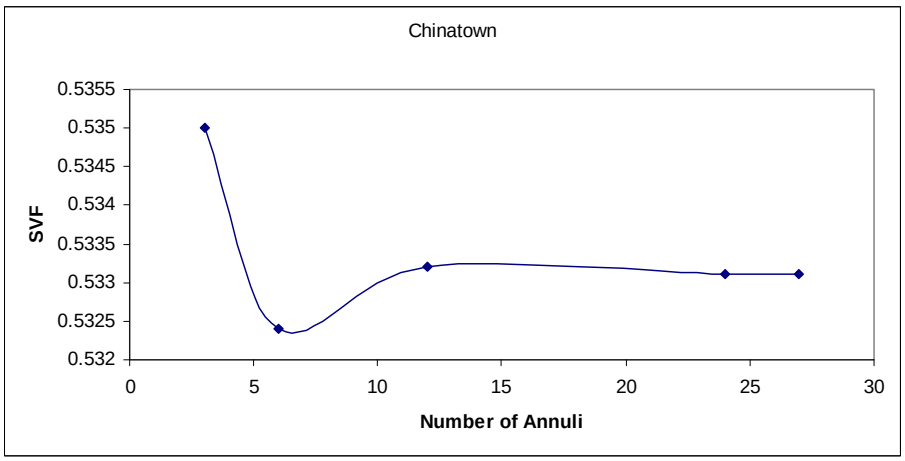

(c)

Figure 4 Convergence of sky view factor (SVF) results by increasing the number of annuli for (a) Oxford Road (b) Oldham Street (c) Chinatown, Manchester.

SVF results from each method are shown below:

	Canyon	Grimmond	Chapman	Matlab
1	Oxford Road	0.481	0.746	0.743
2	Oldham Street	0.328	0.525	0.492
3	Chinatown	0.347	0.541	0.533
4	Pariser	0.507	0.826	0.72
5	Turner Street	0.297	0.443	0.448
6	John Dalton Street	0.342	0.501	0.501
7	Deansgate	0.437	0.717	0.679
8	Alan Turing	0.431	0.672	0.706
9	Brown Street	0.177	0.297	0.271

Table 3 Comparison between SVF results obtained using Grimmond, Chapman and Matlab methods

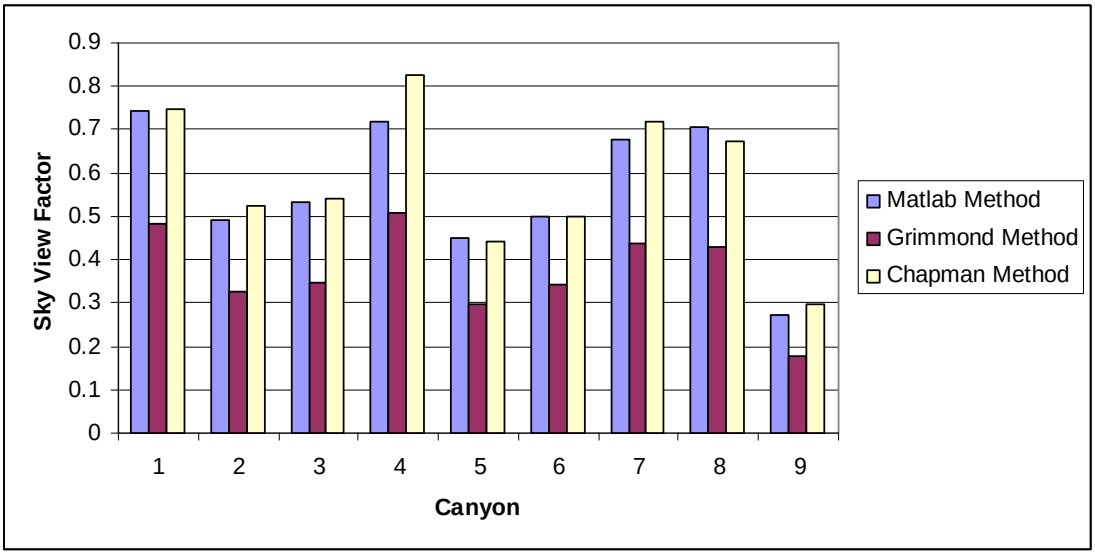

Figure 5 Comparison between Grimmond, Chapman and Matlab methods

Results from the Matlab method agree well with results from the Chapman method, indicating Chapman method is more accurate than Grimmond method.
However, it is assumed the Matlab method is most accurate because it uses a greater image resolution of 723,823 pixels per image.

Therefore SVFs used for further analysis were all calculated by this Matlab method.

SVF measured at different positions inside canyon

An important consideration when correlating SVF to urban heat island intensity is whether it is valid to use images obtained from photographs taken in the centre of each canyon. This is because the temperature sensors are positioned on one side of each canyon, not in the centre, so if the air temperature inside each canyon varies across the horizontal plane, the air temperature at the centre of the canyon could be completely different to the air temperature detected by the temperature sensor.

3.1 Horizontal plane

Before investigating the temperature variation across the horizontal plane, it is important to check if the SVF calculated from different position in the canyon would affect the SVF result. Photos were taken in different horizontal planes inside 14 canyons in Greater Manchester. One side of the canyon was named as side A and the other side was named as side B. All photos were taken in the same height and table 4 shows their SVFs and percentage errors.

	SVFs			% error between Side A and B	% error between both sides and middle	
Street Canyons	A	Middle	B		A	B
Brown Street	0.126	0.190	0.126	0.1	33.7	33.7
China Town	0.301	0.370	0.298	1.2	18.6	19.6
Oxford Road	0.486	0.766	0.472	2.7	36.6	38.4
Turner Street	0.312	0.413	0.304	2.6	24.4	26.4
Concert Lane	0.207	0.213	0.204	1.6	2.8	4.4
Essex Street	0.202	0.213	0.201	0.1	5.4	5.6
Fountain Street	0.289	0.296	0.279	3.3	2.4	5.6
Kent Street	0.188	0.154	0.102	45.9	-22.2	33.8
Marsden Street	0.179	0.196	0.178	0.5	8.4	8.8
Norfolk Street	0.315	0.324	0.314	0.3	2.5	2.8
Pall Mall	0.195	0.209	0.191	2.1	6.6	8.6
Police Street	0.277	0.303	0.275	0.6	8.6	9.1
South King Street	0.297	0.324	0.294	1.1	8.2	9.2
W Mosley Street	0.190	0.200	0.189	0.4	5.2	5.6

Table 4 SVF calculated at different horizontal position in canyons

It could be seen that the SVFs calculated from both sides of a canyon is very similar

(less than 5%) for most of the canyon apart from Kent Street. This is because the canyon is very asymmetrical with very tall building on side B and low building on side A. The percentage error of SVF calculated from one side of canyon compare to the one calculated from middle on canyon varies from 2.4% to 38.4%. This could be caused by different reasons. Therefore, it could be concluded that the most accurate SVF value should be the one taken from middle of canyon.

3.2 Vertical Plane

Photos taken from heights of 0.55m and 1.44m in the centre of canyons are obtained to investigate whether varying the height at which photos are taken effects results for SVF. Four canyons were selected for this experiment. Table 5 shows the result.

	SVF		
Street Canyons	High (1.44m)	Low (0.55m)	Percentage Error
Brown Street	0.190	0.185	0.10%
China Town	0.370	0.366	0.14%
Oxford Road	0.766	0.737	2.26%
Turner Street	0.413	0.406	0.31%

Table 5 SVF calculated at different vertical position in canyons

As can be seen from table 5, there is no significant difference in results when varying height. This is explained by the difference in height between the change of camera position to the building heights in the canyons. For example the height of the buildings on each side of the Oxford Road canyon are 31.2m and 23.3m respectively, which are much greater than the insignificant change in camera height of 0.89m.
Since the air temperature inside each canyon is recorded in the canopy layer close to the canyon surface, it is valid to capture images for SVF from a height of 1.44m, as this the greatest height the tripod can reach and little difference in SVF is shown for small changes in the vertical position the image is captured from.

3.3 variation of temperature horizontally across the canyon

To investigate this air temperature data was obtained at three positions across Oxford Road and Turner Street throughout a still clear day using a mercury thermometer to investigate how air temperature varies across the canyons. The experiment was conducted throughout a morning when solar radiation input into the canyon varies with position due to the obstruction of buildings as the sun rises from the East. Hence

this is the most likely time for there to be air temperature differences inside the canyon. It is important to choose a still day so that wind does not transport heat out of the canyon and disrupt temperature at local positions inside a canyon due to turbulence.

The temperature sensor in the Oxford Road canyon is on the East side, and the north east side in Turner Street. Temperature data from three positions across these canyons is obtained to see how air temperature varies across the canyons.

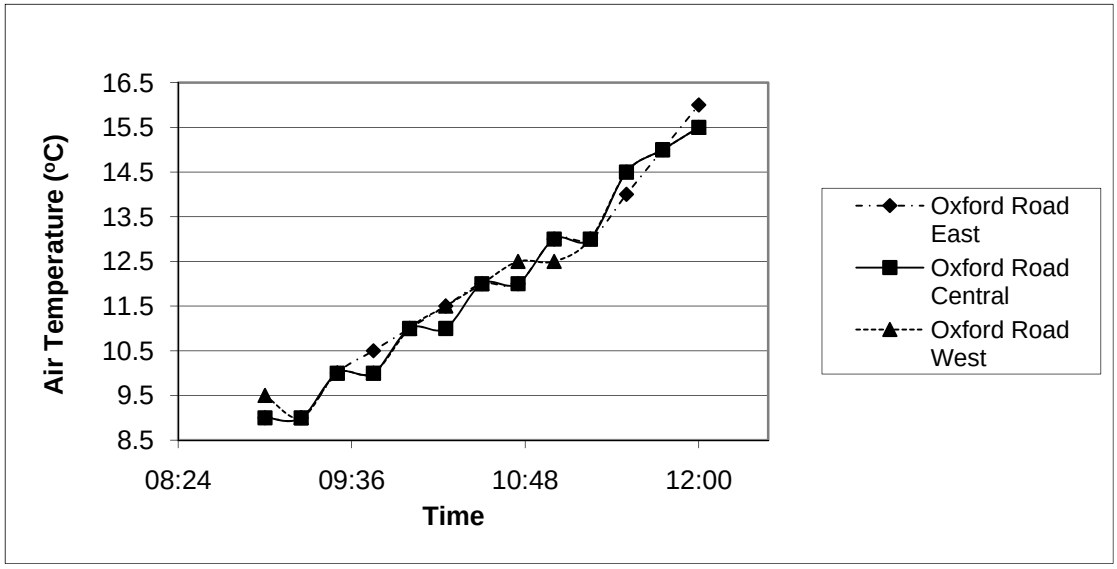

Figure 6 Air Temperature across Oxford Road and Turner Street canyon on 12/04/2010

Due to the resolution of the mercury thermometer, both canyons were found to have exactly the same temperature variations shown in figure 6. From the data obtained from the two canyons it can be seen that temperature does not vary significantly across the two canyons. The reason for this is believed to be that turbulent air flow inside the canyon is sufficient even on still days to mix the air so that there is a uniform temperature across the canyon. This validates obtaining photographic images from the centre of each canyon to calculate SVF because air temperature is not dependant on horizontal position inside the canyon, however the relative position inside each canyon must be consistent. Therefore in order to obtain SVF data for each canyon, photos are taken from the centre of each canyon.

4.0 SVF and the Urban Heat Island (UHI) effect in Manchester

Oke (1981) stated that the urban heat island effect should be at maximum on clear

calm nights. Clear and calm periods were therefore filtered from Feb to Apr data for the Manchester "rural" MetO site of Woodford (15miles south of Manchester city centre). (Snow was present in Manchester on some the clear days in Jan which might result in inaccuracy of data) with the following criteria:

1. Cloud cover at Woodford was smaller than or equal to 2 oktas
2. Wind speed at Woodford was smaller than or equal to 2.5ms^{-1}
3. The total time period with condition 1 and 2 occurring should last for at least four hours.

Average half hourly heat island intensities were then calculated from these clear and calm periods. The number of data sets used to calculate average half hourly data in each half hour interval were different. However this averaging method was still adopted because there was no other consecutive period long enough with clear and calm weather conditions in Manchester in these three months. Figure 6.7 and 6.8 below shows the urban heat island intensity over a time period of 24 hours. The points on the graphs were averaged half hourly data. The two graphs use data from three canyons each with the same orientation.

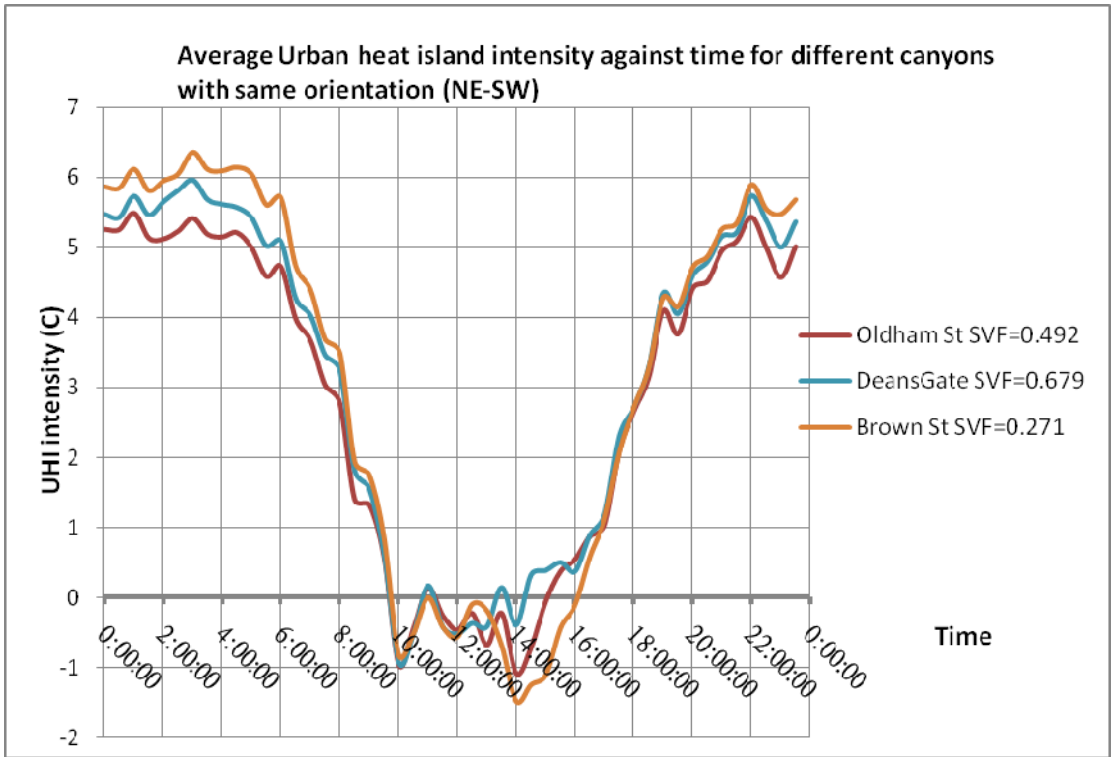

Figure 8 Average UHI intensity against time for different canyons with orientation of NE to SW

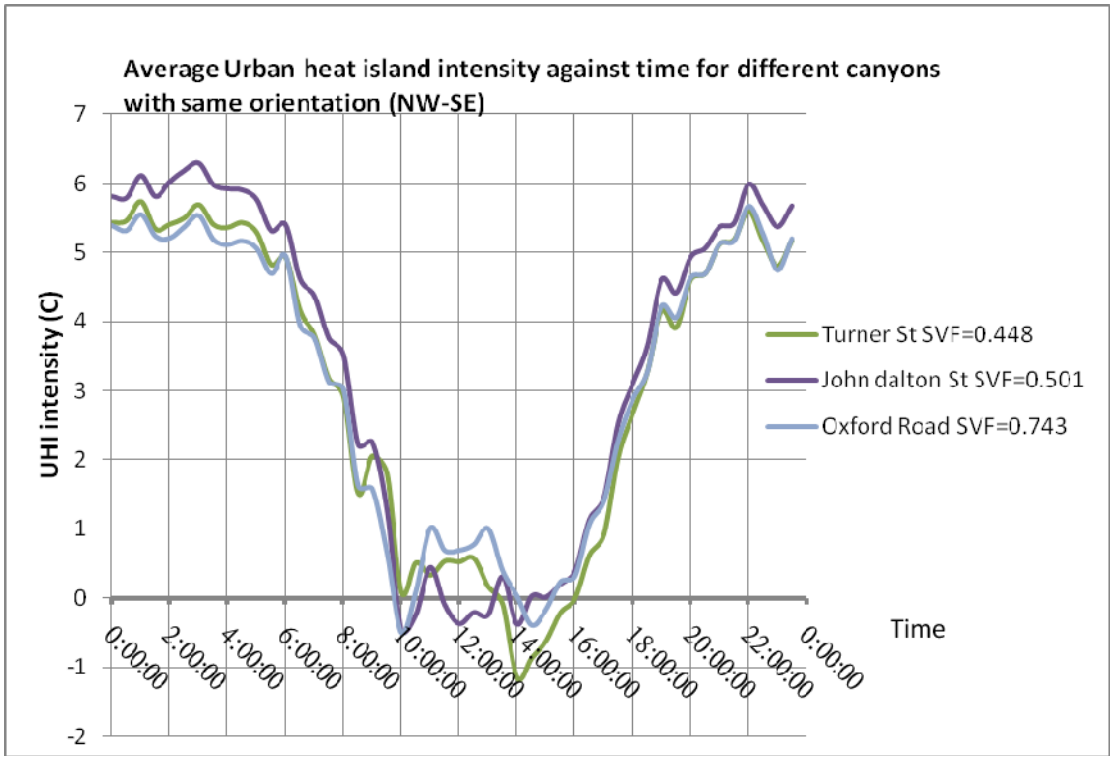

Figure 9 Average UHI intensity against time for different canyons with orientation of NW to SE

In Fig.9 Brown Street (SVF=0.271) has the smallest SVF compared to the other two canyons and it has the largest heat island intensity during night time when UHI intensity should be a maximum. However, John Dalton Street has the largest UHI effect but does not have the lowest SVF. Similarly, in Fig.10, Oxford Road has the largest SVF but not the smallest heat island intensity as shown in Fig. 10. These results do not fully agree with the prediction suggested by Oke's model (1981) with the empirical equation for the maximum UHI effect (ΔTu-r(max)):

$$\Delta T_{u-r(\max)} = 15.27 - 13.88\psi_s \qquad \text{eq.4}$$

However, there are other factors, apart from SVF, (varying building facades and their heat emissions, traffic, etc [Smith *et al.,* (2008) (2009)]) that affect the urban heat island intensity.

However, a similar relationship to Oke's is found from the Manchester data for the UHI intensity against SVFs in the night time (Fig.11):

$$UHImax = 5.12 - 1.06SVF \qquad \text{eq.5}$$

However, the UHI effect during the day is not as large as the maximum at night and shows a reverse regression (Fig. 12):

$$UHImax = 0.88SVF - 0.12 \quad \text{eq.6}$$

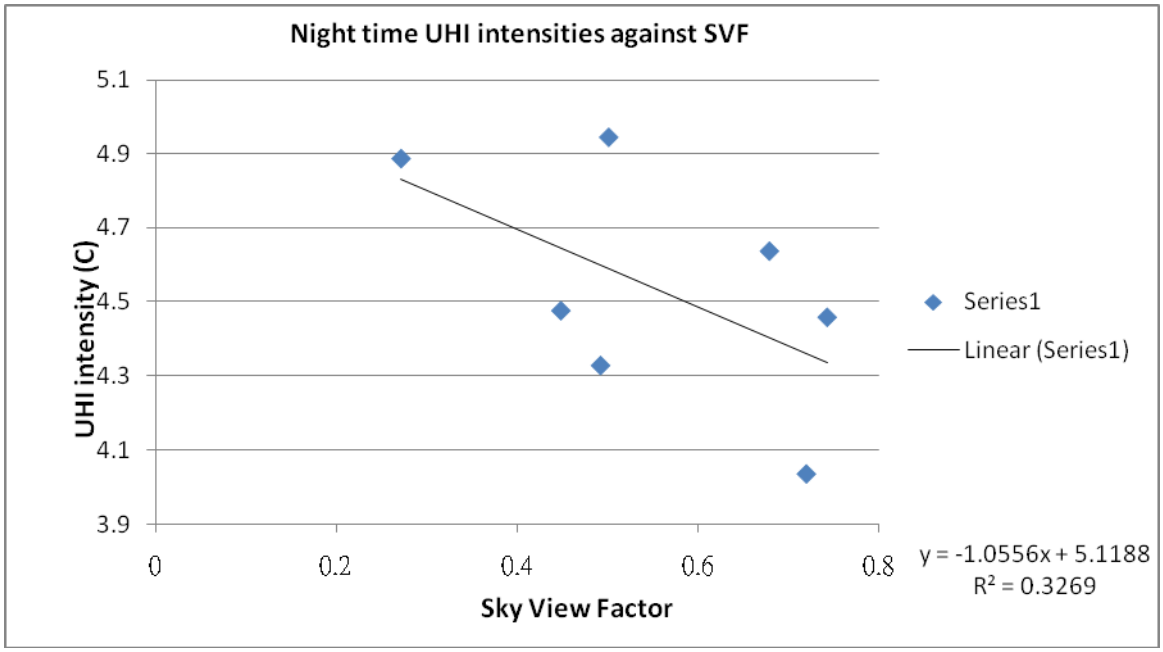

Fig 10 Night time UHI intensities against SVF

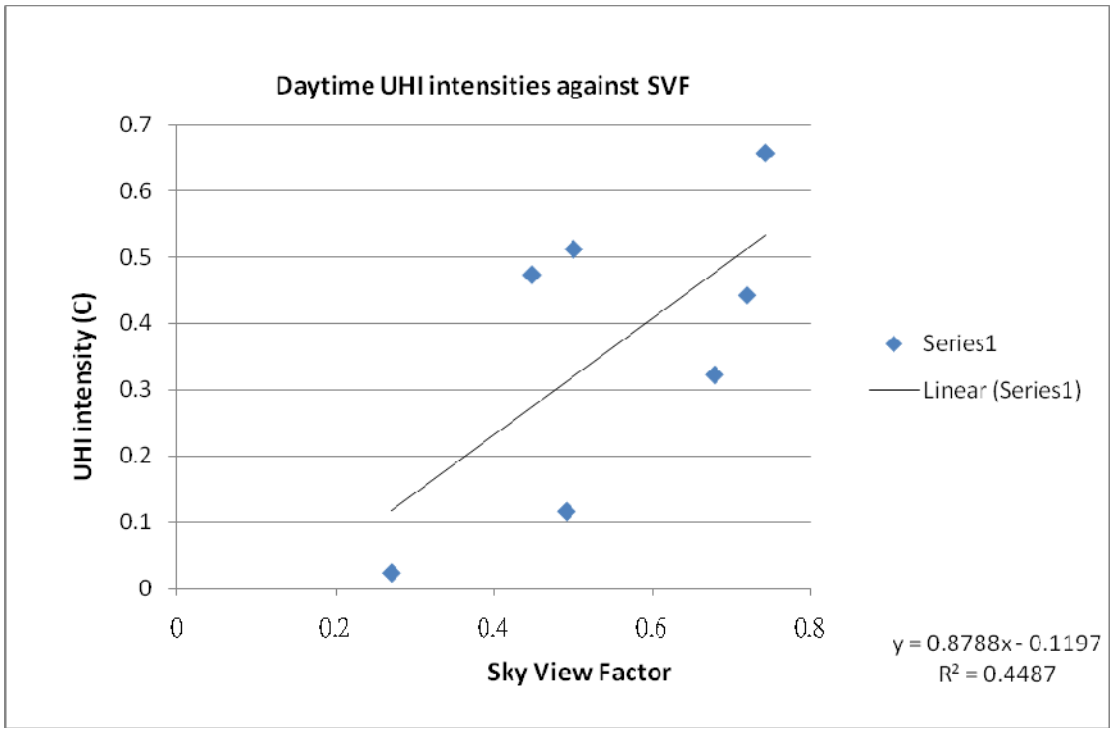

Fig 11 Day time UHI intensities against SVF

During the night time, a negative slope was found from Fig. 11 in general agreement with Oke but with a shallower slope (indicating a smaller SVF influence on the UHI effect than Oke's work). 4. Nevertheless, a positive slope was found from Fig. during the daytime which means a canyon with a small SVF would have a low UHI effect. Such a result could be explained by the cool island during the day time. However, the R^2 values for the slopes in Fig. 11 and Fig.12 are not that high and t-tests give 1.57 for night-time and 2.02 for daytime with a critical t-value of 2.44 for a 95% confidence level.

Conclusions:

- Discuss the relevance of the correlations found.

Reference

http://ams.allenpress.com/perlserv/?request-get, viewed on 22/03/2010

L C.L Souza, D S.Rodrigues, J.F.G.Mendes, Sky View Factors Estimation using a 3D-GIS Extension, 2003, Methodology for SVF Assesment, pg 2

Yamashita .Shuji, On Relationships between Heat Island Effect and Sky View Factor in Cities of Tana River Basin Japan, 1985, 4.Some Considerations, pg 685

Cheung. H., Levermore. G. and Watkins. R. (2010) A low cost, easily fabricated radiation shield for temperature measurements to monitor dry bulb air temperature in built up urban areas. *Building services engineering research technology* 31, 3

Dr Parkinson, J. B. *Department of Mathematics The university of Manchester.* Private communication in July 2010

Reference

[1] Oke, T., R., (1978) Boundary Layer Climate *Routledge* ISBN:0415043190

[2] Population reference bureau (2007). *2007 World Population Data Sheet.* Population Reference

[3] United Nations. (2005) Department of economic and social affairs, Population Division Word Urbanisation Prospects: The 2005 Revision. Working Paper Np. ESA/P/WP/200

[4] Stone, B. and Rogers, M., O. (2001) Urban form and thermal efficiency – How the design of cities influences the urban heat island effect. *Journal of the American Planning Association* 62(2), 186-198

[5] Lowry., W., P. (1977) Empirical estimation of urban effects on climate: a problem analysis, *Journal of Applied Meteorology* 16, 129-135

[6] Magee, N., Curtis, J., Wendler, G., (1999) The urban heat island effect at Fairbanks, Alaska. *Theoretical and Applied Climatology* 64, 39-47

[7] Kim, Y. and Baik, J., (2005) Spatial and temporal structure of the urban heat island in Seoul *Journal of Applied Meteorology* 44, 591-605

[8] Arnfield, A, J. (2003) Two decades of urban climate research: a review of turbulence, exchange of energy and water, and the urban heat island. *International Journal of Climatology,* 23(1), 1-26

[9] Kanda, M. (2007) Progress in Urban Meteorology: A Review, *Journal of the Meteorological Society of Jamal*. 85B, 363-383

[10] Eliasson, I. (1996) Urban Nocturnal temperatures, street geometry and land use. *Atmospheric Environment*, Vol. 30(3), 379-392

[11] Girdharan, R., Lau, S.S.Y., Ganesan, S. and Givoni, B. (2007) Urban design factors influencing heat island intensity in high-rise high-density environments of Hong Kong. *Building and Environment*, 42(10), 3669-3684.

[12] Watkins, R., Palmer. J., Kolokotroni. M. and Littlefair, P. (2002) The London Heat Island: results from summertime monitoring. *Building services engineering research technology*. 23(2), 97-106

[13] Wilby, R, L. (2003) Past and projected trends in London's heat island intensity. *Weather,* 58(7), 251-260

[14] Baik, J, J., Kim, Y, H., Kim, J, J. and Han, J, Y. (2007) Effects of boundary-layer stability on urban heat island-induced circulation. *Theoretical and Applied Climatology* 89(1-2), 73-81

[15] Hulme,M., Jenkins,G.J., Lu,X., Turnpenny,J.R., Mitchell,T.D., Jones,R.G., Lowe,J., Murphy,J.M., Hassell,D., Boorman,P., McDonald,R. and Hill,S. (2002) Climate Change Scenarios for the United Kingdom: The UKCIP02 Scientific Report, *Tyndall Centre for Climate Change Research, School of Environmental Sciences, University of East Anglia, Norwich*, UK. 120pp

[16] ASCCUE Final Report (2006) EPSRC Funded http://www.sed.manchester.ac.uk/research/cure/downloads/asccue_epsrc_report.pdf *The University of Manchester* [accessed on 27/4/2011]

[17] SCORCHIO EPSRC funded http://www.sed.manchester.ac.uk/research/cure/research/scorchio/ *The University of Manchester* [accessed on 27/4/2011]

[18] IPCC Fourth Assessment Report (2007) Working Group III "Mitigation of Climate Change". Cambridge University Press

[19] Chow, D., Levermore, G., Jones, P., Lister, D., Laycock, P, L. and Page, J. (2002) Extreme and near-extreme climate change data in relation to building and plant design. *Building Services Engineering Research and Technology*, 23(4), 233-242

[20] Konopacki, S. and Akbari, H. (2002) Energy saving for heat island reduction strategies in Chicago and Huston (including updates for Baton Rouge, Sacramento and Salt Lake city) *Final Report LBNL-49638* University of California, Berkeley

[21] Parkinson, J., Wright, A., Levermore, G. and Muneer, T. (2004) Weather data with climate change scenarios, *CIBSE TM34.* London

[22] CIBSE Guide A (2006) *Chartered Institute of Building Service Engineering*

[23] Levremore, G. and Parkinson, J. (2006) Analysis and algorithms for new Test Reference Years and Design Summer Years for the UK. *Building servicers Engineering Research and Technology*, 27(4), 311-325.

[24] UK Climate Impact Programme (2009), UKCP, http://www.ukcip.org.uk/index.php [accessed 28/06/10]

[25] Coincident Probabilistic climate change weather data for a Sustainable built Environment (COPSE) (2008) Case for support

[26] UK Climate Projection (2009) Section 5.13 http://ukclimateprojections.defra.gov.uk/content/view/2002/500/ [accessed 27/4/2011]

[27] Howards. L., (1818) The climate of London, deduced from Meteorological observations, made at different places in the neighbourhood of the metropolis, II. London.

[28] Mitchell, J., M. (1953) On the causes of instrumentally observed secular temperature trends *Journal of Meteorology* 10, 244-261

[29] Gartland, L. (2008) Heat islands understanding and mitigating heat in urban areas. *Earthscan* London. ISBN:9781844072507

[30] Morris, C. and Simmonds, I. (2001) Quantification of the Influences of Wind and Cloud on the Nocturnal urban heat island of a large city. *Journal of applied meteorology* 40(2), 169-182

[31] Jauregui, E. (1997) Heat island development in Mexico City. *Atmospheric Environement* 31, 3821-31

[32] Moll, G. and C. Berish (1996) Atlanta's changing environment *American Forests* Spring 26-29

[33] Van Weverberg K., De Ridder K., Van Rompaey A. (2008) *Modelling* the contribution of the Brussels heat island to a long temperature time series. *Journal of Applied Meteorology and Climatology* 47, 976-90

[34] Yamashita, S. (1996) Detailed structure of heat island phenomena from moving observations from electric tram-cars in metropolitan Tokyo *Atmospheric Environment* 30(3), 429-435

[35] Moreno-Garcia, M., C. (1994) Intensity and form of the urban heat island in Barcelona. *International Journal of Climatology* 14,705-10

[36] Gedzeman, S. D., Austin S., Cermak, R., Stefano, N., Partridge, S., Quesenberry, S. and Robinson, D. A. Mesoscale aspects of the urban heat island around New York City. *Theoretical and Applied Climatology* 75,29-42

[37] Montacez, J. P., A. Rodriguez and J. I. Jimenez (2000) A study of the urban heat island of Granada. *International Journal of Climatology* 20,899-911

[38] Santamouris, M. (1995) The Athens urban climate experiment. *In PLEA '98 1995 June 1998* (Lisbon). James & James Science Publishers Ltd 1998:147-52

[39] Ludwig, F. L. (1968) Urban temperature filed. In: *Symposium on urban climates and building climatology 1968* (Brussels). World Meteorological Organisation, 1968:80-107

[40] Steinecke, K. (1999) Urban climatological studies in the Reykjavik subarctic environment, Iceland. *Atmospheric Environment* 33, 4157-4162

[41] Brazel, A., N. Selover, R. Vose and G. M. Heisler (2000) The tale of two climates – Baltimore and Phoenix urban LTER sites. *Climate Research* 15, 123-135

[42] Kolokotroni, M. and Giridharan, R. (2008) Urban heat island intensity in London: An investigation of the impact of physical characteristics on changes in outdoor air temperature during summer. *Solar Energy* 82, 986-998

[43] Giridharan, R. and Kolokotroni, M. (2009) Urban heat island characteristics in London during winter. *Solar Energy* 83, 1668-1682

[44] Watkins, R., (2002) Phd Thesis *Mechanical Engineering Brunel University*, UK

[45] Peterson, T. C., Galoo, K. P., Lawrimore, J., Owen, T. W., Huang, A. and Mckittrick, D. A. (1999) Global rural temperature trends *Geophysical Research Letter* 26(3), 329-332

[46] Mccarthy, M., Best, M. and Betts, R. (2009) Cities under a changing climate. *Paper B9-5 : The 7th International Conference on Urban Climate.* Yokohama, Japan, 2009

[47] Changnon, S. A., Jr, Kuynkel, K.E. and Reinke, B. C. (1996) Impacts and responses to the 1995 heat wave: A call to action. *Bulletin of the American Meteorological Society* 77, 1497-1506

[48] Wright, A. J., Young, A. J. and Natarajan, S. (2005) Dwelling temperatures and comfort during the August 2003 heat wave. *Building Services Engineering Research & Technology* 26, 285-300.

[49] Sarrat, C., Lemonsu, A., Masson, V. and Guedalia, D. (2006) Impact of urban heat island on regional atmospheric pollution. *Atmospheric Environment* 40, 1743-1758

[50] Voogt, James, A. (2004) Urban heat islands: Hotter cities. Web article for *ActionBioscience* http://www.actionbioscience.org/environment/voogt.html [accessed on 25/5/2010]

[51] Memon, R. A., Leung, D. Y. C., and Chunho, L, I, U. (2008a) A review on the generation, determination and mitigation of Urban heat island. *Journal of Environmental Science-China* 20(1), 120-128

[52] Memon, R. A., Leung, D.Y.C., Liu, C. H. (2008b) Impacts of important environmental variables on the urban heating. *Journal of environmental science* 22(12), 1903-1909

[53] Unger, J., Sumeghy, Z. and Zoboki, J. (2001) Temperature cross-section feature in an urban area. *Atmospheric Research* 58, 117-127

[54] Hafner, J. and Kidder, S.Q. (1999) Urban heat island modelling in conjunction with satellite-derived surface/soil parameter. *Journal of Applied Meteorology* 38, 448-465

[55] Poreh, M. (1996) Investigation of heat island using small scale model. *Atmospheric Environment* 30(3) 467-474

[56] Oke, T. R. (1981) Canyon Geometry and the nocturnal urban heat island: Comparison of scale model and field observations. *Journal of Climatology* 1, 237-254

[57] Yamashita, S., Sekine, K., Shoda, M., Yamashita, K. and Hara, Y. (1986) On the relationships between heat island and sky view factor in the cities of Tama River Basin, Japan. *Atmospheric Environment* 20, 681-686

[58] Eliasson, I. (1992) Infrared thermography and urban temperature patterns. *International Journal of Remote Sensing* 13(5), 869-879

[59] Goh, K. C. and Chang, C. H. (1999) The relationship between height to width ratios and the heat island intensity at 22:00h for Singapore. *International Journal of Climatology* 19, 1011-1023

[60] Santos, I.G., Lima, H.G. and Assis, E.S. (2003) A comprehensive approach of the sky view factor and building mass in an urban area of the city of Belo Horizonte, Brazil. In: Klysik, K, Oke, T.R., Fortuniak, K., Grimmond, C.S.B., Wibug, J. (eds) Proc 5th International Conference on Urban Climate, Vol. 2 *University of Lodz,* Lodz 367-370

[61] Unger, J. (2004) Intra-urban relationship between surface geometry and urban heat island: review and new approach. *Climate Research* 27,253-264

[62] Eumorfopoulou, E. A. and Kontoleon, K. J (2009) Experimental approach to the contribution of plant-covered walls to the thermal behaviour of building envelopes. *Building and Environment*. 44, 1024-1038

[63] Jusuf, S. K., Wong, N, H., Emlyn, H., Anggoro, R. and Hong, Y. (2007) The influence of land use on the urban heat island in Singapore. *Habitat International* 31(2), 232-242

[64] Gill, S., Handley, J., Ennos, A., and Pauleit, S. (2007) Adapting cities for climate change: The Role of the Green Infrastructure. *Built Environment.* 3, 115-133

[65] Eliasson, I and Svensson, M. K. (2003) Spatial air temperature variations and urban land use- a statistical approach. *Meteorology Applications* 10, 135-149

[66] Golany, G. S. (1996) Urban design morphology and thermal performance. *Atmospheric Environment* 30(3), 455-465

[67] Upmanis, H., Eliasson, I. and Lindquist, S. (1998) The influence of green areas on nocturnal temperatures in a high latitude city (Goteborg, Sweden). *Inthernational Journal of Climatology* 18, 681-700

[68] Upmanis, H. and Chen, D. L. (1999) Influence of geographical factors and meteorological variables on nocturnal urban-park temperature differences – a case study of summer 1995 in Goteborg, Sweden. *Climate Research* 13, 125-139

[69] Bottyan, Z., A. Kircsi, Szegedi, S. and Unger, J. (2005) The relationship between built-up areas and the spatial development of the mean maximum urban heat island in Debrecen, Hungary. *International Journal of Climatology* 25(3), 405-418

[70] Taha, H. (1997) *Modelling* the impacts of large-scale albedo changes on ozone air quality in the South Coast Air Basin. *Atmospheric Environment* 31(11), 1667-1676

[71] Giridharan, R., Ganesan, S, and Lau, S, S, Y. (2004) Daytime urban heat island effect in high-rise and high-density residential developments in Hong Kong. *Energy and Building* 36(6), 525-534

[72] Hamilton, I, G., Davies, M., Steadman, P., Stone, A., Ridley, A. and Evans, S. (2008) The significance of the anthropogenic heat emissions of London's buildings: A comparison against captured shortwave solar radiation. *Building and Environment*, 44(4), 807-817

[73] Smith, C., Lindley, S. and Levermore, G. (2009) Estimating spatial and temporal patterns of urban anthropogenic heat fluxes for UK cities: the case of Manchester. *Theoretical and Applied Climatology*. 98, 19-35

[74] Tereshchenko, I, E. and Filonov, A, E. (2001) Air temperature fluctuations in Guadalajara, Mexico, from 1926 to 1994 in relation to urban growth. *International Journal of Climatology* 21(4), 483-494

[75] Oke, T. R., Jonson, G., T. Johnson, Steyn, D. G. and Watson, I. D. (1991) Simulation of surface urban heat islands under "Ideal" conditions at night Part 2: Diagnosis of causation. *Boundary-Layer Meteorology* 56, 339-358

[76] Kolokotroni, M., Davies, M., Croxford, B., Bhuiyan, S. and Mavrogianni, A (2010) A validated methodology for the prediction of heating and cooling energy demand for buildings within the urban heat island: Case-study of London. *Solar Energy* 84, 2246-2255

[77] Santamouris, M., Mihalakakou, G., Papanikolaou, N. and Asimakopoulos, D.N. (1999) A neural network approach for modelling the heat island phenomenon in urban areas during the summer period. *Geophysical Research Letters* 26(3), 337-340

[78] Kolokotronim, M, Zhang, Y. and Giridharan, R. (2009) Heating and cooling degree day prediction within the London urban heat island area. *Building Services Engineering Research and Technology* 30(3), 183-202

[79] Gobakis, K., Kolokotsa, D., Synnefa, A., Saliari, M., Giannopoulou, K. and Santamouris, M. (2011) Development of a model from urban heat island prediction using neural network techniques. *Sustainable Cities and Society* 1, 103-115

[80] Masson, V. (2000) A physically based scheme for the urban energy budget in atmospheric models. *Boundary Layer Meteorology* 94, 357-397

[81] Masson, V., Grimmond, C. S. B., Oke, T.R. (2002) Evaluation of the town energy balance (TEB) Scheme with Direct Measurements from Dry Districts in Two cities. *American Meteorological Society Journals.* 41(10), 1011-1026

[82] Arnfield, A, J. (2000) A simple model of urban canyon energy budget and its validation. *Physical Geography* 21(4), 305-326

[83] Kusaka, H., Konodo, H., Kikegawa, Y. and Kimura. F. (2001) A simple single-layer urban canopy model for atmospheric models: comparison with multi-layer and slab models. *Boundary-Layer Meteorology* 101(3), 329-358

[84] Kanda, M., Kawai, T., Kanega, M., Moriwaki, R., Narita, K. and Hagishima, A. (2005) A simple energy balance model for regular building arrays. *Boundary-Layer Meteorology*, 116(3), 423-443

[85] Uno, I., Ueda, H. and Wakamatsu, S. (1989) Numerical modelling of the nocturnal urban boundary layer. *Boundary-Layer Meteorology* 46(1-2), 77-98

[86] Ashie, Y., Vu Thanh, C. and Asaeda, T. (1999) Building canopy model for the analysis of urban climate. *Journal of Wind Engineering and Industrial Aerodynamics* 81(1), 237-248.

[87] Vu Thanh, C., Asaeda, T. and Ashie, Y. (1999) Development of a numerical model for the evaluation of the urban thermal environment. *Journal of Wind Engineering and Industrial Aerodynamics* 81(1), 181-196

[88] Vu Thanh, C., Ashie, Y. and Asneda, T. (2002) A k- ε turbulence closure model for the atmospheric boundary layer including urban canopy. *Boundary-Layer Meteorology* 102(3), 459-490

[89] Martilli, A. (2003) A two dimensional numerical study of the impact of a city on atmospheric circulation and pollutant dispersion in a coastal environment. *Boundary-Layer Meteorology* 108(1), 91-119

[90] Tanimoto, J., Hagishima, A. and Chimklai, P. (2004) An approach for coupled simulation of building thermal effects and urban climatology. *Energy and buildings* 36(8), 781-793

[91] Kono, H., Genchi, Y., Kikegawa, Y., Ohashi, Y., Yoshikado, H. and Komiyama, H. (2005) Development of a multi-layer urban canopy model for the analysis of energy consumption in a big city: structure of the urban canopy model and its basic performance. *Boundary-Layer Meteorology* 116 (3), 395-421

[92] Grimmond, C,S,B., Blackett, M., Best, M,J., Barlow, J., Baik, J,J., Belcher, S,E., Bohnenstengel, S,I., Calmet, I., Chen, F., Dandou, A., Fortuniak, K., Gouvea, M, L., Hamdi, R., Hendry, M., Kawai, T., Kawamoto, Y., Kondo, H., Krayenhoff, E,S., Lee, S, H., Loridan, T., Martilli, A., Masson, V., Miao, S., Oleson, K., Pigeon, G., Porson, A., Ryu, Y, H., Salamanca, F., Shashua-Bar, L., Steeneveld, G, J., Tombrou, M., Voogt, J., Young, D. and Zhang, N. (2010) The international urban energy balance models compartison project: First results from phase 1. *Journal of applied meteorology and climatology* 49, 1268-1292

[93] Grimmond, C,S,B., Blackett, M., Best, M,J., Baik, J,J., Belcher, S,E., Beringer, J., Bohnenstengel, S,I., Calmet, I., Chen, F., Coutts, A., Fortuniak, K., Gouvea, M, L., Hamdi, R., Hendry, M., Kanda, M., Kawai, T., Kawamoto, Y., Kondo, H., Krayenhoff, E,S., Lee, S, H., Loridan, T., Martilli, A., Masson, V., Miao, S., Oleson, K., Ooka, R., Pigeon, G., Porson, A., Ryu, Y, H., Salamanca, F., Steeneveld, G, J., Tombrou, M., Voogt, J,A., Young, D,T., and Zhang, N. (2011) Initial results from phase 2 of the international urban energy balance model comparison. *International Journal of Climatology* 31, 244-272

[94] Mavrogianni, A., Davies, M., Batty, M., Belcher, S, E., Bohnenstengel, S, I., Carruthers, D., Chalabi, Z., Croxford, B., Demanuele, D., Evans, S., Giridharan, R., Hacker, J,N., Hamilton, I., Hogg, C., Milner, J., Rajapaksha, I., Ridley, I., Steadman, J, P., Stocker, J., Wilkinson, P. and Ye, Z. (2011) The comfort, energy and health implications of London's urban heat island *Building Service Engineering Research and Technology* 0, 1-18

[95] The development of a Local Urban Climate model and its application to the Intelligent Design of cities (LUCID) EPSRC funded project http://www.lucid-project.org.uk/ [accessed on 24/7/2011]

[96] Tso, C. P., Chan, B. K., and Hashim, M. A. (1990) An Improvement to the basic energy balance model for urban thermal environment analysis. *Energy and Buildings,* 14(2), 143-152.

[97] Tso, C. P., Chan, B. K. and Hashim, M. A. (1991) Analytical solutions to the near-neutral atmospheric surface energy balance with and without heat storage for urban climatological studies. *Journal of Applied Meteorology,* 30(4), 413-424

[98] Johnson, G, T., Oke, T, R., Lyon, T, J., Steyn, D, G., Watson, I, D. and Voogt, J, A. (1991) Simulation of surface urban heat islands under 'Ideal' conditions at night Part 1: Theory and tests against field data. *Boundary Layer Meteorology.* 56, 275-294

[99] Mills, G. M. (1993) Simulation of the energy budget of an urban canyon – I. Model structure and sensitivity test. *Atmospheric Environment* 27B(2), 157-170

[100] Erell, E. and Williamson, T. (2006) Simulating air temperature in an urban street canyon in all weather conditions using measured data at a reference meteorological station. *International Journal of Climatology* 26, 1671-1694

[101] Gill, S.(2009) PhD Thesis *Centre for Urban and Regional Ecology, School of Environment and Development*, University of Manchester

[102] Whitford, V (2001) MSc Thesis *University of Manchester*

[103] Whitford, V., Ennos, A. R. and Handley, J. F. (2001) "City form and natural process" indicators for the ecological performance of urban areas and their application to Merseyside. UK *Landscape and Urban Planning,* 57(2), 91-103

[104] Kershaw, T., Sanderson, M., Coley, D and Eames, M. (2010) Estimation of the urban heat island for UK climate change projections. *Building Services Engineering Research and Technology* 0, 1-13

[105] Cheung. H., Levermore. G. and Watkins. R. (2010) A low cost, easily fabricated radiation shield for temperature measurements to monitor dry bulb air temperature in built up urban areas. *Building services engineering research technology* 31(4), 371-380

[106] Rotronic (2010) data logger data sheet http://www.rotronic.co.uk/_upload/gen_downloads/FE_Katalog_RAG_CH_eng_data_loggers.pdf [accessed 26/09/2009]

[107] Tinytag temperature logger data sheet http://www.geminidataloggers.com/file/loggers_variant/datasheet/tgp-4017.pdf [accessed 26/09/2009]

[108] Maxim. (2009) Temperature Logger iButton with 8kb Data Log Memory Rev 8. http://datasheets.maxim-ic.com/en/ds/DS1922L-DS1922T.pdf [accessed 26/09/2009]

[109] Sunshine Sensor type BF-3 Data sheet, *Delta T Device Ltd*, Cambridge UK

[110] Skye Lux Sensor SKL-310 Data sheet, *Skye Instrument Ltd,* Powys UK

[111] Pakinson, J. (2010) Private communication *Department of Mathematics* The University of Manchester

[112] British Atmosphere Data Centre (BASC) Met Office - MIDAS Land Surface Observation Stations Data. http://badc.nerc.ac.uk/data/ukmo-midas/ [accessed 23/02/2010]

[113] Stull R. B. (1995) Meteorology today for scientists and engineers A technical companion book. *West Publishing Company* USA. ISBN 0314064710

[114] http://www.timeanddate.com/worldclock/astronomy.html?n=302&month=1&year=2011&obj=sun&afl=-11&day=1 [accessed on 02/03/2011]

[115] Landsberg, H. E., (1981) The urban climate. *New York NY Academic Press*, ISBN: 0124359604

[116] Tumanov, S., A. Stan-Sion, A. Lupu, C. Soci and C. Opera (1999) Influences of the city of Bucharest of weather and climate parameter. *Atmospheric Environment* 33:, 4137-4183

[117] Souza, L C.L, Rodrigues, D. S. and Mendes, J.F.G. *(*2003) Sky View Factors Estimation using a 3D-GIS Extension, *Eighth International IBPSA Conference*, Abstract, pg 1

[118] Johnson. G. T. and Watson. I. D (1984) The Determination of View-Factors in Urban Canyons. , *Journal of Climate and Applied Meteorology*, pg 329-335

[119] Daniel Coles (2010) *BEng Thesis* University of Manchester

[120] Daniel Reaney (2009) *BEng Thesis* University of Manchester

[121] Grimmond, C,S,B, Potter, S, K., Zutter, H, N. and Souch, C. (2001) Rapid methods to estimate sky-view factors applied to urban areas *International Journal of Climatology* 21, 903-913

[122] Chapman, L., Thornes, J, E., and Bradley, A, V. (2000) Rapid determination of canyon geometry parameters for use in surface radiation budgets. *Theoretical and Applied Climatology* 69, 81-89

[123] Cheung H, Coles D, Levermore G. Sky view factor and urban heat island in Manchester. *Drafting Paper* found in appendix C

[124] Land Use Consultants (LUC), (1993) Trees in Towns: Report to the Department of Environment. HMSO, London

[125] Gill, S., Handley, J., Ennos, A., Pauleit, S., Theuray, N. and Lindley, S. (2008) Characterising the urban environment of UK cities and towns: a template for landscape planning. *Landscape and urban planning*. 87, 2010-222

[126] Erell, E. and Williamson, T. (2007) Intra-urban differences in canopy layer air temperature at a mid latitude city. *International journal of climatology.* 27, 1243-1255

[127] ESRI. (2006) What is ARcGIS 9.2 *Documents attached with the installation of ArcGIS v9.2*

[128] Smith C (2009) Private communication *Department of Geography The University of Manchester*

[129] SPSS Inc (2008). *SPSS for Windows: rel 16.0.2.* Chicago, lL: SPSS Inc.

[130] Lindley, S. (2009) Private communication *Department of Geography* The University of Manchester

[131] Laycock, P (2011) Private communication *Department of Mathematics* The University of Manchester

[132] Levermore, G. and Cheung, H. (2011) A low order canyon model to estimate the influence of canyon shape on the maximum urban heat island effect. *Building services engineering research technology* [accepted in Jun 2011]

[133] ERA Report 69-30 (Part B). (1989.) Sustained Current Ratings for Cables Thermosetting Insulation to BS 5467:1989 and BS 6724 1986 (AC 50Hz and DC. ERA Technology Ltd.

[134] CIBSE 2006. TRY for Manchester UK. CIBSE, London.